Development and Evaluation of Teriflunomide and Quercetin Loaded Topical Transferosomal Gel for the Treatment of Rheumatoid Arthritis

THESIS

Submitted in partial fulfillment
of the requirements for the degree of

DOCTOR OF PHILOSOPHY

by

KARNAM SRIRAVALI
ID. No. 2019PHXF0071P

Under the Supervision of
Prof. PAUL ATISH TULSHIRAM

and

Co-supervision of
Prof. ANIL B. JINDAL

BITS Pilani

Pilani | Dubai | Goa | Hyderabad | Mumbai

BIRLA INSTITUTE OF TECHNOLOGY & SCIENCE, PILANI
2024

Dedicated to My Father

Late Shri. Karnam Amar Veer Chisthy

DECLARATION

I hereby declare that the work carried out in this thesis titled **"Development and Evaluation of Teriflunomide and Quercetin Loaded Topical Transferosomal Gel for the Treatment of Rheumatoid Arthritis"** is an original piece of research work carried out under the supervision of **Prof. Paul Atish Tulshiram** with co-supervision by **Prof. Anil B. Jindal** at Department of Pharmacy, Birla Institute of Technology and Science, Pilani (BITS-Pilani), Pilani Campus. This thesis has not been submitted by me for the award of any other degree of any other University/Institute.

Karnam Sriravali
2019PHXF0071P
Research scholar
BITS-Pilani, Pilani Campus
Date: 11/9/2024

BIRLA INSTITUTE OF TECHNOLOGY AND SCIENCE, PILANI

CERTIFICATE

This is to certify that the thesis entitled **"Development and Evaluation of Teriflunomide and Quercetin Loaded Topical Transferosomal Gel for the Treatment of Rheumatoid Arthritis"** submitted by **Karnam Sriravali**, ID. No. **2019PHXF0071P** for award of Ph.D. degree of the institute, embodies original work done by her under our supervision.

Supervisor
Prof. Paul Atish Tulshiram
Associate Professor,
Department of Pharmacy,
BITS-Pilani, Pilani Campus, Rajasthan
Date: 11/9/2024

Co-Supervisor
Prof. Anil B. Jindal
Associate Professor,
Department of Pharmacy,
BITS-Pilani, Pilani Campus, Rajasthan
Date:11/9/2024

ACKNOWLEDGEMENT

Abstract

Rheumatoid arthritis (RA) manifests as a multifaceted autoimmune condition, primarily targeting joints and synovial membrane. In 2020, it was estimated that around 17.6 million individuals globally were diagnosed with RA. Projections indicate that this number could rise to 30 million by 2050. In RA, immune cells, such as lymphocytes (T-cells, B-cells, and natural killer cells) and monocytes (macrophages and dendritic cells), along with mast cells, are prominently contributes to the pathogenesis of the disease. Hence, thorough comprehension of the intricate mechanisms involved in RA pathogenesis is imperative for formulating precise therapeutic strategies tailored to mitigate the varied stages of disease progression.

The European League Against Rheumatism (EULAR) has established guidelines for RA treatment, endorsing monotherapy or combination therapy consisting of synthetic Disease-modifying antirheumatic drugs (DMARDs), corticosteroids, biological DMARDs, or targeted DMARDs. Several guidelines promote the implementation of initial combination therapy with synthetic DMARDs as a preventive measure against progressive joint damage. Also, the effectiveness of combination of synthetic molecules with natural products for the management of RA has been investigated. Teriflunomide (TFD) the drug of choice, it is an active metabolite of Leflunomide, (categorized as synthetic DMARD) that acts by inhibiting the mitochondrial enzyme dihydroorotate dehydrogenase (DHODH), which is a critical component of the *de-novo* pyrimidine synthesis pathway, ultimately leading to the suppression of proliferation of active lymphocytes. Oral administration of TFD has been associated with significant hepatotoxicity and systemic adverse effects. Apart from the synthetic drugs, natural products have been documented to exhibit anti-inflammatory and anti-arthritic properties through acting by multiple pathways. Natural products also often exhibit insufficient solubility and bioavailability when administered orally. Therefore, adopting a topical delivery method is crucial, aiming for localized effectiveness within joint tissue while minimizing systemic levels through dose reduction.

However, there remains limited exploration regarding the efficacy of combining TFD with natural products for the treatment of RA. Based on the literature, well-known anti-inflammatory natural products namely Andrographolide (ANG), Quercetin (QCN), Resveratrol (RES), Rutin (RUT), and Tanshinone IIA (TAN) were selected for combination development with TFD. Thus, aim of the present dissertation was to develop "TFD and Natural Products Loaded Transferosomes for Treatment of Rheumatoid Arthritis."

Prior to the evaluation of *in-vivo* activity of the combination, the *in-vitro* synergistic anti-inflammatory activity of selected natural products in combination with TFD, in LPS stimulated RAW 264.7 cells was evaluated to identify the most effective combination exhibiting high synergy. The initial screening was performed using nitric oxide (NO) assay to determine the IC_{50}, with prior determination of the safest concentration range using the MTT assay. Synergistic analysis was performed using a constant ratio design using NO assay, and calculating combination index (CI), isobologram analysis and dose reduction index (DRI). Among the tested combinations, QCN, RES, and TAN with TFD displayed low CI values (0.484 to 0.957) and were evaluated for proinflammatory cytokines inhibition using ELISA based assay. Notably, the combination of QCN and TFD showed significant synergistic activity, with CI values of 0.470 and 0.607 (at Fa = 0.5) for TNF-α and IL-6, respectively. Intracellular ROS measurement with this combination revealed greater synergistic activity, suggesting a promising combination for RA treatment. Hence, the combination of TFD and QCN was further selected for the evaluation of efficacy in RA.

A simple and cost-effective UV-Visible spectrophotometric method was developed for the simultaneous estimation of TFD and QCN using absorption factor method and validated as per ICH guidelines. Also, rapid, and sensitive simultaneous Reversed-phase high-performance liquid chromatography (RP-HPLC) method was developed by implementing analytical quality by design (AQbD). The developed method was also validated as per the ICH guidelines. The developed method can be applicable for the estimation of TFD and QCN in the prepared topical formulation.

TFD and QCN loaded transferosomes were prepared separately using QbD approach, employing 3-level, 3-factorial Box-Behnken design (BBD). The independent variables, including the quantities of Phospholipon® 90 G (PL 90G), sodium cholate, and tween 80, were chosen to operate at three distinct levels (+1, 0, -1 represents high, intermediate, and low level) against dependent variables such as vesicle size (nm) and entrapment efficiency (%EE). The ANOVA analysis indicated the quadratic model to be the most suitable fit for the experimental results with p > 0.001 and regression coefficient of for all variables were > 0.98. The composition was optimized using numerical and desirability methods with the optimized composition falling within the design space.

The transferosomes were prepared by thin film hydration method and optimized composition exhibited a vesicular size of 107.80 ± 2.68 nm (PDI of 0.283 ± 0.008) and the zeta potential

(ZP) of -32. ± 1.98 mV for TFD transferosomes. Similarly, for QCN transferosomes the vesicular size was found to be 96.32 ± 3.32 nm (PDI of 0.289 ± 0.005) and the ZP values were determined to be -30.7 ± 1.14 mV. The % EE was found to be 79.92 ± 0.20 % and 89.55 ± 0.10 % for TFD and QCN transferosomes, respectively. The *in-vitro* drug release showed a sustained release up to 10 hrs by TFD transferosomes and 12 h by QCN transferosomes, whereas both the free drugs solutions showed drug release within 2 h. For preparation of transferosomal combination gel, TFD and QCN at a ratio of 1:3.5 was taken based on the *in-vitro* screening study and formulated using Carbopol 974P. The topical combination gel underwent thorough evaluation of rheology. The transferosomal gel exhibited enhanced permeability, as evident from the *ex-vivo* skin permeation and retention studies using excised rat abdominal skin. The synergistic combination of TFD and QCN transferosomal gel effectively suppressed NO, TNF-α and IL-6 levels in *in-vitro* LPS induced RAW 264.7 cells. The cytotoxicity study in HaCaT cells indicated non-toxicity of the gel, that was further confirmed by skin irritation study conducted in rats.

The *in-vivo* anti-arthritic activity was evaluated in complete freund's adjuvant induced paw edema model in female Wistar rats for a period of 28 days. The evaluation was carried out for various parameters such as paw volume, arthritic score, X-ray analysis, inhibition of proinflammatory cytokines in serum & paw tissue, and histopathological examination of paw & liver tissues. The findings indicated that the transferosomal gel demonstrated greater anti-arthritic activity compared to the free drug loaded gel. Histopathology of the liver revealed marginal changes in hepatocellular structure with oral administration of TFD, in contrast to the topical transferosomal gel. Also, the topical combinational transferosomal gel exhibited reduced collagen deposition and decreased levels of TNF-α and IL-6 in paw tissue. The comprehensive study concluded that the combination of TFD and QCN transferosomal gel holds promise for the effective treatment of RA through localized delivery, and may allow for the dose reduction thereby mitigating systemic side effects of TFD.

Table of Contents

List of Figures

List of Tables

List of Abbreviations and Symbols

α	Alpha
Å	Amstrong
ω	Angular Frequency
β	Beta
cm	Centimeter
°C	Degree Celsius
=	Equal to
J	Flux
γ	Gamma
g	Gram
g/mol	Gram per mole
h	Hour/Hours
IC_{50}	Inhibitory Concentration
λ_{max}	Lambda Max
<	Less than
≤	Less than equal to
G"	Loss Moduli
C_{max}	Maximum Concentration
μg	Microgram
μm	Micrometer
μL	Microliter
μM	Micromolar
>	More than
≥	More than equal to
ng	Nanogram
nM	Nanomolar
nm	Nanometer
Log P	Partition Coefficient
%	Percentage
S	Seconds
$\dot{\gamma}$	Shear Rate

τ	Shear Stress
Jss	Steady-state flux
G'	Storage Moduli
σ_0	Yield Stress
w/v	Weight per volume
w/w	Weight per weight
ACPA	Anti-Citrullinated Protein Antibody
ACR	American College of Rheumatology
APLAR	Asia Pacific League of Associations for Rheumatology
AQbD	Analytical Quality by Design
ALT	Alanine Aminotransferase
ANG	Andrographolide
ANOVA	Analysis of Variance
AP-1	Activator Protein-1
APCs	Antigen Presenting Cells
API	Active Pharmaceutical Ingredient
ATP	Analytical Target Profile
ATR-IR	Attenuated Total Reflectance- Infrared
BBD	Box–Behnken Design
CAA	Critical Analytical Attributes
CAM	Complementary and Alternative Medicine
CAMK2A	Calcium/Calmodulin-dependent Protein Kinase II alpha
CCD	Center Composition Design
CFA	Complete Freund's Adjuvant
CI	Combination Index
CMA	Critical Material Attributes
COX	Cyclooxygenase
CPP	Critical Process Parameters
CQA	Critical Quality Attributes
CRF	Code of Federal Regulations
CRP	C-Reactive Protein
CYP	Cytochrome
DCs	Dendritic Cells

DHODH	Dihydroorotate Dehydrogenase
DIP	Distal Interphalangeal
DL	Drug Loading
DLS	Dynamic Light Scattering
DMARD	Disease Modifying Anti-Rheumatic Drugs
bDMARDs	Biological Disease Modifying Anti-Rheumatic Drugs
sDMARDs	Synthetic Disease Modifying Anti-Rheumatic Drugs
tsDMARDs	Targeted Disease Modifying Anti-Rheumatic Drugs
DCFDA	2′,7′-Dichlorodihydrofluorescein Diacetate
DMEM	Dulbecco's Modified Eagle's Medium
DMSO	Dimethyl Sulfoxide
DOE	Design of Experiments
DRI	Dose Reduction Index
DSC	Differential Scanning Calorimetry
EE	Encapsulation Efficiency
ELISA	Enzyme-Linked Immunosorbent Assay
EULAR	European League Against Rheumatism
ERK	Extracellular Signal-Regulated Kinase
ESR	Erythrocyte Sedimentation Rate
FBS	Fetal Bovine Serum
FCP	Fibrous Connective Tissue Proliferation
FDA	Food and Drug Administration
FESEM	Field Emission Scanning Electron Microscopy
FFD	Fractional Factorial Design
FLS	Fibroblast like Synoviocytes
FMEA	Failure Mode Effects and Analysis
FRK	Fyn-related Kinase
FST	Frequency Sweep Test
GI	Gastrointestinal
GRAS	Generally Recognized as Safe
GSK-3β	Glycogen Synthase Kinase 3 beta
H&E	Hematoxylin and eosin stain
HIF	Hypoxia Inducible Factor

HPLC	High-pressure liquid chromatography
HQC	High Quality Control
IAEC	Institutional animal ethical committee
IC	Inflammatory cell infiltration
*i*NOS	Inducible nitric oxide synthase
ICH	International Council for Harmonisation of Technical Requirements of Pharmaceuticals for Human Use
IFN-γ	Interferon-gamma
IL	Interleukins
IS	Internal Standard
JAK	Janus Kinase-Signal Transducer
JAK-STAT	Janus Kinase-Signal Transducer and Activator of Transcription
JNK	c-Jun N-terminal kinase
KDa	Kilo Daltons
Kp	Permeability Coefficient
kV	Kilo Volt
L	Liter
LC-MS	Liquid Chromatography-Mass Spectrometry
LOD	Limit of Detection
LOQ	Limit of Quantification
LPS	Lipopolysaccharide
LQC	Lower Quality Control
LVR	Linear Viscoelastic Region
LRP	Lipoprotein Receptor-Related Protein
M	Molar
MAPK	Mitogen-Activated Protein Kinase
MHC	Major Histocompatibility Complex
MMPs	Matrix Metalloproteinases
MP	Mobile Phase
MQC	Medium Quality control
mg	Milligram
min	Minutes
MLRA	Multiple Linear Regression Analysis

mL	Milliliter
mm	Millimetre
mM	Millimolar
MODR	Method Operable Design Region
mPa.s	Millipascal per Second
MP	Metacarpophalangeal
MPP	Matrix Metalloproteinase
MTT	3-(4,5-dimethylthiazol-2-yl)-2,5-diphenyl tetrazolium bromide
Mv	Milli Volts
NCCS	National Centre for Cell Science
NF-κB	Nuclear Factor Kappa B
NEDD	N-(1-naphthyl) Ethylenediamine Dihydrochloride
NK	Natural Killer Cells
NO	Nitric Oxide
Nrf2	Nuclear factor erythroid 2-related factor 2
NSAIDS	Nonsteroidal Anti-inflammatory Drug
PBS	Phosphate Buffer Saline
PDA	Photodiode Array
PDI	Poly Dispersibility Index
PGE_2	Prostaglandin E2
PI	Portal Inflammation
PI3K-Akt	Phosphatidylinositol 3 kinase
PDK1	Phosphoinositide-dependent Protein Kinase-1
PAD4	Protein Arginine Deiminase 4
PIP	Proximal Interphalangeal
PIP2	Phosphatidylinositol 4,5-bisphosphate
PIP3	Phosphatidylinositol 3,4,5-trisphosphate
PKA	Protein Kinase A
PKC	Protein Kinase C
PL 90 G	Phospholipon 90 G
QbD	Quality by Design
QC	Quality Control
QCN	Quercetin

QTPP	Quality Target Product Profile
RA	Rheumatoid Arthritis
R^2	Coefficient of Correlation
RANK	Receptor Activator of Nuclear Factor κB
RANKL	Receptor Activator of Nuclear Factor κB Ligand
RF	Rheumatoid Factor
REM	Risk Estimation Matrix
RES	Resveratrol
ROS	Reactive Oxygen species
RP-HPLC	Reverse phase high performance liquid chromatography
RPM	Rotations per minutes
RPN	Risk Priority Number
RSD	Relative Standard Deviation
RUT	Rutin
SD	Standard Deviation
SLNs	Solid Lipid Nanoparticles
SYK-BTK	Spleen tyrosine kinase bruton's tyrosine kinase pathway
TAN	Tanshinone IIA
TFD	Teriflunomide
Tfh Cells	T Follicular Cells
Th	T Helper Cells
TLR	Toll-like Receptor
Treg Cells	T Regulatory Cells
TNF-α	Tumor Necrosis Factor alpha
USFDA	United States Food and Drug Administration
WHO	World Health Organization
Wnt	Wingless/Integrated
ZP	Zeta Potential

Chapter 1

Introduction

Chapter 1

1.1. Introduction

Rheumatoid arthritis (RA) manifests as a multifaceted autoimmune condition, primarily targeting joints with inflammatory arthritis and also with extra articular manifestations [1,2]. The development of RA arises from a combination of genetic predisposition and various environmental factors, that collectively contribute to the complex interplay which triggers and exacerbates the condition [3]. The World Health Organization (WHO) reported that, in 2019 approximately 1% of the global population was affected by RA, impacting an estimated 18 million people. Notably, around 70% of those affected by RA are women, with a significant portion (55%) are over the age of 55. It is estimated that this number could rise to 30 million by 2050 [4]. RA typically initiates in smaller joints, that progress symmetrically. Persistent inflammation and immune dysregulation in RA potentially culminate in erosive synovitis and progressive joint destruction in the absence of therapeutic intervention [1,5]. The clinical manifestations and characteristics associated with RA have been delineated in **Figure 1.1**. The primary symptoms linked with RA encompass discomfort in the joints, swelling, stiffness, and warmth in the affected joints, ultimately resulting in a reduction in joint mobility. The clinical manifestation of RA is marked by hyperplasia or hypertrophy of synovial membrane, infiltration of immune cells secretion of inflammatory cytokines and proteolytic enzymes into synovium, new blood vessel formation (angiogenesis), activation of osteoclasts (leading to bone erosion), proliferation of fibroblast-like synoviocytes (FLS), and pannus formation, all contributing to the chronic inflammatory process and joint destruction observed in the disease [6,7].
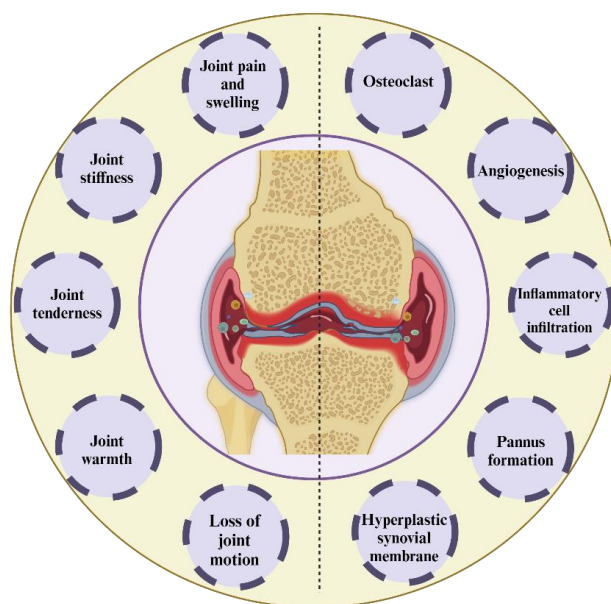
Figure 1.1. Clinical manifestations (on left) and characteristics (on right) associated with RA

1.2. Pathophysiology of RA

The pathophysiological cascade of RA encompasses a multifaceted interplay among diverse immune cells, cytokines, and inflammatory mediators [8]. A thorough comprehension of these intricate mechanisms is imperative for formulating precise therapeutic strategies to address the different stages of disease progression [9]. Ding et al. 2023 outlined the triphasic progression of RA, commencing with an initial non-specific inflammatory phase characterized by immune cell proliferation within the synovium, followed by a chronic inflammatory phase and culminating in a final phase of tissue damage orchestrated by the production of diverse inflammatory cytokines [10].

1.2.1. Role of immune cells in the pathogenesis of RA

In RA, various immune cells, including lymphocytes (T-cells, B-cells, natural killer cells), monocytes (macrophages, dendritic cells DCs), and mast cells, play significant role in disease development. Specifically, T-cells, B-cells, and macrophages that are found in the synovium or circulating in peripheral blood crucially contribute to RA pathogenesis [11]. RA is said to be triggered by diverse genetic and environmental factors, leading to activation of the immune system [12]. The adaptive and innate immune systems are both involved in RA pathogenesis. The innate immune response promptly triggers inflammation and tissue damage in response to stimuli, while the adaptive immune system mounts a precise, antigen-specific reaction, culminating in autoantibody production and sustained inflammation in RA [13,14]. This dual activation by adaptive and innate immunity perpetuates the chronic inflammation and joint damage as characteristics of the disease [15,16].

Upon encountering specific susceptibility factors, this activation prompts post-translational modifications of arginine residues in proteins, transitioning them to citrulline in a process known as citrullination and prompts the antigen-presenting cells (APCs) to recognize altered proteins containing peptidyl arginine and peptidyl citrulline residues [12,17]. The APCs (comprising dendritic cells, macrophages, and B cells) instigate the T cell activation through a sequence of intricate interactions that entail antigen presentation alongside co-stimulatory signals [18]. APCs internalize antigens from their microenvironment and subsequently enzymatically process them into peptides. These peptides are then displayed on the APC surface and bound to major histocompatibility complex (MHC) molecules. Upon encountering a peptide-MHC complex, the T cell receptor on a naive CD4+ T cell forms an immunological synapse with the APC, initiating downstream signaling by phosphatidylinositol 3 kinase (PI3K) pathway cascades that culminate in CD4+ T cell activation [19]. Additionally, co-stimulatory

molecules on the APC surface, such as CD80 and CD86, interact with corresponding receptors on the T cell, providing the second signal necessary for full T cell activation and proliferation. This activation process is crucial for initiating and orchestrating adaptive immune responses against pathogens or self-antigens, in RA [20,21]. Following activation, naive CD4+ T cells undergo differentiation into specific T helper (Th) subpopulations, including Th1, Th2, T regulatory cell (Treg), Th17, T19, T22 and T follicular cells (Tfh), each producing a distinct array of cytokines crucial for modulating immune responses, as depicted in the **Figure 1.2.** Subsets like Th1, Th17, Th9, Th22, and Tfh cells collectively contribute to the generation of diverse inflammatory cytokines and matrix metalloproteinases (MMPs), fostering inflammation. Conversely, Treg and Th2 cells play pivotal roles in immune regulation by secreting anti-inflammatory cytokines, thus suppressing the immune responses [21,22].

Further, B cells undergo differentiation into plasma cells, which is driven by T cell-derived signals and cytokines. These plasma cells generate autoantibodies such as rheumatoid factor (RF) and anti-citrullinated protein antibodies (ACPAs), targeting self-antigens within the synovial tissue. The resulting formation of immune complexes exacerbates chronic inflammation, leading to tissue damage and joint destruction typical of RA [23]. Furthermore, activated B cells can present autoantigens to T cells, intensifying the immune response and sustaining the autoimmune cascade in RA [24]. T cell-derived cytokines such as tumor necrosis factor-alpha (TNF-α), interferon-gamma (IFN-γ), and interleukin-17 (IL-17) directly stimulate macrophages, leading to their activation and production of inflammatory mediators [11,25,26] Similarly, activated B cells , can also stimulate macrophages through antigen presentation to T cell and cytokine secretion [24]. Activated macrophages contribute to inflammation by releasing pro-inflammatory cytokines, such as TNF-α, IL-1β, and IL-6, as well as by producing reactive oxygen species and tissue-degrading enzymes, collectively promoting synovial inflammation, cartilage degradation, and joint damage in RA [21,27]. The various cytokines produced by T, B cells and macrophages are represented in **Figure 1.2**.

Apart from the immune cells, fibroblast like synoviocytes (FLS) undergo aberrant proliferation triggered by receptor activator of nuclear factor kappa B ligand (RANKL) interaction, activating nuclear factor kappa B (NF-κB) pathways in response to inflammatory cytokines. Macrophages release RANKL upon activation by TNF-α and IL-1β, IL-6 and IL-17 crucial for osteoclastogenesis. Subsequently, RANKL binds osteoclast precursors, initiating NF-κB cascades, promoting differentiation into mature osteoclasts, ultimately contributing to bone resorption [21,28]. Besides their pro-inflammatory functions, cytokines such as TNF-α and IL-1 stimulate chondrocytes, the key cells regulating cartilage homeostasis, to secrete matrix-

degrading enzymes [11,29]. This enzymatic activity results in the degradation of vital cartilage components like collagen and proteoglycans, leading to structural deterioration and functional impairment of cartilage. Consequently, this mechanism significantly contributes to the progressive cartilage degradation observed in RA, ultimately worsening joint damage and impairing joint function [29].
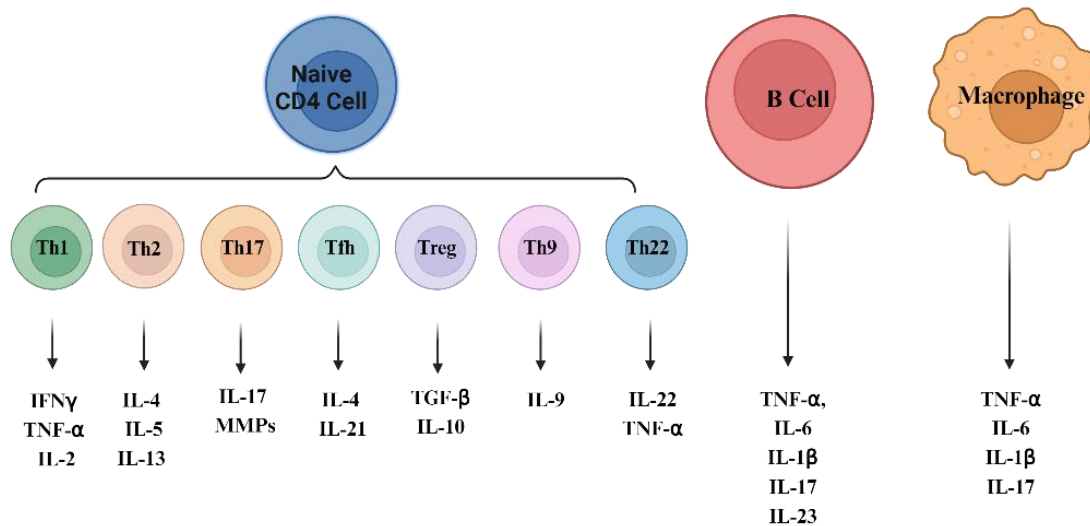
Figure 1.2. Various cytokines produced by T cells, B cells and macrophages

Other immune cells like mast cells, DCs, and natural killer (NK) cells contribute to RA pathogenesis [11]. Mast cells in synovium promote inflammation in RA, although their exact role is still unclear [30]. Elevated activated DCs in RA synovial tissues act as antigen-presenting cells, initiating and sustaining joint inflammation. Research studies has been conducted using tolerogenic DCs (tolDCs) to suppress autoimmune responses in RA therapy [31,32]. CD56+ NK cells overexpress in inflamed joints, producing higher IFN-γ levels, highlighting their pathogenic role in RA [33].Thus, understanding these immune cell dynamics is crucial for advancing RA therapeutic regimen. The intricate mechanisms underlying the pathogenesis of RA are visually depicted in **Figure 1.3**.
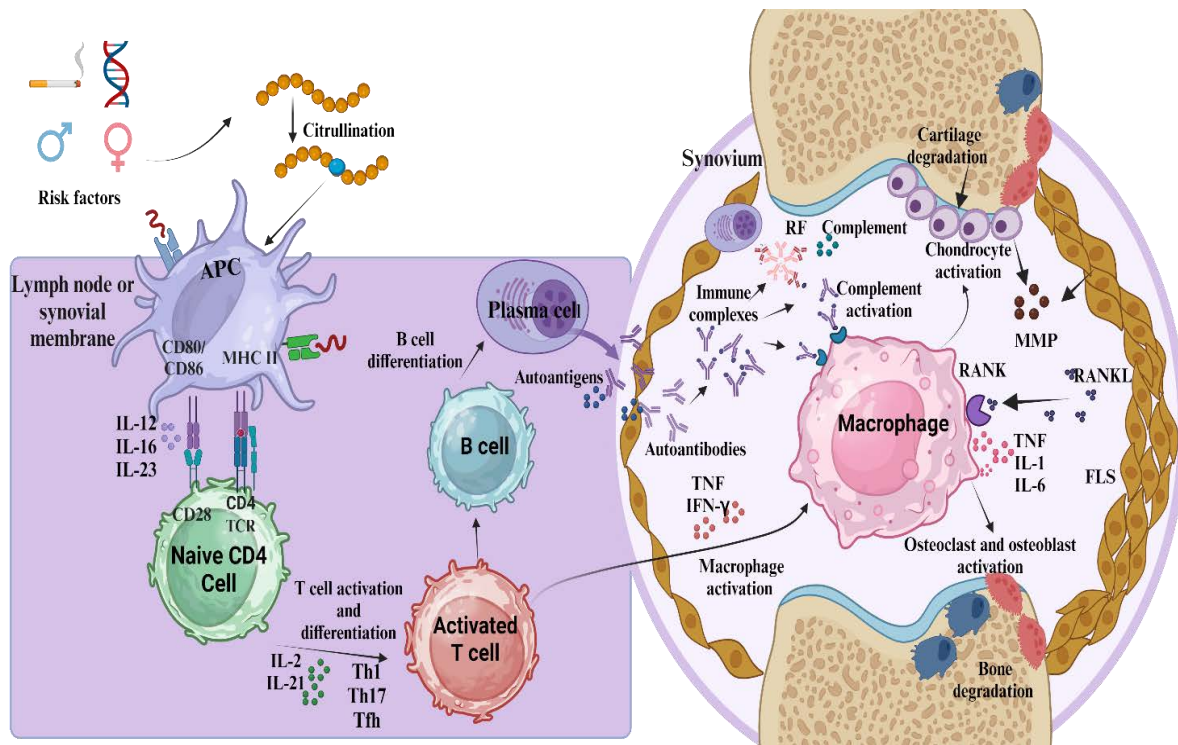
Figure 1.3. Mechanism underlying the pathogenesis of RA

1.2.2. Signaling pathway involved in RA

The progression of RA involves intricate dysregulation across pivotal signaling pathways such as Janus kinase-signal transducer and activator of transcription (JAK-STAT), mitogen-activated protein kinase (MAPK), NF-κB, phosphoinositide 3-kinase-Akt (PI3K-Akt), and Wingless/Integrated (Wnt) pathways (**Figure 1.4**) [10,17]. The mechanistic insights into the intricate molecular pathways underlying RA pathogenesis presents potential targets for therapeutic intervention aimed at attenuating disease progression.

1.2.2.1. JAK/STAT pathway

In RA, the activation of the JAK/STAT pathway is triggered by diverse cytokines, including interleukins and interferons. Upon cytokine binding to their receptors, JAK kinases are activated, leading to the phosphorylation of STAT proteins. Phosphorylated STAT molecules then form dimers and translocate to the nucleus, where they regulate the expression of genes involved in inflammation, immune response, and tissue degradation. This intricate signaling cascade involves the JAK family, including JAK1, JAK2, JAK3, and TyK2, collaborating with the STAT family, which encompasses STAT1-4, STAT5A, STAT5B, and STAT6, thereby contributing to the multifaceted cellular processes and regulatory mechanisms underlying RA pathogenesis [10,34].
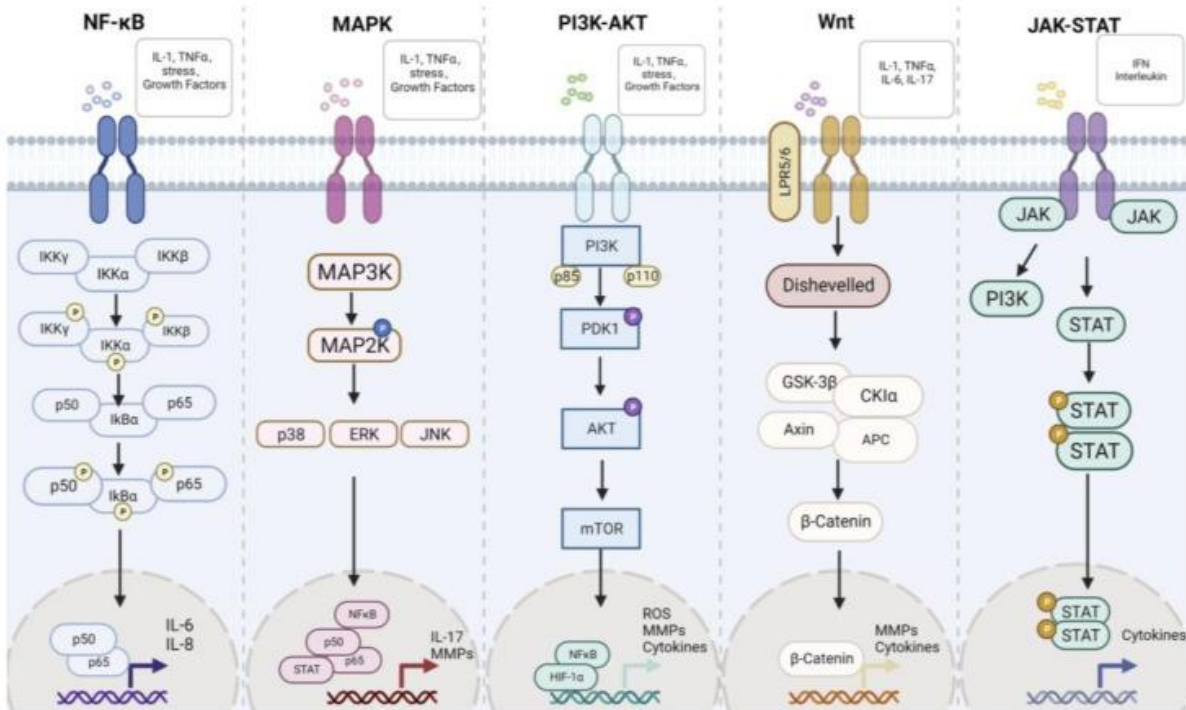
Figure 1.4. Various signaling pathways involved in the RA pathogenesis [17]

1.2.2.2. MAPK pathway

Activation of MAPKs, namely p38 kinases, extracellular signal-regulated kinase (ERK), and c-Jun N-terminal kinase (JNK), leads to the transcription and activation of genes encoding inflammatory cytokines such as TNF-α, IL-1, and IL-6. These cytokines further perpetuate inflammation, contributing to synovial hyperplasia, cartilage degradation, and joint damage characteristic of RA [10]. ERK1 and ERK2 responds to various stimuli like ischemia, oxidative stress, and neurotransmitters, playing a pivotal role in cell differentiation, proliferation, and survival regulation [35]. In RA, JNK MAPKs primarily contribute to cartilage degradation through MMP activation [36]. Conversely, P38, a prominent member of the MAPK family, is closely associated with the inflammatory response in RA, emphasizing its significance in the disease process [37].

1.2.2.3. PI3K-Akt pathway

The PI3K-Akt pathway is pivotal in RA, that orchestrates cellular functions such as proliferation, metabolism, angiogenesis, and cell survival in response to various stimuli, thereby contributing to the inflammatory cascade.

The PI3K dimer consists of a regulatory subunit (p85) and a catalytic subunit (p110), forming an active enzyme complex. Activation of PI3K can occur through conformational changes within the dimer or by the interaction with Ras and p110. Upon activation, PI3K phosphorylates phosphatidylinositol lipids, converting phosphatidylinositol 4,5-bisphosphate

(PIP2) to phosphatidylinositol 3,4,5-trisphosphate (PIP3), thereby initiating downstream signaling cascades [38]. Akt (protein kinase B) pathway is activated by PIP3 and 3-phosphoinositide-dependent protein kinase-1 (PDK1). PIP3 recruits Akt and PDK1 to the plasma membrane, where PDK1 phosphorylates Akt, leading to its activation. Once activated, Akt phosphorylates various downstream targets, including lipid kinases, transcription factors, regulators of small G proteins, and metabolic enzymes, among others. This cascade of events influences cell survival, proliferation, and metabolism, thereby playing a role in the development of RA [17,39].

1.2.2.4. Wnt pathway

The Wnt signaling pathway, that is crucial in cancer and embryonic development, is also involved in RA, impacting synovial inflammation and bone metabolism regulation. RA involves two Wnt pathways: canonical (beta-catenin-dependent) and non-canonical (beta-catenin-independent). In the canonical Wnt pathway, Wnt binds to Frizzled (Fz) family receptors and co-receptors, low-density lipoprotein receptor-related protein 5 (LRP5) and low-density lipoprotein receptor-related protein 6 (LRP6). This interaction activates cytoplasmic proteins including glycogen synthase kinase 3 beta (GSK-3β), axin 1, adenomatous polyposis coli (APC), disheveled (DVL1), casein kinase 1 alpha 1 (CSNK1A1), and beta-catenin, initiating signal transduction.

In the noncanonical Wnt pathway, Wnt5A initiates signaling through DVL1, leading to intracellular Ca^{+2} release and activation of calcium/calmodulin-dependent protein kinase II alpha (CAMK2A) and protein kinase C (PKC). This cascade promotes NF-κB transcription factor activation, inducing the expression of proinflammatory cytokines/chemokines. Additionally, noncanonical signaling *via* the planar cell polarity pathway, involved in DVL1 activation of Rac and Rho proteins, regulation of cytoskeleton organization and cell differentiation/growth [40].

1.2.2.5. NF-κB signaling pathway

NF-κB comprises dimeric transcription factors such as RelA (p65), c-Rel, RelB, NF-κB1 (p50), and NF-κB2, with the most common form in activated cells being the RelA/NF-κB1 (p65/p50) heterodimer, often referred to as the 'classic' NF-κB [41]. NF-κB activation triggers transcription of TNF-α, IL-1β, and IL-6, contributing to chronic inflammation in affected joints. Stimuli like reactive oxygen species (ROS) activate IκB kinase (IKK), resulting in the proteasomal degradation of IκB and the subsequent release of NF-κB. NF-κB translocate to the nucleus, and regulates the inflammation-related gene expression. The signal-induced

processing of IκB involves a series of steps including phosphorylation, ubiquitination, and proteasomal degradation, governed by three major multiprotein complexes: IKK, IκB ubiquitin ligase, and the 26S proteasome [17,42].

1.2.2.6. Other transcriptional factors

Several transcription factors, including, Nuclear factor erythroid 2-related factor 2 (Nrf2), hypoxia-inducible factor (HIF), and Activator Protein-1 (AP-1) play crucial roles in the pathogenesis of RA. Nrf2 is involved in cellular defense mechanisms against oxidative stress, which is implicated in RA pathology. HIF regulates responses to hypoxia, a condition observed in the inflamed synovium of RA patients. AP-1 controls the expression of genes involved in inflammation and tissue destruction in RA. Collectively, dysregulation of these transcription factors contributes to the complex pathogenesis of RA [10,43].

1.3. Diagnosis

The primary objective for the management of RA is early diagnosis and prompt initiation of treatment to mitigate the risk of irreversible structural damage to the joints [4]. The American College of Rheumatology (ACR) and the European League Against Rheumatism (EULAR) have established the guidelines and criteria for diagnosis, treatment recommendations, and management strategies for RA. The aim of these guidelines is to improve patient outcomes and quality of life based on set of variables including risk factors, assessing the extent and type of joint involvement, and symptom duration [32].Employing differential diagnosis to confirm RA possess a significant challenge and thus underscores the importance of preferred medical strategy for distinguishing it from osteoarthritis and other related conditions. The pattern of synovitis varies across different rheumatic conditions. RA typically manifests symmetrically, affecting larger joints such as the proximal interphalangeal (PIP) and metacarpophalangeal (MP) joints. Conversely, in ankylosing spondylitis, synovitis is limited to smaller joints, while in psoriatic arthropathy, it develops asymmetrically, including involvement of the toes. Moreover, inflammation tends to be more severe in RA compared to osteoarthritis, which typically exhibits asymmetric inflammation, primarily affecting the distal interphalangeal (DIP) joints [1,21].

In RA, the diagnostic biomarkers encompass serological indicators like RF and ACPAs antibodies, indicative of an autoimmune condition. Inflammatory biomarkers such as C-Reactive Protein (CRP) and Erythrocyte Sedimentation Rate (ESR) provide insights into disease activity [44]. Imaging techniques such as X-rays and magnetic resonance imaging (MRI), and ultrasonography elucidate structural joint changes indicative of RA progression

[45]. Synovial fluid biomarkers, notably cytokines and chemokines, reflect the intensity of synovial inflammation. MMPs and tissue inhibitors are pivotal in the joint remodeling processes associated with RA pathogenesis [46]. Genome-wide association studies (GWAS) employing single nucleotide polymorphism (SNP) analysis have identified numerous genes linked to RA susceptibility, particularly those encoding immunoregulatory factors . Over 35 risk loci have been identified as potential biomarkers for RA. Notably, the HLA (human leukocyte antigen)-DR4 and shared epitope (SE) alleles at the HLA–DRB1 locus collectively contribute to approximately 15% of the overall RA disease risk [47]. These diverse biomarkers collectively facilitate accurate diagnosis, ongoing disease monitoring, and tailored therapeutic interventions in RA management.

1.4. Treatment and management of RA

NSAIDs are employed in RA treatment during the acute phase response to alleviate pain by mitigating inflammation. These drugs act by inhibiting inflammatory mediators generated in the cyclooxygenase (COX) pathway [48]. NSAIDs can be categorized based on their mechanisms into nonselective NSAIDs (e.g., ibuprofen, naproxen), semi-selective NSAIDs (e.g., diclofenac, indomethacin), and coxibs (e.g. rofecoxib, celecoxib). These drugs have varying side effects and toxicities, including cardiovascular, gastrointestinal, renal, and hematologic effects [41].

On the other hand, glucocorticoids, such as prednisone, methylprednisolone, prednisolone, hydrocortisone, dexamethasone, and triamcinolone, exhibit higher potency and efficacy in treating RA compared to NSAIDs, owing to their intricate anti-inflammatory and immunosuppressive mechanisms. However, they entail a greater risk of side effects compared to NSAIDs and are therefore recommended for short-term use at low doses in RA management [4]. The anti-inflammatory effects of glucocorticoids stem from their binding to glucocorticoid receptors, forming a receptor-glucocorticoid complex. This complex interacts with DNA sequences called glucocorticoid response elements, modifying the transcription of various genes involved in the inflammatory response [42].

Disease-modifying antirheumatic drugs (DMARDs) constitute an important group of medications employed to induce remission by suppressing autoimmune activity and delaying or preventing joint degeneration [43]. These drugs possess both immunosuppressive and immunomodulatory properties and are classified into conventional synthetic DMARDs (sDMARDs), targeted synthetic DMARDs (tsDMARDs) or small molecule DMRDS, and biologic DMARDs (bDMARDs) [34,40]. Conventional sDMARDs encompass a diverse range

of medications, including methotrexate, leflunomide, hydroxychloroquine, and sulfasalazine that are commonly used for treatments of RA [44]. Additionally, gold salts such as aurothioglucose, auranofin, and gold sodium thiomalate, along with D-penicillamine, are frequently employed. Other compounds such as azathioprine, cyclosporine, minocycline, and cyclophosphamide are prescribed in RA when the disease is particularly aggressive or refractory to other treatments [45]. tsDMARDs function by selectively inhibiting signaling pathways involved in the inflammatory cascade of RA. These include JAK inhibitors (e.g., tofacitinib) [46], JAK-STAT pathway inhibitors (eg. peficitinib, baricitinib and ruxolitinib), spleen tyrosine kinase bruton's tyrosine kinase pathway (SYK-BTK) inhibitors (evobrutinib, spebrutinib and tirabrutinib), and those that interfere with NF-κB pathway (eg. Iguratimod) [40,47]. bDMARDs exhibit high specificity, targeting precise pathways within the immune system. Examples of bDMARDs include TNF inhibitors (e.g., adalimumab, etanercept), interleukin inhibitors (e.g., tocilizumab, sarilumab), and B-cell inhibitors (e.g., rituximab). Conventional sDMARDs are commonly employed as first-line therapy and administered promptly after the diagnosis of the disease to mitigate disease progression. If first-line therapy is not well tolerated or if it proves to be ineffective, bDMARDs or tsDMARDs are recommended [40,48].

1.5. Combination delivery used in RA treatment (Preclinical and Clinical studies)

In 2022, EULAR has issued 11 treatment recommendations for RA treatment. It consists of three phases. In Phase I, newly diagnosed RA patients are advised to initiate DMARDs promptly, with methotrexate being the preferred initial treatment, and if not well tolerated, alternatives such as leflunomide, sulfasalazine, or sDMARDs are prescribed. The combination with short-term glucocorticoids is well recommended to instant pain relief. If the target is not achieved within 6 months, phase II entails switching to another synthetic DMARD, alone or in combination, with the addition of glucocorticoid. In case of high disease activity bDMARDs or JAK inhibitors are recommended based on risk assessment. Phase III involves considering alternative TNF-α antagonists, cell-targeted therapy, or cytokine antagonists if the desired clinical outcomes aren't met within the specified time frame [49,50].

Taking into account the factors outlined in treatment guidelines by EULAR, the co-delivery or combination of DMARDS with glucocorticoids or other NSAIDs has proven effective in managing RA [51,52]. By targeting various pathways implicated in RA's pathogenesis, combination therapy offers a more efficacious approach to treatment. This strategy aids in retarding joint degradation, negating long-term toxicity, lowering drug resistance, increasing

targeting ability, and enhancing the overall quality of life for patients [53]. A study highlighted the benefits of using glucocorticoids as adjunctive therapy with DMARDs. The findings emphasized that medium to high doses of glucocorticoids represented a valuable approach in bridging the temporal interval between the initiation of DMARDs and the manifestation of their therapeutic effects [54]. Similarly, in a randomized trial conducted by Calgüneri, M.et al. 1999 found that the triple combination of methotrexate, sulfasalazine, and hydroxychloroquine produced superior efficacy compared to both monotherapy and two-drug combinations [55]. Also, DMARDs in conjunction with corticosteroids or anti-TNF drugs present an appealing choice as components of combination therapy for early RA, given their ability to swiftly alleviate RA [56].

The primary goal in RA treatment is to achieve complete remission and to explore the potential use of combination therapies particularly in patients with very early RA. There have been various strategies utilized in the administration of combination therapy, each presenting its own set of advantages and disadvantages. These strategies encompass both the step-up and step-down approaches. In the step-up approach, treatment typically begins with monotherapy, reserving combination therapy for patients who do not respond adequately to monotherapy. Conversely, the step-down approach involves initiating aggressive treatment initially to effectively suppress inflammation in RA. Once the disease is controlled, medications with higher toxicity profiles are gradually withdrawn, and treatment is continued with the agent offering the optimal balance between efficacy and toxicity [57]. Administering aggressive combination therapy, even for a short duration during the early established phase of RA, leads to long-term advantages compared to monotherapy. According to a report by Verschueren, P. et. al 2008, in a routine clinical practice, employing a step-down treatment strategy for early RA proves to be more effective than a step-up approach [58]. Similarly in a two-year COBRA-Slim regimen (15 mg methotrexate weekly and a weekly step-down scheme of oral prednisone) for RA treatment achieved the most favorable balance between effectiveness and safety, regardless of the patients' prognosis [59]. Despite this, step-up therapy involving methotrexate, sulfasalazine, and cyclosporin has proven to be effective in treating RA, with 40% of patients receiving combination therapy and 21% receiving monotherapy after three years [60]. Apart from these various combinations of therapeutic agents in clinical trials for their effectiveness in RA treatment are summarized in **Table 1.1** [61]**.** Although there are promising findings, the current evidence is not enough to support the use of combination DMARD therapy for all early RA patients due to concerns about potential adverse effects. Therefore, it is essential to evaluate

the effectiveness of different treatment strategies, particularly among those with early RA, to determine the most suitable initial approach [57].

Additionally, various research endeavors have explored the impact of the combination of different agents either conventional or encapsulated within nanocarriers, in both *in-vitro* and *in-vivo* model, aiming for enhanced treatment efficacy, with reduced side effects [53]. In addition to synthetic agents, natural products have demonstrated anti-inflammatory and immunomodulatory effects by targeting multiple pathways involved in RA [62,63]. The most reported natural products for RA treatment include andrographolide, boswellic acid, curcumin, quercetin, resveratrol, rutin, tanshinone IIA etc. These agents, whether used alone or in combination with synthetic DMARDs, have been extensively studied in the literature for the treatment of RA [64]. According to the 21.CFR guidelines, combining two or more drugs in a single dosage form is referred to as fixed combination products. This approach is specially considered in cases where the combination of drugs can enhance the safety or effectiveness of the primary active component and minimize the risk of abuse of primary component. **Table 1.2** summarizes the various combination of drugs and their effectiveness in *in-vivo* animal models for treatment of RA.

Table 1.1. Clinical trials of various combinations *via* oral route for RA treatment

Trail No	Name of the combination drugs	Study Title	Phase
NCT00252668	Etanercept and Methotrexate	Study Evaluating the Combination of Etanercept and Methotrexate in Rheumatoid Arthritis Subjects	Phase 4
NCT00579878	Leflunomide, Methotrexate, Sulfasalazine and Hydroxychloroquine	Triple III Comparison of Leflunomide Alone *Vs* Two DMARD Combinations in the Treatment of Rheumatoid Arthritis	Phase 3
NCT00154336	Imatinib and Methotrexate	A Study of Imatinib 400 mg Once Daily in Combination with Methotrexate in the Treatment of Rheumatoid Arthritis.	Phase 2
NCT01987479	Tocilizumab and Methotrexate	A Study on Safety and Efficacy of Tocilizumab (RoActemra/Actemra) Alone or in Combination with Non-Biologic Antirheumatics in Participants with Rheumatoid Arthritis	Phase 3
NCT00579644	Minocycline and Methotrexate	Treatment of Early RA: Minocycline in Combination with Methotrexate *Vs* Methotrexate Alone	Phase 3
NCT02076659	F8IL10 and Methotrexate	Combination Therapy of F8IL10 and Methotrexate in Rheumatoid Arthritis Patients	Phase 3
NCT02046603	Tocilizumab, Oral Corticosteroids and Methotrexate	A Study of Tocilizumab (RoActemra/Actemra) in Monotherapy or in Combination with Methotrexate or Other Non-Biologic DMARDs in Participants with Active Rheumatoid Arthritis and an Inadequate Response to Current Non-Biologic DMARD Therapy or the First Anti-TNF Biologic Agent	Phase 3

NCT00908089	Trexan, Salazopyrin, Oxiklorin, prednisolone and infliximab	TNF-blocking Therapy in Combination with Disease-modifying Antirheumatic Drugs in Early Rheumatoid Arthritis	Phase 4
NCT01941095	Azathioprine, Chloroquine, Hydroxychloroquine, Leflunomide, Sulfasalazine, Tocilizumab	A Study of Subcutaneous Tocilizumab as Monotherapy and/or in Combination with Non-Biologic Disease Modifying Anti-Rheumatic Drugs (DMARDs) in Participants with Rheumatoid Arthritis	Phase 3
NCT00420927	Adalimumab and Methotrexate	Study of the Optimal Protocol for Methotrexate and Adalimumab Combination Therapy in Early Rheumatoid Arthritis	Phase 4
NCT01521923	Certolizumab Pegol + Methotrexate	A Multi-center, Randomized, Double-blind, Placebo-controlled Study to Evaluate the Efficacy and Safety of Certolizumab Pegol in Combination with Methotrexate in the Treatment of Disease Modifying Antirheumatic Drugs (DMARD)-naïve Adults with Early Active Rheumatoid Arthritis	Phase 3
NCT02222493	PF-06438179, Infliximab and Methotrexate	A Study of PF-06438179 (Infliximab-Pfizer) and Infliximab in Combination with Methotrexate in Subjects with Active Rheumatoid Arthritis (REFLECTIONS B537-02).	Phase 3
NCT00913432	Masitinib and Methotrexate	Masitinib in Combination with Methotrexate, in Treatment of Patients with Active Rheumatoid Arthritis	Phase 2
NCT00485589	Ocrelizumab and Methotrexate	A Study of Ocrelizumab in Combination with Methotrexate in Patients with Rheumatoid Arthritis Who Are Naive to Methotrexate (FILM)	Phase 3
NCT04230213	PF-06410293 and adalimumab	A Comparative Study Between PF-06410293 and Humira® in Combination with Methotrexate in Participants with Active Rheumatoid Arthritis	Phase 3

NCT04227366	BCD- 89 and Methotrexate	Study of the Efficacy and Safety of BCD-089 in Combination with Methotrexate in Patients with Active Rheumatoid Arthritis (SOLAR)	Phase 3
NCT02762838	BCD-055, Remicade® and Methotrexate	Comparative Clinical Trial of Efficacy and Safety of BCD-055 and Remicade® in Combination with Methotrexate in Patients with Active Rheumatoid Arthritis	Phase 3
NCT02886728	Filgotinib and Methotrexate	Filgotinib Alone and in Combination with Methotrexate in Adults with Moderately to Severely Active Rheumatoid Arthritis Who Are Naive to Methotrexate Therapy (FINCH 3)	Phase 3
NCT01283399	Rituximab in Combination with Methotrexate	An Observational Study of Rituximab in Combination with Methotrexate in Participants with Active Rheumatoid Arthritis	Phase 3
NCT00162279	Abatacept and Etanercept	The Study of Abatacept in Combination with Etanercept	Phase 2
NCT01384461	RoActemra/Actemra and methotrexate	An Observational Study of RoActemra/Actemra (Tocilizumab) in Combination with Methotrexate in Patients with Rheumatoid Arthritis (ACTIVATE)	Phase 3

Table 1.2. Summary of reported combination delivery and their effectiveness in *in-vivo* animal studies for treatment of RA

S. No	Combination of drugs	Route	Dosage form	Target	Therapeutic outcomes	Ref
1	Diclofenac and Teriflunomide	Transdermal	Patch	Diclofenac inhibits Cyclooxygenase (COX) and prostaglandin. Teriflunomide inhibits dihydroorotate dehydrogenase enzyme (DHODH)	Compound patch presented better anti-inflammatory and analgesic effects in the study of adjuvant arthritis in rats and acetic acid-induced writhing syndrome in mice.	[65]
2	Teriflunomide and Ketoprofen	Transdermal	Patch	Ketoprofen inhibits COX and prostaglandin. Teriflunomide inhibits DHODH	The skin permeation and dynamic activity of combination patch was increased compared with teriflunomide and ketoprofen individual patches.	[66]
3	Teriflunomide and Methotrexate	Subcutaneous delivery	Hydroxy-apatite nanoparticles	Methotrexate inhibits purine and pyrimidine synthesis. Teriflunomide inhibits DHODH	In arthritic assessment study, it showed a significant reduction in ankle diameter, arthritis score and less hepatotoxicity with the combination of nanoparticles	[67]
4	Teriflunomide and Lornoxicam	Intra-articular	Topical patch	Teriflunomide inhibits DHODH. Lornoxicam inhibits COX enzymes	The combination showed enhanced inhibition of swelling on primary arthritis of bilateral hind paws	[68]

5	Methotrexate and Teriflunomide	Intra-articular	Hyaluronate-functionalized hydroxyapatite nanoparticles	Methotrexate inhibits purine and pyrimidine synthesis. Teriflunomide inhibits DHODH	Greater accumulation of nanoparticles in the synovial region. The nanoparticles exhibited synergistic effect in the treatment of RA.	[69]
6	Loxoprofen and Tofacitinib	Transdermal	Photothermal Microneedles	Tofacitinib targets TNF-α, IL-1β, iNOS, JAK2, JAK3, and STAT3. Lornoxicam inhibits COX enzyme	Carrageenan induced arthritis rat model exhibited reduced joint swelling, muscle atrophy, and cartilage destruction with the combination patch. Also, downregulated the mRNA expression levels of proinflammatory cytokines	[70]
7	Pioglitazone and Prednisolone	Oral	Suspension	Pioglitazone acts on Peroxisome proliferator-activated receptor-gamma (PPAR-γ). Prednisolone inhibits inflammatory cytokines by binding to glucocorticoid receptor	Treatment with combination in the arthritic animals showed significant reductions in paw volume, and tibiotarsal joint thickness Also, it significantly decreased plasma levels of TNF-α and IL-6.	[71]
8	Naproxen, Prednisolone and Hydroxyc hloroquine	Oral	Solution	Naproxen acts on COX pathway. Prednisolone acts by binding to glucocorticoid receptor.	The combination effectively ameliorated the CFA-induced arthritis and were more effective in combination as compared to individual drug therapy	[72]

				Hydroxychloroquine acts by inhibiting toll-like receptor (TLR) signaling pathways.		
9	Aceclofenac and Methotrexate	Topical and Intravenous	Nano particles	Methotrexate inhibits purine and pyrimidine synthesis. Aceclofenac inhibits COX enzyme	In *in-vivo* RA experimental model demonstrated that the combination regains the structure of paw bones and joints is similar to the market formulations.	[73]
10	Tofacitinib and Dexamethasone	Subcutaneous	Solution	Dexamethasone inhibits NF-κB and AP1 transcription factor signaling. Tofacitinib inhibits the phosphorylation and activation of Janus kinase	Combined effect has shown good inhibitory effect on RA paw edema compared to monotherapy.	[74]
11	Leflunomide and Methotrexate	Oral	Suspension	Methotrexate inhibits purine and pyrimidine synthesis. Leflunomide inhibits DHODH	COX 2 and VEGF levels decreased with combination therapy compared to individual drug treatment. It also improved the ankle circumference and clinical scores compared to monotherapy	[75]
12	Bucillamine and Etanercept	Oral and Subcutaneous	Suspension	Bucillamine acts by NF-κB inhibition. Etanercept is a anti-TNF biologic agent.	Bucillamine and etanercept combination treatment also reduced serum IL-1α and granulocyte macrophage colony-stimulating	[76]

				factor and tended to reduce serum IL-1β and IL-6 levels.	
13	Curcumin and Diclofenac Sodium	Oral	Nanoparticles	Curcumin acts by inhibiting NF-κB. Diclofenac inhibits COX and prostaglandin.	Combination of curcumin and diclofenac nanoparticle resulted in reduced pain and inflammatory cytokines (TNF-α, IL-6, and IL-1β)	[77]
14	Methotrexate and Quercetin	Intra peritoneal	Suspension	Quercetin acts by inhibiting COX-2, NF-κB and AP-1 activity. Methotrexate inhibits purine and pyrimidine synthesis.	Combination of quercetin exhibited enhancement in anti-inflammatory activity and reduced toxicity associated with methotrexate in CFA induced rat	[64]
15	Curcumin and Methotrexate	Intra peritoneal	Suspension	Curcumin acts by inhibiting NF-κB. Methotrexate inhibits purine and pyrimidine synthesis	The combination curcumin reduces the hepatotoxicity induced by methotrexate in CFA induced rat	[78]
16	Prednisolone and Curcumin	Intravenous	Human Serum Albumin Nanoparticle	Curcumin acts by inhibiting NF-κB. Prednisolone acts by binding to glucocorticoid receptor	The combination exhibited a synergistic activity in CFA induced rat compared to single drug nanoparticles and free drug	[79]

Table 1.1. underscores the importance of utilizing oral combination delivery consisting of dual therapy, triple therapy, or quadruple therapy for RA treatment. These includes sDMARDs (leflunomide, methotrexate, hydroxychloroquine, sulfasalazine, minocycline, azathioprine), tsDMARDs (filgotinib, abatacept, etanercept), bDMARDs (tocilizumab, infliximab, adalimumab, certolizumab, ocrelizumab, rituximab), tyrosine kinase inhibitors (imatinib, masitinib) and corticosteroids (prednisolone). All of these combinations are at various phases of clinical trials, with the combinations of trexan, salazopyrin, oxiklorin, prednisolone, and infliximab (NCT00908089) and adalimumab and methotrexate (NCT00420927) currently in phase 4 trials.

The data depicted in **Table 1.2.** illustrates documented combinations of various synthetic molecules utilized in the treatment of RA as reported in the literature. These include sDMARDs (methotrexate, teriflunomide, hydroxychloroquine, bucillamine), tsDMARDs (tofacitinib, etanercept), NSAIDs (aceclofenac, diclofenac, ketoprofen, lornoxicam, naproxen) and glucocorticoids (prednisolone, dexamethasone). Apart from these, the combination of synthetic drugs with natural products namely curcumin and diclofenac Sodium; methotrexate and quercetin; methotrexate and curcumin; prednisolone and curcumin have also been reported. These highlights the potential efficacy of such combinations for RA treatment.

1.6. Problems associated with conventional dosage forms in RA

Various conventional formulations, including tablets, capsules, oral liquids, and parenteral preparations, play a crucial role in the therapeutic approach to RA [80]. The conventional management of RA typically involves the administration of NSAIDs, glucocorticoids, and synthetic DMARDs, either alone or in combination, with the primary goal of alleviating pain and inhibiting disease progression [1]. However, the prolonged use of NSAIDs is linked to adverse effects such as gastrointestinal bleeding, cardiovascular effects, and nephrotoxicity [81]. Similarly, extended administration of glucocorticoid agents may precipitate complications including muscle atrophy, osteoporosis, suppression of the hypothalamic-pituitary-adrenal axis, glaucoma, and diabetes [82]. Systemic adverse effects are common among synthetic DMARDs used to RA, affecting various physiological systems. These effects include hematologic abnormalities such as leukopenia and anemia, hepatotoxicity indicated by elevated liver enzymes, and pulmonary complications such as interstitial lung disease. Furthermore, potential risks include lymphomas and non-melanoma skin cancers, renal toxicity leading to impaired renal function, allergic reactions, bone marrow suppression, and an elevated susceptibility to both common and serious infections [83]. **Table 1.3** presents a

compilation of conventional medications alongside their documented adverse effects as reported on the labels of respective brands from drug products approved by the United States Food and Drug Administration (US FDA).

Table 1.3. Various adverse effects reported for conventional dosage forms by USFDA

	Drug	Dosage form	Brand	Adverse effects
NSAIDS	Ibuprofen	Tablet	Advil	GI discomfort and bleeding increase the risk of heart attack, and severe allergic reactions to people using aspirin
	Aspirin	Capsule	Vazalore	GI discomfort, allergic reactions, Reye's syndrome
	Naproxen	Tablet	Aleve	GI discomfort, increase the risk of heart attack, severe allergic reactions to people using aspirin
	Celecoxib	Capsule	Celebrex	GI discomfort, anaphylactoid reactions, increase the risk of cardiovascular risk, upper respiratory tract infection
	Meloxicam	Tablet and oral suspension	Mobic	GI discomfort, anaphylactoid Reactions, and anemia
Glucocorticoids	Prednisone	Tablets	Rayos	Fluid retention, alteration in glucose tolerance, elevation in blood pressure, increased appetite and weight gain
DMARDs	Methotrexate	Tablets	Trexal	Ulcerative stomatitis, leukopenia, nausea, and abdominal distress
	Leflunomide	Tablets	Arava	Hepatotoxicity, teratogenicity diarrhea, respiratory infection, nausea, headache, rash, abnormal liver enzymes, dyspepsia.

Oral administration of natural products presents disadvantages including inadequate systemic absorption, variability in efficacy, and a lack of specificity for RA-affected organs/tissues [84].

Additionally, due to their short half-life and inadequate concentration at the target site, natural products often require frequent dosing, which can lead to patient non-compliance. Therefore, careful monitoring of adverse effects is vital for optimizing RA therapy and ensuring patient safety [85].

In terms of drug delivery precise targeting to the afflicted joint presents a notable challenge, affecting both efficacy and systemic exposure control. To overcome these challenges associated with oral administration, research efforts require innovation in topical delivery methods. In this endeavor, the objective should be to enhance stability, refine targeting mechanisms, ensure safety, optimize drug release, and comply with regulatory standards for the efficacious treatment of RA. Topical delivery address the above challenges of conventional dosage form by presenting numerous benefits, including avoidance of hepatic metabolism, sustained drug release, dosage adaptability, and protection against gastrointestinal degradation.

1.7. Challenges in topical delivery

In recent years, there has been a surge of interest in topical drug administration due to its non-invasive nature and high patient compliance facilitated by its ease of application. Additionally, dermal delivery presents numerous benefits, including sustained drug release, dosage adaptability, reduced adverse effects, avoidance of hepatic metabolism, and protection against gastrointestinal degradation. The effectiveness of topical drug delivery depends on intricate interplays between the skin's physiological traits, intrinsic attributes of drug molecules (including size, solubility, and lipophilicity), and application techniques (such as nanotechnology, microneedle, electroporation, iontophoresis, and sonophoresis) [86,87].

The skin, as the largest organ in the human body, acts as a pivotal barrier modulating the permeability of topically applied drugs, representing roughly 15% of an adult's total body weight [88]. In topical drug delivery, the skin barrier is the initial obstacle that comprises of three layers - the epidermis, dermis, and subcutaneous hypodermis. The epidermis encompasses the non-viable *stratum corneum* and the viable epidermis, with the former forming a dense barrier due to its multiple layers of keratinocytes and lipid bilayers. The dermis, situated beneath the epidermis, is rich in fibroblasts, adipocytes, blood vessels, and skin appendages, serving as the primary site for drug absorption. Meanwhile, the hypodermis, situated below the dermis, primarily consists of loose connective tissue and adipose cells, that play a role in heat insulation and energy storage [80,89,90].

Drug absorption through the skin encompasses two main pathways: The trans epidermal route and the skin appendage route. The trans epidermal route includes the transcellular and

intercellular routes. In the transcellular route, drugs traverse the lipid membrane structure of the *stratum corneum*, hindered by hydrated keratin-filled cells, requiring a delicate hydrophilic-lipophilic balance. Conversely, in the intercellular pathway, drug molecules penetrate the dermis through the lipid matrix between keratinocytes. Capillaries in the dermis efficiently facilitate drug absorption into circulation, making the intercellular pathway the primary route. Skin appendage absorption involves drugs penetrating through hair follicles, sweat glands, and sebaceous glands. This route typically offers a faster penetration rate compared to the transepidermal route. However, the skin appendages cover a small area, making them a secondary pathway for transdermal drug absorption [80,91].

Ensuring drug delivery to the synovial tissues holds paramount importance in the treatment of RA, the effective delivery of topically applied drugs into deeper tissues is imperative for eliciting therapeutic effects by efficiently inhibiting various inflammatory pathways. The efficacy of topical or transdermal products in alleviating inflammation within joints is widely reported [92]. However, the process of transporting drugs into the deeper layers of synovial tissues following topical application to the joints remains ambiguous [68]. The intricate mechanisms governing topical drug movement may involve local enhanced delivery, possibly facilitated by the local vasculature. This mechanism generates a convective force, propelling topically applied drugs deeper into the underlying tissue before systemic distribution ensues [93].

In topical delivery, drugs can reach the synovial cavity *via* direct diffusion at the application site and systemic circulation. At the dermal level, drugs may enter local blood vessels for distribution to deeper inflamed tissues [94], with the possibility of uptake into the systemic circulation through dermal microcirculation resulting in low systemic exposure [95,96]. Topically applied drugs can exhibit a depot effect, leading to their prolonged accumulation in various skin layers such as the *stratum corneum*, epidermis, dermis, and subcutaneous fatty tissue, thereby forming a reservoir for sustained drug release into surrounding tissues [97,98]. The efficiency of this reservoir depends on the drug's properties, including solubility, protein-binding capacity, absorption, concentration, clearance, application time, and mode [99,100]. Drug movement through the skin primarily occurs through passive diffusion, driven by concentration gradients and tissue partitioning, following Fick's Law [101–103]. Topical application of NSAIDs like diclofenac, ketoprofen, methyl salicylate, and felbinac has been found to cause notably higher drug concentrations in treated knee joint tissues, including synovial fluid, compared to systemic levels or untreated sites. This suggests direct diffusion and local blood redistribution that play significant role in this effect [104,105]. Comparable

findings have been documented by Bae, J et.al 2016 for leflunomide administered topically, with concentrations 6.5 to 5.0 fold higher in the synovial fluid than at non-application sites following the use of leflunomide topical solution or patch [93].

1.8. Topical nano formulations for treatment of RA

Given the availability of various conventional methods for topical RA treatment, nanoparticles have emerged as a significant advancement in drug delivery. Topical nano carriers serve as crucial components in the delivery of drugs for RA by augmenting drug penetration through the skin barrier, primarily the *stratum corneum,* consequently enhancing localized therapeutic effectiveness. These carriers enable targeted delivery to inflamed joints, reducing systemic side effects of conventional oral medications, while also ensuring sustained drug release for prolonged therapeutic effects and enhanced patient compliance [106,107]. Moreover, they provide a versatile platform for incorporating various drugs and therapeutic agents, allowing tailored combination therapies to meet individual patient needs. Nano formulations like nanoemulsion, solid lipid nanoparticles (SLNs), niosomes, transferosomes, and ethosomes have emerged to enhance drug permeation in topical applications for RA treatment [86].

1.9. Transferosomes in drug delivery

In recent years, there has been an increase in the study of novel drug delivery systems aimed at improving efficacy, patient compliance, and therapeutic outcomes in the pharmaceutical sciences. Among these advances, transferosomes have emerged as a new lipid-based bilayered vesicular carrier technology, offering exceptional potential in topical drug administration [108]. Transferosomes, also known as ultra-deformable vesicles, differ significantly from traditional liposomal carriers because of their remarkable flexibility and elasticity [109]. The inherent deformability of transferosomes enables them to traverse the *stratum corneum,* the primary barrier of the skin, thereby facilitating enhanced penetration into the deeper layers of the epidermis. As a result, transferosomes present a promising approach for achieving more efficient and precise transdermal drug delivery by surmounting the challenges posed by the epidermal barrier [110]. The diagram illustrating the structure of transferosomes is presented in **Figure 1.5**.
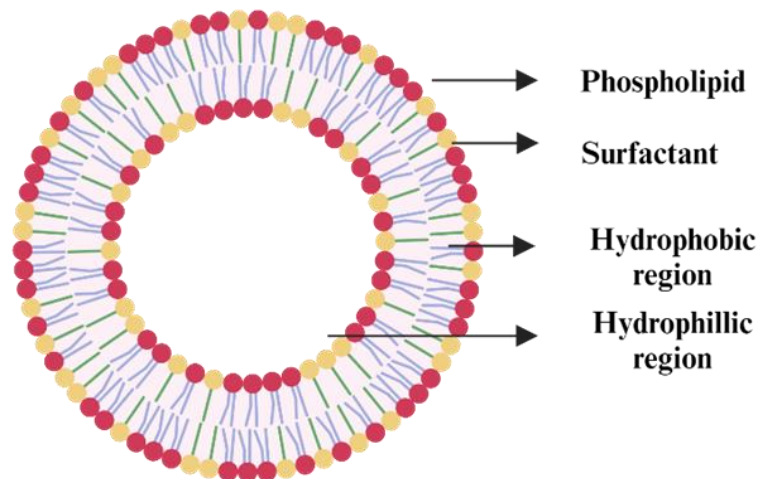
Figure 1.5. Structure of transferosomes

Transferosomes are composed of phospholipids along with edge activators such as surfactants or bile salts. Phospholipids are amphiphilic molecules characterized by a hydrophilic head group containing phosphates and a hydrophobic tail composed of both saturated and unsaturated fatty acids connected by a glycerol moiety. The phospholipid bilayer structure of transferosomes closely resembles the natural lipid bilayers found in the skin. This similarity enhances the biocompatibility of transferosomes, making them well-suited for interaction with biological systems without causing adverse effects [111]. Apart from these the surfactants have the unusual capacity to deform and squeeze through narrow pores, including the intercellular spaces of the *stratum corneum*. The specifics of the composition, along with examples, are provided in **Table 1.4**. Moreover, the composition of transferosomes can be tailored to accommodate a diverse array of drugs, encompassing hydrophilic, lipophilic, and amphiphilic substances. This versatility renders transferosomes an attractive foundation for formulating an extensive array of in pharmaceutical industry [112].

Several hypotheses have been proposed to understand the permeability of lipid vesicles across skin membranes. The potential mechanism for drug transportation through the skin *via* vesicular systems is depicted in **Figure 1.6**. These include free drug mechanism, where the drug penetration into skin independently after vesicle release, focusing on drug properties rather than vesicle composition; penetration enhancing properties of vesicles, in which the presence of surfactant demonstrate to improve transdermal drug delivery by reducing skin permeability barriers and interacting with the stratum corneum; fusion with the *stratum corneum* where the lipid vesicle merge with the *stratum corneum* or attach to surface *via* adsorption leading to enhancement in penetration of active moieties; intact vesicle penetration

into the epidermal layer; and penetration of vesicles through the hair follicle (trans appendageal route) [113].

Table 1.4. Composition of transferosomes

Component	Examples	Function
Phospholipids	Soya phosphatidyl choline, Dimyristoly phosphatidylcholine (DMPC), Hydrogenated soya phosphatidylcholine (HSPC), and other modified phospholipids	A crucial element for the formation of a lipid bilayer vesicle
Surfactants	Span 60, Span 80, Tween 60, Tween 80 and sodium cholate, sodium deoxycholate, stearyl amine	Membrane softening agent provides elasticity and deformity
Hydrating media	Aqueous media or pH buffer	The formation of self-assembled vesicles occurs in hydrating media

Transferosomes, with their hydrophilic surface, respond to dermal hydration gradients, propelling vesicles through skin channels as noninvasive drug carriers. Their high membrane flexibility and skin permeability enable simultaneous modulation of skin components. Under local hydration stresses, transferosomal vesicles deform and autonomously navigate through pores significantly smaller than their average diameter in a self-regulated manner. Hydrostatic pressure differences facilitate their passage through the *stratum corneum*, driven by hydrotaxis and governed by elastomechanics principles [113].

Transferosomes have demonstrated effectiveness in delivering topical treatments for RA, as evidenced by reported studies. Zeb A. et.al 2017 reported that the topical delivery of methotrexate using ultra deformable vesicles, that exhibited potential *in-vivo* activity in CFA model. It reduced the paw volume and pro-inflammatory cytokine expression in paw tissue compared to other conventional liposomes and free drug loaded gel [114]. Similarly Taymouri, et.al 2021 reported that transferosomal gel exhibited more paw edema inhibition compared to imatinib gel in CFA induced rat model [115]. In addition to synthetic molecules, natural product-loaded transferosomes have been also assessed for their efficacy in treating RA. Sarwa et al. 2015 demonstrated that in carrageenan-induced rats, the transferosomal gel containing capsaicin exhibited superior inhibitory activity compared to Thermagel (a marketed

formulation) [116]. Similarly, Sana et.al 2021 reported that curcumin transferosomal gel increased the antiarthritic activity in CFA induced mice compared to conventional gel. Also it reduced the TNF-α and IL-6 levels in paw tissue [117].
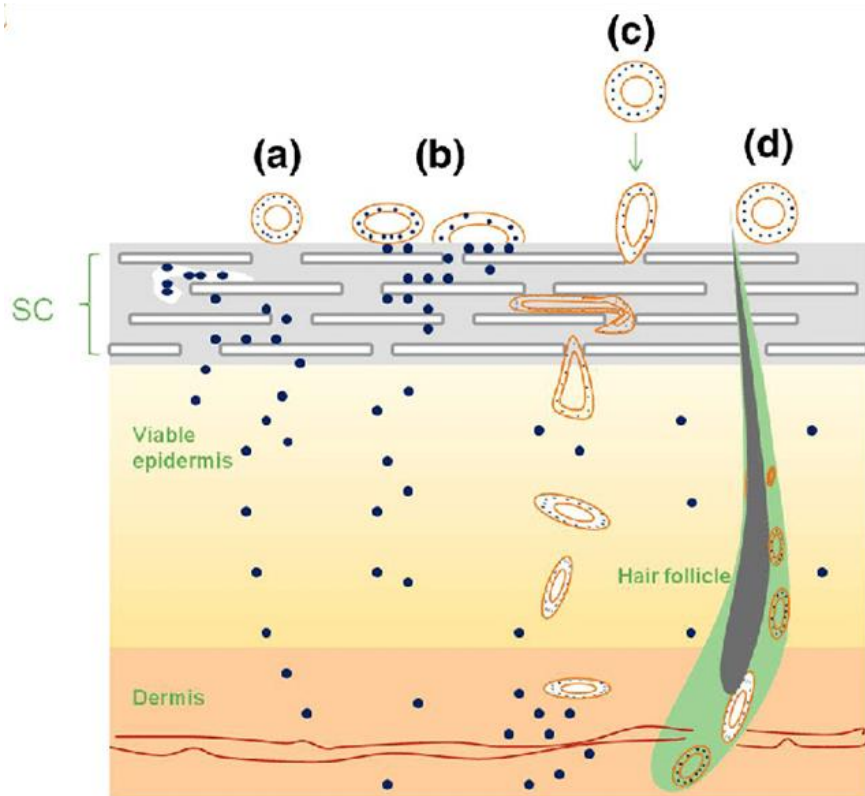
Figure 1.6. Mechanism of permeation of lipid vesicles, a) the penetration enhancing mechanism; b) vesicle adsorption to and/or fusion with the *stratum corneum*; c) intact vesicular penetration mechanism (intact vesicles penetration into intact skin); d) trans-appendageal penetration [118].

Based on the data and existing literature, the transferosomes represent a promising platform for topical drug delivery, offering a versatile and effective means of overcoming the skin's barrier properties for the effective treatment of RA.

1.10. Conclusion

Management of RA effectively requires a combination therapy to address its diverse underlying pathways. Following EULAR guidelines, initiating DMARD treatment upon diagnosis aims to slow disease progression. Drug combinations are tailored based on disease severity, typically involving sDMARDs with glucocorticoids or bDMARDs/tsDMARDs. Clinical studies have explored both step-down and step-up approaches, employing double or triple treatments for

long-term RA management. Researchers have explored the combination of DMARDs with corticosteroids or NSAIDs in both *in-vitro* and *in-vivo* models to investigate their potential synergistic effects in managing RA. In addition to this, natural products have been reported to demonstrate anti-arthritic activity either as monotherapy or in combination with synthetic molecules. Systemic administration of medications is often linked to numerous adverse effects and hence delivering combination therapies *via* topical routes presents challenges, as it can mitigate systemic effects by exerting localized action, as elucidated by Fick's law of diffusion. Topical nano carriers such as transferosomes incorporating combination drugs represent a promising strategy for delivering medications into deeper tissues, such as the synovium while reducing systemic effects.

Chapter 1

References

1. Bullock, J., Rizvi, S. A. A., Saleh, A. M., Ahmed, S. S., Do, D. P., Ansari, R. A., & Ahmed, J. (2019). Rheumatoid arthritis: A brief overview of the treatment. *Medical Principles and Practice*, *27*(6), 501–507.

2. Pitzalis, C. (2014). Pathogenesis of rheumatoid arthritis: From systemic autoimmunity to localised joint disease. *Drug Discovery Today*, *19*(8), 1152–1154.

3. Karlson, E. W., & Deane, K. (2012). Environmental and gene-environment interactions and risk of rheumatoid arthritis. *Rheumatic Diseases Clinics of North America*, *38*(2), 426.

4. Black RJ, Cross M, Haile LM, Culbreth GT, Steinmetz JD, Hagins H, Kopec JA, Brooks PM, Woolf AD, Ong KL, Kopansky-Giles DR (2023). Global, regional, and national burden of rheumatoid arthritis, 1990–2020, and projections to 2050: A systematic analysis of the Global Burden of Disease Study 2021. *The Lancet Rheumatology*, *5*(10), e594-e610.

5. Sparks, J. A. (2019). Rheumatoid Arthritis. *Annals of Internal Medicine*, *170*(1), ITC1–15.

6. Ferrari, M., Onuoha, S. C., & Pitzalis, C. (2016). Going with the flow: Harnessing the power of the vasculature for targeted therapy in rheumatoid arthritis. *Drug Discovery Today*, *21*(1), 172–179.

7. Janakiraman, K., Krishnaswami, V., Rajendran, V., Natesan, S., & Kandasamy, R. (2018). Novel nano therapeutic materials for the effective treatment of rheumatoid arthritis-recent insights. *Materials Today Communications*, *17*, 200–213.

8. Choy, E. (2012). Understanding the dynamics: Pathways involved in the pathogenesis of rheumatoid arthritis. *Rheumatology*, *51*, v3-11.

9. Smolen, J. S., & Steiner, G. (2003). Therapeutic strategies for rheumatoid arthritis. *Nature Reviews. Drug Discovery*, *2*(6), 473–488.

10. Ding, Q., Hu, W., Wang, R., Yang, Q., Zhu, M., Li, M., Cai, J., Rose, P., Mao, J., & Zhu, Y. Z. (2023). Signaling pathways in rheumatoid arthritis: Implications for targeted therapy. *Signal Transduction and Targeted Therapy*, *8*(1), 68.

11. Yap, H.-Y., Zi-Yi Tee, S., Mei-Theng Wong, M., Chow, S.-K., Peh, S.-C., & Teow, S.-Y. (2018). Pathogenic role of immune cells in rheumatoid arthritis: Implications in clinical treatment and biomarker development. *Cells*, *7*(10), 161.

12. Dhule, K. D., & Nandgude, T. D. (2023). Lipid nano-system based topical drug delivery for management of rheumatoid arthritis: An overview. *Advanced Pharmaceutical Bulletin*, *13*(4), 663–677.

13. Jang, S., Kwon, E. J., & Lee, J. J. (2022). Rheumatoid arthritis: Pathogenic roles of diverse immune cells. *International Journal of Molecular Sciences*, *23*(2), 905.

14. Yamada, H. (2022). Adaptive immunity in the joint of rheumatoid arthritis. *Immunological Medicine*, *45*(1), 1–11.

15. Chimenti, M. S., Triggianese, P., Conigliaro, P., Candi, E., Melino, G., & Perricone, R. (2015). The interplay between inflammation and metabolism in rheumatoid arthritis. *Cell Death & Disease*, *6*(9), e1887.

16. Malmström, V., Trollmo, C., & Klareskog, L. (2004). The additive role of innate and adaptive immunity in the development of arthritis. *The American Journal of the Medical Sciences*, *327*(4), 196–201.

17. Zhu, M., Ding, Q., Lin, Z., Fu, R., Zhang, F., Li, Z., Zhang, M., & Zhu, Y. (2023). New Targets and strategies for rheumatoid arthritis: From signal transduction to epigenetic aspect. *Biomolecules*, *13*(5), 766.

18. Huang, Q., & Anandasabapathy, N. (2020). Ex vivo assessment of in vivo DC-targeted antibodies in pre-clinical models. *Methods in Enzymology*, *632*, 417–430.

19. Iwasaki, A., & Medzhitov, R. (2010). Regulation of adaptive immunity by the innate immune system. *Science*, *327*(5963), 295.

20. Blüml, S., Sahin, E., Saferding, V., Goncalves-Alves, E., Hainzl, E., Niederreiter, B., Hladik, A., Lohmeyer, T., Brunner, J.S., Bonelli, M. & Koenders, M.I. (2015). Phosphatase and tensin homolog (PTEN) in antigen-presenting cells controls Th17-mediated autoimmune arthritis. *Arthritis Research & Therapy*, *17*(1), 230.

21. Aletaha, D., & Smolen, J. S. (2018). Diagnosis and management of rheumatoid arthritis: A review. *JAMA*, *320*(13), 1360–1372.

22. Luo, P., Wang, P., Xu, J., Hou, W., Xu, P., Xu, K., & Liu, L. (2022). Immunomodulatory role of T helper cells in rheumatoid arthritis : A comprehensive research review. *Bone & Joint Research*, *11*(7), 426–438.

23. Wu, F., Gao, J., Kang, J., Wang, X., Niu, Q., Liu, J., & Zhang, L. (2021). B cells in rheumatoid arthritis : Pathogenic mechanisms and treatment prospects. *Frontiers in Immunology*, *12*, 750753.

24. Silverman, G. J., & Carson, D. A. (2003). Roles of B cells in rheumatoid arthritis. *Arthritis Research & Therapy*, *5*, 1-6.

25. Jovanovic, D. V., Di Battista, J. A., Martel-Pelletier, J., Jolicoeur, F. C., He, Y., Zhang, M., Mineau, F., & Pelletier, J.-P. (1998). IL-17 Stimulates the production and expression of proinflammatory cytokines, IL-β and TNF-α, by Human macrophages. *The Journal of Immunology*, *160*(7), 3513–3521.

26. Parameswaran, N., & Patial, S. (2010). Tumor necrosis factor-α signaling in macrophages. *Critical Reviews in Eukaryotic Gene Expression*, *20*(2), 103.

27. Kinne, R. W., Bräuer, R., Stuhlmüller, B., Palombo-Kinne, E., & Burmester, G. R. (2000). Macrophages in rheumatoid arthritis. *Arthritis Research*, *2*, 1-14.

28. Kondo, N., Kuroda, T., & Kobayashi, D. (2021). Cytokine networks in the pathogenesis of rheumatoid arthritis. *International Journal of Molecular Sciences*, *22*(20), 10922.

29. Tseng, C. C., Chen, Y. J., Chang, W. A., Tsai, W. C., Ou, T. T., Wu, C. C., Sung, W. Y., Yen, J. H., & Kuo, P. L. (2020). Dual role of chondrocytes in rheumatoid arthritis: The chicken and the egg. *International Journal of Molecular Sciences*, *21*(3), 1071.

30. Rivellese, F., Nerviani, A., Rossi, F. W., Marone, G., Matucci-Cerinic, M., de Paulis, A., & Pitzalis, C. (2017). Mast cells in rheumatoid arthritis: Friends or foes? *Autoimmunity Reviews*, *16*(6), 557–563.

31. Yu, M. B., & Langridge, W. H. R. (2017). The function of myeloid dendritic cells in rheumatoid arthritis. *Rheumatology International*, *37*(7), 1043–1051.

32. Hilkens, C. M. U., & Isaacs, J. D. (2013). Tolerogenic dendritic cell therapy for rheumatoid arthritis: Where are we now? *Clinical and Experimental Immunology*, *172*(2), 148–157.

33. Shegarfi, H., Naddafi, F., & Mirshafiey, A. (2012). Natural killer cells and their role in rheumatoid arthritis: Friend or foe? *The Scientific World Journal*, *2012*, 491974.

34. Banerjee, S., Biehl, A., Gadina, M., Hasni, S., & Schwartz, D. M. (2017). JAK–STAT Signaling as a target for inflammatory and autoimmune diseases: Current and future prospects. *Drugs 2017 77:5*, *77*(5), 521–546.

35. Ohori, M. (2008). ERK inhibitors as a potential new therapy for rheumatoid arthritis. *Drug News & Perspectives*, *21*(5), 245–250.

36. Kanai, T., Kondo, N., Okada, M., Sano, H., Okumura, G., Kijima, Y., Ogose, A., Kawashima, H., & Endo, N. (2020). The JNK pathway represents a novel target in the treatment of rheumatoid arthritis through the suppression of MMP-3. *Journal of Orthopaedic Surgery and Research*, *15*, 87.

37. Lemaire, M., Froment, C., Boutros, R., Mondesert, O., Nebreda, A. R., Monsarrat, B., & Ducommun, B. (2021). Stress relief techniques: P38 MAPK determines the balance of cell cycle and apoptosis pathways. *Biomolecules 11*(10), 1444.

38. Ito, Y., Hart, J. R., & Vogt, P. K. (2018). Isoform-specific activities of the regulatory subunits of phosphatidylinositol 3-kinases potentially novel therapeutic targets. *Expert Opinion on Therapeutic Targets*, *22*(10), 877.

39. Manning, B. D., & Toker, A. (2017). AKT/PKB signaling: Navigating the network. *Cell*,

169(3), 405.

40. Rabelo, F. de S., da Mota, L. M. H., Lima, R. A. C., Lima, F. A. C., Barra, G. B., de Carvalho, J. F., & Amato, A. A. (2010). The Wnt signaling pathway and rheumatoid arthritis. *Autoimmunity Reviews*, *9*(4), 207–210.

41. Makarov, S. S. (2001). NF-kappaB in rheumatoid arthritis: A pivotal regulator of inflammation, hyperplasia, and tissue destruction. *Arthritis Research*, *3*(4), 206.

42. Karin, M., & Ben-Neriah, Y. (2000). Phosphorylation meets ubiquitination: The control of NF-κB activity. *Annual Review of Immunology*, *18*, 621–663.

43. Le Rossignol, S., Ketheesan, N., & Haleagrahara, N. (2018). Redox-sensitive transcription factors play a significant role in the development of rheumatoid arthritis. *International Reviews of Immunology*, *37*(3), 129–143.

44. Atzeni, F., Talotta, R., Masala, I. F., Bongiovanni, S., Boccassini, L., & Sarzi-Puttini, P. (2021). Biomarkers in rheumatoid arthritis. *Cureus*, *13*(5), e15063.

45. Kgoebane, K., Ally, M. M. T. M., Duim-Beytell, M. C., & Suleman, F. E. (2018). The role of imaging in rheumatoid arthritis. *SA Journal of Radiology*, *22*(1), 1316.

46. Meehan, R. T., Regan, E. A., Hoffman, E. D., Wolf, M. L., Gill, M. T., Crooks, J. L., Parmar, P. J., Scheuring, R. A., Hill, J. C., Pacheco, K. A., & Knight, V. (2021). Synovial fluid cytokines, chemokines and mmp levels in osteoarthritis patients with knee pain display a profile similar to many rheumatoid arthritis patients. *Journal of Clinical Medicine*, *10*(21), 5027.

47. Ruyssen-Witrand, A., Constantin, A., Cambon-Thomsen, A., & Thomsen, M. (2012). New insights into the genetics of immune responses in rheumatoid arthritis. *Tissue Antigens*, *80*(2), 105–118.

48. Ben Mrid, R., Bouchmaa, N., Ainani, H., El Fatimy, R., Malka, G., & Mazini, L. (2022). Anti-rheumatoid drugs advancements: New insights into the molecular treatment of rheumatoid arthritis. *Biomedicine & Pharmacotherapy,151*, 113126.

49. Köhler, B. M., Günther, J., Kaudewitz, D., & Lorenz, H. M. (2019). Current therapeutic options in the treatment of rheumatoid arthritis. *Journal of Clinical Medicine*, *8*(7), 938.

50. Smolen, J.S., Landewé, R.B., Bergstra, S.A., Kerschbaumer, A., Sepriano, A., Aletaha, D., Caporali, R., Edwards, C.J., Hyrich, K.L., Pope, J.E. & De Souza, S. (2023). EULAR recommendations for the management of rheumatoid arthritis with synthetic and biological disease-modifying antirheumatic drugs: 2022 update. *Annals of the Rheumatic Diseases*, *82*(1), 3–18.

51. Combe, B., Landewe, R., Daien, C.I., Hua, C., Aletaha, D., Álvaro-Gracia, J.M., Bakkers,

M., Brodin, N., Burmester, G.R., Codreanu, C. & Conway, R.. (2017). 2016 update of the EULAR recommendations for the management of early arthritis. *Annals of the Rheumatic Diseases*, *76*(6), 948–959.

52. Del Grossi Moura, M., Lopes, L. C., Silva, M. T., Barberato-Filho, S., Motta, R. H. L., & De Cássia Bergamaschi, C. (2018). Use of steroid and nonsteroidal anti-inflammatories in the treatment of rheumatoid arthritis: Systematic review protocol. *Medicine*, *97*(41), e12658.

53. Zhang, S., Zhang, M., Li, X., Li, G., Yang, B., Lu, X., Gao, Y., & Sun, F. (2022). Nano-based co-delivery system for treatment of rheumatoid arthritis. *Molecules 27*(18), 5973.

54. Hoes, J. N., Jacobs, J. W. G., Buttgereit, F., & Bijlsma, J. W. J. (2010). Current view of glucocorticoid co-therapy with DMARDs in rheumatoid arthritis. *Nature Reviews. Rheumatology*, *6*(12), 693–702.

55. Çalgüneri, M., Pay, S., Çalişkaner, Z., Apraş, S., Kiraz, S., Ertenli, I., & Çobankara, V. (1999). Combination therapy versus monotherapy for the treatment of patients with rheumatoid arthritis. *Clinical and Experimental Rheumatology*, *17*(6), 699–704.

56. St.Clair, E. W., Van Der Heijde, D. M. F. M., Smolen, J. S., Maini, R. N., Bathon, J. M., Emery, P., Keystone, E., Schiff, M., Kalden, J. R., Wang, B., DeWoody, K., Weiss, R., & Baker, D. (2004). Combination of infliximab and methotrexate therapy for early rheumatoid arthritis: A randomized, controlled trial. *Arthritis and Rheumatism*, *50*(11), 3432–3443.

57. Suresh, E., & Lambert, C. M. (2005). Combination treatment strategies in early rheumatoid arthritis. *Annals of the Rheumatic Diseases*, *64*(9), 1252–1256.

58. Verschueren, P., Esselens, G., & Westhovens, R. (2008). Daily practice effectiveness of a step-down treatment in comparison with a tight step-up for early rheumatoid arthritis. *Rheumatology, 47*(1), 59–64.

59. Stouten, V., Westhovens, R., Pazmino, S., De Cock, D., Van der Elst, K., Joly, J. & Verschueren, P. (2019). Effectiveness of different combinations of DMARDs and glucocorticoid bridging in early rheumatoid arthritis: Two-year results of CareRA. *Rheumatology 58*(12), 2284–2294.

60. Ferraccioli, G. F., Gremese, E., Tomietto, P., Favret, G., Damato, R., & Di Poi, E. (2002). Analysis of improvements, full responses, remission and toxicity in rheumatoid patients treated with step-up combination therapy (methotrexate, cyclosporin A, sulphasalazine) or monotherapy for three years. *Rheumatology, 41*(8), 892–898.

61. ClinicalTrials.gov.https://clinicaltrials.gov/study/NCTxxx. Acessed March 15 2024.

62. Dudics, S., Langan, D., Id, Meka, R. R., Venkatesha, S. H., Berman, B. M., Che, C.-T., & Moudgil, K. D. (2018). Natural products for the treatment of autoimmune arthritis: Their mechanisms of action, targeted delivery, and interplay with the host microbiome. International Journal of Molecular Sciences, 19, 1–21.

63. Yahfoufi, N., Alsadi, N., Jambi, M., & Matar, C. (2018). The immunomodulatory and anti-inflammatory role of polyphenols. Nutrients, 10(11), 1618.

64. Haleagrahara, N., Hodgson, K., Miranda-Hernandez, S., Hughes, S., Kulur, A. B., & Ketheesan, N. (2018). Flavonoid quercetin-methotrexate combination inhibits inflammatory mediators and matrix metalloproteinase expression, providing protection to joints in collagen-induced arthritis. Inflammopharmacology, 26(5), 1219–1232.

65. Zhang, Y., Cun, D., Kong, X., & Fang, L. (2014). Design and evaluation of a novel transdermal patch containing diclofenac and teriflunomide for rheumatoid arthritis therapy. Asian Journal of Pharmaceutical Sciences, 9(5), 251–259.

66. Liu, C., Guan, Y., Tian, Q., Shi, X., & Fang, L. (2019). Transdermal enhancement strategy of ketoprofen and teriflunomide: The effect of enhanced drug-drug intermolecular interaction by permeation enhancer on drug release of compound transdermal patch. International Journal of Pharmaceutics, 572, 118800.

67. Pandey, S., Kumar, V., Leekha, A., Rai, N., Ahmad, F. J., Verma, A. K., & Talegaonkar, S.(2018). Co-delivery of teriflunomide and methotrexate from hydroxyapatite nanoparticles for the treatment of rheumatoid arthritis: In vitro characterization, pharmacodynamic and biochemical investigations. Pharmaceutical Research, 35(11), 1–17.

68. Xi, H., Cun, D., Xiang, R., Guan, Y., Zhang, Y., Li, Y., & Fang, L. (2013). Intra-articular drug delivery from an optimized topical patch containing teriflunomide and lornoxicam for rheumatoid arthritis treatment: Does the topical patch really enhance a local treatment? Journal of Controlled Release, 169(1–2), 73–81.

69. Pandey, S., Rai, N., Mahtab, A., Mittal, D., Ahmad, F. J., Sandal, N., Neupane, Y. R., Verma, A. K., & Talegaonkar, S. (2021). Hyaluronate-functionalized hydroxyapatite nanoparticles laden with methotrexate and teriflunomide for the treatment of rheumatoid arthritis. International Journal of Biological Macromolecules, 171, 502–513.

70. Lu, Y., Xiao, T., Lai, R., Liu, Z., Luo, W., Wang, Y., Fu, S., Chai, G., Jia, J., & Xu, Y. (2023). Co-delivery of loxoprofen and tofacitinib by photothermal microneedles for rheumatoid arthritis treatment. Pharmaceutics, 15(5), 1500.

71. Suke, S. G., Negi, H., Mediratta, P. K., Banerjee, B. D., & Sharma, K. K. (2013). Anti-

arthritic and anti-inflammatory activity of combined pioglitazone and prednisolone on adjuvant-induced arthritis. European Journal of Pharmacology, 718(1–3), 57–62.

72. Akhtar, M. F., Zubair, S., Saleem, A., Alsharif, K. F., & Abdel-Daim, M. M. (2021). Comparison of individual and combination treatments with naproxen, prednisolone and hydroxychloroquine to treat Complete Freund's Adjuvant induced arthritis. Inflammopharmacology, 29(6), 1719–1731

73. Negi, S., Tandel, N., Garg, N. K., Sharma, P., Kumar, R., Sharma, P., Kumar, R., Saini, S., Sharma, A., & Tyagi, R. K. (2024). Co-delivery of aceclofenac and methotrexate nanoparticles presents an effective treatment for rheumatoid arthritis. International Journal of Nanomedicine, 19, 2149–2177.

74. Yu, R., Song, D., DuBois, D. C., Almon, R. R., & Jusko, W. J. (2019). Modeling combined anti-inflammatory effects of dexamethasone and tofacitinib in arthritic rats. The AAPS Journal, 21(5), 93.

75. Bilasy, S. E., Essawy, S. S., Mandour, M. F., Ali, E. A. I., & Zaitone, S. A. (2015). Myelosuppressive and hepatotoxic potential of leflunomide and methotrexate combination in a rat model of rheumatoid arthritis. Pharmacological Reports, 67(1), 102–114.

76. Setoguchi, C., Tsuji, F., Katsuta, O., Okamoto, M., & Aono, H. (2010). Combined effects of bucillamine and etanercept on a rat type II collagen-induced arthritis model. Modern Rheumatology, 20(4), 381–388.

77. Boarescu, I., Pop, R. M., Boarescu, P. M., Bocșan, I. C., Gheban, D., Râjnoveanu, R. M., Râjnoveanu, A., Bulboacă, A. E., Buzoianu, A. D., & Bolboacă, S. D. (2022). Anti-inflammatory and analgesic effects of curcumin nanoparticles associated with diclofenac sodium in experimental acute inflammation. International Journal of Molecular Sciences, 23(19), 11731.

78. Banji, D., Pinnapureddy, J., Banji, O. J. F., Saidulu, A., & Hayath, M. S. (2011). Synergistic activity of curcumin with methotrexate in ameliorating Freund's Complete Adjuvant induced arthritis with reduced hepatotoxicity in experimental animals. European Journal of Pharmacology, 668(1–2), 293–298.

79. Yan, F., Li, H., Zhong, Z., Zhou, M., Lin, Y., Tang, C., & Li, C. (2019). Co-delivery of prednisolone and curcumin in human serum albumin nanoparticles for effective treatment of rheumatoid arthritis. International Journal of Nanomedicine,14,9113–9125.

80. Zhang, Y., Gao, Z., Chao, S., Lu, W., & Zhang, P. (2022). Transdermal delivery of inflammatory factors regulated drugs for rheumatoid arthritis. Drug Delivery, 29(1), 1934–1950.

81. Wongrakpanich, S., Wongrakpanich, A., Melhado, K., & Rangaswami, J. (2018). A comprehensive review of non-steroidal anti-inflammatory drug use in the elderly. Aging and Disease, 9(1), 150.

82. Schäcke, H., Döcke, W. D., & Asadullah, K. (2002). Mechanisms involved in the side effects of glucocorticoids. Pharmacology and Therapeutics, 96(1), 23–43.

83. Benjamin O, Goyal A, Lappin SL. Disease modifying anti-rheumatic drugs (DMARD). StatPearls Publishing; 2018. https://www.ncbi.nlm.nih.gov/books/NBK507863/. Updated 2019 Jan 6. Accessed May 30, 2024.

84. Press, N. J., Joly, E., & Ertl, P. (2019). Natural product drug delivery: A special challenge? Progress in Medicinal Chemistry, 58, 157–187.

85. Pirmardvand Chegini, S., Varshosaz, J., & Taymouri, S. (2018). Recent approaches for targeted drug delivery in rheumatoid arthritis diagnosis and treatment. Artificial Cells, Nanomedicine, and Biotechnology, 46(2), 502–514.

86. Anita, C., Munira, M., Mural, Q., & Shaily, L. (2021). Topical nanocarriers for management of Rheumatoid Arthritis: A review. Biomedicine & Pharmacotherapy, 141, 11880.

87. Kalluri, H., & Banga, A. K. (2011). Transdermal delivery of proteins. AAPS PharmSciTech, 12(1), 431–441.

88. Dąbrowska, A. K., Spano, F., Derler, S., Adlhart, C., Spencer, N. D., & Rossi, R. M. (2018). The relationship between skin function, barrier properties, and body-dependent factors. Skin Research and Technology, 24(2), 165–174.

89. Andrews, S. N., Jeong, E., & Prausnitz, M. R. (2013). Transdermal delivery of molecules is limited by full epidermis, not just stratum corneum. Pharmaceutical Research, 30(4), 1099–1109.

90. Katz, S. I., Gilchrest, B. A., Paller, A. S., & Leffell, D. J. (2008). Fitzpatrick's dermatology in general medicine. K. Wolff, & L. A. Goldsmith (Eds.). New York: McGraw-Hill.

91. Kotla, N. G., Chandrasekar, B., Rooney, P., Sivaraman, G., Larrañaga, A., Krishna, K. V., Pandit, A., & Rochev, Y. (2017). Biomimetic lipid-based nanosystems for enhanced dermal delivery of drugs and bioactive agents. ACS Biomaterials Science & Engineering, 3(7), 1262–1272.

92. Day, R. O., McLachlan, A. J., Graham, G. G., & Williams, K. M. (1999). Pharmacokinetics of nonsteroidal anti-inflammatory drugs in synovial fluid. Clinical Pharmacokinetics, 36(3), 191–210.

93. Bae, J., & Park, J. W. (2016). Topical delivery of leflunomide for rheumatoid arthritis treatment: Evaluation of local tissue deposition of teriflunomide and its anti-inflammatory effects in an arthritis rat model. Drug Development and Industrial Pharmacy, 42(2), 254–262.

94. Scheuplein, R. J. (1965). Mechanism of percutaneous adsorption. I. Routes of penetration and the influence of solubility. The Journal of Investigative Dermatology, 45(5), 334–346.

95. Altman, R., Bosch, B., Brune, K., Patrignani, P., & Young, C. (2015). Advances in NSAID development: Evolution of diclofenac products using pharmaceutical technology. Drugs, 75(8), 877.

96. Singh, P., & Roberts, M. S. (1994). Skin permeability and local tissue concentrations of nonsteroidal anti-inflammatory drugs after topical application. Journal of Pharmacology and Experimental Therapeutics, 268(1), 144–151.

97. Clijsen, R., Baeyens, J. P., Barel, A. O., & Clarys, P. (2015). In vivo determination of the diclofenac skin reservoir: Comparison between passive, occlusive, and iontophoretic application. Drug Design, Development and Therapy, 9, 840.

98. Roberts, M. S., & Cross, S. E. (1999). A physiological pharmacokinetic model for solute disposition in tissues below a topical below a topical application site. Pharmaceutical Research, 16(9), 1392–1398.

99. Roberts MS, Cross SE, A. Y. (2005). The skin reservoir for topically applied solutes. In Bronaugh RL, Maibach H (Eds.), Percutaneous Absorption:Drugs, Cosmetics, Mechanisms, Methods. (pp. pp249-270). CRC Press.

100. Roberts, M. S., Cross, S. E., & Anissimov, Y. G. (2004). Factors affecting the formation of a skin reservoir for topically applied solutes. Skin Pharmacology and Physiology, 17(1), 3–16.

101. Flynn, G. L., Yalkowsky, S. H., & Roseman, T. J. (1974). Mass transport phenomena and models: theoretical concepts. Journal of Pharmaceutical Sciences, 63(4), 479–510.

102. Brown, M. B., Martin, G. P., Jones, S. A., & Akomeah, F. K. (2006). Dermal and transdermal drug delivery systems: current and future prospects. *Drug Delivery*, *13*(3), 175–187.

103. Hagen, M., & Baker, M. (2017). Skin penetration and tissue permeation after topical administration of diclofenac. *Current Medical Research and Opinion*, *33*(9),1623–1634.

104. Mills, P. C., Magnusson, B. M., & Cross, S. E. (2005). Penetration of a topically applied nonsteroidal anti-inflammatory drug into local tissues and synovial fluid of dogs. *American Journal of Veterinary Research*, *66*(7), 1128–1132.

105. Shinkai, N., Korenaga, K., Mizu, H., & Yamauchi, H. (2008). Intra-articular penetration of ketoprofen and analgesic effects after topical patch application in rats. *Journal of Controlled Release, 131*(2), 107–112.

106. Haroutiunian, S., Drennan, D. A., & Lipman, A. G. (2010). Topical NSAID therapy for musculoskeletal pain. *Pain Medicine*, *11*(4), 535–549.

107. Herndon, C. M. (2012). Topical delivery of nonsteroidal anti-inflammatory drugs for osteoarthritis. *Journal of Pain & Palliative Care Pharmacotherapy*, *26*(1), 18–23.

108. Matharoo, N., Mohd, H., & Michniak-Kohn, B. (2024). Transferosomes as a transdermal drug delivery system: Dermal kinetics and recent developments. *Wiley Interdisciplinary Reviews. Nanomedicine and Nanobiotechnology*, *16*(1), e1918.

109. Chacko, I. A., Ghate, V. M., Dsouza, L., & Lewis, S. A. (2020). Lipid vesicles: A versatile drug delivery platform for dermal and transdermal applications. *Colloids and Surfaces B: Biointerfaces*, *195*, 111262.

110. Miatmoko, A., Ayunin, Q., & Soeratri, W. (2021). Ultradeformable vesicles: Concepts and applications relating to the delivery of skin cosmetics.*12*(10), 739–756.

111. Van Hoogevest, P., & Fahr, A. (2019). Phospholipids in cosmetic carriers. In *Nanocosmetics: From Ideas to Products* (pp. 95–140). Springer International Publishing.

112. Khan, I., Needham, R., Yousaf, S., Houacine, C., Islam, Y., Bnyan, R., Sadozai, S. K., Elrayess, M. A., & Elhissi, A. (2021). Impact of phospholipids, surfactants and cholesterol selection on the performance of transfersomes vesicles using medical nebulizers for pulmonary drug delivery. *Journal of Drug Delivery Science and Technology*, *66*, 102822.

113. Ibrahim, M. M., Nair, A. B., Shehata, B. E. A. and T. M., Ibrahim, M. M., Nair, A. B., & Shehata, B. E. A. & T. M. (2017). Hydrogels and their combination with liposomes, niosomes, or transfersomes for dermal and transdermal drug delivery. In A. Catala (Eds.), *Liposomes* (1st ed., pp. pp155-186). IntechOpen.

114. Zeb, A., Qureshi, O. S., Yu, C. H., Akram, M., Kim, H. S., Kim, M. S., Kang, J. H., Majid, A., Chang, S. Y., Bae, O. N., & Kim, J. K. (2017). Enhanced anti-rheumatic activity of methotrexate-entrapped ultradeformable liposomal gel in adjuvant-induced arthritis rat model. *International Journal of Pharmaceutics*, *525*(1), 92–100.

115. Taymouri, S., Hajhashemi, V., Tabbakhian, M., & Torkashvand, M. (2021). Preparation and evaluation of imatinib loaded transfersomal gel for the treatment of rheumatoid arthritis. *Iranian Journal of Pharmaceutical Research, 20*(4), 46.

116. Sarwa, K. K., Mazumder, B., Rudrapal, M., & Verma, V. K. (2015). Potential of capsaicin-loaded transfersomes in arthritic rats. *Drug Delivery*, *22*(5), 638–646.

117. Sana, E., Zeeshan, M., Ain, Q. U., Khan, A. U., Hussain, I., Khan, S., Lepeltier, E., & Ali, H. (2021). Topical delivery of curcumin-loaded transfersomes gel ameliorated rheumatoid arthritis by inhibiting NF-κβ pathway. *Nanomedicine, 16*(10), 819–837.

118. Guo, F., Wang, J., Ma, M., Tan, F., & Li, N. (2015). Skin targeted lipid vesicles as novel nano-carrier of ketoconazole: Characterization, in vitro and in vivo evaluation. *Journal of Materials Science. Materials in Medicine*, 26(4), 1–13.

Chapter 2

Literature Review and Gaps in Existing Research

Chapter 2

2.1. Introduction

sDMARDs constitute a group of distinct compounds primarily utilized in the treatment of RA due to their ability to modify the immune system and alter the progression of the disease. sDMARDs are commonly recommended as the initial treatment for RA by various guidelines, including those from the EULAR, the French Society for Rheumatology, the Asia Pacific League of Associations for Rheumatology (APLAR), the National Institute for Health and Care Excellence, and the Brazilian Society of Rheumatology. sDMARDs are prescribed as the first-line therapy for RA and are preferred over bDMARDs and tsDMARDs due to their efficacy, safety, accessibility, and cost-effectiveness [1].

The commonly used sDMARDs includes methotrexate, leflunomide, sulfasalazine, and hydroxychloroquine. Methotrexate functions by inhibiting dihydrofolate reductase, a crucial enzyme involved in the synthesis of tetrahydrofolate necessary for cell proliferation. This disruption affects various cells, including synovial lymphocytes, ultimately resulting in immunosuppression [2]. Leflunomide inhibits mitochondrial enzyme, crucial for pyrimidine synthesis, leading to decreased production of pyrimidine nucleotides essential for DNA and RNA synthesis in activated lymphocytes [3]. Hydroxychloroquine regulates the immune response by disrupting antigen presentation and T cell activation. Additionally, it inhibits toll-like receptor signaling and decreases the production of pro-inflammatory cytokines. These actions collectively alleviate joint inflammation and mitigate pain in individuals with RA [4]. Sulfasalazine undergoes metabolism into two components: 5-aminosalicylic acid and sulfapyridine. Through this process, it exerts anti-inflammatory effects by suppressing the production of inflammatory mediators and regulating the activity of immune cells that contribute to the inflammatory response [5].

Methotrexate has emerged as the most frequently prescribed medication, either used alone or in combination with other drugs. For patients unable to tolerate methotrexate, leflunomide is often the next preferred treatment of choice [6]. Most studies have reported that both methotrexate and leflunomide are considered effective DMARDs, exhibiting comparable efficacy over the long term [7,8].

2.1.1. Teriflunomide (TFD)
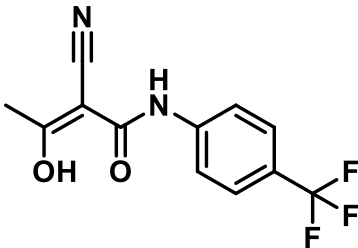
2.1.1.1. Background

Leflunomide is a sDMARDs, that received approval from the United States Food and Drug Administration (US FDA) for the treatment of RA in 1998. It is marketed under the brand name ARAVA and available in oral tablet forms of 10 mg, 20 mg, and 100 mg. Leflunomide is an isoxazole derivative, that undergoes metabolism *via* the cytochrome P450 2C19 enzyme

(CYP2C19) to produce its active metabolite, A77 1726 (formally known as TFD) through the opening of its isoxazole ring [9,10]. The active metabolite TFD exhibits the principal pharmacological effects for treating RA. The physicochemical properties of TFD are represented in **Table 2.1**.

Table 2.1. Physicochemical properties of TFD

Name	Teriflunomide (TFD)
Chemical structure	
IUPAC name	(Z)-2-cyano-3-hydroxy-N-[4-(trifluoromethyl)phenyl]but-2-enamide
Molecular formula	$C_{12}H_9F_3N_2O_2$
Molecular weight	270.21 g/mol
BCS class	Class II
pKa	3.1 at 23 ºC
Log P	2.7
Melting point	228-232 ºC
Solubility	Sparingly soluble in acetone, slightly soluble in polyethylene glycol and ethanol, very slightly soluble in isopropanol and practically insoluble in water. Solubility of TFD is low at pH values below 4.0 and increases at higher pH.

TFD has gained recognition as a DMARD owing to its immunomodulatory and anti-inflammatory characteristics. Subsequently, in 2012, TFD was approved by the US FDA, the European Union, and Canada for treating patients with relapsing forms of multiple sclerosis [10,11]. TFD is marketed under the brand name AUBAGIO® and is available as 7 mg and 14 mg oral tablets.

2.1.1.2. Mechanism of action

TFD exerts its anti-inflammatory and antiproliferative effect by selective and non-competitive inhibition of the enzyme dihydroorotate dehydrogenase (DHODH), a critical component of the *de-novo* pyrimidine synthesis pathway presents in the mitochondria. Blockage of DHODH causes T cells, B cells, and other fast-dividing cells to halt their cell cycle progression specifically in the G1 phase. This interference with DNA and RNA synthesis impedes the proliferation and function of activated lymphocytes, that are pivotal in the pathogenesis of RA [12,13] (**Figure 2.1**).
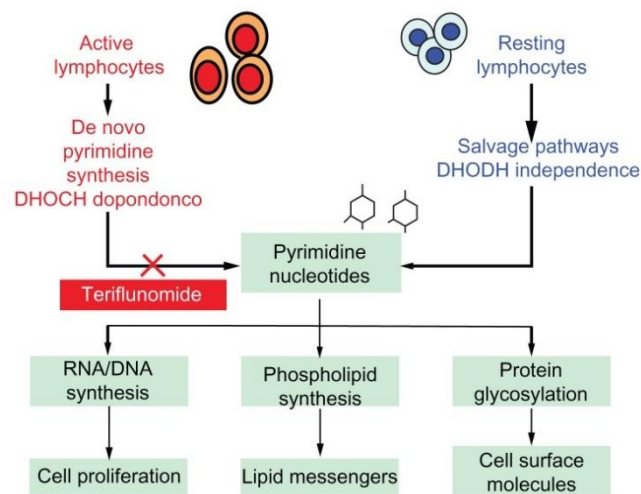
Figure 2.1. Mechanism of action of TFD [13].

TFD has been reported to inhibit tyrosine kinases, including those within the JAK/STAT pathway, playing a vital role in regulating the production of proinflammatory cytokines such as TNF-α and IL-17 [14,15]. In addition to the JAKs, TFD also impede the function of other tyrosine kinases, such as members of the 'Src family,' involved in T cell signal transduction, and epidermal growth factor receptor (EGFR) receptor tyrosine kinase [15,16].

TFD has also been demonstrated to inhibit the NF- κB pathway in T cells, a crucial process for suppressing the expression of various inflammatory cytokines [17,18]. Apart from this, it is also shown to inhibit prostaglandin E2 (PGE_2), MMP1, IL 6 in human, FLS [19], and COX-2 directly both *in-vitro* and *in-vivo* [20].

In summary, TFD mechanism of action involves inhibition of DHODH, modulation of tyrosine kinases, and suppression of pro-inflammatory cytokines, collectively contributing to its therapeutic efficacy in RA.

2.1.1.3.Adverse effects associated with oral administration of TFD

The oral administration of TFD has been demonstrated as an effective treatment for RA, but it is also linked with various adverse effects. Among these, hepatotoxicity is considered the most severe. A boxed warning highlighting the risk of hepatotoxicity has been included on the label of AUBAGIO®. It is essential to monitor liver function by assessing bilirubin and alanine aminotransferase (ALT) levels before initiating treatment with TFD, as well as periodically thereafter, to detect any signs of liver injury. TFD has been associated with teratogenicity and embryo lethality, therefore, it is contraindicated during pregnancy. Furthermore, TFD has been reported to demonstrate bone marrow effects, peripheral neuropathy, increased blood pressure, respiratory effects, hypersensitivity, and serious skin reactions. In addition to these, commonly reported adverse reactions include diarrhea, respiratory infections, nausea, headaches, rashes, abnormal liver enzymes, and dyspepsia [21].

2.2. Natural Products for the treatment of RA

Extensive research has been conducted on natural products across various health conditions, including cancer, infectious diseases, and autoimmune disorders [22]. Synthetic compounds used to treat RA have been linked to various unwanted side effects, in addition to being relatively costly. Consequently, a growing number of patients are exploring natural products as alternatives to alleviate symptoms associated with RA and related conditions, drawn by the desire to avoid these limitations [23]. Complementary and Alternative medicine (CAM) therapies are reported to be utilized by more than 36% of adults in the USA [24]. In this scenario, researchers have explored and documented the potential of natural products to play a role in both the onset and treatment of the disease. This interest also stems from their recognized antioxidant and anti-inflammatory properties. Present strategies for effectively managing RA frequently incorporate CAM approaches, which have garnered attention from both patients and the scientific community in recent years. However, understanding the mechanism of natural products is challenging to evaluate their efficacy resulting in uncertainty in both public and professional communities. Hence, elucidating the mechanism of action of natural products stands as a significant priority, as emphasized by the National Center for Complementary and Integrative Health (NCCIH) and the National Institutes of Health (NIH) in the United States [22].

Natural products exhibit anti-inflammatory and anti-arthritic properties through acting by multiple pathways. These include the suppression of activating molecules like proinflammatory cytokines and chemokines, the modulation of anti-inflammatory mediators such as interleukins (IL-4, IL-10), and regulation of the balance between T-helper type 17 (Th17) and Regulatory

T cells (Tregs) that plays a crucial role in the pathogenesis of the disease, and modulation of the interaction between the immune system and bone tissue [25,26]. These effects can be achieved by intervening in various pathways, including JAK-STAT, MAPK, NF-κB, PI3K-Akt, and Wnt pathways as mentioned in the section 1.2.2.

Dudics, S et.al 2018 reported various natural products including boswellic acids, curcumin, celastrol, harpagoside, carotenoids, flavonoid glycosides, terpenoids, quercetin, resveratrol etc. for treatment of autoimmune arthritis. Curcumin, capsaicin, piperine, quercetin, resveratrol, and tetrandrine have been investigated individually for their potential in treating RA through incorporation into nanoparticles. These investigations have involved evaluations conducted through both *in-vitro* and *in-vivo* studies [27–32]. Among various natural products, andrographolide, quercetin, resveratrol, rutin, and tanshinone IIA were selected for evaluating their synergistic anti-inflammatory activity due to their previously reported effectiveness in RA by targeting multiple pathways. The rationale for selecting these natural products stems from the comprehensive understanding of the detailed mechanisms through which each exhibits activity in RA, as described below.

2.2.1. Andrographolide (ANG)

2.2.1.1. Background
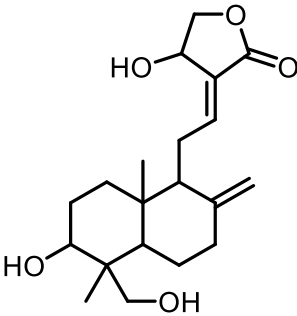
ANG is obtained from the whole plant of *Andrographis paniculata*, belonging to the family Acanthaceae. It is a bioactive diterpene lactone that demonstrates notable anti-inflammatory and immunomodulatory properties, offering potential therapeutic benefits [33]. The physicochemical properties of ANG are represented in **Table 2.2**.

2.2.1.2. Mechanism of action

ANG exhibits significant anti-inflammatory properties in RA by targeting various pathways. It is reported to effectively reduce the production of key pro-inflammatory cytokines such as TNF-α and IL-6, pivotal in the inflammatory process [34]. Moreover, ANG inhibits the activation of NF-κB and STAT3 by modulating the expression of SOCS1 and SOCS3 signaling pathways, leading to the downregulation of inflammatory iNOS and COX-2 gene expression [35]. Additionally, it has demonstrated inhibitory effects on FLS by promoting caspase-3 activation, elevating levels of cell cycle inhibitors p21 and p27, and reducing cyclin-dependent kinase 4 content. By limiting MMPs, ANG is reported to help in preserving joint integrity and function. Furthermore, it decreases the expression of protein arginine deiminase 4 (PAD4), which is involved in promoting neutrophil apoptosis and inhibiting neutrophil autophagy, thereby contributing to its overall therapeutic effects in rheumatoid arthritis [34].

Table 2.2. Physicochemical properties of ANG

Name	Andrographolide (ANG)
Chemical structure	
IUPAC name	(3E,4S)-3-[2-[(1R,4aS,5R,6R,8aS)-6-hydroxy-5-(hydroxymethyl)-5,8a-dimethyl-2-methylidene-3,4,4a,6,7,8-hexahydro-1H-naphthalen-1-yl]ethylidene]-4-hydroxyoxolan-2-one
Molecular formula	$C_{20}H_{30}O_5$
Molecular weight	350.4 g/mol
BCS class	Class II
pKa	13.8 (strong acidic) -2.8 (strong basic)
Log P	2.2
Melting point	235.3°C
Solubility	Slightly soluble in methanol or ethanol, very slightly soluble in chloroform, and almost insoluble in water.

2.2.2. Quercetin (QCN)
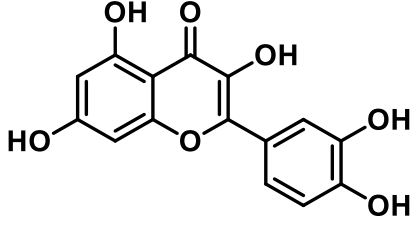
2.2.2.1. Background

QCN is a flavonoid found abundantly in various plant-based foods such as apples, berries, onions, and green leaves. Additionally, citrus fruits, grapes, tomatoes, and green tea are rich sources of this flavonoid. Herbs like parsley, capers, and dill also contain significant amounts of QCN. It is renowned for its antioxidant and anti-inflammatory properties, that are attributed to its ability to modulate signaling pathways involved in inflammation [36]. Also, QCN has been extensively studied for its safety and tolerability in humans, leading to its designation as

Generally Recognized as Safe (GRAS) by the US FDA for use as a dietary supplement in the year 2010 [37]. The physicochemical properties of QCN are represented in **Table 2.3**.

Table 2.3. Physicochemical properties of QCN

Name	Quercetin (QCN)
Chemical structure	
IUPAC name	2-(3,4-dihydroxyphenyl)-3,5,7-trihydroxychromen-4-one
Molecular formula	$C_{15}H_{10}O_7$
Molecular weight	302.23 g/mol
BCS Class	Class II
pKa	6.38 (acidic) -4 (basic)
Log P	1.5
Melting point	316 °C
Solubility	Very soluble in ether, methanol; soluble in ethanol, acetone, pyridine, acetic acid Soluble in alcohol and glacial acetic acid; insoluble in water

2.2.2.2. Mechanism of action

QCN has been documented to show promise in autoimmune diseases by modulating various signaling pathways, including those associated with inflammation and the regulation of immune response [38]. QCN has demonstrated anti-arthritic activity through its immune-regulatory effects, as well as its anti-inflammatory and bone-protective mechanisms [39].

Studies have demonstrated that QCN inhibits the differentiation of TH17 cells, implicated in RA pathogenesis and joint inflammation. Moreover, it promotes regulatory T cells (Tregs) differentiation, that suppresses immune reactions and sustains immune tolerance. By balancing TH17 cells and Tregs, QCN mitigates inflammation and autoimmune responses in RA, potentially through restraining NLRP3 inflammasome activation and activating HO-1-

mediated anti-inflammatory pathways, thus offering therapeutic potential for managing RA [40]. The anti-inflammatory activity of QCN is attributed to its ability to decrease the levels of pro-inflammatory cytokines while increasing anti-inflammatory cytokines by regulating various signaling pathways such as NF-κB, adenosine deaminase, MAPK signaling pathways and GSK-3β [39]. In addition to this, QCN exhibits bone-protective effects by inhibiting MMPs, RANKL, COX-2, and PGE$_2$ production [39,41]. Moreover, its antioxidative activity is manifested through the Nrf2/HO-1 signaling pathway, which helps to alleviate synovial inflammation [39].

2.2.3. Resveratrol (RES)

2.2.3.1. Background
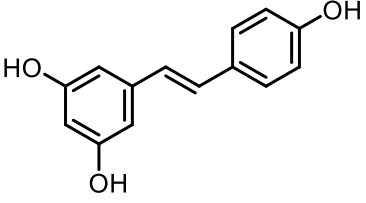
RES, is a natural polyphenolic stilbenoid compound, that was initially isolated from *Veratrum grandiflorum* belonging to the family Melanthiaceae. It occurs in various sources like berries, seeds, and in over 70 plant species [42]. The physicochemical properties of RES are represented in **Table 2.4**.

2.2.3.2. Mechanism of action

RES is reported to suppress the TNF-α triggered PI3/Akt signaling pathway in FLS, leading to the inhibition of IL-1β and MMP3 production [43]. RES activates sirtuin 1 (SIRT1), a member of the sirtuin family of proteins involved in various cellular processes. By activating SIRT1, RES assists in regulating inflammation, oxidative stress, and immune responses associated with RA pathogenesis, achieved in part by downregulating NF-κB and MMP1/MMP13. RES boosts the production of mitochondrial reactive oxygen species (MTROS), lowers the concentrations of autophagic and oxidative stress proteins (Beclin1, LC3A/B, MnSOD), and triggers apoptosis in FLS by modulating the mitochondrial membrane potential. RES exhibits the ability to hinder the adhesion of T cells to chondrocytes mediated through TNF-β, by suppressing the AHR receptor, consequently decreasing the production of CYP1A1. Consequently, this dual action leads to a reduction in the quantity and functionality of Th17 cells in the draining lymph nodes [44]. Additionally, RES inhibits monocyte differentiation by blocking the PMA-induced phosphorylation and nuclear translocation of PU.1 [45].

Table 2.4. Physicochemical properties of RES

Name	Resveratrol (RES)
Chemical structure	
IUPAC name	5-[(E)-2-(4-hydroxyphenyl)ethenyl]benzene-1,3-diol
Molecular formula	$C_{14}H_{12}O_3$
Molecular weight	228.24 g/mol
BCS Class	Class II
pKa	8.49 (strong acidic) -6.2 (strong basic)
Log P	3.10
Melting point	254°C
Solubility	Soluble in methanol, ethanol and DMSO, low water solubility

2.2.4. Rutin (RUT)

2.2.4.1. Background

RUT, is a flavanol glycoside, that is frequently found in a variety of plants, including passionflower, tea, buckwheat, apple, and citrus. It plays a crucial role as a nutritional component within these food sources. Additionally, it is known by alternative names such as rutoside, quercetin-3-rutinoside, and sophorin. Chemically, RUT consists of the flavonolic aglycone QCN combined with the disaccharide rutinose. The term "Rutin" originates from the plant *Ruta graveolens*, which belongs to the Rutaceae family [46]. The physicochemical properties of RUT are represented in **Table 2.5**.
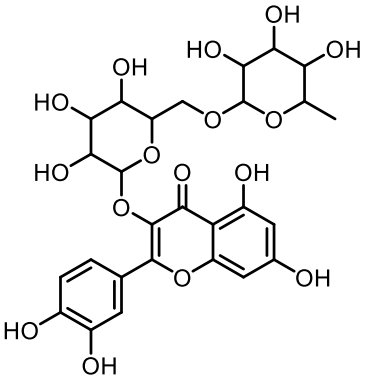
2.2.4.2. Mechanism of action

RUT hinders the development of osteoclasts initiated by RANKL in bone marrow-derived macrophages. This inhibition stems from its ability to suppress reactive oxygen species induced by RANKL, thereby resulting in reduced TNF-α levels. Furthermore, RUT also attenuates the activation of NF-κB in response to RANKL [47]. RUT has been documented to inhibit proinflammatory cytokines like TNF-α and IL-1β in adjuvant-induced RA by suppressing the

expression of NF-κB p65 protein [48]. Additionally, RUT has been noted for its ability to inhibit inflammation and extracellular matrix molecule (ECM) damage induced by advanced glycation end products (AGE) in chondrocytes. This effect is achieved by targeting proteins in the NF-κB/MAPK pathway, such as BCL-2 and TRAF-6 [49]. RUT exhibits notable effectiveness in suppressing various inflammatory markers such as TNF-α, IL-1β, IL-6, IL-13, IL-17, IFN-γ, MMPs, Ob-cadherin, RORγt, Cox-2, and iNOS. Moreover, it enhances the levels of IL-4, IL-5, IL-10, and BMP-6/7. Furthermore, RUT reduces the expression of PI3K, Akt and phosphorylated forms of STAT-1/3, IκB, NF-κB, p38, JNK, and β-catenin [50].

Table 2.5. Physicochemical properties of RUT

Name	Rutin (RUT)
Chemical structure	
IUPAC name	2-(3,4-dihydroxyphenyl)-5,7-dihydroxy-3-[(2S,3R,4S,5S,6R)-3,4,5-trihydroxy-6-[[(2R,3R,4R,5R,6S)-3,4,5-trihydroxy-6-methyloxan-2-yl]oxymethyl]oxan-2-yl]oxychromen-4-one
Molecular formula	$C_{27}H_{30}O_{16}$
Molecular weight	610.5 g/mol
BCS Class	Class II
pKa	6.37 (strong acidic) -3.7 (strong basic)
Log P	-1.3
Melting point	157°C
Solubility	Soluble in methanol, ethanol very slightly soluble in water.
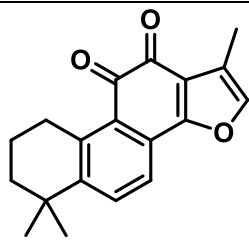
2.2.5. Tanshinone IIA (TAN)

2.2.5.1. Background

TAN is a lipophilic compound classified as a diterpene quinone. It is isolated from the dried roots and rhizomes of the Chinese herb *Salvia miltiorrhiza Bunge*, which belongs to the Lamiaceae family. It has been reported to exhibit a wide array of activities including anti-inflammatory, antiviral, antioxidant, neuroprotective, anti-atherosclerotic, antiallergic, anticonvulsant, antifatigue, anti-Alzheimer, and antiangiogenic [51]. The physicochemical properties of TAN are represented in **Table 2.6**.

Table 2.6. Physicochemical properties of TAN

Name	Tanshinone IIA (TAN)
Chemical structure	
IUPAC name	1,6,6-trimethyl-8,9-dihydro-7H-naphtho[1,2-g][1]benzofuran-10,11-dione
Molecular formula	$C_{19}H_{18}O_3$
Molecular weight	294.3 g/mol
BCS Class	Class II
pKa	-
Log P	4.3
Melting point	205-215ºC
Solubility	Easily soluble in organic solvents such as ethanol, methanol and benzene, and insoluble in water.

2.2.5.2. Mechanism of action

TAN has been documented to suppress the differentiation of osteoclasts by inhibiting lactate dehydrogenase C (LDHC) mediated ROS generation. This leads to a reduction in the levels of IL-17, MMP-9, and tartrate-resistant acid phosphatase (TRAP) [52]. TAN has been observed to inhibit the proliferation of RA fibroblast-like synoviocytes through multiple signaling pathways, including AKT/mTOR (mammalian target of rapamycin), MAPK, NF- κB and HIF-

1 [53]. TAN has also been reported to inhibit the expression of MMP9, receptor for advanced glycation end product (RAGE), and toll-like receptor 9 (TLR9) in both collagen-induced arthritis (CIA) mice and RA-FLS [54]. Additionally, it has been documented that TAN inhibits apoptosis in RA-FLS by blocking the cell cycle in the G2/M phase and *via* the mitochondrial pathway [55].

2.3. Combination delivery of natural products and synthetic compounds

Natural products have been investigated for their potential in effectively managing RA in combination with synthetic molecules. Several studies have reported on this combination approach. Haleagrahara, N et. al 2019 reported the efficacy of combination of methotrexate and QCN in collagen-induced arthritis. The adjuvant therapy with QCN exhibited effective inhibition of joint inflammation by decreasing the expression of TNFα and MMP genes in the ankle joints of arthritic mice [56]. Banji, D et.al 2011 also, reported the combination efficacy of curcumin and methotrexate in CFA induced arthritis. The administration of curcumin markedly decreased methotrexate-induced hepatotoxicity by virtue of its antioxidant properties [57]. The combination of curcumin-diclofenac has been reported to exhibit better efficacy in mitigating pain, suppressing inflammatory cytokines, and ameliorating histological alterations during acute inflammation in carrageenan induced rats [58]. Similarly, co-delivery of curcumin-prednisolone nanoparticles have been found to accumulate within inflamed joints by ELVIS effect (Extravasation through Leaky Vasculature and the subsequent Inflammatory cell–mediated Sequestration). This co-delivery approach have demonstrated superior therapeutic efficacy compared to nanoparticles loaded with monotherapy in adjuvant induced arthritis in rats [59]. Apart from this topical application of a combination of methotrexate and RES nanoemulsion has demonstrated a reduction in a paw volume in carrageen induced rats [60]. Collectively, the above studies indicate that combining synthetic molecules with natural products encompasses an effective approach for treating RA.

2.4. Disadvantages of oral administration of Natural products

Natural products have been extensively studied for their efficacy against a variety of diseases, yet their oral administration presents several challenges. These include issues with poor absorption, distribution and metabolism properties leading to inconsistent bioavailability and therapeutic effects [61]. Additionally concerns arise regarding the stability of these products. Furthermore, the absence of target-specific delivery mechanisms can result in unintended side effects associated with them [62] necessitating alternative routes of administration for effective and localized delivery.

ANG has been reported for its low solubility and limited bioavailability. Additionally, oral administration often leads to vomiting. Large doses of it and related preparations orally can induce epigastric discomfort and diminish appetite [33]. QCN possess low solubility, limited gastrointestinal retention, and rapid excretion. Furthermore, its oral administration often results in poor clinical efficacy due to rapid degradation in alkaline conditions [27]. RES exhibits poor bioavailability following oral administration and has stability issues, leading to suboptimal *in-vivo* pharmacokinetics [63]. RUT has solubility and stability issues ultimately resulting in inadequate oral bioavailability [64]. TAN has also been documented to possess poor solubility and limited bioavailability after oral administration [65, 66].

2.5. Gaps in existing research

RA manifests as immune-mediated inflammation impacting the joints and synovial tissue, eliciting pain and inflammation. Inadequate treatment may result in the progressive deterioration of joint function over time. Numerous inflammatory mediators, (including TNF-α, IL-6, and IL-1β, IL-17) play crucial roles in the pathophysiology of the condition, stemming from the body's immune dysregulation. EULAR, ACR, and other guidelines recommend the early initiation of sDMARDs, either in monotherapy or combination therapy, upon diagnosis of the disease. TFD, acts by inhibiting the mitochondrial enzyme DHODH, leading to the suppression of active lymphocyte proliferation. Several guidelines promote the implementation of initial combination therapy as a preventive measure against progressive joint damage. Clinical trials have consistently demonstrated the superior efficacy of combination therapy as mentioned in **Table 1.1.** Researchers have further investigated the synergistic effects of combination of synthetic as well as natural products for enhanced treatment outcomes in RA, as outlined in **Table 1.2.**

However, based on the literature, the following gaps have been identified in the effective management of RA.

➢ The ongoing scientific exploration involves the combination of synthetic molecules with natural products for the treatment of various diseases. **However, there remains limited exploration regarding the efficacy of combining TFD with natural products for the treatment of RA**

➢ Multiple researchers have documented the efficacy of combination therapies *in-vivo*, **yet there remains a gap in understanding the *in-vitro* potential of these combinations prior to their *in-vivo* exploration**

➢ The oral administration of TFD has been associated with significant hepatotoxicity and systemic adverse effects. Similarly, natural products often exhibit insufficient solubility

and bioavailability when administered orally. **Thus, an alternative delivery approach is imperative, one that ensures localized action, effectively demonstrating activity within joint tissue while minimizing systemic levels through dose reduction.**

2.6. Aim of the study

Given the potential gaps in existing research, our objective is the development of **"Teriflunomide and Natural Products Loaded Topical Transferosomal Gel for the Treatment of Rheumatoid Arthritis."**

2.7. Objectives

1. To evaluate the synergistic anti-inflammatory activity of selected natural products (ANG, QCN, RES, RUT, and TAN) in combination with TFD in LPS stimulated RAW 264.7 cells.

2. Analytical method development and validation of the TFD and the QCN using UV-visible spectroscopy and High-performance liquid chromatography (HPLC).

3. Development and evaluation of combination of TFD and QCN loaded transferosomal gel.

4. *In-vivo* evaluation of antiarthritic activity of combination (TFD and QCN) topical transferosomal gel in complete freund's adjuvant induced rat model.

Chapter 2

References

1. Hill, S., & Frey, N. (2021). Conventional disease-modifying antirheumatic drugs for the treatment of rheumatoid arthritis. *Canadian Journal of Health Technologies*, *1*(5), 1-40

2. Cutolo, M., Sulli, A., Pizzorni, C., Seriolo, B., & Straub, R. H. (2001). Anti-inflammatory mechanisms of methotrexate in rheumatoid arthritis. *Annals of the Rheumatic Diseases*, *60*(8), 729–735.

3. Cohen, S., & Iqbal, I. (2003). Leflunomide. *International Journal of Clinical Practice*, *57*(2), 115–120.

4. Nirk, E. L., Reggiori, F., & Mauthe, M. (2020). Hydroxychloroquine in rheumatic autoimmune disorders and beyond. *EMBO Molecular Medicine*, *12*(8), e12476.

5. Beiranvand, M. (2021). A review of the biological and pharmacological activities of mesalazine or 5-aminosalicylic acid (5-ASA): An anti-ulcer and anti-oxidant drug. *Inflammopharmacology*, *29*(5), 1279–1290.

6. Köhler, B. M., Günther, J., Kaudewitz, D., & Lorenz, H. M. (2019). Current therapeutic options in the treatment of rheumatoid arthritis. *Journal of Clinical Medicine*, *8*(7), 938.

7. Ishaq, M., Muhammad, J. S., Hameed, K., & Mirza, A. I. (2011). Leflunomide or methotrexate? Comparison of clinical efficacy and safety in low socio-economic rheumatoid arthritis patients. *Modern Rheumatology*, *21*(4), 375–380.

8. Schiff, M. H. (1999). Leflunomide versus methotrexate: A comparison of the European and American experience. *Scandinavian Journal of Rheumatology, 112*(112), 31–35.

9. Fajardo-Robledo, N.S., Jacobo-Cuevas, H., Perez-Guerrero, E.E., Corona-Sanchez, E.G., Saldaña-Cruz, A.M., Romero-Tejeda, E.M., Rodriguez-Jimenez, N.A., Totsuka-Sutto, S.E., Lopez-Roa, R.I., Ponce-Guarneros, J.M. & Alcaraz-Lopez, M.F.(2022). Therapeutic response to leflunomide in combo therapy and monotherapy is associated to serum teriflunomide (A77 1726) levels. *Scientific Reports, 12*(1), 1877.

10. Aly, L., Hemmer, B., & Korn, T. (2017). From leflunomide to teriflunomide: Drug development and immuno-suppressive oral drugs in the treatment of multiple sclerosis. *Current Neuropharmacology*, *15*(6), 891.

11. Hernandez, A. L., O'Connor, K. C., & Hafler, D. A. (2014). Multiple Sclerosis. In *The Autoimmune Diseases: Fifth Edition*, Noel R. Rose, Ian R. Mackay (Eds.). 735–756. Academic Press.

12. Sanders, S., & Harisdangkul, V. (2002). Leflunomide for the treatment of rheumatoid arthritis and autoimmunity. *The American Journal of the Medical Sciences*, *323*(4), 190–193.

13. Nwankwo, E., Allington, D. R., Rivey, M. P., & Allington, D. (2012). Emerging oral immunomodulating agents-focus on teriflunomide for the treatment of multiple sclerosis. *Degenerative Neurological and Neuromuscular Disease*, *2,* 15–28.

14. González-Alvaro, I., Ortiz, A. M., Domínguez-Jiménez, C., Aragón-Bodi, A., Díaz Sánchez, B., & Sánchez-Madrid, F. (2009). Inhibition of tumour necrosis factor and IL-17 production by leflunomide involves the JAK/STAT pathway. *Annals of the Rheumatic Diseases*, *68*(10), 1644–1650.

15. Papadopoulou, A., Kappos, L., & Sprenger, T. (2012). Teriflunomide for oral therapy in multiple sclerosis. *Expert Review of Clinical Pharmacology*, *5*(6), 617–628.

16. Xu, X., Williams, J. W., Bremer, E. G., Finnegan, A., & Chong, A. S. F. (1995). Inhibition of protein tyrosine phosphorylation in T cells by a novel immunosuppressive agent, leflunomide. *The Journal of Biological Chemistry*, *270*(21), 12398–12403.

17. Manna, S. K., & Aggarwal, B. B. (1999). Immunosuppressive leflunomide metabolite (A77 1726) blocks TNF-dependent nuclear factor-κB activation and gene expression. *The Journal of Immunology*, *162*(4), 2095–2102.

18. Manna, S. K., Mukhopadhyay, A., & Aggarwal, B. B. (2000). Leflunomide suppresses TNF-induced cellular responses: Effects on NF-kappa B, activator protein-1, C-Jun N-terminal protein kinase, and apoptosis. *Journal of Immunology*, *165*(10), 5962–5969.

19. Burger, D., Begué-Pastor, N., Benavent, S., Gruaz, L., Kaufmann, M.-T., Chicheportiche, R., & Dayer, J.-M. (2003). The active metabolite of leflunomide, A77 1726, inhibits the production of prostaglandin E 2 , matrix metalloproteinase 1 and interleukin 6 in human fibroblast-like synoviocytes. *Rheumatology*, *42*(1), 89–96.

20. Hamilton, L. C., Vojnovic, I., & Warner, T. D. (1999). A771726, the active metabolite of leflunomide, directly inhibits the activity of cyclo-oxygenase-2 in vitro and in vivo in a substrate-sensitive manner. *British Journal of Pharmacology*, *127*(7), 1589–1596.

21. Bar-Or, A. (2014). Teriflunomide (Aubagio®) for the treatment of multiple sclerosis. *Experimental Neurology, 262*, 57-65.

22. Dudics, S., Langan, D., Meka, R. R., Venkatesha, S. H., Berman, B. M., Che, C. T., & Moudgil, K. D. (2018). Natural products for the treatment of autoimmune arthritis: Their mechanisms of action, targeted delivery, and interplay with the host microbiome. *International Journal of Molecular Sciences, 19*(9), 2508.

23. Deligiannidou, G. E., Gougoula, V., Bezirtzoglou, E., Kontogiorgis, C., & Constantinides, T. K. (2021). The role of natural products in rheumatoid arthritis: Current knowledge of basic in vitro and in vivo research. *Antioxidants 10*(4), 599.

24. Barnes, P. M., Bloom, B., & Nahin, R. L. (2008). Complementary and alternative medicine use among adults and children: United States, 2007. *National Health Statistics Reports*, *12*, 1–23.

25. Yahfoufi, N., Alsadi, N., Jambi, M., & Matar, C. (2018). The Immunomodulatory and anti-inflammatory role of polyphenols. *Nutrients*, *10*(11), 1618.

26. Astry, B., Venkatesha, S.H., Laurence, A., Christensen-Quick, A., Garzino-Demo, A., Frieman, M.B., O'Shea, J.J. & Moudgil, K.D.(2015). Celastrol, a Chinese herbal compound, controls autoimmune inflammation by altering the balance of pathogenic and regulatory T cells in the target organ. *Clinical Immunology, 157*(2), 228-238.

27. Gokhale, J. P., Mahajan, H. S., & Surana, S. S. (2019). Quercetin loaded nanoemulsion-based gel for rheumatoid arthritis: In vivo and in vitro studies. *Biomedicine and Pharmacotherapy*, *112*. 108622.

28. Afzal, O., Altamimi, A. S. A., Alamri, M. A., Altharawi, A., Alossaimi, M. A., Akhtar, M. S., Tabassum, F., Almalki, W. H., & Singh, T. (2023). Resveratrol-loaded chia seed oil-based nanogel as an anti-inflammatory in adjuvant-induced arthritis. *Gels, 9*(2), 131.

29. Jeengar, M. K., Rompicharla, S. V. K., Shrivastava, S., Chella, N., Shastri, N. R., Naidu, V. G. M., & Sistla, R. (2016). Emu oil based nano-emulgel for topical delivery of curcumin. *International Journal of Pharmaceutics*, *506*(1–2), 222–236.

30. Fan, C., Li, X., Zhou, Y., Zhao, Y., Ma, S., Li, W., Liu, Y., & Li, G. (2013). Enhanced topical delivery of tetrandrine by ethosomes for treatment of arthritis. *BioMed Research International*, *2013*(1), 161943.

31. Sarwa, K. K., Mazumder, B., Rudrapal, M., & Verma, V. K. (2015). Potential of capsaicin-loaded transfersomes in arthritic rats. *Drug Delivery*, *22*(5), 638–646.

32. Bhalekar, M. R., Madgulkar, A. R., Desale, P. S., & Marium, G. (2017). Formulation of piperine solid lipid nanoparticles (SLN) for treatment of rheumatoid arthritis. *Drug Development and Industrial Pharmacy*, *43*(6), 1003–1010.

33. Yan, Y., Fang, L. H., & Du, G. H. (2018). Andrographolide. In: Natural Small Molecule Drugs from Plants, Springer, 357-362.

34. Li, X., Yuan, W., Wu, J., Zhen, J., Sun, Q., & Yu, M. (2022). Andrographolide, a natural anti-inflammatory agent: An update. *Frontiers in Pharmacology*, *13*, 920435.

35. Lee, K. C., Chang, H. H., Chung, Y. H., & Lee, T. Y. (2011). Andrographolide acts as an anti-inflammatory agent in LPS-stimulated RAW 264.7 macrophages by inhibiting STAT3-mediated suppression of the NF-κB pathway. *Journal of Ethnopharmacology*, *135*(3), 678–684.

36. Li, Y., Yao, J., Han, C., Yang, J., Chaudhry, M.T., Wang, S., Liu, H. & Yin, Y. (2016). Quercetin, inflammation and immunity. *Nutrients, 8*(3), 167.

37. Di Pierro, F., Khan, A., Iqtadar, S., Mumtaz, S.U., Chaudhry, M.N.A., Bertuccioli, A., Derosa, G., Maffioli, P., Togni, S., Riva, A. & Allegrini, P. (2023). Quercetin as a possible complementary agent for early-stage COVID-19: Concluding results of a randomized clinical trial. *Frontiers in Pharmacology, 13,* 1096853.

38. Shen, P., Lin, W., Deng, X., Ba, X., Han, L., Chen, Z., Qin, K., Huang, Y., & Tu, S. (2021). Potential implications of quercetin in autoimmune diseases. *Frontiers in Immunology*, *12*, 689044.

39. Tang, M., Zeng, Y., Peng, W., Xie, X., Yang, Y., Ji, B., & Li, F. (2022). Pharmacological aspects of natural quercetin in rheumatoid arthritis. *Drug Design, Development and Therapy*, *16*, 2043-2053.

40. Yang, Y., Zhang, X., Xu, M., Wu, X., Zhao, F., & Zhao, C. (2018). Quercetin attenuates collagen-induced arthritis by restoration of Th17/Treg balance and activation of Heme Oxygenase 1-mediated anti-inflammatory effect. *International Immunopharmacology*, *54*, 153–162.

41. Sung, M. S., Lee, E. G., Jeon, H. S., Chae, H. J., Park, S. J., Lee, Y. C., & Yoo, W. H. (2012). Quercetin inhibits IL-1β-induced proliferation and production of MMPs, COX-2, and PGE2 by rheumatoid synovial fibroblast. *Inflammation*, *35*(4), 1585–1594.

42. Salehi, B., Mishra, A.P., Nigam, M., Sener, B., Kilic, M., Sharifi-Rad, M., Fokou, P.V.T., Martins, N. & Sharifi-Rad, J (2018). Resveratrol: A double-edged sword in health benefits. *Biomedicines, 6*(3), 91.

43. Tian, J., Chen, J. W., Gao, J. S., Li, L., & Xie, X. (2013). Resveratrol inhibits TNF-α-induced IL-1β, MMP-3 production in human rheumatoid arthritis fibroblast-like synoviocytes via modulation of PI3kinase/Akt pathway. *Rheumatology International*, *33*(7), 1829–1835.

44. Buhrmann, C., Popper, B., Aggarwal, B. B., & Shakibaei, M. (2017). Resveratrol downregulates inflammatory pathway activated by lymphotoxin α (TNF-β) in articular chondrocytes: Comparison with TNF-α. *PloS One*, *12*(11), e0186993.

45. Sheng, S., Wang, X., Liu, X., Hu, X., Shao, Y., Wang, G., Mao, D., Li, C., Chen, B. & Chen, X. (2022). The role of resveratrol on rheumatoid arthritis: From bench to bedside. *Frontiers in Pharmacology, 13*, 829677.

46. Ganeshpurkar, A., & Saluja, A. K. (2017). The Pharmacological potential of rutin. *Saudi Pharmaceutical Journal, 25*(2), 149-164.

47. Kyung, T. W., Lee, J. E., Shin, H. H., & Choi, H. S. (2008). Rutin inhibits osteoclast formation by decreasing reactive oxygen species and TNF-α by inhibiting activation of NF-kappaB. *Experimental & Molecular Medicine*, *40*(1), 52–58.

48. Sun, C. L., Wei, J., & Bi, L. Q. (2017). Rutin attenuates oxidative stress and proinflammatory cytokine level in adjuvant induced rheumatoid arthritis via inhibition of NF-κB. *Pharmacology*, *100*(1–2), 40–49.

49. Chen, X., Yu, M., Xu, W., Zou, L., Ye, J., Liu, Y., Xiao, Y. & Luo, J. (2021). Rutin inhibited the advanced glycation end products-stimulated inflammatory response and extra-cellular matrix degeneration via targeting TRAF-6 and BCL-2 proteins in mouse model of osteoarthritis. *Aging, 13*(18), 22134.

50. Sharma, A., Tirpude, N. V., Bhardwaj, N., Kumar, D., & Padwad, Y. (2022). Berberis lycium fruit extract and its phytoconstituents berberine and rutin mitigate collagen-CFA-induced arthritis (CIA) via improving GSK3β/STAT/Akt/MAPKs/NF-κB signaling axis mediated oxi-inflammation and joint articular damage in murine model. *Inflammopharmacology*, *30*(2), 655–666.

51. Fang, Z., Zhang, M., Liu, J. N., Zhao, X., Zhang, Y. Q., & Fang, L. (2020). Tanshinone IIA: A review of its anticancer effects. *Frontiers in Pharmacology*, *11*, 611087.

52. Peng, Q., Wang, J., Han, M., Zhao, M., Li, K., Lu, T., Guo, Q., & Jiang, Q. (2023). Tanshinone IIA inhibits osteoclastogenesis in rheumatoid arthritis via LDHC-regulated ROS generation. *Chinese Medicine*, *18*, 54.

53. Du, H., Wang, Y., Zeng, Y., Huang, X., Liu, D., Ye, L., Li, Y., Chen, X., Liu, T., Li, H. & Wu, J.(2020). Tanshinone IIA suppresses proliferation and inflammatory cytokine production of synovial fibroblasts from rheumatoid arthritis patients induced by TNF-α and attenuates the inflammatory response in AIA mice. *Frontiers in Pharmacology, 11*, 568.

54. Liu, W., Wu, C., Wang, Q., Kuang, L., & Le, A. (2023). Tanshinone IIA relieves arthritis by inhibiting autophagy of fibroblast-like synoviocytes via matrix metalloproteinase9/receptor for advanced glycation end product/toll-like receptor 9 signal axis in mice with collagen-induced arthritis. *Phytotherapy Research* , *37*(4), 1391–1404.

55. Jie, L., Du, H., Huang, Q., Wei, S., Huang, R., & Sun, W. (2014). Tanshinone IIA induces apoptosis in fibroblast-like synoviocytes in rheumatoid arthritis via blockade of the cell cycle in the G2/M phase and a mitochondrial pathway. *Biological & Pharmaceutical Bulletin*, *37*(8), 1366–1372.

56. Haleagrahara, N., Hodgson, K., Miranda-Hernandez, S., Hughes, S., Kulur, A. B., & Ketheesan, N. (2018). Flavonoid quercetin-methotrexate combination inhibits

inflammatory mediators and matrix metalloproteinase expression, providing protection to joints in collagen-induced arthritis. *Inflammopharmacology*, *26*(5), 1219–1232.

57. Banji, D., Pinnapureddy, J., Banji, O. J. F., Saidulu, A., & Hayath, M. S. (2011). Synergistic activity of curcumin with methotrexate in ameliorating Freund's Complete Adjuvant induced arthritis with reduced hepatotoxicity in experimental animals. *European Journal of Pharmacology*, *668*(1–2), 293–298.

58. Boarescu, I., Pop, R. M., Boarescu, P. M., Bocșan, I. C., Gheban, D., Rājnoveanu, R. M., Rājnoveanu, A., Bulboacă, A. E., Buzoianu, A. D., & Bolboacă, S. D. (2022). Anti-inflammatory and analgesic effects of curcumin nanoparticles associated with diclofenac sodium in experimental acute inflammation. *International Journal of Molecular Sciences*, *23*(19), 11731.

59. Yan, F., Li, H., Zhong, Z., Zhou, M., Lin, Y., Tang, C., & Li, C. (2019). Co-delivery of prednisolone and curcumin in human serum albumin nanoparticles for effective treatment of rheumatoid arthritis. *International Journal of Nanomedicine*, *14*, 9113–9125.

60. Poonia, N., Lather, V., Kaur, B., Kirthanashri, S. V., & Pandita, D. (2020). Optimization and development of methotrexate- and resveratrol-loaded nanoemulsion formulation using box-behnken design for rheumatoid arthritis. *Assay and Drug Development Technologies*, *18*(8), 356–368.

61. Press, N. J., Joly, E., & Ertl, P. (2019). Natural product drug delivery: A special challenge? *Progress in Medicinal Chemistry*, *58*, 157–187.

62. Elkordy, A. A., Haj-Ahmad, R. R., Awaad, A. S., & Zaki, R. M. (2021). An overview on natural product drug formulations from conventional medicines to nanomedicines: Past, present and future. *Journal of Drug Delivery Science and Technology*, *63*, 102459.

63. Shaito, A., Posadino, A.M., Younes, N., Hasan, H., Halabi, S., Alhababi, D., Al-Mohannadi, A., Abdel-Rahman, W.M., Eid, A.H., Nasrallah, G.K. & Pintus, G. (2020). Potential adverse effects of resveratrol: A literature review. *International Journal of Molecular Sciences, 21*(6), 2084.

64. Hassan, A. S., & Soliman, G. M. (2022). Rutin nanocrystals with enhanced anti-inflammatory activity: Preparation and ex vivo/in vivo evaluation in an inflammatory rat model. *Pharmaceutics*, *14*(12), 2727.

65. Zhou, Z. Y., Zhao, W. R., Zhang, J., Chen, X. L., & Tang, J. Y. (2019). Sodium tanshinone IIA sulfonate: A review of pharmacological activity and pharmacokinetics. *Biomedicine & Pharmacotherapy*, *118*, 109362.

66. Hao, H., Wang, G., Cui, N., Li, J., Xie, L., & Ding, Z. (2006). Pharmacokinetics, absorption and tissue distribution of tanshinone IIA solid dispersion. *Planta medica*, *72*(14), 1311-1317.

Chapter 3

Evaluation of Synergistic Anti-Inflammatory Activity of Selected Natural Products in Combination with Teriflunomide in LPS stimulated RAW 264.7 Cells

Chapter 3

3.1. Introduction

Macrophages are an integral component of the immune system, actively engaged in the inflammatory response underlying the pathogenesis of RA. Serving as antigen-presenting cells, they release a multitude of inflammatory cytokines and chemokines, that significantly contribute to the erosion of cartilage, bone, and surrounding tissues [1]. Upon macrophage stimulation, activation of NADPH oxidase complex initiates the production of superoxide radicals, inducing oxidative stress and subsequent ROS generation within the cell [2]. These ROS can activate pro-inflammatory pathways and serve as signaling molecules, influencing cellular functions like proliferation, differentiation, and apoptosis. Additionally, ROS may induce mitochondrial dysfunction and DNA damage, contributing to cellular pathology [3].

The stimulated macrophages produce various inflammatory mediators such as nitric oxide (NO) and inflammatory cytokines (TNF-α and interleukins) [4]. NO that is regulated by nitric oxide synthase (iNOS), contributes to inflammation in RA by influencing tissue damage and disease progression. The inflammatory mediators such as TNF-α and IL-6 are known to play pivotal roles in the pathogenesis of inflammatory arthritis linked to joint destruction in RA [5]. The production of TNF-α and IL-6 are regulated by the JAK-STAT, NF-κB and MAPK signaling pathways, collectively impacting inflammatory responses in RA [4,6]. Therefore, targeting the suppression of pro-inflammatory mediators released by activated macrophages is a beneficial approach in preventing diseases associated with inflammation such as RA.

The utilization of combination therapy has emerged as a successful approach in managing inflammatory RA, given its intricate origin and pathophysiology. Furthermore, combination of synthetic molecules with natural products holds promise as a future avenue for treating RA. This approach exploits the synergistic activity aiming to improve treatment outcomes and mitigate side effects in disease management through dose reduction [7,8]. As mentioned in Chapter 2, various natural products such ANG, QCN, RES, RUT and TAN have been extensively studied for their therapeutic potential in treating RA. The combination of these natural products along with TFD represents a promising approach for improved pharmacological efficacy by targeting multiple inflammatory pathways simultaneously **(Figure 3.1**) [4].

Previously the individual anti-inflammatory activities of above natural products have been reported, however combination of these natural products along with TFD has not been investigated. Thus, the present study aims to investigates the potential synergistic effects of combining TFD with natural products namely ANG, QCN, RES, RUT and TAN in lipopolysaccharide (LPS) stimulated RAW 264.7 cells with the objective of identifying the

most effective combination. The combinations were evaluated for their inhibitory activity against NO production and proinflammatory cytokines, such as TNF-α and IL-6, followed by evaluating reactive oxygen species (ROS) production.
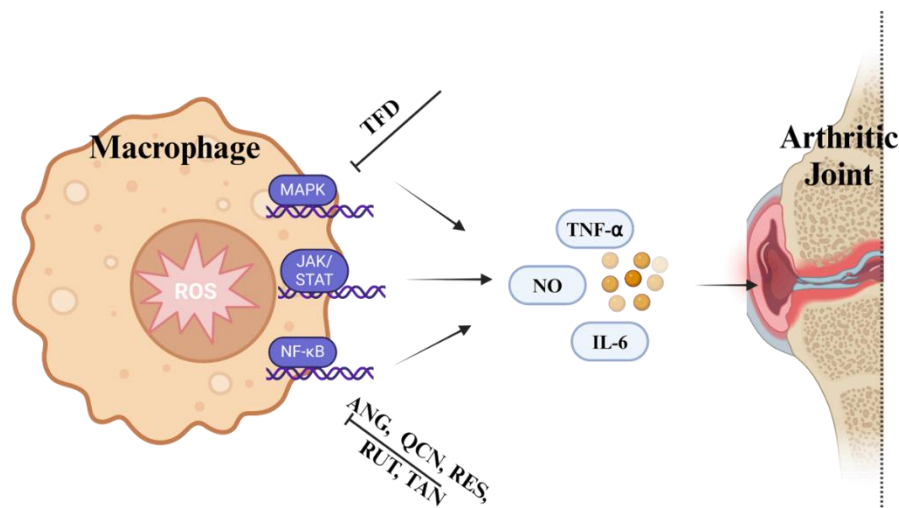
Figure 3.1. Mechanism of inhibition of pro-inflammatory cytokine production in macrophages

3.2. Materials and methods

3.2.1. Materials

TFD (99.9% pure) was obtained as a gift sample from the MSN Laboratories Private Limited (Sangareddy, India). ANG, QCN, RES, RUT and TAN were purchased from the Yucca Enterprises (Mumbai, India) with the purity of > 97%. Dulbecco's Modified Eagle Medium (DMEM) with high glucose was purchased from Gibco (New York, USA). Fetal Bovine Serum (FBS) and Dimethyl Sulfoxide (DMSO) were purchased from Himedia (Mumbai, India). LPS (*E. coli* O26:B6) was purchased from Sigma Aldrich. N-(1-naphthyl) ethylenediamine dihydrochloride (NEDD), 3-(4,5-Dimethylthiazol-2-yl)-2,5-Diphenyltetrazolium Bromide (MTT) and 2′,7′-Dichlorodihydrofluorescein diacetate (DCFDA) were purchased from SRL Pvt. Ltd (Mumbai, India). Sulfanilamide was purchased from Spectrochem Pvt. Ltd (Mumbai, India), TNF-α and IL-6 ELISA kits were purchased from Elabscience (Houston, USA).

3.2.2. Cell culture

RAW 264.7 cells were procured from the National Centre for Cell Science (NCCS), Pune, Maharashtra, India. The cells were cultured in DMEM high glucose media with 10% FBS and supplemented with 1000 U of penicillin and 100 μg of streptomycin per mL under constant temperature of 37 ºC, at humidified atmosphere of 5% CO_2 in an incubator.

3.2.3. Cell viability assay using MTT

The cell viability or cytotoxicity assay for the TFD and selected natural products (ANG, QCN, RES, RUT and TAN) were performed in RAW 264.7 cells using MTT assay. For assessing the cell viability, RAW 264.7 cells were seeded at density of 5×10^3 cells /well in 96 well plate with 100 µL of volume in each well and incubated for 24 h to allow cells to adhere to the plate. After, the cells were treated with different concentrations of TFD and natural products individually in the range of 1-50 µM for 24 h. Then the complete media was removed and MTT was added at a concentration of 0.5mg/mL followed by incubation for another 4 h. The cell supernatant was removed carefully. The formation of formazan crystal was observed visually, and the crystals were further dissolved by the addition of DMSO in each well and kept under rotary orbital shaker at 150 rpm for 30 min. The absorbance was measured at 570 nm with a reference wavelength of 630 nm using microplate reader (Bioteck Synergy H1, Santa Clara, USA) [4].

3.2.4. Nitric oxide (NO) assay

The concentrations with cell viability above 95% were selected for performing the NO assay. The NO assay uses a griess reagent for the detection of NO levels in a sample. RAW 264.7 cells were seeded at density of 2.5×10^4 cells/ well in a 12 well plate and incubated for 24 h. Prior to treatment with LPS at 1µg/mL for 2 h, cells were treated with various concentrations of TFD and natural products individually. After a subsequent incubation period of 24 h, the 100 µL of supernant was collected and treated with equal volume of Griess reagent (a mixture of 2 % sulphanilamide and NEDD in 5% phosphoric acid solution). Finally, the absorbance was measured at 540 nm after 15 min of incubation at room temperature using microplate reader. The concentration of nitrite produced was determined using a standard plot of $NaNO_2$. This plot was generated by measuring the absorbance at 540 nm across a range of concentrations from 10 to 100 µM of $NaNO_2$. Then, the concentration required to produce 50% inhibition of NO (IC_{50}) values were calculated using non-linear regression using Graph pad prism [9–11].

3.2.5. Synergy studies using NO assay

To evaluate the synergy using the NO assay, the IC_{50} value of TFD and natural products were determined. Constant ratio design (**Figure 3.2)** was used to perform the synergistic analysis of the selected natural products in combination with TFD with the help of Compusyn software version 1.0 [4,12,13].
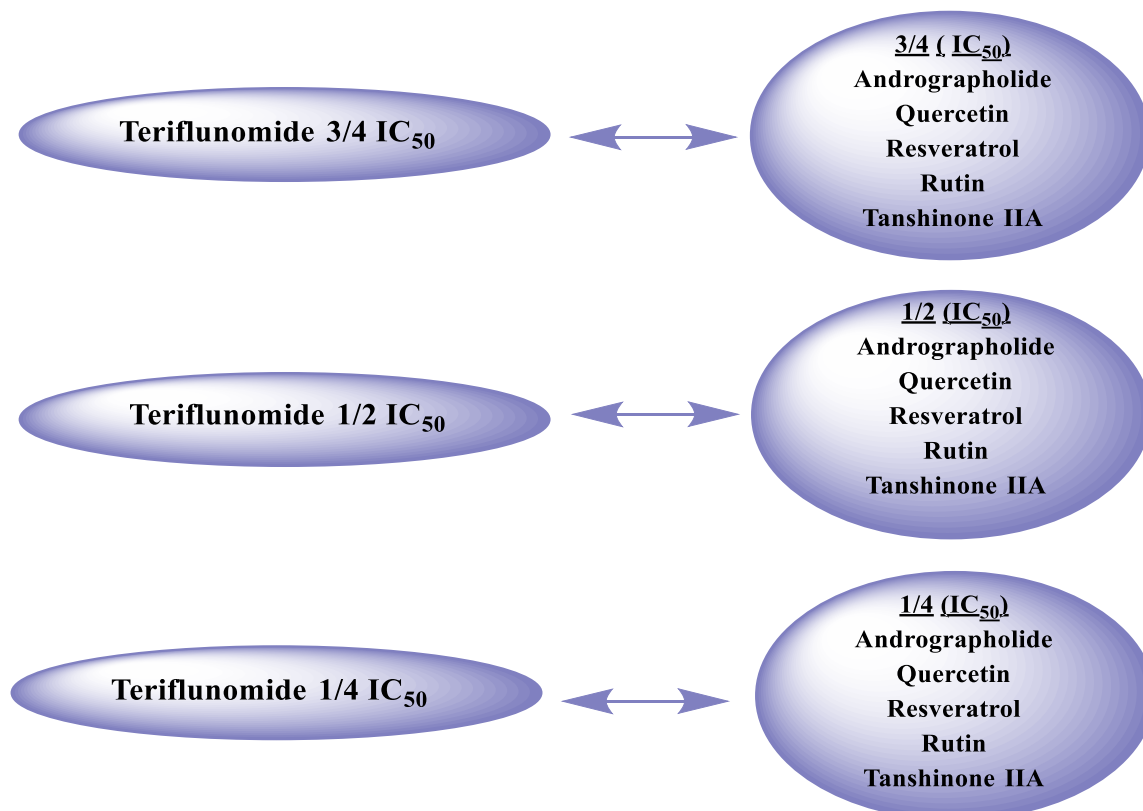
Figure 3.2. Synergistic effect analysis – Constant ratio design

Prior to evaluating synergy, the MTT assay for the combination of TFD with natural products at a same concentration (as outlined in **Figure 3.2)** were conducted on LPS-stimulated RAW 264.7 cells, as per the procedure detailed in section 3.1.3. Further, the NO assay was performed for each natural products alone and in combination with TFD at 3/4, 1/2, 1/4, of IC_{50}. The obtained activity data was keyed into Compusyn software to calculate the Combination Index (CI) value and to generate isobologram curves for the NO measurement. These isobologram representations, alongside the CI value, provided insights into the nature of the interaction, determining whether their effects are synergistic or antagonistic. The CI index values were calculated using following equation 3.1

$$CI = \frac{AX}{A1} + \frac{BX}{B1} \qquad \text{…eq 3.1}$$

Here, *AX* and *BX* indicate the concentration of drugs used in combination to produce X effect, while *A1* and *B1* represent the concentrations used individually to produce the same effect

Synergy is said to occur if the CI < 1, while if CI =1 or CI >1 then it indicates additive or antagonistic effect [4,14]. The isobologram curve interpretation relies on data points' positioning: below for synergy, above for antagonism, and on the line for additivity [4,15]. It assesses combined drug effects compared to individual treatments, guiding treatment optimization. Further the Dose Reduction Index (DRI) values for all combinations were provided, delineating the potential reduction in individual drug dosages while maintaining efficacy. Higher DRI values suggest increased scope for dose reduction in combined therapies, balancing efficacy and side effects [15]. Additionally, polygonogram was utilized to visually depict the effects of combined drug doses, facilitating the analysis of drug interactions within a single graph.

3.2.6. Determination of proinflammatory cytokines inhibition

RA being a complex phenomenon associated with immune-mediated inflammatory diseases, it is imperative to assess the inhibitory potential against various inflammatory mediators. Given that TNF-α and IL-6 play pivotal roles in disease progression, it is essential to assess the inhibitory potential of the selected individual natural products and their combinations with TFD [16,17]. The evaluation of inhibitory activity against TNF-α and IL-6, involved the examination of the combination of a natural products with TFD, specifically focusing on those combinations with the best CI values that were determined through the NO assay. RAW 264.7 cells were seeded at a density of 2.5 x 10^4 cell/well in a 12 well plate and incubated for 24 h. Cells were treated with various concentrations of TFD and Natural products alone or in combination with TFD. Following a 2 h incubation, cells were treated with LPS at a concentration of 1 μg/mL. After a 24 h incubation period, the supernatant was taken and centrifuged at 10000 rpm for 10 min. Further the supernant was analyzed for proinflammatory cytokines such as TNF-α and IL-6 using experimental protocol provided by sandwich ELISA kit and the final absorbance was taken for both at 480 nm. Further assessment involved calculating the CI for synergistic analysis in inhibiting TNF-α and IL-6 using Compusyn software.

3.2.7. Determination of intracellular ROS

ROS generation in RA exacerbates oxidative stress, leading to heightened oxidative damage and inflammation in tissues. Elevated ROS levels also stimulate cytokine production, thereby perpetuating the autoimmune response and promoting joint degradation [18]. Modulating ROS generation offers potential therapeutic interventions to alleviate oxidative injury and manage disease progression in RA and hence was evaluated as follows [19].

3.1.7.1. Fluorescence intensity

The most effective combination against proinflammatory cytokine activity was further assessed for the measurement of ROS using a fluorogenic dye DCF-DA. This allowed to assess the activity of hydroxyl, peroxyl, and other ROS within cellular environments. RAW 264.7 cells were plated in a 96 well plate at a density of 5 x10^3 cells/well and allowed to incubate for 24 h. Following this, the cells were treated with different concentrations of TFD and natural products (exhibiting higher synergy), followed by stimulation with LPS after 2 h. After another 24 h of incubation, the cells were exposed to phosphate buffer saline (PBS) containing 10 µM of DCF-DA and incubated at 37°C for 30 min in the dark. Fluorescence intensity was recorded using microplate reader at excitation wavelength of 485 nm and emission wavelength of 528 nm, respectively [4].

3.1.7.2. Fluorescence microscope

The experiment was conducted following the procedure outlined in the above section. Following a 30 min incubation period with DCF-DA, the cells underwent three washes with ice-cold PBS. Subsequently, fluorescence images were captured using a 40X magnification and a green fluorescent protein channel (ZEISS Vert A1) [4].

3.3. Statistical analysis

All the experiments were performed in triplicates and the data was mentioned as mean ± SD. The IC$_{50}$ values were calculated using nonlinear regression using GraphPad prism version 9.1.0. Two-way analysis of variance (ANOVA) followed by Tukey's multiple comparison test was used to calculate the difference. Synergistic analysis was performed using Compusyn software version 1.0.

3.4. Results and discussion

3.4.1. Effect of TFD and Natural products on cell viability

The cell viability was determined for TFD and natural products (ANG, QCN, RES, RUT and TAN) individually prior to the evaluation of the anti-inflammatory activity in RAW 264.7 cells. In accordance with reported studies, the concentration range of 1-50 µM was evaluated for both TFD and all natural products. A cell viability exceeding 95 % was considered as indicative of non-cytotoxicity. The MTT data for concentration ranges up to 1-30 µM for TFD and all natural products are depicted in **Figure 3.3**. Additionally, these concentrations were utilized for subsequent studies.
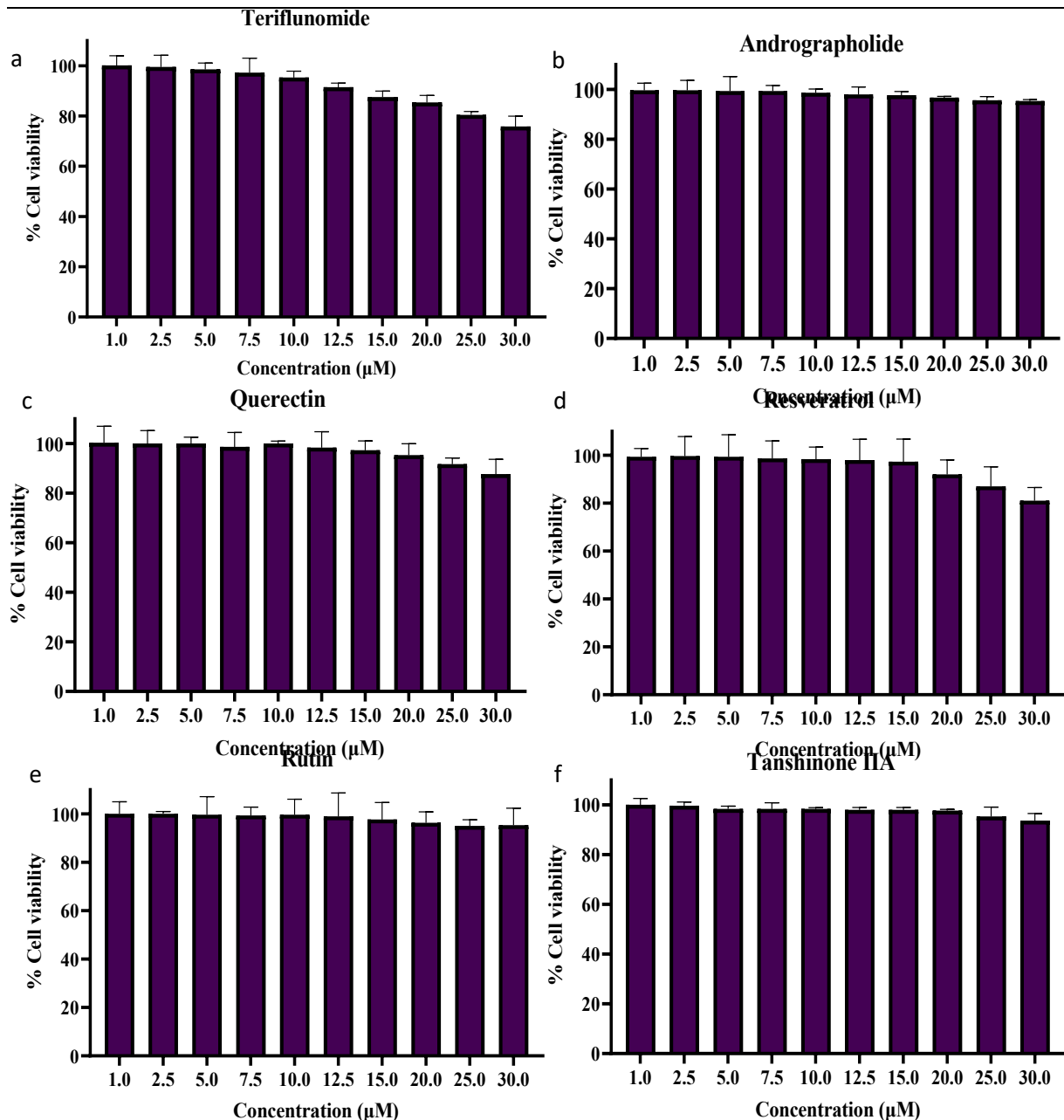
Figure 3.3. MTT assay of a) TFD; b) ANG; c) QCN; d) RES; e) RUT and f) TAN

The MTT assay results indicated that TFD, within the concentration range of 1-10 μM, demonstrated non-cytotoxicity. At 30 μM, it displayed 76 % cell viability, aligning with findings from Pandey et al. 2021. ANG demonstrated no cytotoxic effects within the tested concentration range of 1-30 μM. This corresponded with the observations of Chiou et al. 2000, who noted over 95% cell viability, even at a concentration as high as 50 μM. Similar findings were reported by Lee et. al 2011, where no cell death was observed at the concentration of 50 μM. [20,21]. QCN exhibited cell viability > 95 % with the concentration range of 1-20 μM which was comparable with the results reported by Endale et al. 2013 and

H.N Lee et al. 2018 [22,23]. RES at a concentration range of 1-20 µM was considered as non-cytotoxic and results were in accordance with previous study by Zong et al. 2012 [24]. Rutin exhibited no cytotoxic effects within the concentration range of 1-30 µM, consistent with Chen et al. 2001 report where no cell death was observed at 40 µM [25]. TAN also did not exhibited cytotoxicity 1-25 µM and the results were comparable with the Jang et al. 2006 [26].

3.4.2. NO assay

The MTT assay identified the safest concentration, ensuring cell viability exceeding 95%, which was subsequently utilized for conducting the NO assay. The % NO inhibition for the individual TFD and all natural products at different concentration ranges were tested. The first step entailed constructing the standard curve for NaNO$_2$, with concentration plotted on the X-axis and absorbance on the Y-axis. The regression equation was determined to be y= 0.0093x+ 0.0505 with regression coefficient of 0.999. and the respective graph is represented in **Figure 3.4**

.
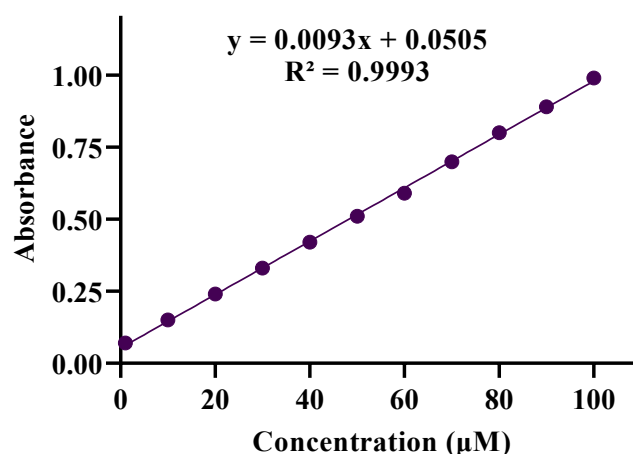
Figure 3.4. Calibration curve for NaNO$_2$

Further, the IC$_{50}$ values for the individual TFD and all the natural products were established *via* non-linear curve fit analysis using GraphPad Prism (version 9.1.0) from dose-response curve [27]. **Figure 3.5** depicts the dose-response curves for the individual TFD and natural products, with log concentration on the X-axis and % NO inhibition on the Y-axis**.** The IC$_{50}$ value for TFD was found to be 3.43 µM. The IC$_{50}$ value for ANG, was determined to be 19.27 µM, that closely aligned with the Chiou et al. 2001 [20]. The IC$_{50}$ value for QCN was found to be 12.08 µM, a result closely resembling to that reported by Yan et al. 2021 [28]. The IC$_{50}$ value of RES was found to be 15.07 µM, that closely aligned with the reported value by Cho et al. 2002 [29]. The IC$_{50}$ of RUT was determined to be 25.77 µM, while Chen

et al. 2001 reported a value of 41.5 µM. The IC_{50} value for TAN was determined to be 15.51 µM, that was consistent with the value reported by Jang et. al 2003 [30].
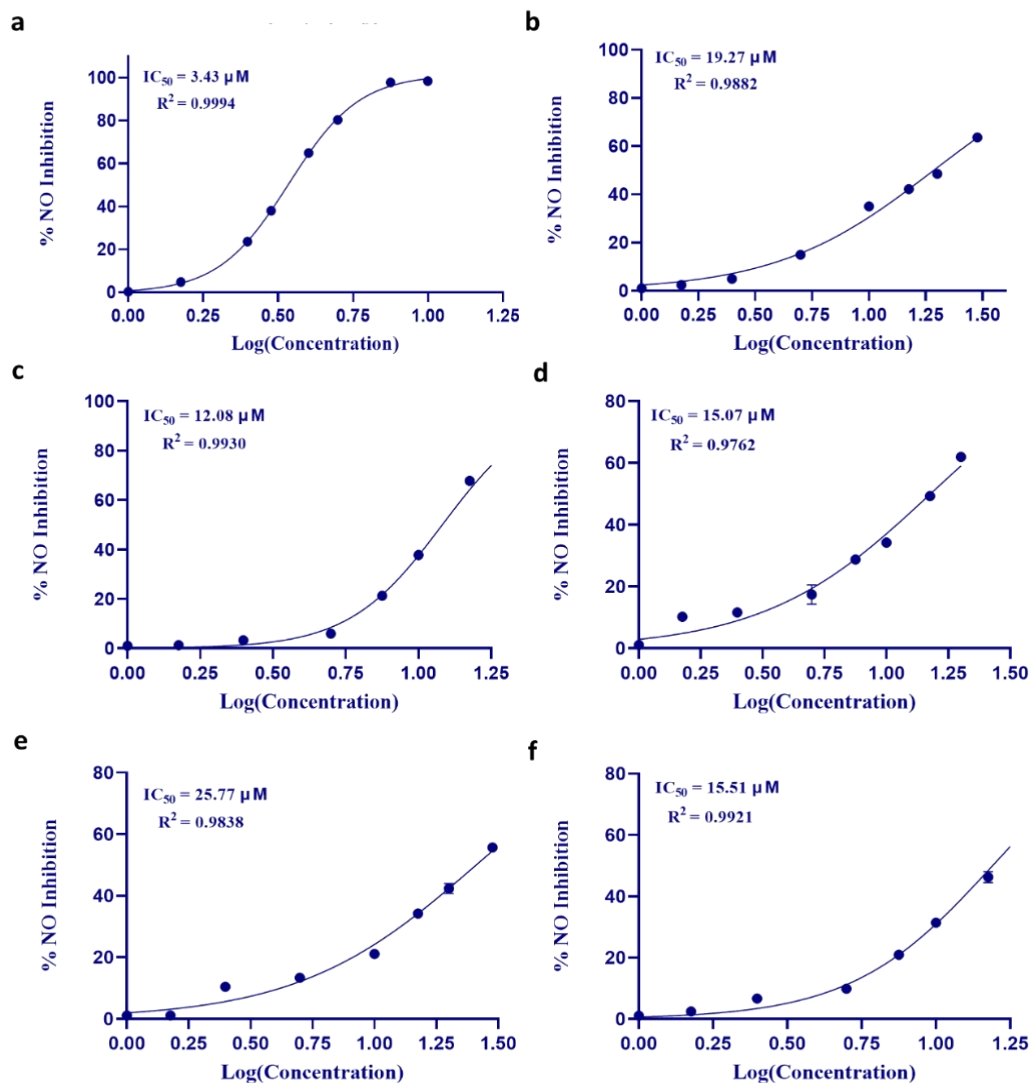
Figure 3.5. Dose-response curve analysis for the NO assay a) TFD; b) ANG; c) QCN; d) RES; e) RUT and f) TAN

3.4.3. Synergistic activity using NO assay

The MTT assay for all natural products in combination with TFD was initially conducted to assess their impact on cell viability in LPS-stimulated RAW 264.7 cells, with the results presented in **Table 3.1.** All combinations exhibited cell viability of approximately 90% or higher within the selected concentration range following LPS stimulation of RAW 264.7 cells.

Table 3.1. % Cell viability for the combinations in LPS stimulated RAW 264.7 cells

Name	% Cell viability at		
	3/4th IC_{50}	1/2nd IC_{50}	1/4th IC_{50}
TFD-ANG	90.16	91.96	93.25
TFD-QCN	90.54	93.26	95.19
TFD-RES	90.92	92.51	95.82
TFD-RUT	89.67	91.84	93.51
TFD-TAN	90.90	92.47	92.98

The synergistic activity of all natural products (ANG, QCN, RES, RUT and TAN) in combination with TFD was conducted using Compusyn software, utilizing the NO assay in LPS-stimulated RAW 264.7 cells. Initially the % nitrite inhibition at 3/4, 1/2, 1/4, of their respective IC_{50} was assessed individually and then for combination of natural products with TFD. The respective dose response curves for individual and combinations are represented in **Figure 3.6a and 3.6b,** respectively**.** Subsequently, a synergistic study for the NO was performed using a constant ratio design. The CI values corresponding to 50% inhibition (Fa = 0.50) were calculated using Compusyn software. The CI values ranged from 0.484 to 0.957 indicating synergistic activity for all the tested combinations. The respective CI plots have been depicted in **Figure 3.6c** and the values are represented in **Table 3.2**. TFD-QCN demonstrated the highest synergistic activity, followed by TFD-RES > TFD-TAN > TFA-RUT > TFD-ANG.

The isobologram analysis for the tested combinations is depicted in **Figure 3.7.** The individual doses of natural products and TFD to achieve Fa=0.9, Fa=0.75 and Fa=0.5 were calculated and shown as green, red and blue lines, respectively and the data was plotted on X-axis (for natural products) *Vs* y-axis (for TFD) using Compusyn software. As shown in **Figure 3.7**, the combination of natural products along with TFD to achieve Fa=0.9, Fa=0.75 and Fa=0.5 inhibition was present below the respective lines represented by green triangle, red square and blue circle symbols, respectively. Thus, results proved that all tested combinations exhibited synergistic activity. However, from the image, it is evident that the dose required to exhibit synergy varied. For e.g. QCN requires a lower dose (as indicated by its narrow plot) when compared to RUT that requires a higher dose (as indicated by its broader plot) when combined with TFD.
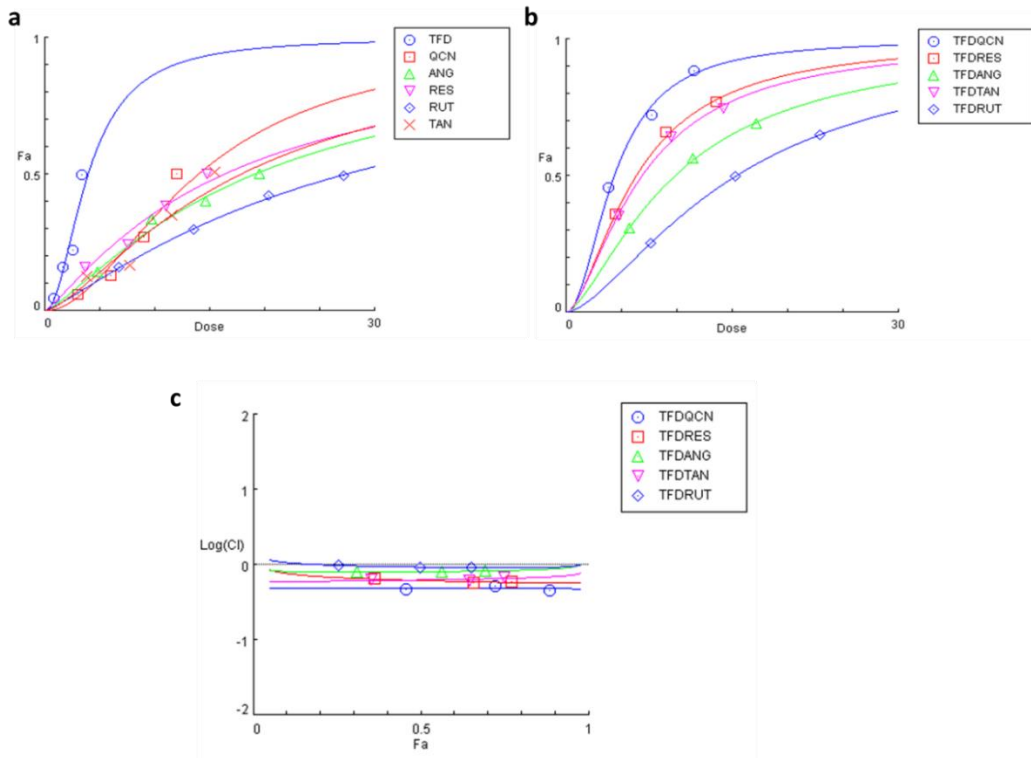
Figure 3.6. Dose-response curve using NO assay for a) TFD and natural products individually; b) natural products in combination with TFD; c) CI plots
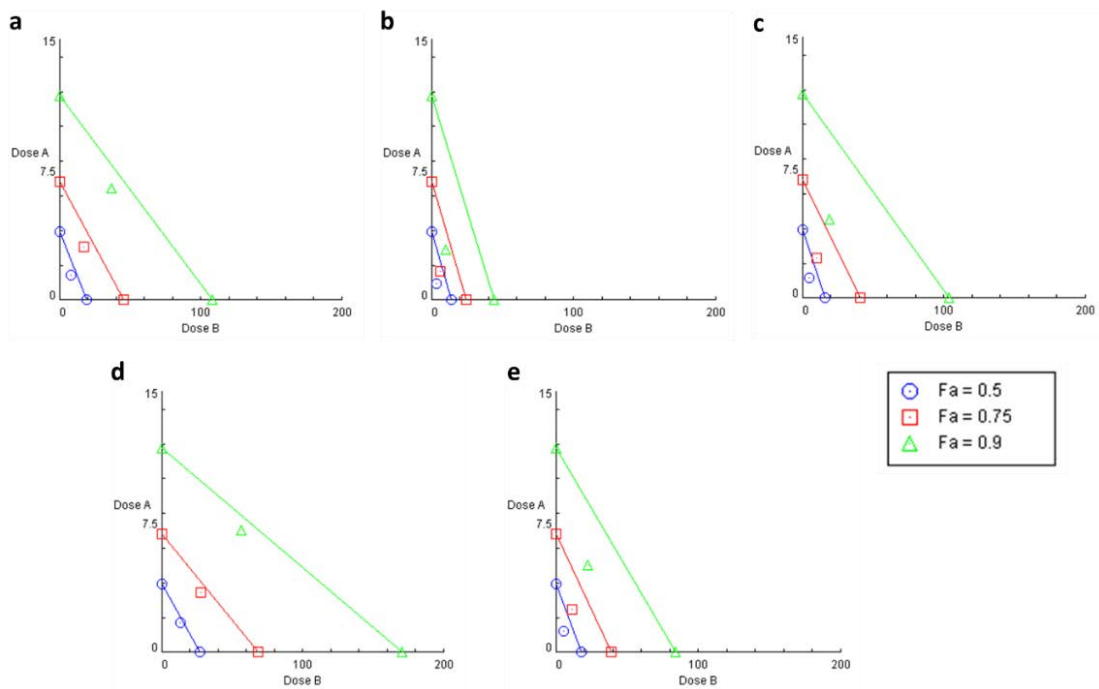
Figure 3.7. Isobologram analysis using NO assay for a) TFD & ANG; b) TFD & QCN; c) TFD & RES; d) TFD & RUT; e) TFD & TAN

The DRI values for all combinations were calculated and are presented in **Figure 3.8** and in the corresponding **Table 3.2**.
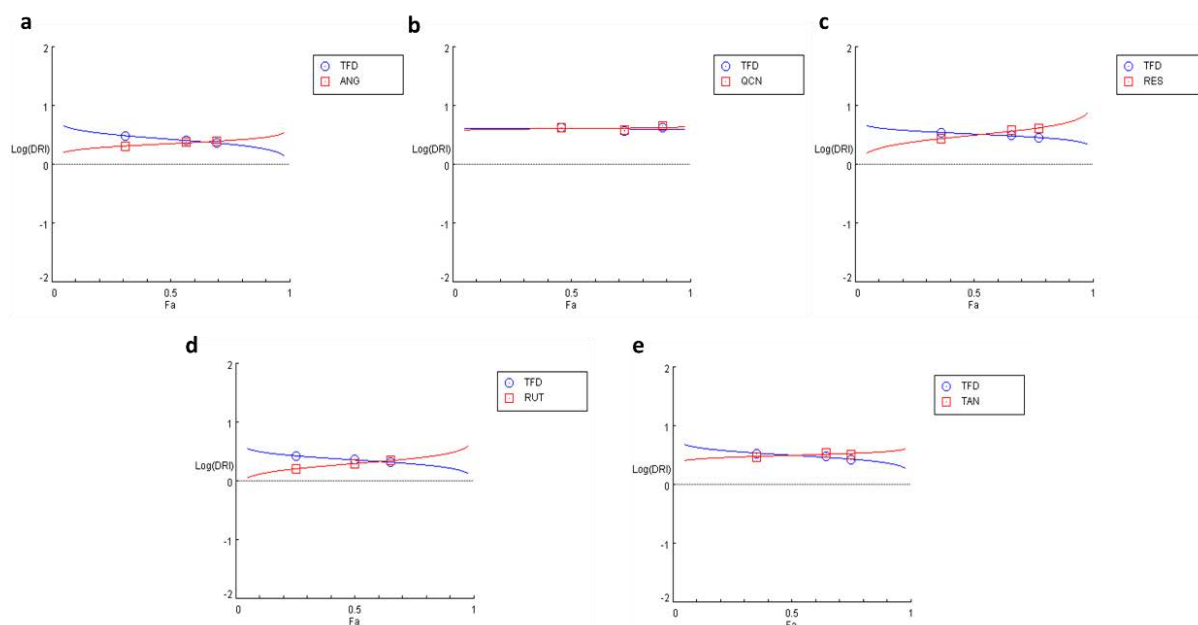
Figure 3.8. DRI plots for a) TFD & ANG; b) TFD & QCN; c) TFD & RES; d) TFD & RUT; e) TFD & TAN using NO assay

From the above data, it is evident that the DRI_{TFD} was high for TFD-QCN combination with the value of 4.09 (Fa= 0.5).

Table 3.2. Inhibitory activity of individual and combinations for synergistic effect against NO

Natural Products	Combination ratio [TFD : Natural product]	CI value	DRI TFD
ANG	1: 5.7	0.809	2.69
QCN	1: 3.5	**0.487**	4.09
RES	1: 4.3	0.617	3.30
RUT	1: 8	0.933	2.30
TAN	1: 4.5	0.628	3.18

The polygonogram depicted in **Figure 3.9** illustrates a notably thicker line associated with the TFD-QCN combination, indicating more synergy compared to other combinations. Conversely, the TFD-RUT combination shows a thinner line, suggesting comparatively less

synergy. This visual representation may signify the varying degrees of synergistic activity among different combinations in targeting inflammatory pathways.
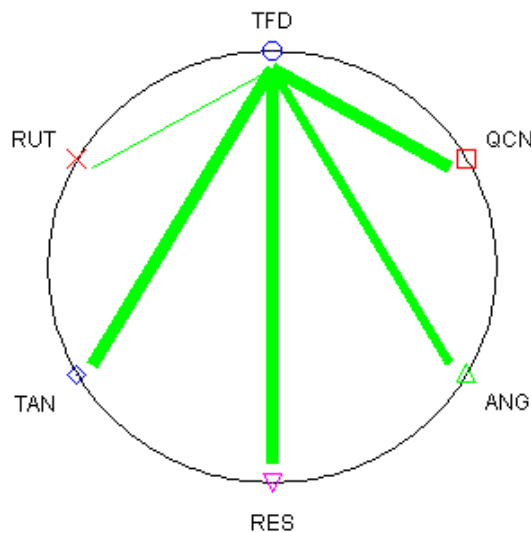
Figure 3.9. Polygonogram

The analysis of CI index, isobologram, and polygonogram collectively demonstrates that the TFD-QCN combination, at a ratio of 1:3.5, exhibited superior synergistic activity compared to the other combinations assessed. Specifically, the combination of TFD-QCN demonstrated the lowest CI values of 0.487 at Fa=0.5, indicative of greater synergistic activity. Moreover, the DRI values further supports this by demonstrating that the use of QCN could potentially enable a more significant reduction in dose of TFD in the combination. Followed by this, TFD-RES combination and TFD-TAN showed synergistic activity with CI values of 0.617 and 0.628 respectively. Furthermore, based on their CI values, the combinations of TFD-QCN, TFD-RES, and TFD-TAN were chosen for evaluating their activity against TNF-α and IL-6 in RAW 264.7 cells.

3.4.4. Determination of proinflammatory cytokines inhibition

The inhibitory potential against proinflammatory cytokines (TNF-α and IL-6) was evaluated for the combinations of TFD-QCN, TFD-RES, and TFD-TAN in RAW 264.7 cells at the ratio of 1:3.5, 1:4.4 and 1:4.5, respectively. **Figures 3.10** depict the inhibitory activity of these combinations against TNF-α and IL-6.
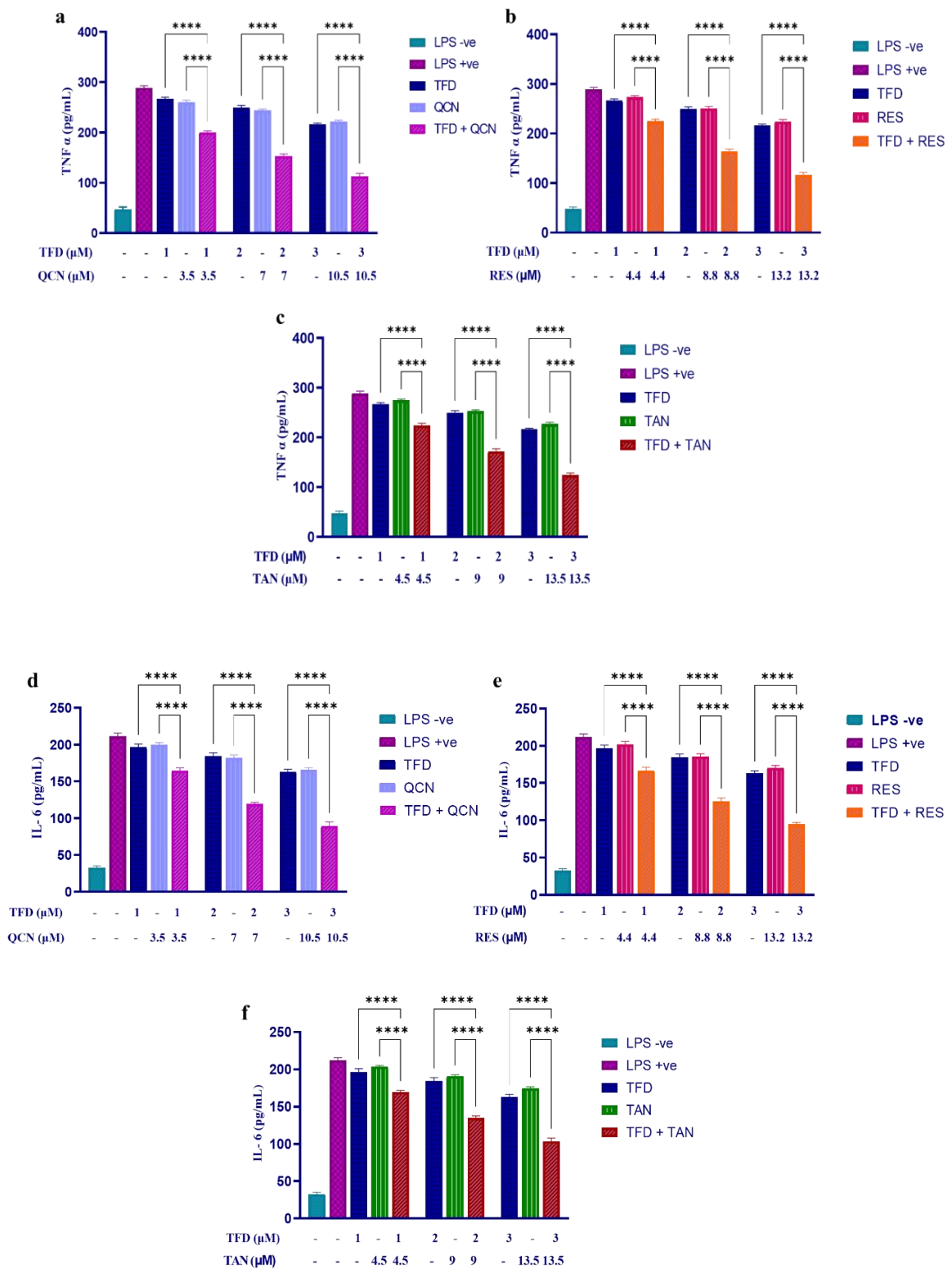
Figure 3.10. Inhibitory activity against TNF-α for a) TFD-QCN; b) TFD-RES; c) TFD-TAN; and Inhibitory activity against IL-6 for d) TFD-QCN; e) TFD-RES; and f) TFD-TAN (n=3, Mean ± SD). **** $p < 0.0001$; *** $p < 0.001$; ** $p < 0.01$; * $p < 0.05$

The baseline levels of TNF-α and IL-6 were 47.60 ± 4.07 pg/mL and 32.38 ± 2.85 pg/mL respectively. However, upon LPS stimulation, these levels increased significantly to 289.90 ± 2.71 pg/mL for TNF-α and 211.75 ± 3.96 pg/mL for IL-6. Treatment with the combination of TFD-QCN, TFD-RES, and TFD-TAN showed a statistically significant difference ($p < 0.0001$) compared to individual treatments against both TNF-α and IL-6 across all three tested concentration ranges, demonstrating dose-dependent activity. The TFD-QCN (at a concentration of 3µM of TFD and 10.5 µM of QCN) exhibited decreased TNF-α and IL-6 level with the values of 112.15 ± 4.08 pg/mL, 89.37 ± 5.46 pg/mL respectively. For TFD-RES (at a concentration of 3µM of TFD and 13.2 µM of RES) resulted in 125.99 ± 2.61 pg/mL, 99.52 ± 2.18 pg/mL for TNF-α and IL-6 respectively. Similarly, for TFD-TAN (at a concentration of 3µM of TFD and 13.5 µM of TAN) resulted in 129.00 ± 2.69 pg/mL for TNF-α , 103.00 ± 4.27 pg/mL for IL-6.

Additionally, the CI values were computed for the above combinations for TNF-α and IL-6 inhibition**.** The data indicated that the TFD-QCN combination demonstrated greater synergistic activity in comparison to TFD-RES and TFD-TAN. Specifically, TFD-QCN exhibited synergistic activity with CI values of 0.470 and 0.607 (at Fa = 0.5) for TNF-α and IL-6 inhibition, respectively. TFD-RES demonstrated CI values of 0.651 and 0.640, whereas for TFD-TAN, the values were 0.699 and 0.693 for inhibition of TNF-α and IL-6, respectively. The corresponding CI plots are represented in **Figure 3.11.**
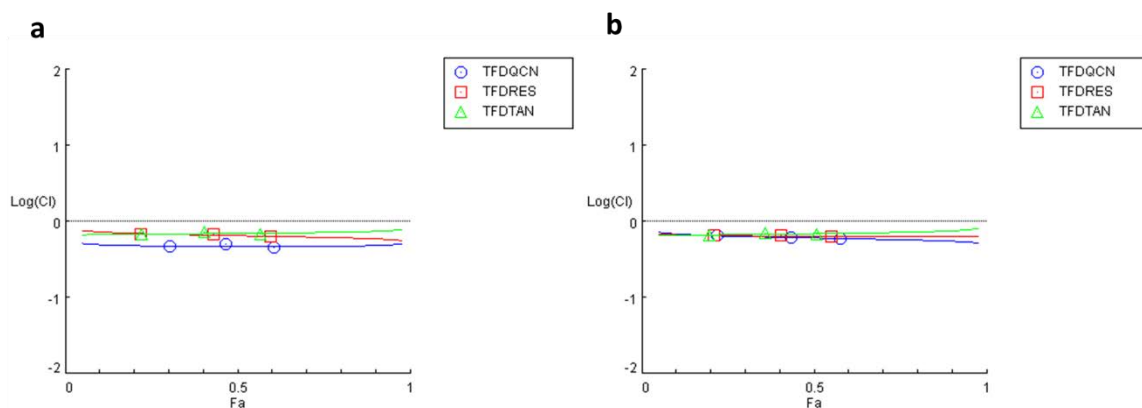
Figure 3.11. CI plots of combinations for the inhibitory activity against a) TNF-α; b) IL-6 production

3.4.5. Determination of intracellular ROS

3.3.5.1. Fluorescence intensity

Given that the TFD-QCN combination demonstrated superior synergistic activity in both the NO assay and proinflammatory cytokine assessments, this particular combination was chosen for subsequent evaluation of intracellular ROS levels using DCFDA. The combination of TFD and QCN at a ratio of 1:3.5 was tested across three concentration ranges. The relative fluorescence intensity of the tested combination is depicted in **Figure 3.12a.** The data revealed a dose-dependent activity of the combination, demonstrating a statistically significant difference ($p < 0.001$) in their ability to inhibit ROS generation for the combination when compared to both individual treatments.

3.3.5.2. Fluorescence microscopy

The acquired fluorescence images for the TFD,QCN and their combinations at different concentrations are represented in **Figure 3.12b.** From the data it is evident that the combination of TFD-QCN exhibited a decrease in ROS production significantly ($p < 0.001$) as compared to both TFD and QCN individually, consequently mitigating the oxidative stress within the cell.

As the TFD-QCN combination exhibited significant synergistic activity, understanding the mechanism is crucial. The mechanism of TFD is well established *via* inhibition of DHODH and cell proliferation. It has been reported to inhibit JAK/STAT and NF-κB pathways in T cells. QCN is reported exhibits of immune-mediated responses by balancing TH17 cells and Tregs. It is also reported to inhibits NF-κB, adenosine deaminase, MAPK signaling pathways [31,32]. Addition to this, the QCN exhibits bone-protective effects by inhibiting MMPs, RANKL production, COX-2, and PGE$_2$ production [32]. Macrophages have been observed to manifest inflammation through diverse pathways, including NF-κB, MAPK, PI3K/Akt, and JAK/STAT [33]. The observed anti-inflammatory effects of the TFD-QCN combination against NO, TNF-α, and IL-6 in RAW 264.7 cells may stem from its modulation of these diverse signaling pathways. Additionally, TFD is known to induce hepatotoxicity upon oral administration. However, the high DRI values obtained for the TFD-QCN combination using the NO assay suggested the potential for reducing the dose of TFD, which could help mitigate the adverse effects associated with TFD.
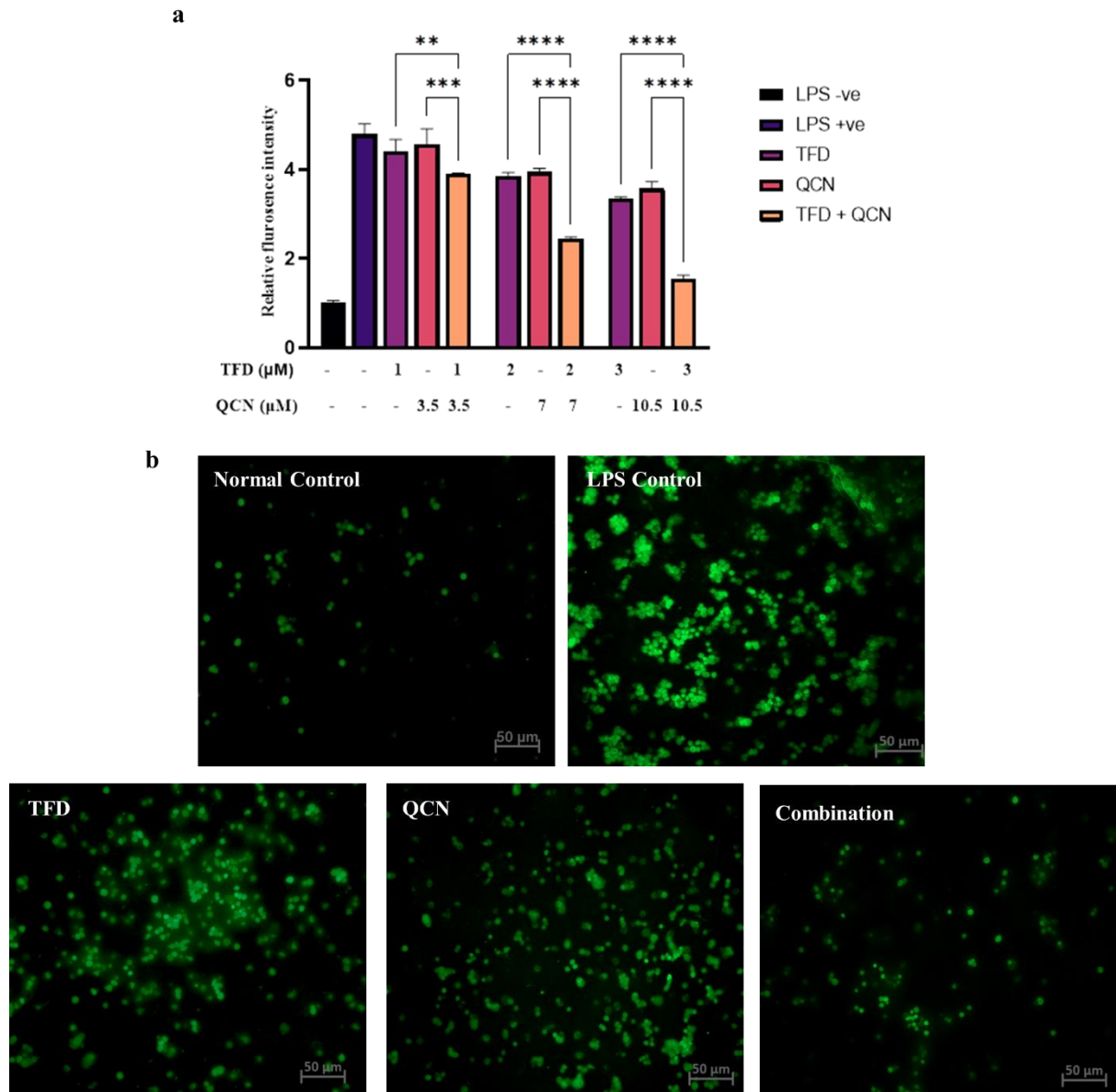
Figure 3.12. a) Fluorescence intensity (n=3, Mean ± SD); b) Fluorescence images for of TFD-QCN combination against ROS production in LPS stimulated RAW 264.7 cells

**** $p < 0.0001$; *** $p < 0.001$; ** $p < 0.01$; * $p < 0.05$

3.5. Conclusion

The current study demonstrates the effectiveness of combination therapy in combating the inflammatory responses produced by the macrophage cell line upon stimulation. The combination of TFD along with the natural products were tested in RAW 264.7 cells. Specifically, among the tested natural products such as ANG, QCN, RES, RUT, and TAN, the TFD-QCN combination emerged as the most potent, exhibiting significant synergistic activity against NO inhibition compared to other combinations. The low CI value and high DRI value for TFD-QCN demonstrate that the combination is effective and may lead to a dose reduction of TFD, indicating its potential for optimizing therapeutic outcomes. Also, the combination of TFD-QCN demonstrated a synergistic reduction in TNF-α, and IL-6 production in LPS-stimulated RAW 264.7 cells. Furthermore, the combination of TFD-QCN resulted in reduction in ROS, indicating a promising therapeutic approach for treating RA by mitigating inflammation resulting from oxidative stress. Based on the findings from the synergy studies, TFD and QCN were chosen for the analytical method development using UV and HPLC, as well as for the development and evaluation of topical formulation.

Chapter 3

References

1. Laria, A., Lurati, A., Marrazza, M., Mazzocchi, D., Re, K. A., & Scarpellini, M. (2016). The macrophages in rheumatic diseases. *Journal of Inflammation Research*, *9*, 1–11.

2. Woo, C.-H., Lim, J.-H., & Kim, J.-H. (2004). Lipopolysaccharide induces matrix metalloproteinase-9 expression via a mitochondrial reactive oxygen species-p38 kinase-activator protein-1 pathway in RAW 264.7 cells. *Journal of Immunology 173*(11), 6973–6980.

3. Kwon, D. H., Cha, H. J., Lee, H., Hong, S. H., Park, C., Park, S. H., Kim, G. Y., Kim, S., Kim, H. S.,& Choi, Y. H. (2019). Protective Effect of glutathione against oxidative stress-induced cytotoxicity in RAW 264.7 macrophages through activating the nuclear factor erythroid 2-related factor-2/heme oxygenase-1 pathway. *Antioxidants*, *8*(4), 82.

4. Chen, J., Li, D. L., Xie, L. N., Ma, Y. ran, Wu, P. P., Li, C., Liu, W. F., Zhang, K., Zhou, R. P., Xu, X. T., Zheng, X., & Liu, X. (2020). Synergistic anti-inflammatory effects of silibinin and thymol combination on LPS-induced RAW264.7 cells by inhibition of NF-κB and MAPK activation. *Phytomedicine*, *78*, 153309.

5. Yokota, K., Sato, K., Miyazaki, T., Aizaki, Y., Tanaka, S., Sekikawa, M., Kozu, N., Kadono, Y., Oda, H., & Mimura, T. (2021). Characterization and function of tumor necrosis factor and interleukin-6-induced osteoclasts in rheumatoid arthritis. *Arthritis & Rheumatology* , *73*(7), 1145–1154.

6. Lee, S. Bin, Lee, W. S., Shin, J. S., Jang, D. S., & Lee, K. T. (2017). Xanthotoxin suppresses LPS-induced expression of iNOS, COX-2, TNF-α, and IL-6 via AP-1, NF-κB, and JAK-STAT inactivation in RAW 264.7 macrophages. *International Immunopharmacology*, *49*, 21–29.

7. Ulrich-Merzenich, G. S. (2014). Combination screening of synthetic drugs and plant derived natural products. Potential and challenges for drug development. *Synergy*, *1*(1), 59–69.

8. Haleagrahara, N., Hodgson, K., Miranda-Hernandez, S., Hughes, S., Kulur, A. B., & Ketheesan, N. (2018). Flavonoid quercetin-methotrexate combination inhibits inflammatory mediators and matrix metalloproteinase expression, providing protection to joints in collagen-induced arthritis. *Inflammopharmacology*, *26*(5), 1219–1232.

9. Tundis, R., Bonesi, M., Deguin, B., Loizzo, M. R., Menichini, F., Conforti, F., Tillequin, F., & Menichini, F. (2009). Cytotoxic activity and inhibitory effect on nitric oxide production of triterpene saponins from the roots of Physospermum verticillatum (Waldst & Kit) (Apiaceae). *Bioorganic & Medicinal Chemistry*, *17*(13), 4542–4547.

10. Cho, H., Yun, C. W., Park, W. K., Kong, J. Y., Kim, K. S., Park, Y., Lee, S., & Kim, B. K. (2004). Modulation of the activity of pro-inflammatory enzymes, COX-2 and iNOS, by chrysin derivatives. *Pharmacological Research*, *49*(1), 37–43.

11. Tenuta, M. C., Deguin, B., Loizzo, M. R., Dugay, A., Acquaviva, R., Malfa, G. A., Bonesi, M., Bouzidi, C., & Tundis, R. (2020). Contribution of flavonoids and iridoids to the hypoglycaemic, antioxidant, and nitric oxide (NO) Inhibitory activities of Arbutus unedo L. *Antioxidants*, *9*(2), 184.

12. Chou, T. C. (2006). Theoretical basis, experimental design, and computerized simulation of synergism and antagonism in drug combination studies. *Pharmacological Reviews*, *58*(3), 621–681.

13. Kamran, S., Sinniah, A., Chik, Z., & Alshawsh, M. A. (2022). Diosmetin exerts synergistic effects in combination with 5-fluorouracil in colorectal cancer cells. *Biomedicines*, *10*(3), 531.

14. Hong, S., Dia, V. P., & Zhong, Q. (2021). Synergistic anti-inflammatory activity of apigenin and curcumin co-encapsulated in caseins assessed with lipopolysaccharide-stimulated RAW 264.7 macrophages. *International Journal of Biological Macromolecules*, *193*, 702–712.

15. George, G., Sridhar SNC, S., & Paul, A. T. (2020). Investigation of synergistic potential of green tea polyphenols and orlistat combinations using pancreatic lipase assay-based synergy directed fractionation strategy. *South African Journal of Botany*, *135*, 50–57.

16. Matsuno, H., Yudoh, K., Katayama, R., Nakazawa, F., Uzuki, M., Sawai, T., Yonezawa, T., Saeki, Y., Panayi, G. S., Pitzalis, C., & Kimura, T. (2002). The role of TNF-alpha in the pathogenesis of inflammation and joint destruction in rheumatoid arthritis (RA): A study using a human RA/SCID mouse chimera. *Rheumatology*, *41*(3), 329–337.

17. Srirangan, S., & Choy, E. H. (2010). The role of interleukin 6 in the pathophysiology of rheumatoid arthritis. *Therapeutic Advances in Musculoskeletal Disease*, *2*(5), 247–256.

18. Wang, X., Fan, D., Cao, X., Ye, Q., Wang, Q., Zhang, M., & Xiao, C. (2022). The role of reactive oxygen species in the rheumatoid arthritis-associated synovial microenvironment. *Antioxidants*, *11*(6), 1153.

19. Baek, S. H., Cho, Y., Lee, J., Choi, B. Y., Choi, Y., Park, J. S., Kim, H., Sul, J., Kim, E., Park, J. H., & Jo, D.-G. (2018). Intracellular and mitochondrial reactive oxygen species measurement in primary cultured neurons. *Bio-Protocol*, *8*(11), e2871.

20. Chiou, W. F., Chen, C. F., & Lin, J. J. (2000). Mechanisms of suppression of inducible nitric oxide synthase (iNOS) expression in RAW 264.7 cells by andrographolide. *British*

Journal of Pharmacology, *129*(8), 1553–1560.

21. Lee, K. C., Chang, H. H., Chung, Y. H., & Lee, T. Y. (2011). Andrographolide acts as an anti-inflammatory agent in LPS-stimulated RAW264.7 macrophages by inhibiting STAT3-mediated suppression of the NF-κB pathway. *Journal of Ethnopharmacology*, *135*(3), 678–684.

22. Endale, M., Park, S. C., Kim, S., Kim, S. H., Yang, Y., Cho, J. Y., & Rhee, M. H. (2013). Quercetin disrupts tyrosine-phosphorylated phosphatidylinositol 3-kinase and myeloid differentiation factor-88 association, and inhibits MAPK/AP-1 and IKK/NF-κB-induced inflammatory mediators production in RAW 264.7 cells. *Immunobiology*, *218*(12), 1452–1467.

23. Lee, H. N., Shin, S. A., Choo, G. S., Kim, H. J., Park, Y. S., Kim, B. S., Kim, S. K., Cho, S. D., Nam, J. S., Choi, C. S., Che, J. H., Park, B. K., & Jung, J. Y. (2018). Anti-inflammatory effect of quercetin and galangin in LPS-stimulated RAW264.7 macrophages and DNCB-induced atopic dermatitis animal models. *International Journal of Molecular Medicine*, *41*(2), 888–898.

24. Zong, Y., Sun, L., Liu, B., Deng, Y. S., Zhan, D., Chen, Y. L., He, Y., Liu, J., Zhang, Z. J., Sun, J., & Lu, D. (2012). Resveratrol Inhibits LPS-Induced MAPKs activation via activation of the phosphatidylinositol 3-kinase pathway in murine RAW 264.7 macrophage cells. *PloS One*, *7*(8), e44107.

25. Chen, Y. C., Shen, S. C., Lee, W. R., Hou, W. C., & Lee, T. J. F. (2001). Inhibition of nitric oxide synthase inhibitors and lipopolysaccharide induced inducible NOS and cyclooxygenase-2 gene expressions by rutin, quercetin, and quercetin pentaacetate in RAW 264.7 macrophages. *Journal of Cellular Biochemistry*, *82*(4), 537–548.

26. Il Jang, S., Jin Kim, H., Kim, Y. J., Jeong, S. Il, & You, Y. O. (2006). Tanshinone IIA inhibits LPS-induced NF-kappaB activation in RAW 264.7 cells: Possible involvement of the NIK-IKK, ERK1/2, p38 and JNK pathways. *European Journal of Pharmacology*, *542*(1–3), 1–7.

27. Marques, R. V., Sestito, S. E., Bourgaud, F., Miguel, S., Cailotto, F., Reboul, P., Jouzeau, J. Y., Rahuel-Clermont, S., Boschi-Muller, S., Simonsen, H. T., & Moulin, D. (2022). Anti-Inflammatory activity of bryophytes extracts in LPS-stimulated RAW264.7 Murine macrophages. *Molecules*, *27*(6), 1940.

28. Yan, X. L., Fan, R. Z., Sang, J., Xie, X. L., Tang, G. H., & Yin, S. (2021). Euphanoids A and B, two new lathyrane diterpenoids with nitric oxide (NO) inhibitory activity from Euphorbia kansuensis. *Natural Product Research*, *35*(22), 4402–4408.

29. Cho, D. I., Koo, N. Y., Chung, W. J., Kim, T. S., Ryu, S. Y., Im, S. Y., & Kim, K. M. (2002). Effects of resveratrol-related hydroxystilbenes on the nitric oxide production in macrophage cells: Structural requirements and mechanism of action. *Life Sciences*, *71*(17), 2071–2082.

30. Jang, S. Il, Jeong, S. Il, Kim, K. J., Kim, H. J., Yu, H. H., Park, R., Kim, H. M., & You, Y. O. (2003). Tanshinone IIA from Salvia miltiorrhiza inhibits inducible nitric oxide synthase expression and production of TNF-α, IL-1β and IL-6 in activated RAW 264.7 cells. *Planta Medica*, *69*(11), 1057–1059.

31. Sung, M. S., Lee, E. G., Jeon, H. S., Chae, H. J., Park, S. J., Lee, Y. C., & Yoo, W. H. (2012). Quercetin inhibits IL-1β-induced proliferation and production of MMPs, COX-2, and PGE2 by rheumatoid synovial fibroblast. *Inflammation*, *35*(4), 1585–1594.

32. Tang, M., Zeng, Y., Peng, W., Xie, X., Yang, Y., Ji, B., & Li, F. (2022). Pharmacological aspects of natural quercetin in rheumatoid arthritis. *Drug Design, Development and Therapy*, *16*, 2053.

33. Xu, N., Yuan, H., Liu, W., Li, S., Liu, Y., Wan, J.,& Chang, Y. (2013). Activation of RAW264.7 mouse macrophage cells in vitro through treatment with recombinant ricin toxin-binding subunit B: Involvement of protein tyrosine, NF-κB and JAK-STAT kinase signaling pathways. *International Journal of Molecular Medicine*, 32(3), 729–735

Chapter 4

Analytical Method Development and Validation

87

(a) Simultaneous Estimation of Teriflunomide and Querectin using UV- visible Spectrophotometric Approach Utilizing the Absorption Factor Method

Chapter 4

4.1. Introduction

The UV spectrophotometer that is known for its simplicity and cost-effectiveness, measures ultraviolet light absorption to quantify analytes in various fields like chemistry, biology, and pharmaceuticals [1]. Its ease of use and affordability make it indispensable for laboratories, ensuring efficient and reliable sample analysis. UV methods for both TFD and QCN have been reported previously [2–4], but to the best of our knowledge no UV method has been reported for the simultaneous estimation of both drugs. Multicomponent UV spectroscopy, through the simultaneous analysis of distinct absorption spectra from sample mixture, is extensively applied in chemical analysis for the identification and quantification of analytes within mixtures. The discriminative capability of UV spectroscopy facilitates the efficient investigation of intricate sample compositions. The utilization of this technique guarantees precise multicomponent analysis, establishing it as a valuable asset in the field of analytical chemistry [5,6].

In the realm of analytical chemistry, numerous multicomponent spectroscopic methods have been developed for the simultaneous determination of multiple substances within complex mixtures. These includes, simultaneous equation method, absorbance ratio spectra, absorptivity factor method, derivative ratio spectra, derivative spectrophotometry, difference spectrophotometry, Q-absorbance ratio method, successive ratio-derivative spectra, dual wavelength method, isosbestic point method and multivariate chemometric methods [7,8]. In the specific context of analyzing TFD and QCN in a sample mixture, the "absorption factor method" was chosen as the preferred technique [9,10]. This method has been applied for the multiple components in a binary mixture containing X & Y with absorption maxima of λ_x and λ_y respectively, and especially when an overlapped spectra is observed. In this method, X does not show interference at the λ_y but Y shows interfere at the λ_x. As X does not exhibit any interference at λ_y, the concentration of Y can be directly found at the λ_y, while the concentration X in a binary mixture can be calculated by following equation 4.1.1[5,6].

$$Absorption\ of\ X\ at\ \lambda\text{x} = A_{x+y}\lambda_{x1} - \frac{A_{y1}\lambda_{x1}}{A_{y1}\lambda_{y2}} \times A_{x+y}\lambda_{y1} \qquad \text{…eq.4.1.1}$$

Where, $A_{x+y}\lambda_{x1}$ is Absorption of mixture at λ_x

$A_{y1}\lambda_{x1} / A_{y1}\lambda_{y1}$ is Absorption factor for Y

$A_{x+y}\lambda_{y1}$ is Absorption of mixture at λ_y

To find out the absorption factor for Y, different standard solutions of Y are scanned through the entire UV region, and the average value of absorbance are noted and calculated by using following equation 4.1.2

$$Absorption\ factor = \frac{A_{y1}\lambda_{x1}}{A_{y1}\lambda_{y1}} \qquad \text{...eq 4.1.2}$$

Where, $A_{y1}\lambda_{x1}$ – is Absorption of Y at λ_x

$A_{y1}\lambda_{y1}$ – is Absorption of Y at λ_y

The aim of the study was to develop a validated UV spectroscopic method for the simultaneous estimation of TFD and QCN by applying the absorption factor method.

4.1.1. Materials and Methods

As mentioned in chapter 3, TFD (99.9% pure) was obtained as a gift sample from the MSN Laboratories Private Limited (Sangareddy, India). QCN (> 98% purity) was purchased from Yucca Enterprises (Mumbai, India). Analytical grade solvents such as acetonitrile and methanol were purchased from Merck Life Sciences. All other chemicals used were of analytical grade.

4.1.1.1. Instrument

UV-Visible spectrophotometer (Jasco V-750, Japan) utilizing Spectra Manager software with a spectral bandwidth of 1 nm was employed for all spectroscopic measurements, using a pair of 1.0 cm quartz cells.

4.1.1.2. Method development

Acetonitrile was selected as a common solvent for studying spectral characteristics of the selected drugs. A standard stock solution (1 mg/mL) of TFD and QCN were made separately in the acetonitrile. A primary stock solution (100 µg/mL) was prepared from the standard stock solutions (1 mg/mL) using acetonitrile. Further 10µg/mL was prepared from primary stock solution and used for the determination of λ_{max}. The samples were scanned through entire UV-Visible region (200-800 nm) using UV spectrophotometer in the full spectrum mode.

4.1.1.3. Method validation

The developed method was validated for linearity, range, accuracy, precision, limit of detection (LOD), limit of quantification (LOQ), selectivity, robustness, and ruggedness as per the International Council for Harmonisation of Technical Requirements for Pharmaceuticals for Human Use (ICH Q2(R1)) guidelines [11].

Linearity, range, LOD and LOQ

Six calibration standards (2, 4, 6, 8, 10, 12 µg/mL) for TFD as well as for QCN were prepared separately in the acetonitrile and analyzed for evaluating the linearity of the developed method at their respective λ_{max}. (n=3). A linearity curve was plotted with concentration on X-axis and absorbance on Y-axis with the obtained data. From the linearity curve the regression analysis i.e., slope, intercept, and correlation coefficient (r^2) were determined. The obtained results are

considered as acceptable only if the r² value was ≥ 0.99. LOD and LOQ of the drug were derived by calculating the signal-to-noise ratio (S/N ratio of 3.3 for LOD and 10 for LOQ) using the following equations (4.1.3 and 4.1.4) designated by ICH.

$$LOD = 3.3 \times \frac{\sigma}{S} \qquad \qquad \text{...eq 4.1.3}$$

$$LOQ = 10 \times \frac{\sigma}{S} \qquad \qquad \text{...eq 4.1.4}$$

Where "σ" indicates standard deviation of the response and "S" indicates slope of the calibration curve. Both σ and S were determined using Standard Error of estimates (STEYX) in linear regression [12,13]. The range was determined for both TFD and QCN with acceptable linearity, accuracy, and precision.

Accuracy

To ascertain the accuracy of the proposed method, recovery study was carried out by the standard addition method at three different levels i.e., 50, 100 and 150 % representing the concentrations of 2, 6 and 8 µg/mL for both TFD and QCN separately in acetonitrile. The study was performed in triplicates by spiking a standard solution of 2 µg/mL of each drug into the respective samples.

Precision

Precision was studied to find out intra and inter-day variations in the test method for TFD and QCN. The samples were run in triplicates on the same day at three different time points (Intra-day) and for three days (Inter-day) at three different concentration levels and % RSD (relative standard deviation) was calculated.

Robustness

Robustness of the proposed method was carried out by making a deliberate changes in λmax (±2) for both TFD and QCN. The absorbance of the samples at different wavelengths were analyzed at three different levels in triplicates and results were mentioned in terms of % RSD

Ruggedness

The ruggedness of the developed method was carried out to check the reproducibility under normal and expected operated conditions using UV Spectrophotometer by operating with different analysts on different days. The samples were analyzed in triplicates at three different levels and the results were depicted in terms of % RSD.

4.1.1.4. Selectivity of the method using Absorption factor method

The selectivity of the proposed method using absorption factor method was initially applied for the estimation of individual components in a laboratory prepared mixtures in different ratios

(1:1; 2:1; 3:1 and 4:1 ratio of TFD to QCN) [5,6]. A minimum of four standards solutions of QCN i.e., 4, 6, 8,10 µg/mL were analyzed through the entire UV range (200-400 nm) and average value of absorption factor was calculated using equation 4.1.5.

$$Absorption\ factor = \frac{A_{y1}\lambda_{x1}}{A_{y1}\lambda_{y1}}$$ ...eq 4.1.5

Where, $A_{y1}\lambda_{x1}$ – Absorption of QCN at 280nm

$A_{y1}\lambda_{y1}$ – Absorption of QCN at 367nm

4.1.2. Results and Discussion

4.1.2.1. Method development

Various solvents, including methanol, ethanol, and acetonitrile, were employed in the method development. Among these, acetonitrile was chosen due to the favorable solubility of both analytes in this solvent. A standard solution of 10 µg/mL for both TFD and QCN in acetonitrile was scanned through the entire UV range of 200-800 nm and full spectrum was shown in **Figure 4.1.1**. From the UV spectrum, the λ_{max} of TFD was found to be 280 nm and for QCN it was found to be 367 nm. Absorption factor method was applied for the simultaneous estimation of TFD and QCN in a binary mixture because QCN showed interference at the λ_{max} of TFD, while TFD didn't showed any interference at the λ_{max} of QCN.
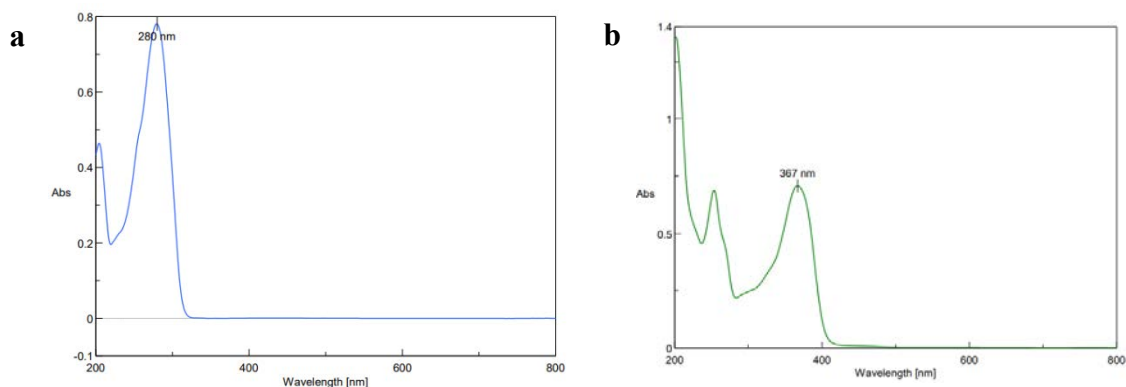
Figure 4.1.1. UV-visible spectrum of a) TFD and b) QCN

4.1.2.2. Method validation

Linearity, range, LOD and LOQ

The developed method was linear with the concentrations of 2, 4, 6, 8, 10 and 12 µg/mL for both TFD and QCN (n=3), as with the increase in concentration absorbance also increased. The regression coefficient (r^2) value was found to be 0.9982 for TFD and 0.9993 for QCN. The

linear regression equation were determined as y = 0.08038x – 0.01146 and y = 0.06536x + 0.00427 for TFD and QCN, respectively. The linearity graph (Concentration vs Absorbance) for both drugs are shown in **Figure 4.1.2**.
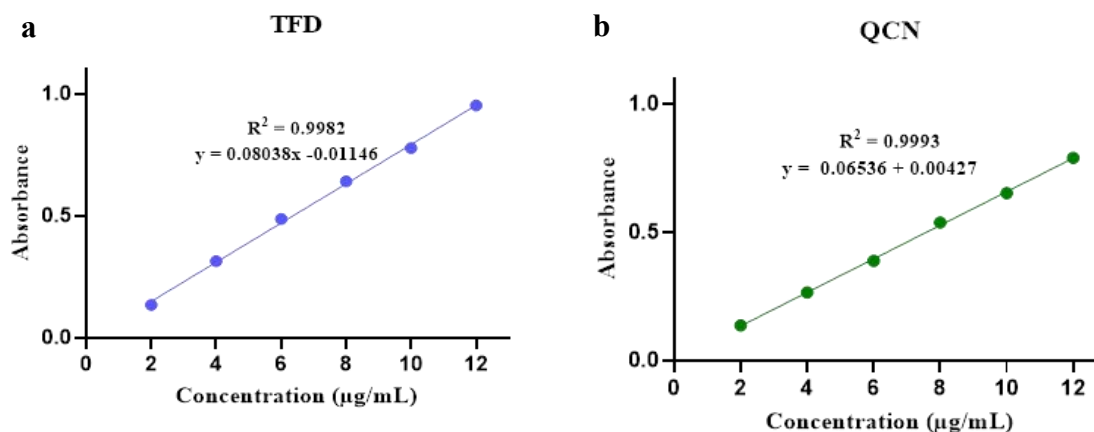
Figure 4.1.2. Linearity graph of a) TFD at 280 nm and b) QCN at 367 nm

The regression analysis parameters are mentioned in **Table 4.1.1**. The LOD & LOQ were found to be 0.585 & 1.772 µg/mL for TFD and 0.358 and 1.087 µg/mL for QCN.

Table 4.1.1. Regression analysis and validation parameters for TFD and QCN

	TFD	QCN
Regression analysis		
Slope	0.08038	0.06536
Intercept	-0.01146	0.00427
Regression coefficient	0.9982	0.99993
Validation parameters		
Linearity range	2-12 µg/mL	2-12 µg/mL
limit of detection	0.585	0.358
limit of quantification	1.772	1.087

The overlay spectrums of the concentration range of 2-12 µg/mL for both drugs are represented in the **Figure 4.1.3.**
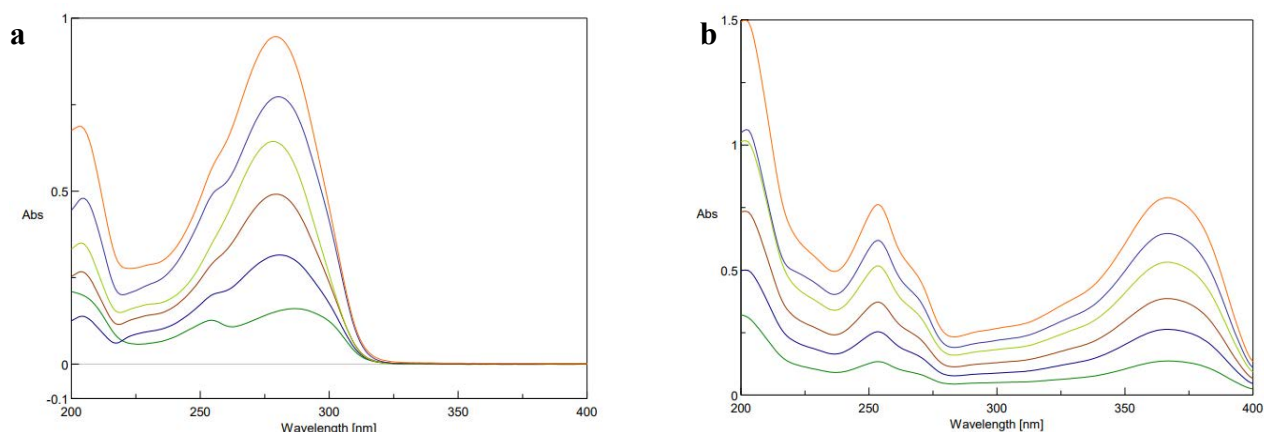
Figure 4.1.3. Overlay UV spectrum of a) TFD and b) QCN

Accuracy

The % recovery of the sample at three levels i.e., 50, 100 and 150 % in triplicates were calculated and the % recovery was found to be in the range of 98.02 to 101.19 for TFD and 98.40 to 101.49 for QCN with % RSD below 2%. The results of accuracy are represented in **Table 4.1.2**.

Table 4.1.2. Accuracy or recovery of TFD and QCN at three different levels

Drug	Recovery levels (%)	Initial amount (μg/mL)	Amount added (μg/mL)	% Recovery	% RSD
TFD	50%	4	2	98.02 ± 1.027	1.048
	100%	4	4	101.19 ± 1.310	1.282
	150%	4	6	99.31 ± 1.946	1.959
QCN	50%	4	2	98.40 ± 1.373	1.395
	100%	4	4	101.49 ± 1.639	1.599
	150%	4	6	99.23 ± 1.243	1.253

Precision

The inter-day and intra-day precision was determined at three concentration levels (50, 100, 150 %) and absorbance was noted. The % RSD was found to be < 2% for both TFD and QCN and the results are represented in **Table 4.1.3**. The consistent and low % RSD values validate the reliability and reproducibility of the method, affirming its suitability for practical application in pharmaceutical analysis.

Table 4.1.3. Inter-day and intra-day precision for TFD and QCN

Drug	Concentration level	Intra-day Precision Mean (±SD)	%RSD	Inter-day Precision Mean (±SD)	%RSD
	50%	0.148 ± 0.001	0.149	0.146 ± 0.002	1.310
TFD	100%	0.342 ± 0.003	0.824	0.307 ± 0.005	1.624
	150%	0.459 ±0.005	1.006	0.440 ± 0.003	0.705
	50%	0.146 ± 0.002	1.458	0.146 ± 0.002	1.502
QCN	100%	0.289 ± 0.002	0.894	0.289 ± 0.001	0.302
	150%	0.428 ± 0.003	0.795	0.427 ± 0.001	0.269

Robustness

To access the robustness of the method the absorbance was noted at different wavelengths (±1 of λ_{max}) and results are mentioned in the **Table 4.1.4.** For both the drugs the % RSD was found to be below 2 %. This demonstrated the stability and reliability of the method that was not affected with slight changes in the wavelengths, confirming its robustness in quantifying the drugs accurately.

Table 4.1.4. Robustness of the developed method for TFD and QCN

Drug	Concentration level	At 279 nm Mean (±SD)	%RSD	At 280 nm Mean (±SD)	%RSD	At 281 nm Mean (±SD)	%RSD
	50%	0.132±0.003	1.906	0.136±0.002	1.761	0.133±0.003	1.902
TFD	100%	0.311±0.004	1.247	0.314±0.001	0.358	0.316±0.001	0.389
	150%	0.486±0.04	0.778	0.487±0.003	0.654	0.486±0.002	0.485
		At 366 nm		**At 367 nm**		**At 368 nm**	
	50%	0.137±0.001	0.534	0.137±0.001	0.511	0.136±0.01	0.532
QCN	100%	0.265±0.003	1.150	0.265±0.003	1.162	0.265±0.03	1.196
	150%	0.388±0.04	0.997	0.388±0.004	0.980	0.387±0.04	0.986

Ruggedness

The results of the ruggedness are mentioned in **Table 4.1.5** by two different analysts under the same operating condition on different days. The % RSD was determined for both drugs, and it

was found to be < 2%. This signifies the method's ruggedness and its ability to generate reliable and consistent results even when executed by different analysts on different days under the same experimental parameters

Table 4.1.5. Ruggedness of the developed method for TFD and QCN

Drug	Concentration level	Analyst 1 Mean (±SD)	%RSD	Analyst 2 Mean (±SD)	%RSD
TFD	50%	0.138 ± 0.003	1.921	0.133 ± 0.001	1.098
	100%	0.323 ± 0.004	1.283	0.308 ± 0.004	1.227
	150%	0.456 ± 0.002	0.541	0.444 ± 0.004	0.797
QCN	50%	0.153 ± 0.001	0.736	0.158 ± 0.001	0.890
	100%	0.295 ± 0.006	1.955	0.306 ± 0.001	0.299
	150%	0.434 ± 0.002	0.393	0.452 ± 0.001	0.268

4.1.2.3. Selectivity of the method using Absorption factor method

The absorption factor for QCN was calculated by taking the absorption spectra of standard concentrations i.e., 4, 6, 8, 10 µg/mL in the UV range of 200-400 nm using eq 4.1.2. The average value of the absorption factor for QCN was found to be 0.309. The QCN concentration was directly determined at 367 nm whereas, quantitative estimation of TFD in the laboratory prepared mixture (1:1; 2:1; 3:1 and 4:1) was calculated from proposed absorption factor method using following equation 4.1.6.

$$Absorption\ of\ Teriflunomide\ at\ 280nm = A_{x+y}\,\lambda_{x1} - \frac{A_{y1}\lambda_{x1}}{A_{y1}\lambda_{y2}} \times A_{x+y}\,\lambda_{y1}\ \text{...eq 4.1.6}$$

Where, $A_{x+y}\,\lambda_{x1}$ – is Absorption of mixture at 280nm

$A_{y1}\,\lambda_{x1}$ / $A_{y1}\,\lambda_{y1}$ - is Absorption factor for QCN

$A_{x+y}\,\lambda_{x1}$ – is Absorption of mixture at 367nm

The amount present in the sample mixture was calculated and the results are represented in the **Table 4.1.6**. The ratio of QCN was kept constant in a sample mixture and its concentration was directly determined at 367 nm. Whereas for TFD, an increase in the ratio of TFD in the sample mixture led to a corresponding increase in its concentration. These findings underscore the selectivity of the proposed absorption factor method for simultaneously quantifying both drugs in a mixture.

Chapter 4

Table 4.1.6. Concentration determination by absorption factor method

Mixture of TFD and QCN in the ratios	Concentration of TFD found		Concentration of QCN found	
	Mean (±SD)	%RSD	Mean (±SD)	%RSD
1:1	2.089 ± 0.006	0.264	2.053 ± 0.007	0.336
2:1	4.099 ± 0.003	0.077	2.038 ± 0.012	0.586
3:1	6.087 ± 0.071	1.165	2.034 ± 0.003	0.130
4:1	8.034 ± 0.060	0.748	2.016 ± 0.016	0.778

4.1.3. Conclusion

A simple and cost-effective UV-visible spectrophotometric method was developed for the simultaneous estimation of TFD and QCN. The TFD and QCN showed absorption maxima at 280 nm and 367 nm, respectively. The method underwent validation in accordance with ICH guidelines, and the results were within acceptable limits. The absorption factor method was employed for the simultaneous estimation of TFD and QCN in the formulation. This developed UV method was applied for the determination of encapsulation efficiency of the transferosomes.

(b) Implementing Analytical Quality by Design in Reversed Phase-High Performance Liquid Chromatography for Simultaneous Estimation of Teriflunomide and Querectin

Chapter 4

4.2. Introduction

The development of an analytical method plays a pivotal role in pharmaceutical analysis, facilitating the accurate estimation of drug content in various formulations. TFD has been demonstrated to be effective in treating RA by inhibiting T cell activation [14]. Its pKa value has been determined to be 3.1 at room temperature, with a pH-dependent solubility [15]. On the other hand, QCN exhibits a pKa value of 6.38 and has been reported to possess potential for treating various inflammatory conditions, including RA. QCN acts by inhibiting inflammatory cytokine release, lowering COX-2 levels induced by lipopolysaccharides, and hindering bone resorption *via* NF-kβ and AP-1 activity suppression [16,17]. The combination of TFD and QCN showed potential as a promising therapy against the production of inflammatory mediators. Hence, a new, efficient, simple, and reproducible analytical method was necessary to quantify both analytes in any pharmaceutical dosage forms [18].

In recent years, there have been various reports on analytical methods such as Liquid chromatography–mass spectrometry (LC–MS) [19,20], UV–Vis spectrophotometry [2,21] and High-Performance Liquid Chromatography (HPLC) [22,23] for quantitative detection of either TFD or QCN individually. Reversed phase-HPLC (RP-HPLC) methods for the combination of either TFD or QCN with other drugs have been also reported [24,25]. However, no method has been established yet for their simultaneous detection. Given that TFD and QCN have distinct pKa, it presents a significant challenge for analytical chemists in devising a dependable HPLC method for simultaneous detection. Thus, the focus of this study was to develop an efficient RP-HPLC method to optimize the retention time of TFD and QCN, while also achieving high resolution and improved peak shape. Traditional trial-and-error methods for controlling all variables are challenging, prompting the use of the analytical quality by design (AQbD) approach, which is known for its cost-effectiveness, rapid identification, and quantification of multiple drugs in a single formulation [26,27].

QbD plays a crucial role in identifying different sources of risk and science-based variability and helps to comprehend predefined objectives through risk assessment. Investigation trials help in identifying high-risk variables that significantly impact method performance, and further optimization of these variables enhances the method's overall performance [28]. Various studies have advocated for AQbD in analytical method development in diverse fields such as for small molecules analysis in various dosage forms, protein and peptide analysis in pharmaceutical industry [29–34]. The overall focus of the research work was on developing an economical, sensitive, robust, simple, rapid, and effective HPLC method for the simultaneous detection of TFD and QCN using the AQbD approach. The developed method was validated

according to the International Council for Harmonization of Technical Requirements for Registration of Pharmaceuticals for Human Use (ICH) guidelines. Furthermore, the greenness profile of the developed method was calculated for establishing its environmental sustainability and ecological impact.

4.2.1. Materials and Methods

As mentioned in chapter 3, TFD (99.9% pure) was obtained as a gift sample from the MSN Laboratories Private Limited (Sangareddy, India). QCN (> 98% purity) was purchased from Yucca Enterprises (Mumbai, India). Ammonium acetate, potassium dihydrogen phosphate, acetic acid, formic acid, trifluoro acetic acid (TFA) were purchased from Thermos Fisher Scientific Pvt Ltd (Mumbai, India). Milli-Q water was obtained from the Merck Milli-Q purification system. All other chemicals used in the experiment were HPLC and analytical grade.

4.2.1.1. Instruments and chromatographic conditions

Chromatography separation for the analysis of TFD and QCN were performed using Shimadzu HPLC (Japan), with binary pump (LC-20AD) and UV/Vis detector (SPD -20A) containing autosampler (SIL- 20AC HT, Shimadzu, Japan). TFD and QCN separation were carried out using Hibar, Lichospher 100 RP-18e column (250 x 4.6 mm, 5µm). The analysis was carried out with a detection wavelength of 280 nm for TFD and 367 nm for QCN. LC solution software version 1.24 SP1 was used for method development and data analysis.

4.2.1.2. Preparation of standard solutions

Primary standard stock solution of 1 mg/mL of TFD and QCN were prepared in acetonitrile separately. A secondary stock solution of 100 µg/mL was prepared from primary stock solution. The working standard solution (10 µg/mL), calibration standards and quality control samples containing both drugs were prepared from secondary stock solutions by serial dilution with acetonitrile and water (90:10 %, v/v).

4.2.1.3. Experimental design for method optimization using AQbD

Study design

The concept of AQbD represents a comprehensive methodology that fosters comprehension and regulation of products and processes through a foundation rooted in deep scientific principles and effective management of quality risks. A roadmap for the simultaneous estimation of TFD and QCN by AQbD approach are represented in **Figure 4.2.1**.
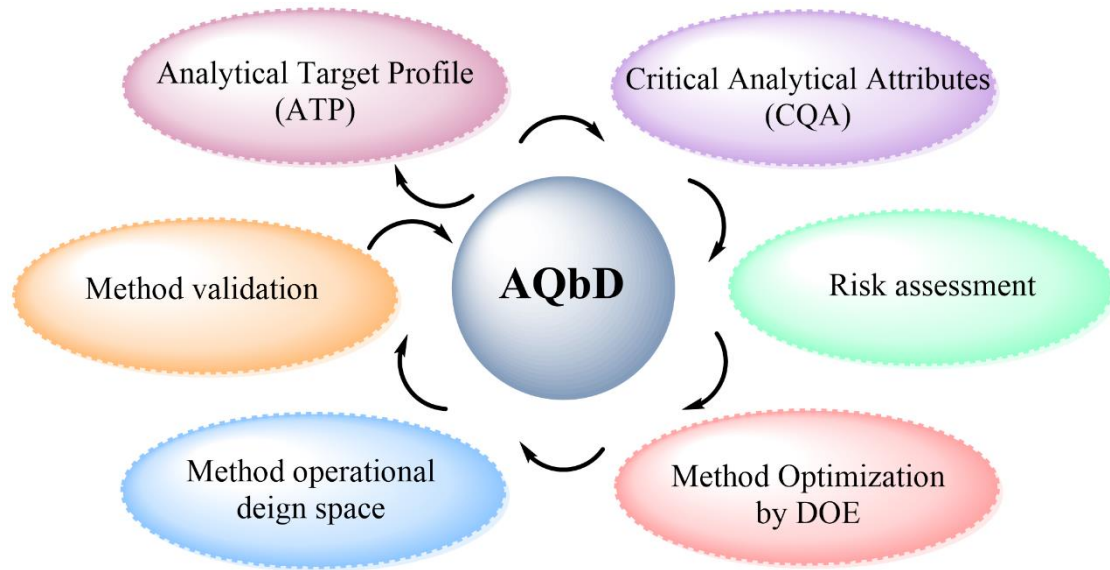
Figure 4.2.1. Roadmap for the simultaneous estimation of TFD and QCN by AQbD approach

Within the AQbD paradigm, the analytical target profile (ATP) serves as a prescriptive outline for the intended method quality, encompassing ideal quality attributes, safety benchmarks, and the efficiency of the developed method. In the initial stages of ATP establishment, a spectrum of variables liable to impact the different parameters involved in the development of the analytical method were taken into account. Also, the recognition and understanding of critical analytical attributes (CAAs), that holds immense importance, as these attributes direct the essential qualities of the method. These attributes play a pivotal role in ensuring the method's accuracy, reliability, and effectiveness in achieving its intended analytical goals. Notably, the essential role of CAAs lies in ensuring thorough alignment of the final method with the required criteria for analysis. The key factors that regulate CAAs were opted from the ATP as mentioned in **Table 4.2.1**. Based on the ATP requirement, a comprehensive literature analysis and the Ishikawa diagram (**Figure 4.2.2**) was prepared to identify the key factors that regulate ATP and CAAs. To determine their relative significance, these factors were evaluated through the risk estimation matrix (REM), categorizing their potential impact as low, medium, and high in their criticality (**Table 4.2.2**). Following this, a meticulous assessment utilizing the failure mode effective and analysis (FMEA) approach was employed to gauge the severity(S), detectability(D), and occurrence(O) of each distinct factor. The criticality of these parameters culminated in the derivation of the risk priority number (RPN) score, which was calculated using equation 4.2.1 and were assigned with ranking number within a scale of 0 to 10 [31,35].

Risk Priority Number (RPN) = Severity (S) * Detectability(D)* Occurrence (O)   … eq 4.2.1

Chapter 4

Table 4.2.1 Analytical target profile (ATP) for the simultaneous estimation of TFD and QCN using RP-HPLC

ATP	Target	Explanation
Sample	Active molecule	Analytical method development for simultaneous estimation of molecules in pharmaceutical dosage form
Type of method	Reversed Phase	The retention of molecules is enhanced by the use of a non-polar stationary phase with end-capping
Instrument	Autosampler HPLC with binary pump	A great resolution of the molecules will be achieved
Nature of the sample	Liquid	To assure complete miscibility, the analyte must be in liquid form
Standard Preparation	Linear method of dilution	Standard medication solution dilution to ensure optimal elution
Sample Preparation	Manual handling	Manual weighing of the sample is the first step in the preparation process, which is then followed by the mixing of the sample with the diluent.
Method application	Estimation of TFD and QCN	The method is applicable for the simultaneous estimation of TFD and QCN in microemulsion
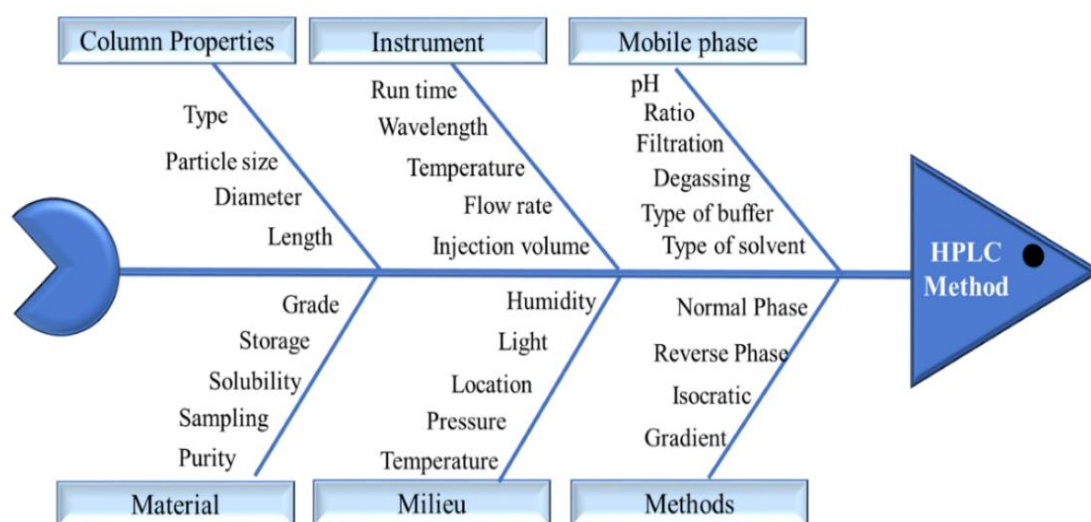
Figure 4.2.2. Ishikawa diagram

Factor optimization study using face centered Central-Composite Design (CCD)

The optimization process prioritizes the use of face-centered central composite design (CCD). Based on insights gained from initial investigations, the selection of variables for enhancing

the analytical method was keyed in face centered CCD. This approach investigates the impact of three independent variables on identified dependent variables across three levels (low, medium, and high), while maintaining consistency in other factors throughout the exploration. To understand the intricate interactions between factors and the desired responsive characteristics, a meticulously crafted design matrix comprising 16 experimental runs was employed (**Table 4.2.3**). This design matrix incorporated center points with alpha value of 1. The culmination of this systematic exploration ultimately led to the optimization of the method with remarkable efficiency through a minimized number of trial iterations. The core of this optimization process revolved around the strategic application of Design-Expert 7.0.0 software.

Optimization data analysis and model validation

For the optimization data analysis and model validation, Design Expert® software. 7.0.0 was utilized. The best fit model (quadratic, linear, modified, cubic, 2 factor interaction) was evaluated by keeping experimental data aiding in the estimation of the effect on various responses under study. Further, model significance was further analyzed by analysis of variance (ANOVA) that specifically took into consideration of coefficients with p values < 0.0001. The relationship between factors and responses were visually explored through the use of 3-D response plots and 2-D contour plots. Also, residual analysis was performed to predict the responses. By employing numerical, graphical optimization and a desirability function (desirable value near to 1), the optimal chromatographic conditions were identified. Further, the optimized composition was carried out for the analytical validation.

4.2.1.4. Method validation

In accordance with the ICH Q2(R1) guidelines, the analytical approach underwent validation pertaining to attributes such as system suitability, linearity, accuracy, range, precision, specificity and robustness, alongside adherence to the system suitability criteria as outlined in the USP [11]

System suitability

System suitability in HPLC ensures reliable results by assessing parameters like retention time, peak resolution, and symmetry. The system suitability was performed by injecting six injections of 10 μg/mL of TFD and QCN mixture and % RSD of the peak area was reported.

Linearity and range

The linearity of TFD and QCN solutions was assessed across eight distinct concentration levels of 0.05, 0.1, 0.5, 1, 5, 10, 15, 20 μg/mL. Triplicate preparations of each concentration level were subjected to analysis utilizing the HPLC system. Subsequently, the peak area responses

for TFD and QCN were recorded at each level, followed by the construction of concentration *Vs* peak area graphs and subsequent regression analysis.

Accuracy

To assess accuracy, triplicates of TFD and QCN solutions at three different quality control (QC) levels, namely low quality control (LQC), medium quality control (MQC), and high quality control (HQC), were analyzed. The results were expressed in terms of percentage recovery. As outlined in the ICH guidelines, the specified acceptance criterion for % recovery was established at 98–102 % [36].

Precision

Precision was assessed by determining the intra-day and inter-day precision of TFD and QCN solutions at LQC, MQC, HQC level. Intra-day precision was evaluated by analyzing three different concentration levels of TFD and QCN triplicate on the same day. Inter-day precision was determined by analyzing the same concentration of TFD and QCN on three successive days. The result was reported as the percentage of RSD. According to the guidelines, the acceptance criterion for % RSD was specified to be below 2 % [36].

Limit of detection and limit of quantification

The limit of detection (LOD) and limit of quantification (LOQ) of the developed method for the TFD and QCN were calculated based on the standard deviation of the response and the slope using the following equation 4.1.3 and 4.1.4. as per ICH guidelines.

Robustness

As per ICH guidelines, robustness is the fitness of analytical practice that is not exaggerated by tiny variations but by significant changes in the experimental factors. Here, the developed method was screened by slight changes in the operating conditions such as column temperature, percentage of acetonitrile and pH of the buffer. The specified acceptance criteria for the calculated %RSD of peak area was below 2 %.

Specificity

Specificity pertains to the ability of the analytical method to distinguish between the analyte(s) and other substances within the sample matrix. The assessment of specificity included introducing blank solution, placebo formulation and formulations containing TFD and QCN, into the chromatographic system. The interference of formulation excipients on the retention of TFD and QCN will be assessed during the analysis.

4.2.1.5. Forced degradation studies

Forced degradation studies were conducted to assess the stability-indicating and specificity properties of the developed assay method. These studies were performed following the

guidelines provided by the ICH and other recommended conditions [37]. The sample preparations for the stress studies were made at a concentration of 0.5 mg/mL for combined mixture and were subjected to different stress conditions. All samples were then appropriately diluted to achieve a final concentration of 5 µg/mL and neutralization was performed wherever necessary. Subsequently, the samples were filtered through 0.22 µm membrane filters before injection, and control samples were also prepared and used during the analysis. The degradation studies were carried out till 10% degradation exceeded in each condition.

Oxidation studies

For oxidation studies, the sample containing both TFD and QCN was carried out using 3% H_2O_2 solution. Samples were heated at 60°C in hot air oven. Samples were withdrawn at specified time intervals and diluted as described above.

Acid and alkali degradation

Samples for acid and alkali degradation studies were prepared using 0.01 N hydrochloric acid (HCl) and 0.01 N sodium hydroxide (NaOH), respectively. Samples were heated at 60°C in hot air oven. Subsequently, the samples were neutralized and diluted as described above.

Thermal Degradation

For thermal degradation, samples were exposed to 60°C in hot air oven. Subsequently, samples were withdrawn, cooled, and diluted as described above.

4.2.1.6. Assessment of greenness profile of the developed method

Evaluating the greenness profile of the HPLC method includes assessing factors like solvent usage, waste generation and energy consumption. This comprehensive analysis ensures the incorporation of eco-friendly practices in analytical procedures, promoting sustainability. Various metrics are available for the assessment of the greenness profile of a method. These include the analytical method greenness score (AMGS), green solvent selection tool (GSST), analytical eco-scale, green analytical procedure index (GAPI), analytical greenness (AGREE), and national environmental methods index (NEMI) [38]. Among these the AMGS calculator was utilized for the assessment of greenness profile of the developed HPLC method.

4.2.2. Results and Discussion

Utilizing HPLC for quantification is widely accepted, but it is yet challenging due to the separation complexities arising from the distinct pKa values of both TFD and QCN. So, a new and efficient RP-HPLC method for the simultaneous quantification of TFD and QCN was developed using AQbD principles [38]. Employing AQbD principles in HPLC method development enables systematic optimization, ensuring robustness, reliability, and compliance

with regulations. This approach fosters a comprehensive understanding of crucial method parameters like column chemistry, mobile phase composition, and detection conditions, leading to the creation of efficient and effective methods. Additionally, it aids in recognizing and addressing potential risks, resulting in improved method performance, minimized variability, and better analytical outcomes. Overall, AQbD empowers researchers to craft HPLC methods that consistently produce accurate and precise results, thereby enhancing product quality and safety across pharmaceutical industry.

4.2.2.1. Development and optimization of the method using AQbD

A thorough literature review was used to conduct preliminary investigation for the development of the simultaneous estimation using RP-HPLC method for the TFD and QCN. The initial trials were carried out with different mobile phase compositions that encompassed buffer salts with varying pH levels, along with a range of solvents such as methanol and acetonitrile. Additionally, various C18 columns with differing specifications were utilized in the preliminary optimization phase. These included columns such as inertsil (4.6 x 250 mm, 5 µm), waters Nova pack (3.9 x 150 mm, 4 µm) and Hibar Lichospher 100 RP-18 end-capped column (250 x 4.6 mm, 5 µm). Following this, the Hibar Lichospher column was selected due to its ability to facilitate the separation of a broad spectrum of analytes (including neutral, acidic, and weak basic ones) with observed satisfactory peak properties. Acetonitrile and 10 mM ammonium acetate buffer combination produced good peak properties, and further trials were carried out using acetonitrile and ammonium acetate buffer at various pH levels to identify the CAAs that impact the ATP. The ATP chosen for analytical method development are shown in **Table 4.2.1**. The CAAs from the ATP were selected because they were reported for their ability to influence the method development. Retention time and resolution between both analytes were identified as CAAs of analytical method development that had a significant impact on quality of the developed method.

The risk assessment was conducted, and the Ishikawa diagram shown in **Figure 4.2.2** was used to identify ATP and CAA. The percentage of acetonitrile, pH of the buffer, flow rate, injection volume, and column temperature were all considered as potential risk factors against retention time and resolution. FMEA was used to assign RPN scores based on risk potentiality and the scores were given based on reported studies. The REM and RPN scores of the CAAs and CPPs are shown in **Table 4.2.2**. A RPN score of more than 50 was regarded as critical for optimizing critical attributes. Here, the percentage of acetonitrile (Factor A), flow rate (Factor B) and pH of the buffer (Factor C), were considered as critical factors.

Table 4.2.2. Risk estimation matrix (REM) and risk priority number (RPN) score

Different Variables	CAAs		FMEA			
	Retention time	Resolution	Severity	Detectability	Occurrence	RPN score
Acetonitrile	High	High	9	9	9	729
pH	High	Medium	8	7	6	336
Injection volume	Low	Low	2	2	2	8
Column temperature	Medium	Low	5	3	3	45
Flow rate	High	High	9	8	8	576

Factors optimizing studies

The risk assessment studies report emphasized the importance of factors like the percentage of acetonitrile, pH of the buffer, and flow rate. These were identified as critical factors influencing CAAs such as retention time and resolution. The process of method optimization utilized face centered CCD with 16 runs, that was evaluated by Design-Expert 7.0.0 software. This optimization encompassed the exploration of percentage acetonitrile, pH of the buffer, flow rate at three different levels, while keeping injection volume (10 µL) and column temperature (25ºC) constant. The face centered CCD with three components and 3 levels generated response values, that are presented in **Table 4.2.3**.

Table 4.2.3. Experimental design using face centered CCD runs and responses

Run	Factor 1 A: Acetonitrile	Factor 2 B: Flow rate	Factor 3 C: pH	Response 1 Retention time of TFD	Response 2 Retention time of QCN	Response 3 Resolution
1	50	1.20	4.00	2.24	3.58	6.38
2	40	1.00	3.50	4.22	5.98	4.11
3	30	1.20	4.00	12.90	15.39	3.46
4	50	0.80	3.00	3.54	5.10	4.36
5	40	0.80	3.50	5.11	7.81	4.51
6	40	1.00	4.00	3.85	6.11	4.69
7	30	0.80	3.00	15.73	17.25	1.14
8	30	1.00	3.50	12.11	14.83	2.32
9	30	1.20	3.00	12.85	14.08	1.19
10	50	0.80	4.00	3.37	5.07	6.79
11	40	1.00	3.00	5.14	6.56	2.64
12	40	1.20	3.50	4.17	6.32	4.17
13	50	1.20	3.00	2.69	3.87	3.69
14	30	0.80	4.00	14.32	16.87	3.86
15	50	1.00	3.50	2.93	4.36	4.48
16	40	1.00	3.50	3.96	5.80	4.00

The efficiency of the model and the significance of the variables were established through ANOVA analysis. The statistical summary indicated the suitability of a quadratic model for the responses with $p < 0.0001$. The R^2 value demonstrated a strong correlation between the fitted model and experimental data. The comprehensive details of the ANOVA analysis have been meticulously presented within the confines of **Table 4.2.4.**

Table 4.2.4. ANOVA analysis for responses

Parameter	Response 1 Retention time of TFD	Response 2 Retention time of QCN	Response 3 Resolution
Standard deviation	0.60	0.49	0.28
Mean	6.82	8.69	3.86
C.V %	8.74	5.59	7.19
R-squared	0.9939	0.9963	0.9869
Adjusted R-squared	0.9847	0.9907	0.9674
Pred R-squared	0.9323	0.9533	0.8754
Adequate precision	27.879	34.260	22.199

Furthermore, the p-values corresponding to each factor associated with various responses and lack of fit values were also delineated and are reported in the **Table 4.2.5**

Table 4.2.5. ANOVA analysis depicting the p-values for each factor

Source	p-value		
	Response 1 Retention time of TFD	Response 2 Retention time of QCN	Response 3 Resolution
A	0.0001	< 0.0001	< 0.0001
B	0.0087	0.0012	0.0904
C	0.1337	0.9205	< 0.0001
AB	0.2182	0.2098	0.3885
AC	0.6763	0.3982	0.8740
BC	0.5104	0.3382	0.8169
A^2	0.0001	< 0.0001	0.0487
B^2	0.1907	0.0494	0.0231
C^2	0.3216	0.9877	0.3948
Lack of fit	0.2199	0.1805	0.1929

Effect of independent variables on retention time

Retention time of TFD ranged from 2.24 to 15.73 min and for QCN, retention time ranged from 3.58 to 17.25 min over 16 trails. The F-values of 108.44 and 177.76 for TFD and QCN in the quadratic model were determined to be statistically significant. The *p*-values corresponding to each factor's effect on the retention time of TFD and QCN were documented (**Table 4.2.5**). Analysis of the data indicated that model terms A, B, and A^2 were statistically significant in influencing the retention time of TFD, whereas the model terms A, B, A^2 and B^2 influenced the retention time of QCN. The respective contour and 3D plots for the effect of percentage of acetonitrile, pH and flow rate on retention time of TFD and QCN are represented in **Figure. 4.2.3 & 4.2.4** respectively. Equation 4.2.2 & 4.2.3 contain coded factors for both TFD and QCN, with positive symbol indicating collusive effect and negative symbol denoting hostile effect. The 3D graphical representations and polynomial equation provided empirical support for the decline in retention time of TFD and QCN as the acetonitrile percentage increased (**Figure. 4.2.3a, 4.2.3b & 4.2.4a, 4.2.4b**). Concurrently, a gradual increase in flow rate and pH resulted in a modest reduction in TFD's retention (**Figure. 4.2.3c**). Conversely, QCN's retention time decreased with higher flow rate and slightly increased with elevated pH (**Figure. 4.2.4c**).

Retention time of TFD = + 4.10 - 5.31 A - 0.72B - 0.33 C + 0.29 AB + 0.093 AC + 0.15 BC + 3.42 A^2 + 0.54 B^2 + 0.40 C^2 ...eq 4.2.2

Retention time of QCN = + 6.18 - 5.64 A - 0.89 B + 0.016 C + 0.24 AB - 0.16 AC + 0.18 BC +3.26 A^2 + 0.73 B^2 -0.048 C^2 ...eq 4.2.3

Here, Factor A- percentage of acetonitrile; Factor B- flow rate; Factor C - pH of the buffer

Effect of independent variables on Resolution

For both TFD and QCN resolution ranged from 1.14 to 6.79 over executed 16 trials. The Quadratic model's F-value 50.39 suggested the model was significant. Data analysis reveals that model terms A, C, A^2 and B^2 exhibited statistical significance in influencing the resolution between the two analytes and the respective contour and 3D plots for the effect of percentage of acetonitrile, pH and flow rate on resolution has been illustrated in **Figure. 4.2.5**. Equation 4.2.4 contained coded values of chosen factors. An increase in acetonitrile percentage and pH levels yielded an increase in resolution (**Figure. 4.2.5a & 4.2.5b**), while an increase in flow rate resulted in a marginal reduction in resolution (**Figure. 4.2.5c**).

Resolution = + 3.90 + 1.37 A - 0.18 B + 1.22 C -0.091 AB + 0.016 AC -0.024 BC -0.42 A^2 + 0.52 B^2 - 0.16 C^2 ...eq 4.2.4
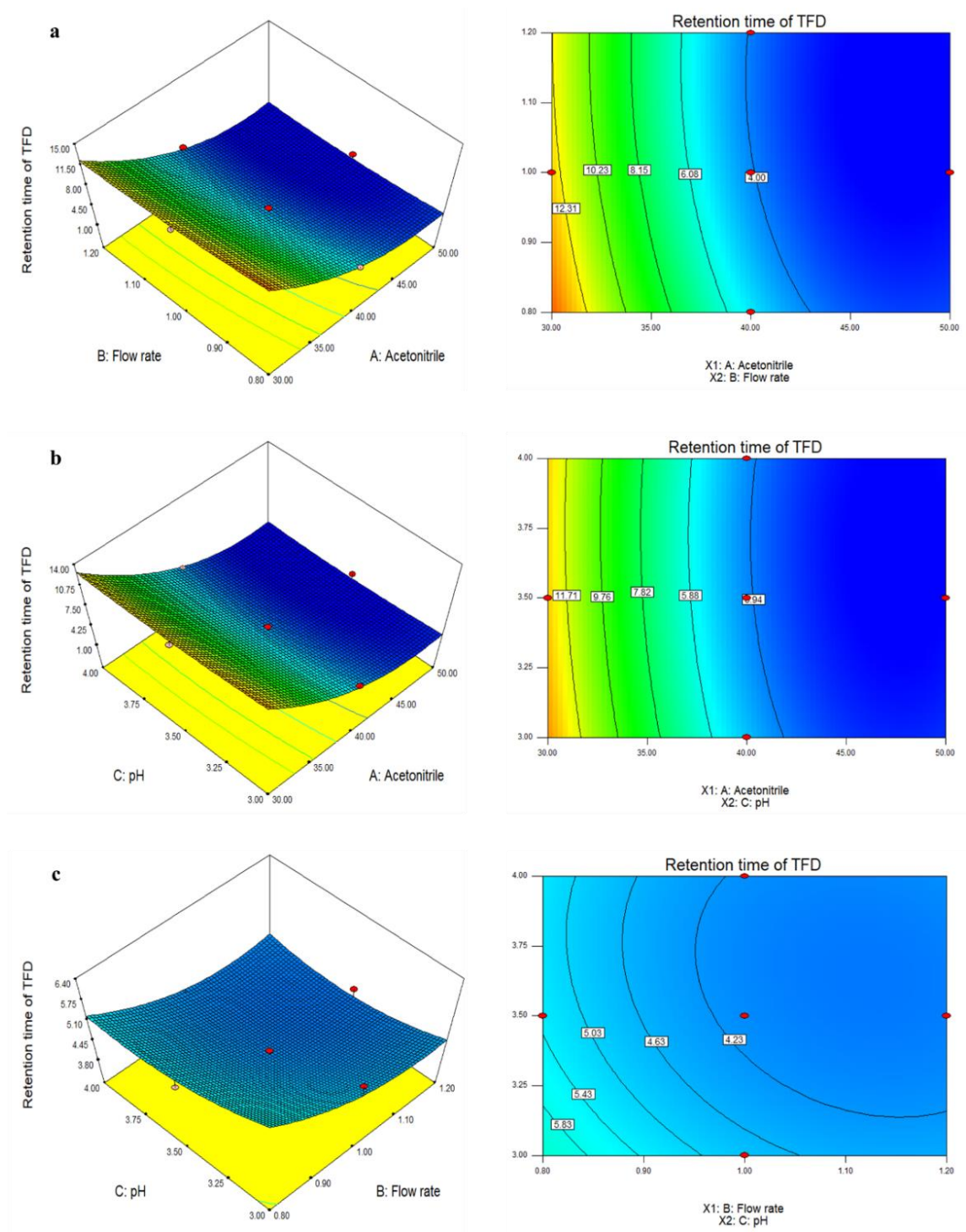
Figure 4.2.3. 3D and Contour plots for the effect of critical factors on the retention time of TFD
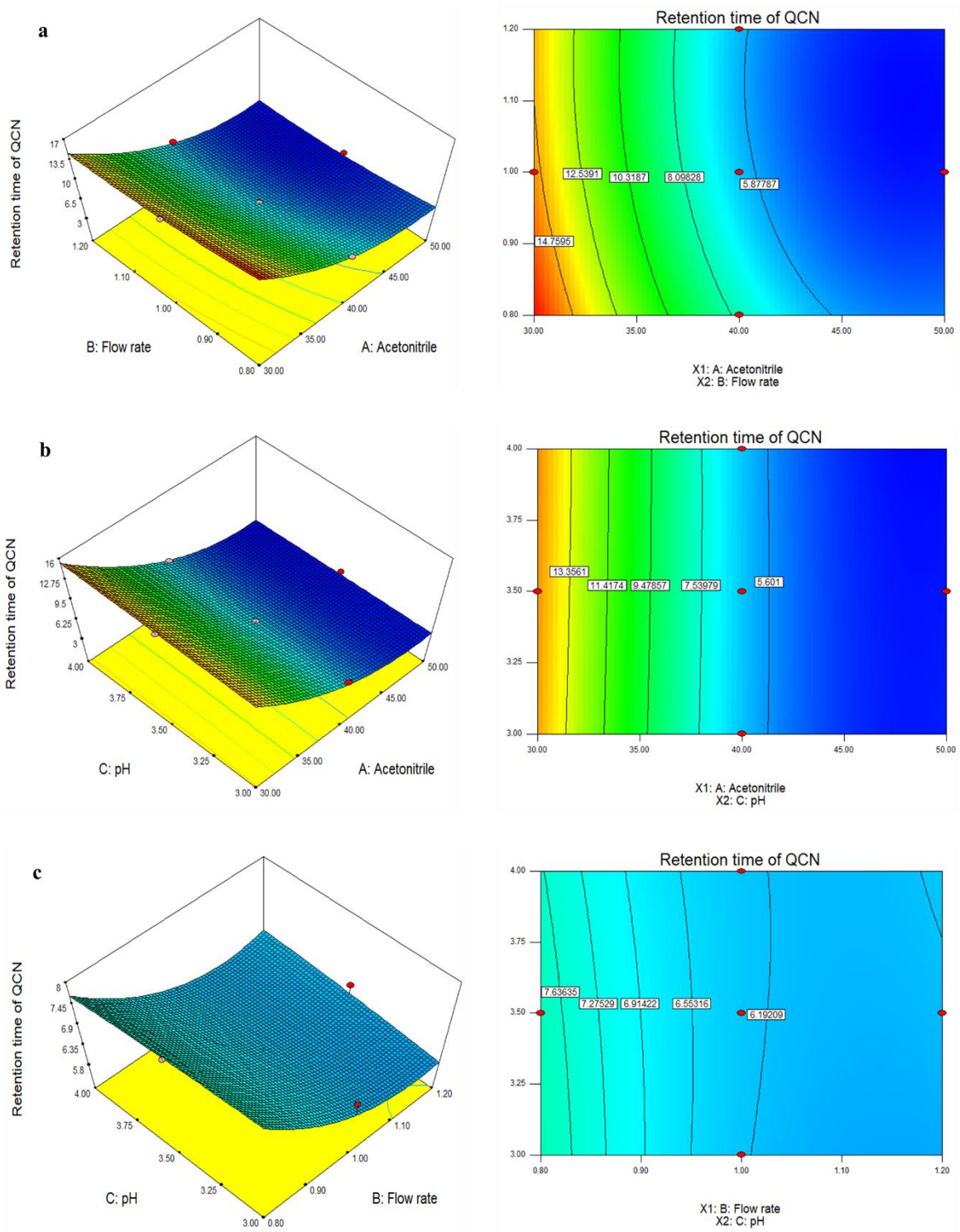
Figure 4.2.4. 3D and Contour plots for the effect of critical factors on the retention time of QCN
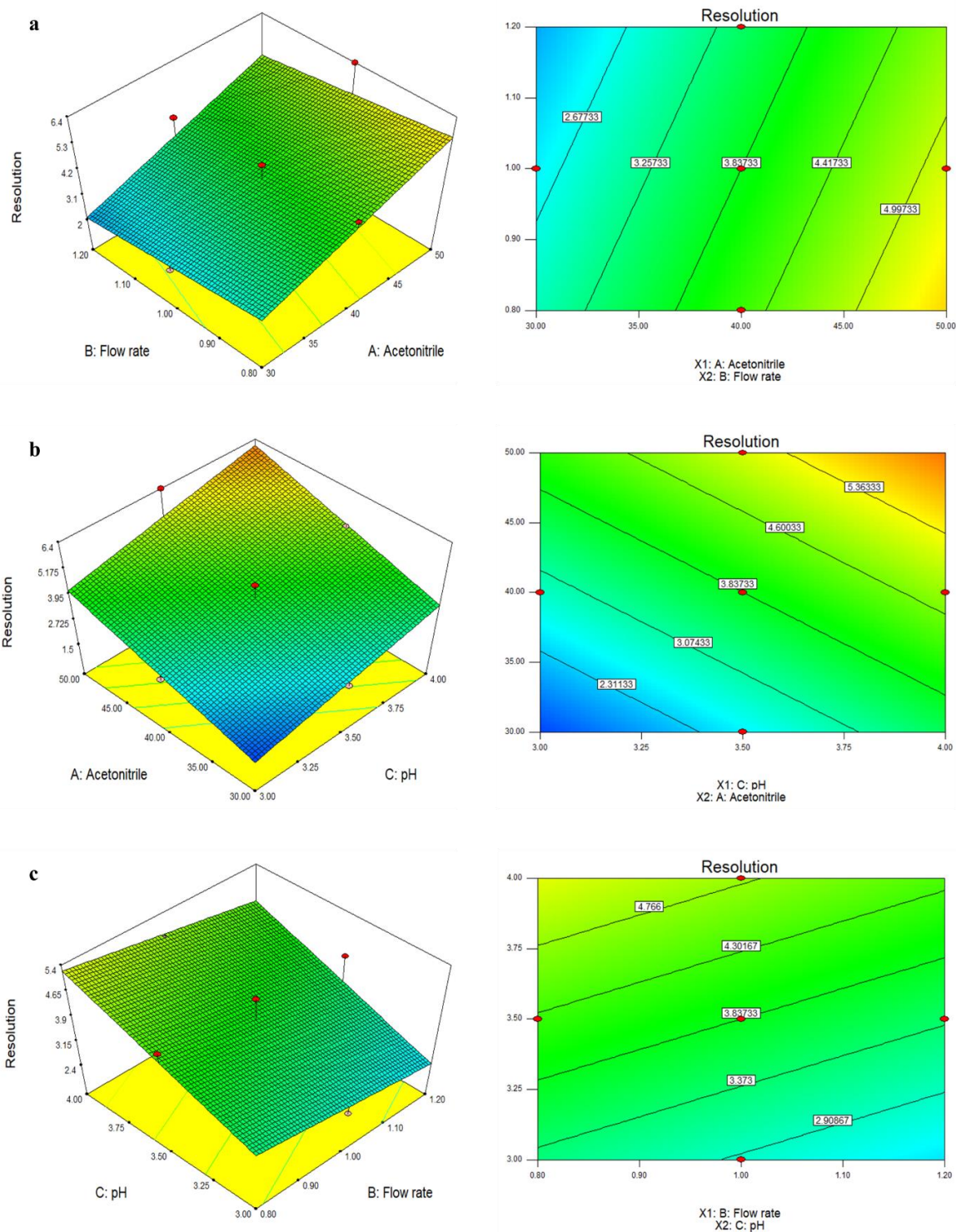
Figure 4.2.5. 3D and Contour plots for the effect of critical factors on resolution

Chapter 4

Validation of the design to select an optimized method

The developed experimental model was further used to predict the responses such as retention time of TFD, QCN and resolution with help of residual plots. The **Figure 4.2.6** display the normal plot of residuals for each response, indicating that the residuals generally conform to a straight line. This observation suggests that errors are uniformly distributed, indicating a satisfactory fit of the model to the data.
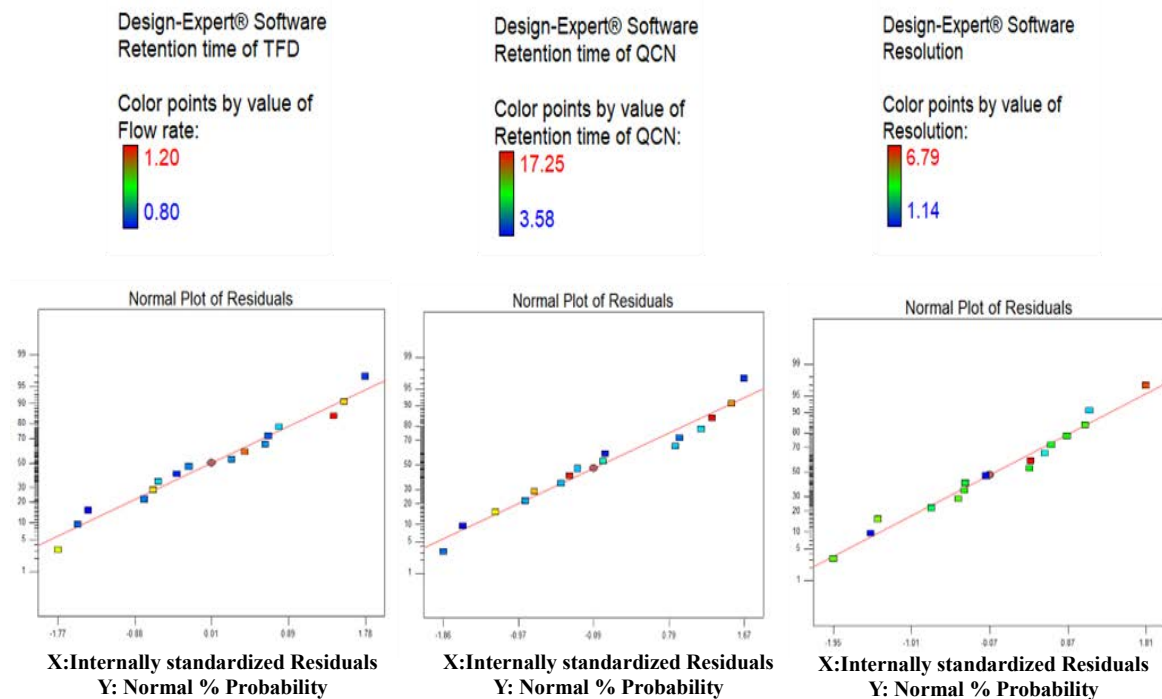
Figure 4.2.6. Normal plot of residual for responses

Further, the analytical method was optimized through a combination of numerical and graphical approaches aiming to improve retention time and resolution. Employing Design Expert software, a set of 16 solutions were generated, and method operable design region (MODR) was established. The MODR serves as a valuable tool for identifying optimal operational parameters to attain the desired quality of outcomes. In **Figure.4.2.7** the MODR was visually depicted through an overlay plot, with the highlighted yellow region indicating the optimized zone. The predicted solution was identified by a flag in this zone with a specific focus on choosing those with desirability values that approached 1 (the desirability graphs have been illustrated in **Figure 4.2.8**).
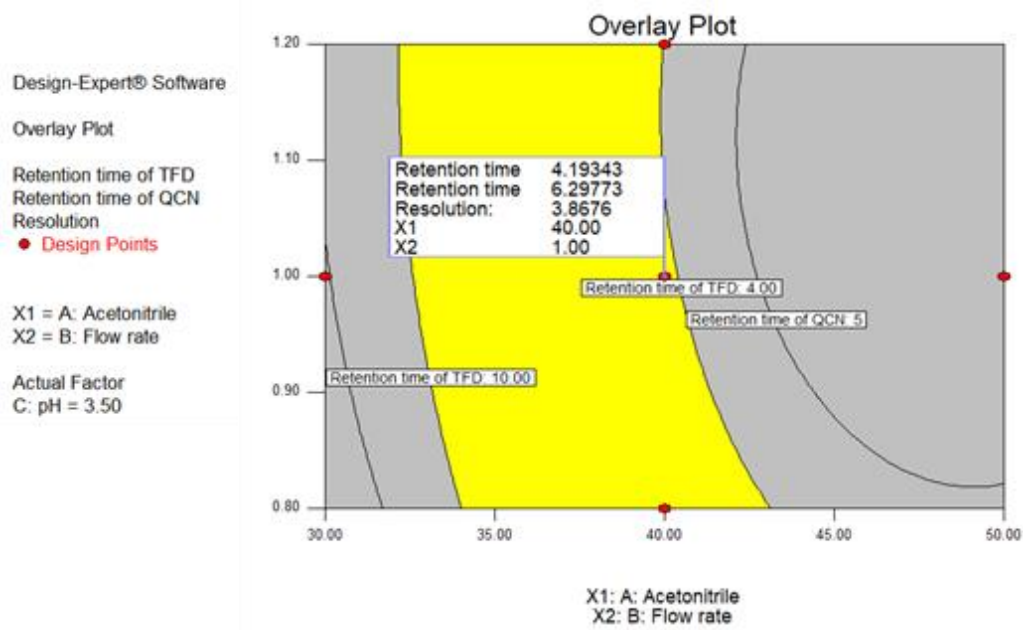
Figure 4.2.7. MODR overlay plot with optimized zone for TFD and QCN
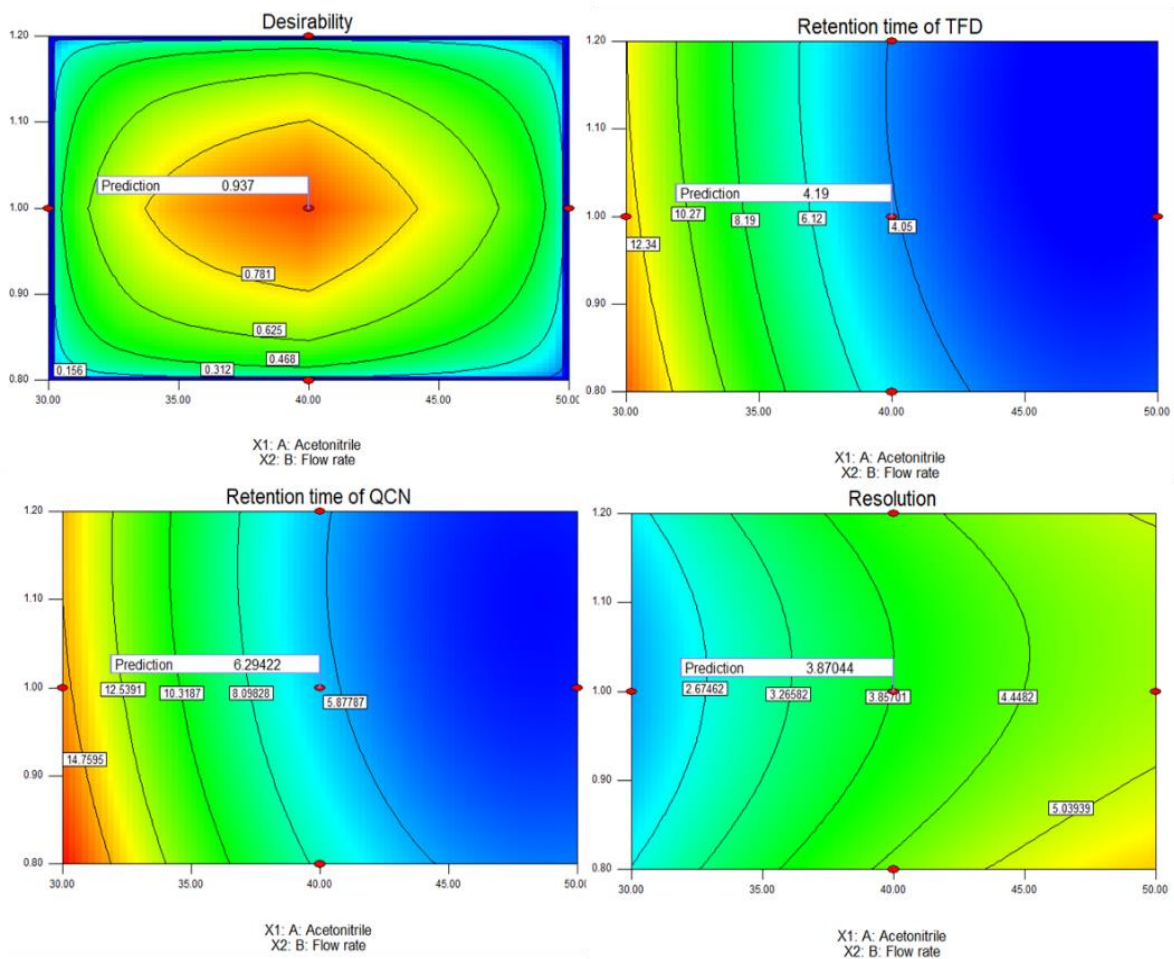
Figure 4.2.8. Desirability graphs for the method optimization

The optimized run employed a mobile phase that consisted of 40% acetonitrile and 60% ammonium acetate buffer (pH of 3.5), with a flow rate of 1 mL/min. These selected conditions resulted in retention times of 3.96 min and 5.94 min for TFD and QCN, respectively. The resolution achieved between these two analytes was determined to be 4.11, showing a close predicted-actual values and design's desirability. The tailing factor was found to be 1.1 and 1.39 for TFD and QCN, respectively. TFD exhibited its peak absorbance at 280 nm, while QCN also manifested absorbance at this specific wavelength with absorption maxima at 367 nm. The representative chromatograms are depicted in **Figure. 4.2.9.**
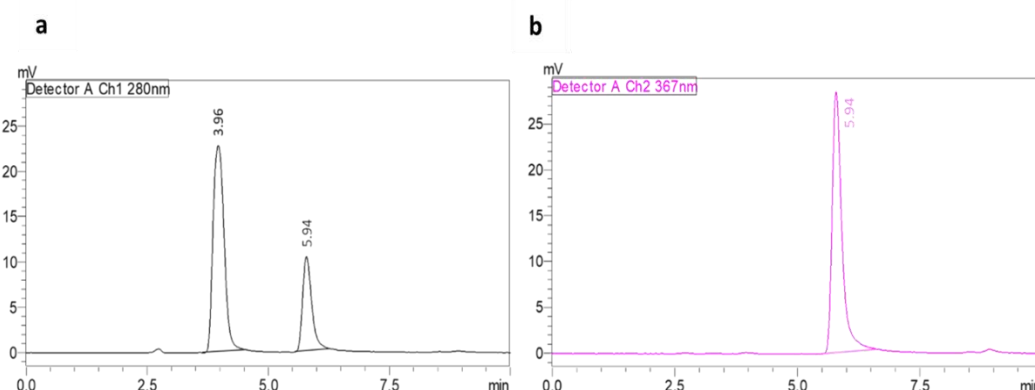
Figure 4.2.9. Chromatogram of a) TFD at 280 nm; b) QCN nm at 367 nm

4.2.2.2. Method validation

Following the ICH Q2 (R1) guidelines validation of the developed HPLC method was conducted to ensure the dependability of the analytical results across various parameters, including system suitability, linearity, range, accuracy, precision, robustness, ruggedness, limit of quantitation (LOQ), limit of detection (LOD), and specificity.

System suitability

The method devised was utilized to assess system suitability, entailing six injections. Calculation of the % RSD for peak areas yielded a value below 2.0%, signifying commendable system precision (chromatogram overlay is depicted in **Figure 4.2.10**).
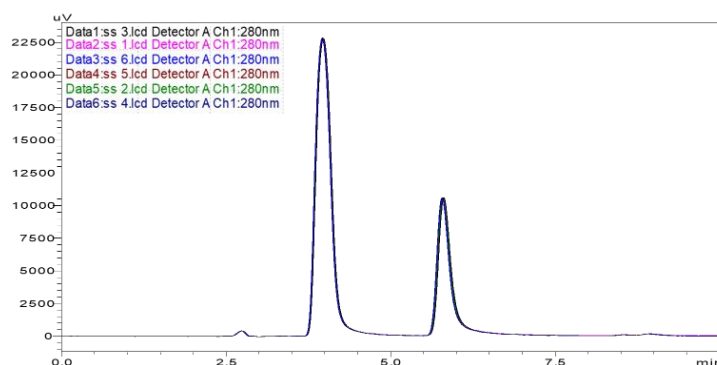
Figure 4.2.10. System suitability for TFD and QCN at 280 nm

Linearity and range

The developed method exhibited linearity across the investigated concentration range from 0.05 to 20 μg/mL. The correlation coefficients for TFD and QCN were determined as 0.999 and 0.998, respectively (**Figure 4.2.11**).
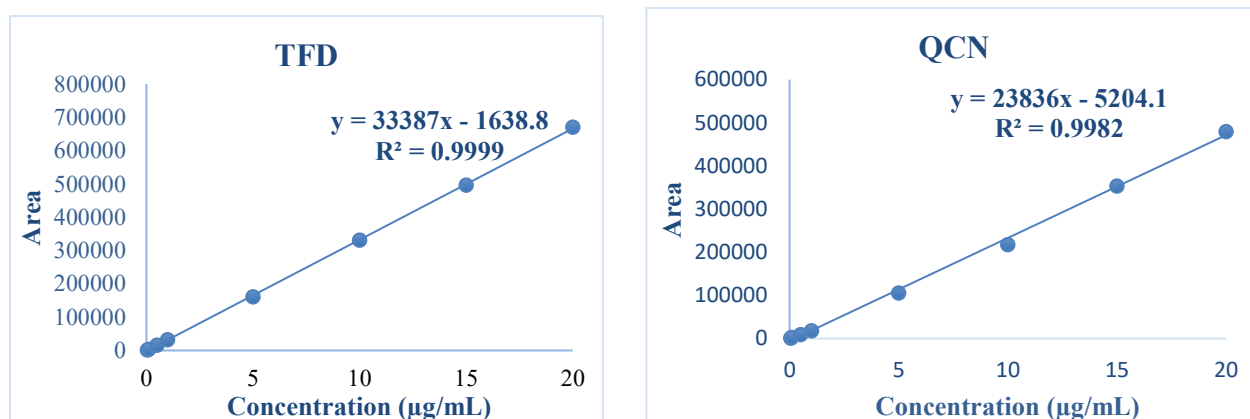
Figure 4.2.11. Calibration curve for TFD and QCN

Accuracy

The observed percentage recovery was within the range of 99.30% to 100.93%, with % RSD of less than 2. Accuracy results for TFD and QCN across LQC, MQC and HQC levels have been tabulated in **Table 4.2.6**. These findings align with regulatory standards, thus confirming the heightened accuracy of the recently developed analytical approach, enabling simultaneous estimation of TFD and QCN

Precision

The interday and intraday precision values for three quality control samples of TFD and QCN demonstrated % RSDs within 2%. These results have been detailed in **Table 4.2.6**, substantiating the precision achieved by the developed HPLC method.

Table 4.2.6. Accuracy and precision for the TFD and QCN

Drug	Concentration level	Inter-day Precision (%RSD)	Intra-day Precision (%RSD)	% Recovery	
				(±SD)	% RSD
TFD	LQC	0.71	0.35	99.30 ± 0.61	0.62
	MQC	1.83	0.41	99.89 ± 1.45	1.46
	HQC	0.32	0.30	100.10 ± 1.12	1.12
QCN	LQC	1.55	1.66	100.93± 1.65	1.63
	MQC	1.17	0.48	99.47 ± 1.80	1.81
	HQC	1.13	0.33	100.55 ± 0.66	0.66

Robustness

Minor changes in column temperature, mobile phase composition, and buffer pH yielded no discernible alterations, with the % RSD measuring below 2% (**Table 4.2.7**).

Table 4.2.7. Robustness

	TFD		QCN	
	% Recovery	**%RSD**	**% Recovery**	**%RSD**
Column temperature - 23°C	99.51	0.70	100.98	1.38
Column temperature -27°C	99.64	0.52	100.14	0.20
Mobile phase – 38% ACN	100.60	0.85	99.61	0.55
Mobile phase – 42% ACN	99.13	1.23	100.46	0.65
pH of buffer – 3.3	99.35	0.92	100.81	1.14
pH of buffer – 3.7	99.41	0.83	99.23	1.09

LOD and LOQ determination

The LOD and LOQ was determined using equation 4.1.3 and 4.1.4. The LOD of TFD and QCN was found to be 0.016 µg/mL and 0.017 µg/mL, respectively. The LOQ of TFD and QCN was determined to be 0.049 µg/mL and 0.051 µg/mL, respectively.

Specificity

The assessment of specificity for the developed method was conducted in the presence of formulation excipients (Phospholipon 90 G, sodium cholate and tween 80) which were anticipated to potentially interfere with the sample. The chromatograms of the blank, sample, placebo, and formulation were depicted in **Figure 4.2.12**. These chromatograms revealed no interference from the formulation excipients with the retention time of TFD and QCN, indicating the specificity of the developed method.
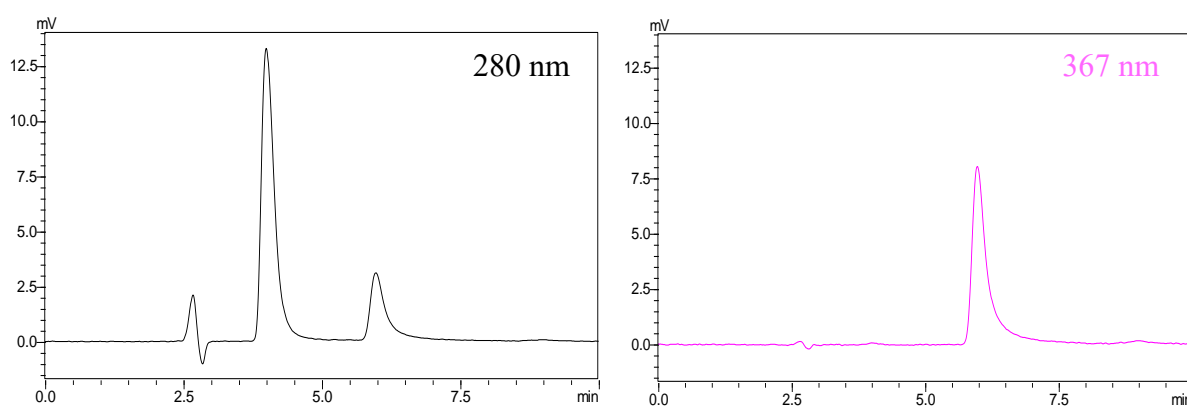
Figure 4.2.12. Specificity of the developed method

4.2.2.3. Forced Degradation studies

The forced degradation studies for combination of TFD and QCN standard sample, blank, placebo and formulations were performed by exposing to different stress conditions such as peroxide, acid, alkali and thermal degradation. The quantified reduction in assay percentage was computed for each condition, and the corresponding outcomes are documented in **Table 4.2.8**.

Table 4.2.8. Forced degradation studies of TFD and QCN

Stress Condition	Degradation of TFD	Degradation of QCN
Standard sample	0 %	0 %
0.01N NaOH	3.03 % in 12 h	> 10 % in 30min
0.01N HCl	> 10 % in 30min	11.50 % in 12 h
3% H_2O_2	> 10 % in 30min	> 10 % in 30min
Thermal	8.92 % in 12h	3.35 % in 24h

The results of the forced degradation analysis revealed that TFD exhibited a more pronounced degradation under acidic conditions compared to alkali. A study reporting forced degradation investigations of TFD under diverse conditions, also indicated a greater degradation rate in acidic environment [39]. Whereas, QCN exhibited significant degradation under alkaline conditions, with degradation exceeding 10% within 30 min. In alkaline degradation at RT 3.3 min a degradation peak of QCN was detected at 280 nm that was confirmed by spiking individual drug. Under oxidative stress conditions, both TFD and QCN displayed substantial degradation i.e. > 10% within 30 mins, whereas the degradation was less pronounced under thermal stress conditions. The chromatograms of the standard samples under normal condition and under various stressed conditions are visually presented in **Figure. 4.2.13a** and **Figure. 4.2.13 (b-e),** respectively. This visual representation confirmed the absence of interference from any other peak.
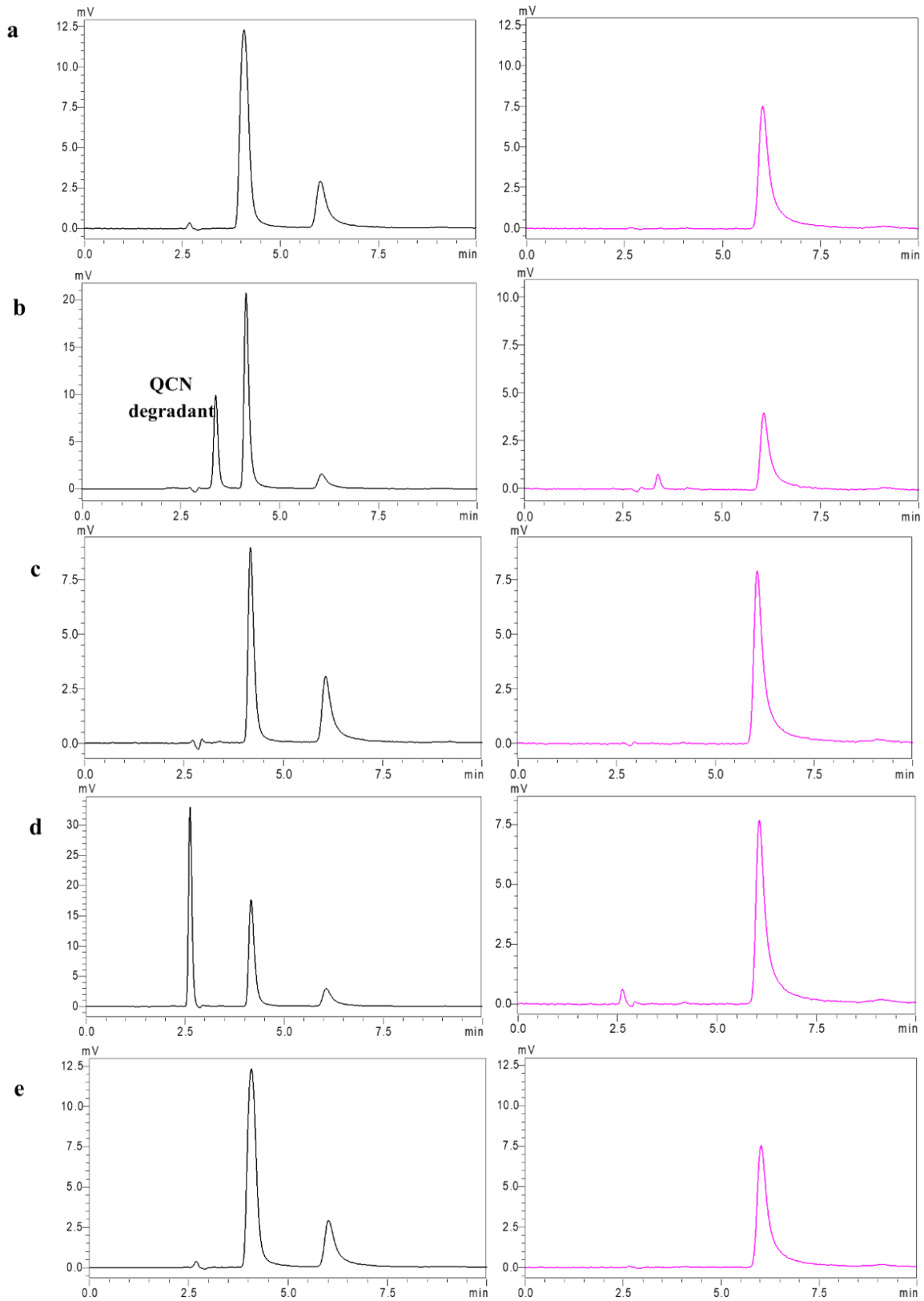
Figure 4.2.13. a) Standard sample under normal condition; forced degradation sample at b) alkali; c) acidic; d) oxidation; e) thermal

Currently, various individual analytical methods have been documented for TFD and QCN. However, employing a AQbD approach facilitates the development of an RP-HPLC method for the quantification of TFD and QCN with a reduced number of experimental trials, while ensuring high resolution. Additionally, the method exhibits specificity by demonstrating no interference with the formulation excipients. Both analytes exhibited a retention time of less than 10 min, thereby reducing the overall method run time. Also, the method demonstrates enhanced sensitivity compared to prior methods. For TFD, the LOD and LOQ were found to be 0.016 μg/mL and 0.049 μg/mL, respectively, indicating improved sensitivity over previous HPLC approaches [39,40]. Similarly, for QCN, the LOD and LOQ were determined as 0.017 μg/mL and 0.051 μg/mL, respectively [41,42], indicating that the method was suitable for detecting and quantifying TFD and QCN across a broad range of concentrations.

4.2.2.4. Assessment of greenness profile of the developed method

The greenness profile of the developed method was evaluated using the AMGS calculator, indicating a greener and more cost-effective approach with a lower AMGS score [38]. Specifically, the proposed method demonstrated a favorable AGMS score of 30.02. The corresponding data for greenness assessment has been summarized in **Table 4.2.9.**

Table 4.2.9. Assessment of the greenness profile of proposed method

Number of analytes of interest	2
Organic modifier	Acetonitrile
Flow rate	1 mL/min
Run time	10 min
Mobile phase A	Acetonitrile (40%)
Mobile phase B	Buffer (60%0
Instrument energy score	8.59 (28.61%)
Solvent energy score	15.48 (51.58%)
Solvent EHS score	5.95 (19.81%)
Total AMGS score	30.02

4.2.3. Conclusion

A new RP-HPLC technique was developed employing the AQbD approach for the simultaneous estimation of TFD and QCN. The method underwent optimization using response surface design *via* face centered CCD. Based on FMEA and RPN score, the critical factors were identified as percentage of acetonitrile (Factor A), flow rate (Factor B) were and pH of the buffer (Factor C), affecting the retention time and resolution of the analytical method. The established design conformed to a quadratic model with a *p*-value of <0.0001 indicating the statistical significance of the model. Numerical and graphical optimization was employed to unveil the ideal chromatographic conditions using MODR, that revealed the optimized zone. The optimized conditions included a mobile phase comprised of 60:40, % v/v of ammonium acetate buffer with pH 3.5 and acetonitrile with a flow rate of 1.0 mL/min. These conditions resulted in a retention time of 3.96 and 5.94 min for TFD and QCN respectively, with the resolution of 4.11. The method underwent validation in accordance with ICH guidelines. The developed analytical method exhibited suitability for analysis without interference from excipients. The validated technique will possess broad applicability, capable of analyzing TFD and QCN individually and in dual drug-loaded formulations. This method offers modern, eco-friendly separation of TFD and QCN in their dual drug loaded formulation, providing efficient and cost-effective results.

Chapter 4

References

1. Dadi, M., & Yasir, M. (2022). Spectroscopy and spectrophotometry: Principles and applications for colorimetric and related other analysis. *Colorimetry.1*, 81-102.

2. Vishwas T. S., & Gurupadayya B. M. (2019). View of novel UV spectrophotometric method for the determination of teriflunomide in tablet dosage form. *International Journal of Current Pharmaceutical Research*, *11*(5), 81–84.

3. Patel, B., Patel, K., Prajapati, H., Chudhary, D., Patel, K. K., & Patel, C. N. (2021). Spectrophotometric method development for estimation of teriflunomide in dosage form. *Indo American Journal of Pharmaceutical Sciences*, *08*(08), 248-254.

4. Patel, M. K., Shah, S. K., Tyagi, C. K., & Usman, M. R. M. (2020). Method development and validation for estimation of quercetin using UV and RP-HPLC in bulk and formulation. *Plant Archives*, 20(2), 4343-4347.

5. Kamal, A. H., El-Malla, S. F., Hammad, S. F., & Kamal, H. (2016). A review on UV spectrophotometric methods for simultaneous multicomponent analysis. *European Journal of Pharmaceutical and Medical Research*, *3*(2), 348–360.

6. Atole, D. M., & Rajput, H. H. (2018). Ultraviolet spectroscopy and its pharmaceutical applications- A brief review. *Asian Journal of Pharmaceutical and Clinical Research*, *11*(2), 59–66.

7. Mukherjee, P., Dutta Chakraborty, D., Chakraborty, P., Shrestha, B., & Ranjan Bhuyan, N. (2021). Different ultraviolet spectroscopic methods: A retrospective study on its application from the viewpoint of analytical chemistry. *Asian Journal of Pharmaceutical and Clinical Research*, *14*(9), 1-11.

8. Medina-Lopez, J. R., Gonzalez-Salazar, O. A., & Contreras-Jimenez, J. M. (2022). Simultaneous quantification of acetylsalicylic acid and caffeine in tablets by first-order derivative spectroscopy. *International Journal of Applied Pharmaceutics*,*14*(4), 200–204.

9. Osman, I., Reid, A., Farid, M., & Eltayeb, S. O. (2021). Simple spectrophotometric methods for the determination of amlodipine and atorvastatin in bulk and tablets. *Future Journal of Pharmaceutical Sciences*, *7*(1), 1–8.

10. Doshi, N., Sheth, A., Patel, T., Dave, J.B. and Patel, C.N. (2010). Spectrophotometric absorption factor method development and validation for estimation of rosuvastatin calcium and telmisartan in solid dosage form. *Journal of Chemical and Pharmaceutical Research., 2*(3), 15-24.

11. International council on harmonisation of technical requirements for registration of pharmaceuticals for human use. Validation of analytical procedures*:* Text and

methodology Q2(R1). (1994).

12. Baldania, S., Bhatt, K., Mehta, R., Shah, D., & Gandhi, T. (2008). RP-HPLC estimation of venlafaxine hydrochloride in tablet dosage forms. *Indian Journal of Pharmaceutical Sciences*, *70*(1), 124.

13. Mowaka, S., Ayoub, B. M., Hassan, M. A., & Zaghary, W. A. (2018). Different spectrophotometric methods for simultaneous determination of trelagliptin and its acid degradation product. *Journal of Analytical Methods in Chemistry*, *2018*(1), 7370651.

14. Cohen, S., & Iqbal, I. (2003). Leflunomide. *International Journal of Clinical Practice*, *57*(2), 115–120.

15. Nadella, N. P., Ratnakaram, V. N., & Srinivasu, N. (2017). Quality-by-design-based development and validation of a stability-indicating UPLC method for quantification of teriflunomide in the presence of degradation products and its application to in-vitro dissolution. *Journal of Liquid Chromatography & Related Technologies*, *40*(10), 517–527.

16. El-Said, K. S., Atta, A., Mobasher, M. A., Germoush, M. O., Mohamed, T. M., & Salem, M. M. (2022). Quercetin mitigates rheumatoid arthritis by inhibiting adenosine deaminase in rats. *Molecular Medicine*, *28*(24) 1-13.

17. Ghasemi, M., Rahmani, M., & Khajeh, M. (2023). Development of a liquid-phase microextraction method prior to HPLC analysis of quercetin in food samples. *Journal of Chromatographic Science. 62*(4), 390-398.

18. Wadie, M., Abdel-Moety, E. M., Rezk, M. R., & Marzouk, H. M. (2024). A novel eco-friendly HPLC method with dual detection modes for versatile quantification of dutasteride and silodosin in pharmaceutical formulation, dissolution testing and spiked human plasma. *Microchemical Journal*, *197*, 109753.

19. Rule, G. S., Rockwood, A. L., & Johnson-Davis, K. L. (2019). LC-MS/MS method for the quantification of the leflunomide metabolite, teriflunomide, in human serum/plasma. *Methods in Molecular Biology*, *1872*, 75–83.

20. Kumar, V. D., Verma, P. R. P., Singh, S. K., & Viswanathan, S. (2015). LC-ESI-MS/MS analysis of quercetin in rat plasma after oral administration of biodegradable nanoparticles. *Biomedical Chromatography*, *29*(11), 1731–1736.

21. Dowd, L. E. (1959). Spectrophotometric determination of quercetin. *Analytical Chemistry*, *31*(7), 1184–1187.

22. Kashid, A. M., Polshettiwar, P. P., & Bhosale, K. M. (2022). Analytical method development and validation of teriflunomide active pharmaceutical ingredient by RP-

UHPLC. *Asian Journal of Pharmaceutical Analysis*, *12*(3), 166–172.

23. Abdelkawy, K. S., Balyshev, M. E., & Elbarbry, F. (2017). A new validated HPLC method for the determination of quercetin: Application to study pharmacokinetics in rats. *Biomedical Chromatography*, *31*(3), 1–8.

24. Pandey, S., Mahtab, A., Singh, A., Ahmad, F. J., Aqil, M., & Talegaonkar, S. (2018). Development and validation of stability indicating reversed-phase liquid chromatographic method for simultaneous quantification of methotrexate and teriflunomide in nanoparticles and marketed formulation. *Biomedical Chromatography*, *32*(12), 1–11.

25. Ramaswamy, S., Gowthamarajan, K., Priyanka Dwarampudi, L., Bhaskaran, M., & Kadiyala, M. (2021). Analytical method development, validation and forced degradation studies for rutin, quercetin, curcumin, and piperine by RP-UFLC method. *Drug Development and Industrial Pharmacy*, *47*(4), 562–568.

26. Adin, S. N., Gupta, I., Aqil, M., & Mujeeb, M. (2023). Application of QbD based approach in development and validation of RP-HPLC method for simultaneous estimation of methotrexate and baicalin in dual-drug-loaded liposomes. *Biomedical Chromatography*, *37*(4), e5581.

27. Gupta, I., Adin, S. N., Aqil, M., Mujeeb, M., & Akhtar, M. (2023). Application of QbD-based approach to the development and validation of an RP-HPLC method for simultaneous estimation of pregabalin and naringin in dual-drug loaded liposomes. *Biomedical Chromatography*, *37*(6), e5623.

28. Sandhu, P. S., Beg, S., Katare, O. P., & Singh, B. (2016). QbD-driven development and validation of a HPLC method for estimation of tamoxifen citrate with improved performance. *Journal of Chromatographic Science*, *54*(8), 1373–1384.

29. Shah, J., Kotadiya, R., & Patel, R. (2022). Analytical quality by design-based robust RP-HPLC method for quantitative estimation of pregabalin and etoricoxib in fixed-dose combination tablet formulation. *Journal of AOAC International*, *105*(6), 1536–1547.

30. Kochling, J., Wu, W., Hua, Y., Guan, Q., & Castaneda-Merced, J. (2016). A platform analytical quality by design (AQbD) approach for multiple UHPLC-UV and UHPLC–MS methods development for protein analysis. *Journal of Pharmaceutical and Biomedical Analysis*, *125*, 130–139.

31. Fukuda, I. M., Pinto, C. F. F., Moreira, C. D. S., Saviano, A. M., & Lourenço, F. R. (2018). Design of experiments (DoE) applied to pharmaceutical and analytical quality by design (QbD). *Brazilian Journal of Pharmaceutical Sciences*, *54*(Special Issue), e01006.

32. Patel, R. B., & Patel, M. R. (2022). A novel validated stability indicating analytical

HPTLC method for quantitation of hydrochlorothiazide and lisinopril in tablet formulation. *Indian Drugs*, *59*(6), 47–51

33. Abdel-Moety, E. M., Rezk, M. R., Wadie, M., & Tantawy, M. A. (2021). A combined approach of green chemistry and quality-by-design for sustainable and robust analysis of two newly introduced pharmaceutical formulations treating benign prostate hyperplasia. *Microchemical Journal*, *160*, 105711.

34. Ahmed, D. A., Hussein, O. G., Rezk, M. R., Abdelkawy, M., & Rostom, Y. (2024). Impressive merger between green analytical approaches and quality- by- design for alcaftadine determination in eye drops and rabbit aqueous humor; Application to stability study by two validated chromatographic methods. *Microchemical Journal*, *196*, 109717.

35. Verch, T., Campa, C., Chéry, C. C., Frenkel, R., Graul, T., Jaya, N., Nakhle, B., Springall, J., Starkey, J., Wypych, J., & Ranheim, T. (2022). Analytical quality by design, life cycle management, and method control. *AAPS Journal*, *24*(1), 1–21.

36. Vikas, A., Rashmin, P., Mrunali, P., Sandip, M., & Kaushik, T. (2020). RP-HPLC method for quantitative estimation of efinaconazole in topical microemulsion and microemulsion-based-gel formulations and in presence of its degradation products. *Microchemical Journal*, *155*, 104753.

37. Baertschi, S. W., Alsante, K. M., & Tønnesen, H. H. (2010). A critical assessment of the ICH guideline on photostability testing of new drug substances and products (Q1B): Recommendation for revision. *Journal of Pharmaceutical Sciences*, *99*(7), 2934–2940.

38. Wadie, M., Abdel-Moety, E. M., Rezk, M. R., & Tantawy, M. A. (2021). Eco-friendly chiral HPLC method for determination of alfuzosin enantiomers and solifenacin in their newly pharmaceutical combination: Method optimization via central composite design. *Microchemical Journal*, *165*, 106095.

39. Mehta, B., Prajapat, P., & Gohil, Y. (2017). Development and validation of stability indicating RP-HPLC method for estimation of teriflunomide in active pharmaceutical ingredient. *The Pharma Innovation Journal*, *6*(9), 440–449.

40. Upadhyay Priya Shitalaprasad, Dr Vinay C. Darji, Bhumi Patel, Jaymin Patel. (2018). Development and validation of stability indicating assay method for estimation of teriflunomide in tablet dosage form. *Indo American Journal of Pharmaceutical Sciences*, *5*(04), 3209–3219.

41. Khursheed, R., Singh, S. K., Kapoor, B., Gulati, M., Wadhwa, S., Gupta, S., Prasher, P., Kumar, D., Dua, K., Kumar, L. M. S., Babu, U. V., Sharma, M., Soni, H. K., & Kumar, V. (2021). Development and validation of RP-HPLC method for simultaneous

determination of curcumin and quercetin in extracts, marketed formulations, and self-nanoemulsifying drug delivery system. *Re: Gen Open, 1*(1), 43–52.

42. Sanghavi, N., Bhosale, S. D., & Malode, Y. (2014). RP-HPLC method development and validation of quercetin isolated from the plant Tridax procumbens L. *Journal of Scientific and Innovative Research*, *3*(6), 594–597.

Chapter 5

Quality by Design-based Optimization of Teriflunomide and Quercetin Loaded Topical Combinational Transferosomal Gel

Chapter 5

5.1. Introduction

The combination of TFD and QCN demonstrated significant synergistic activity in *in-vitro* cell line studies (as mentioned the chapter 3), and hence was selected for the formulation development through a meticulous process. Oral administration of TFD is associated with significant systemic side effects such as hepatotoxicity, bone marrow effects, peripheral neuropathy, increased blood pressure, respiratory effects, and hypersensitivity [1] as detailed in the section no 2.1.1.3. Similarly, QCN has low bioavailability which is attributable to its inadequate gastric retention. It also results in poor clinical efficacy due to rapid degradation in alkaline conditions [2]. Thus, an alternative route of administration is required for the effective treatment in RA with reduced dose. Achieving precise targeting of affected joints poses a significant hurdle in drug delivery, impacting both the effectiveness of treatment and the control of systemic exposure. To address these challenges linked with oral administration, topical delivery could be promising approach in mitigating these side effects and enhanced efficacy *via* localized action [3,4]. In recent years, topical administration of transferosomes have emerged as a promising approach [3]. Transferosomes are composed of a phospholipid bilayer and surfactant that augment skin permeability, enabling precise localized action. Their ability to accommodate both hydrophilic and lipophilic molecules makes them an ideal choice for combination delivery of TFD and QCN for the treatment of RA [5]. The phospholipid bilayer structure of transferosomes closely resembles the natural lipid bilayers found in the skin, making them biocompatible with the skin. Also, the inherent deformability of transferosomes allows them to cross the skin's main barrier (*stratum corneum*), thus facilitating enhanced penetration into the deeper layers of the epidermis [6]. Section 1.9 provides a detailed description of transferosomes, and the various molecules reported for transferosomes delivery in RA.

Given the diverse array of combination therapies in the realm of RA treatment, a systematic evaluation was done for the potential effect of a combination therapy involving transferosomes loaded with TFD and QCN. This investigation was prompted by the earlier-discussed findings (Chapter 3), with a specific focus on localized delivery strategies for RA. The objective of the present work was to design TFD and QCN loaded topical transferosomes using QbD approach incorporating Box-Behnken design (BBD) and further subject them to comprehensive evaluation across various parameters. Moreover, this study also aimed to enhance skin permeation *via* transferosomes loaded gel followed by assessing its efficacy in reducing levels of pro-inflammatory cytokines and NO in in-*vitro* cell lines.

Chapter 5

5.2. Materials and methods

5.2.1. Materials

As mentioned in chapter 3, TFD (99.9% pure) was obtained as a gift sample from the MSN Laboratories Private Limited (Sangareddy, India). Querectin was purchased from the Yucca Enterprises (Mumbai, India) with the purity in the ranges of > 97%. Phospholipon 90G (PL 90G) was obtained as gift sample from Lipoid (Germany). Sodium cholate, tween 80, NEED and MTT were purchased from SRL Pvt. Ltd, (Mumbai, India). Carbopol 974P was purchased from Lubrizol (Belgium, Europe). HPLC-grade acetone, methanol, chloroform and acetonitrile were purchased from Merck Life Sciences Pvt Ltd, (Mumbai, India). DMEM with high glucose was purchased from Gibco (New York USA). FBS, dialysis membrane and DMSO were purchased from Himedia (Mumbai, India). LPS (*E. coli* O26:B6) was purchased from Sigma Aldrich (Bengaluru, India). TNF-α and IL-6 ELISA kits were purchased from Elabscience (Houston, USA).

5.2.2. Preparation of transferosomes

Transferosomes loaded with TFD and QCN were formulated using the thin film hydration method as reported previously with some modifications [7]. Briefly, TFD or QCN, phospholipid (PL 90G), and sodium cholate were dissolved in a mixture of chloroform and methanol in a 3:1 ratio. The organic solvent was removed using a rotary vacuum evaporator (Heidolph rotary evaporator) at 45°C and 120 rpm until a distinct thin film was formed. Thereafter the thin film was hydrated with an aqueous tween 80 solution, at a temperature of 60°C (exceeding the lipid phase transition temperature), and was stirred for 30 min at 120 rpm [8]. Additionally, the hydration process was done for 1 h to ensure adequate swelling of the nanovesicles. Thereafter, the above aqueous dispersion was sonicated for 10 min using a bath sonicator, followed by probe sonication (Vibra cell^{TM}) with a 3 mm probe at 20 % amplitude, utilizing a 15-second on and 10-second off cycle for a duration of 1 min [7,9].

5.2.3. Optimization of transferosomes using BBD

In developing transferosomes loaded with TFD or QCN, a systematic QbD approach was employed. This encompassed the application of the BBD within response surface methodology, leveraging its robust and advantageous framework [2]. The statistical experimental design of BBD facilitates the concurrent investigation of multiple factors, enabling the precise optimization of formulations through a systematic evaluation of quadratic model parameters. It also aids in constructing efficient experimental models, ensuring a comprehensive exploration of the design space. Furthermore, BBD plays a crucial role in discerning the adequacy of the model by identifying lack of fit, enhancing the reliability and accuracy of

formulation development processes. Furthermore, the design proves instrumental in circumventing experimentation under extreme conditions, thereby mitigating the potential for suboptimal responses.

A three-factor, three-level BBD experimental approach was employed for understanding the effect of independent variables on the formulation of nanovesicles. The independent variables, including the quantities of PL 90G (A), sodium cholate (B), and tween 80 (C), were chosen to operate at three distinct levels (+1, 0, -1 representing high, intermediate and low level). Simultaneously, vesicle size (nm) and entrapment efficiency (%EE) were designated as dependent variables for the optimization of the formulation. In accordance with initial investigations, the quantities of PL 90G (A), sodium cholate (B), and tween 80 (C) were chosen within the specified ranges of 200 to 400 mg, 25 to 55 mg, and 10 to 50 mg, respectively. A total of 15 experimental runs, including 3 center points, were generated using Design Expert software version 7.0.0 with the BBD experimental design for TFD and QCN transferosomes. A batch size of 10 mL was prepared, and all other process parameters were maintained constant throughout the experiment. In addition to the aforementioned dependent variables, polydispersity index (PDI), zeta potential (ZP), and % assay were evaluated. The nanovesicles prepared through the QbD approach underwent further examination for precipitation during overnight observation.

The main goal of the BBD design is to optimize the composition of transferosomes by determining the ideal concentrations of PL 90G (A), sodium cholate (B), and tween 80 (C), using QbD. The 15 runs recommended by QbD were prepared using thin film hydration method separately for both TFD and QCN transferosomes. Subsequently, the results pertaining to vesicle size (nm) and EE (%) were assessed and entered into the software for further analysis. The evaluation of the optimal fitting model involved a comprehensive analysis of experimental data across various configurations, including quadratic, linear, modified, cubic, and 2-factor interaction models. This approach allowed a thorough exploration of the data to identify the most suitable model for the study.

Additionally, the model's significance was determined *via* ANOVA. The relationship between independent and dependent variables was visually explored through the utilization of 3D response plots and 2D contour plots. Polynomial models, comprising interaction and quadratic terms, were derived for all dependent variables employing a multiple linear regression analysis (MLRA) methodology. The residual plots were utilized to ascertain the variance between the theoretical and predicted values. The method operable design region (MODR) was further

established to get the optimized zone for the formulation. Eventually, formulation optimization was attained through the utilization of numerical methods and the desirability function.

5.2.4. Characterization of the transferosomes

5.2.4.1. Vesicular size, poly dispersity index (PDI) and zeta potential (ZP) determination

The TFD or QCN transferosomes, prepared through a QbD approach, were characterized for vesicle size, PDI, and ZP utilizing dynamic light scattering (DLS) with a Zetasizer (Malvern Instruments, Ltd., UK) after appropriate dilution with Milli-Q water [10].

5.2.4.2. Percent entrapment efficiency (% EE)

The % EE was determined using the dialysis bag method, utilizing a specially crafted snake skin dialysis membrane composed of regenerated cellulose with a molecular cut-off of 3500 Da (Thermo Scientific, Rockford, USA). The dialysis membrane was first cut into segments approximately 2.5 cm in length. Subsequently, 500 µL of free drug solution and transferosome solution of TFD or QCN was introduced into the bag separately, and securely tied at both ends. The formulation was subjected to dialysis in 100 mL of Milli-Q water, with constant stirring at 100 rpm, for a period determined by the time required to attain a minimum of 90% drug release from the free drug solution. The experiment typically lasted around 2 h . Afterward, the sample was filtered using a syringe filter and the free drug was analyzed spectroscopically using a validated UV- visible spectrophotometric method (Section 4.1), at maximum wavelengths (λ_{max}) of 280 nm for TFD and 367 nm for QCN. Further, the % EE was calculated using the following equation 5.1 and the drug loading was calculated using equation 5.2 [11–13].

$$\%EE = \frac{T_{total\ drug} - T_{free\ drug}}{T_{total\ drug}} \qquad \text{...eq 5.1}$$

$$\%\ Drug\ loading = \frac{T_{total\ drug} - T_{free\ drug}}{W_{lipid+surfactant}} \qquad \text{...eq 5.2}$$

Where, $T_{total\ drug}$ = Total amount of either TFD or QCN incorporated into transferosomes

$T_{free\ drug}$ = The amount of unbound drug acquired from the filtrate post-dialysis

$W_{lipid+surfactant}$= Total weight of lipid and surfactant used in transferosomes

5.2.4.3. Drug content determination

To determine the total drug content, 100 µL of TFD or QCN transferosomes were lysed by adding 900 µL of methanol, followed by sonication for 10 min. Subsequently, the solution was centrifuged at 3500 rpm for 15 min, and the supernatant was collected. The above supernatant

was appropriately diluted and analyzed using a validated UV-visible spectrophotometric method. The results are represented as a percentage assay [2,14].

5.2.4.4. ATR-IR

The IR spectra of TFD, QCN, blank transferosomes, TFD-loaded transferosomes, and QCN-loaded transferosomes were obtained using Bruker's ATR-IR in the range of 4000 to 400 cm^{-1} [15].

5.2.4.5. *In-vitro* drug release

The *in-vitro* drug release studies of free drug solution and transferosomes of both TFD and QCN were performed using a Franz diffusion cell having a capacity of 30 mL. The experiment utilized a dialysis membrane with an average molecular weight of 12,000 Da (Himedia, India). The release media was selected based on the solubility characteristics of both drugs. It was comprised of phosphate buffer solution (pH 6.8) with 20% acetone. Before starting the experiment, the membrane was immersed overnight in the release media [14,16]. In order to carry out the experiment the diffusion cell was filled with media, maintained at a temperature of 37 ± 0.5°C, under magnetic stirring at 200 rpm. About 500 µL of transferosomes of individual TFD and QCN was placed on the donor compartment and samples were withdrawn at predetermined time points (0, 0.5, 1, 2, 4, 6, 8 10, 12 and 14 h) and replaced with same amount of fresh medium to maintain sink condition. The samples were filtered using syringe filters and further analyzed by validated simultaneous HPLC method (section 4.2) [17].

5.2.5. Lab scale-up studies

The optimized TFD and QCN transferosomes underwent a laboratory scale-up process, increasing the batch size from 10 mL to 50 mL. The laboratory scale-up involved a systematic evaluation of different process parameters to understand their impact on the vesicle size. This step was crucial in ensuring the transferosomes maintain their optimized properties at a larger scale. The investigation provided valuable insights into the scalability of the formulations, guiding future efforts toward potential industrial applications. **Table 5.1** delineates the various process parameters for both 10 mL and 50 mL batch sizes. Subsequently, the prepared transferosomes underwent further evaluation for vesicular size, PDI, ZP and % EE.

5.2.6. Preparation of TFD and QCN combination transferosomal gel

The optimized composition of TFD and QCN transferosomes was subsequently chosen for the formulation of the topical gel. The selection of the TFD and QCN combination at a ratio of 1:3.5 was based on the *in-vitro* cell line study conducted in RAW264.7 cells (Chapter 3). Carbopol 974P was selected because of its wide range of applicability in topical delivery. Transferosomes containing TFD and QCN at an equivalent concentration of 0.05% and 0.175%

respectively, were loaded into the gel formulation. In the preparation process, the required amount of water was added to transferosomes loaded with TFD and QCN. Subsequently, Carbopol 974P at a concentration of 0.5 % was added to the above solution under mechanical stirring at 500 rpm. The Carbopol 974P dispersion was allowed to swell for 15 min to ensure a uniform dispersion. Finally, the gel was neutralized using a 0.1% NaOH solution, and stirring was continued until a uniform gel consistency was achieved [18,19].

Table 5.1. Process parameters for preparing transferosomes in 10mL and 50mL batch size

Parameter	10 mL	50 mL
RBF size	50 mL	250 mL
RPM	100	120
Sonication time	10 min	10 min
Probe diameter	3 mm	13 mm
Probe sonication	20 % Amplitude for 1 min (15 sec on, 10 sec off cycle)	25 % Amplitude for 1 min (15 sec on,10 sec off cycle)

5.2.7. Evaluation of the combination transferosomal Gel

5.2.7.1 Physical appearance and pH determination

The gel formulation containing TFD and QCN was assessed visually for smoothness, homogeneity, and clarity. The pH of the gels was measured using a calibrated handheld pH meter. About 1 gm of gel was taken and dispersed in 9 mL Milli-Q water, and the pH measurement was taken at room temperature.

5.2.7.2. Drug content determination

To quantify the total drug content in the topical gel, 1 gm of gel was subjected to lysis by adding 9 mL of methanol, followed by sonication for 10 min. The resulting solution was centrifuged at 3500 rpm for 15 min, and the supernatant was collected [2]. This supernatant was appropriately diluted and subjected to additional analysis utilizing a validated HPLC method (section 4.2) [17].

5.2.7.3. Vesicle size, PDI and ZP of combination loaded gel

The combination gel, consisting of 1 gm of TFD and QCN, was dispersed in 10 mL of Milli-Q water to achieve a uniform dispersion. As mentioned in the earlier section 5.2.4.1, the gel was analyzed for vesicle size, PDI and ZP.

5.2.7.4. Rheology

The rheological characteristics of the gel formulation were assessed utilizing a rheometer (Anton Paar MCR 92, Australia) with flat-faced spindle set to a controlled temperature of 25°C. This analytical instrument enables precise measurement and analysis of rheological behavior of gel, including its viscosity, elasticity, and flow properties. By subjecting the gel to controlled stress and strain conditions, the rheometer provides valuable insights into the gel's structural integrity, consistency, and response to external forces.

Viscosity and flow curves

The viscosity of the combination gel was initially assessed at a constant shear rate (γ) of 10 1/s at 25°C. The average viscosity of the twenty measurements was taken into consideration for analysis. The viscosity of the gel was further assessed by measuring it at varying shear rates ranging from 0.1 to 100 1/s. This evaluation aimed to determine whether the gel exhibits Newtonian or non-Newtonian flow behavior. To further examine flow characteristics of gel, flow curves were generated where shear stress (τ) was plotted as a function of shear rate (γ). All flow curves were generated using a continuous ramp step, gradually decreasing the shear rate from 100 to 0.1 1/s with 25 data points being captured [19,20].

Amplitude sweep test

The amplitude sweep test for topical gels evaluates their mechanical stability and viscoelastic behavior under varying stress amplitudes, providing insights into their performance and suitability for application. The amplitude sweep test of the prepared topical gel was performed at angular frequency (ω) of 10 1/s. The graph was plotted for the storage (G') and loss (G") moduli as a function of the imposed shear stress amplitude (τa), ranging from 0.01 to 100 Pa [19].

Frequency sweep test

The frequency sweep test for topical gels assesses their viscoelastic properties over a range of frequencies, aiding in the understanding how the gel responds to dynamic conditions, ensuring its stability and performance during various application scenarios. The frequency sweep test for the prepared formulations was performed at constant stress amplitude. The graph was plotted as storage (G') and loss (G") moduli against imposed angular frequency of 0.001 to 100 rad/sec [19].

5.2.8. *In-vitro* cell culture studies

5.2.8.1. NO assay

RAW 264.7 cells were utilized for the study of anti-inflammatory activities due to their established role as a model system for investigating macrophage-mediated immune responses and inflammatory processes. The cells were maintained in a nutrient media composed of DMEM with 10 % FBS using an incubator at 37° C with 5% CO_2 and saturated humidity. The cells were seeded at a density of 2.5 x 10^4 cells /well in 12 well plate and incubated for 24 h. Further, the cells were treated with various concentrations of free TFD (1,2,3 µM), free QCN (3.5,7,10.5 µM), TFD transferosomes (1,2,3 µM), QCN transferosomes (3.5,7,10.5 µM), free drug combinational gel and transferosomal combination gel (TFD-1,2,3 µM and QCN-3.5,7,10.5 µM). After 4 h of incubation, cells were stimulated by LPS at 1 µg/mL for next 18 h. The following day, the cell supernatant was collected and centrifuged at 5000 rpm for 10 min. The supernatant was analyzed for nitrite content using Griess reagent and the absorbance was measured at 540 nm after 15 min of incubation at room temperature using a microplate reader. The concentration of nitrite produced was determined using a standard plot of $NaNO_2$ as mentioned the section no 3.4.2.

5.2.8.2. Effect of formulations on the production of TNF-α and IL-6

In RA, TNF-α and IL-6 act as pivotal pro-inflammatory cytokines, actively contributing to the persistent inflammation and joint damage associated with the condition. Therapeutic approaches targeting these cytokines are fundamental in RA management, aiming to regulate the immune response and mitigate symptoms [21–23]. The experiment was carried out following the procedure detailed in the above section. The supernatant was collected after centrifugation and analyzed for TNF-α and IL-6 levels using ELISA kit according to the manufacturer's protocol. The measurement was taken using microplate reader at 450 nm.

5.2.8.3. Cell viability in HaCaT cell lines

HaCaT cells, that originate from Human Keratinocytes, have been used as a standard model for assessing the cytotoxicity and potential adverse effects of topical formulated products on human skin cells. The cells were maintained in a nutrient media composed of DMEM with 10 % FBS maintained in an incubator at 37° C with 5% CO_2 and saturated humidity. The cytotoxicity was performed using MTT assay. For assessing the cytotoxicity, $5x10^3$ cells per well were seeded in a 96-well plate and incubated for 24 h . Following day, the cells were treated with free TFD (1,2,3 µM), free QCN (3.5,7,10.5 µM), TFD transferosomes (1,2,3 µM), QCN transferosomes (3.5,7,10.5 µM), free drug combinational gel and transferosomal combination gel (TFD-1,2,3 µM and QCN-3.5,7,10.5 µM). After 24 h of further incubation

with various formulations and free drug solution, the media was removed and replaced by 0.5 mg/mL of MTT. After 4 h of incubation, the MTT solution was replaced and formed formazan crystals were dissolved by the addition of DMSO. The readings were taken after 30 min using microplate reader at 570 nm with a reference wavelength of 630 nm [24].

5.2.9. *Ex-vivo* skin permeation and skin retention studies

A comparative *ex-vivo* permeation study was carried out for the free drug combination loaded topical gel and transferosomes loaded combination topical gel. The *ex-vivo* study was performed using Franz diffusion cell with 20 mL volume and having a diffusion area of 1 cm^2. The release media consisting of phosphate buffer (pH 6.8) with 20 % acetone. The abdominal skin of the rat was excised, washed with buffer, and positioned on the diffusion cell with the dorsal side facing towards the donor compartment. Approximately 0.25 gm of the gel was placed on the donor compartment of the Franz diffusion cell and kept at 300 rpm at room temperature. The sample was collected at regular time intervals of 0, 2, 4, 8, 12, 16, 20 and 24 h, with replacement of fresh medium. The sample was filtered using a syringe filter of 22μm and analyzed using validated HPLC method (section 4.2) [17]. The amount of drug permeated per unit skin surface area (μg/cm^2) was plotted against time (h). The steady-state flux (Jss, μg/cm^2 h) was determined by calculating the slope of the linear segment of the plot using linear regression analysis.

After 24 h of incubation, the skin samples were thoroughly washed to remove any un permeated gel and then cut into small pieces. The drug present in the tissue matrix was extracted by adding methanol, followed by further homogenization for 10 min at 10,000 rpm [25]. Subsequently, the sample were centrifuged, the supernatant was collected, and the amount of drug deposited in the skin was determined by analyzing it using the HPLC method [17].

5.2.10. Storage stability

The prepared combinational gel was subjected to stability studies at 4–8°C for 45 days. Changes in vesicle size, PDI, and ZP were evaluated using DLS according to the procedure described in section 5.2.4.1 [7].

5.3. Statistical analysis

Each experiment was conducted thrice, and the findings are presented as the mean with standard deviation. Statistical analysis involved employing two-way ANOVA for *in-vitro* cell line studies and *ex-vivo* permeation studies. One -way ANOVA for *ex-vivo* skin retention study, through GraphPad Prism (v 7.0), with significance levels set at $p < 0.05$.

5.4. Results and discussion

5.4.1. Optimization of transferosomes by BBD

Transferosomes loaded with TFD or QCN were formulated using the conventional thin film hydration method. The fundamental structure of transferosomes comprises of phospholipid and surfactant. PL 90G, that was chosen as the phospholipid, consists of phosphatidylcholine (at least 94.0%) and lysophosphatidylcholine (not exceeding 4.0 %). This component contributes to the structural integrity and stability of the transferosome. Its amphiphilic properties facilitate the formation of flexible lipid bilayers, promoting enhanced permeation through the skin and ensuring biocompatibility [26]. Tween 80 and sodium cholate were opted as edge activators, that augmented the deformability and elasticity of nanovesicles. This characteristic enables them to easily traverse narrow pores, ensuring efficient skin penetration [26,27]. Different nanovesicles have been documented for topical and transdermal delivery, employing PL 90G, sodium cholate, and tween 80 [8,14,25]. It has been hypothesized that TFD becomes integrated into the hydrophobic matrix of the phospholipid bilayer due to its hydrophobicity. On the contrary, QCN possesses both hydrophobic and hydroxyl groups that renders it an amphiphilic nature, facilitating its localization within the membrane at the polar–nonpolar interface (**Figure 5.1**) [28,29].
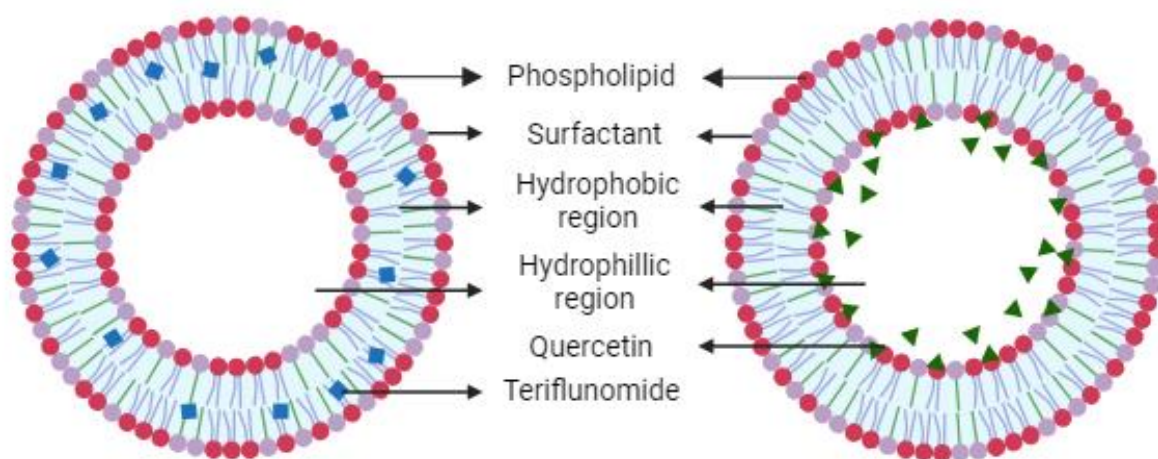
Figure 5.1. Transferosomes encapsulating TFD and QCN

In the preliminary trials, the combination of sodium cholate and tween 80 as surfactant yielded favorable results compared to using either component alone. This could be attributed to the enhanced interaction resulting from the combination of anionic surfactants such as sodium cholate with non-ionic surfactants like tween 80 [30]. Further, the composition of the formulation was optimized through the QbD approach. The initial ranges for PL 90G (200 to

400 mg) [14], sodium cholate (25 to 55 mg), and tween 80 (10 to 50 mg) were decided based on the preliminary trials. Concentrations of PL 90G below 100 mg led to inadequate loading, while concentrations above 400 mg resulted in aggregation [31]. Insufficient concentrations of tween 80 and sodium cholate resulted in inadequate vesicle formation, leading to suboptimal entrapment efficiency. An optimal balance of these components were crucial for the formation of well-structured vesicles with high encapsulation capacity [32]. The remaining process parameters, including film hydration time, sonication time, and probe sonication, were optimized through preliminary experimental trials.

A total of 15 experimental trails were conducted in accordance with QbD principles. The prepared transferosomes loaded with TFD and QCN are represented in **Figure 5.2**.
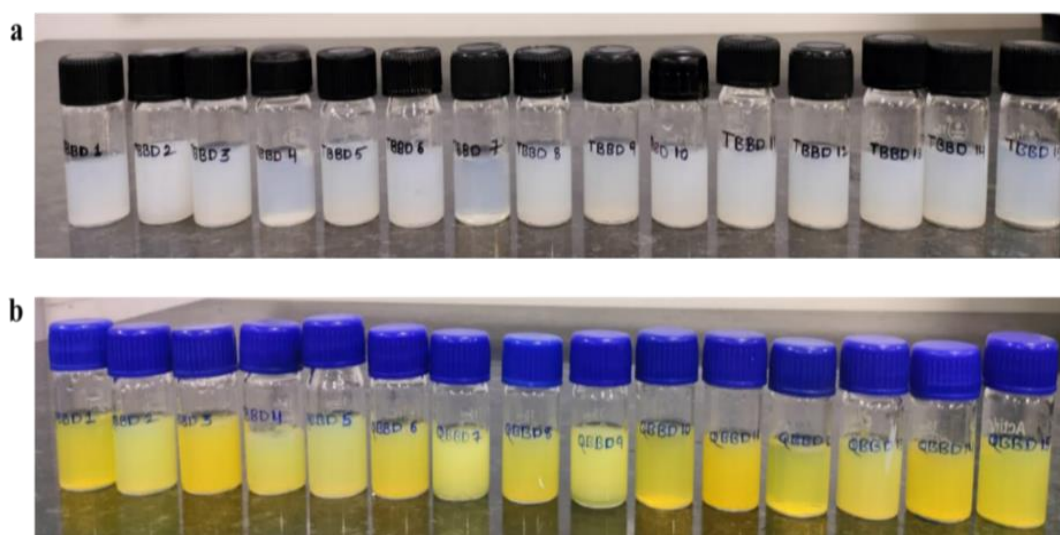
Figure 5.2. Formulations prepared using BBD design a) TFD transferosomes and b) QCN transferosomes

The vesicle size (nm) and %EE were determined, and the corresponding results are shown in **Table 5.2** and **Table 5.3** for TFD and QCN transferosomes, respectively. Apart from the dependent variables, PDI, ZP and % assay were also evaluated for the prepared transferosomes.

Table 5.2. BBD experimental design runs and responses for TFD loaded transferosomes

Factor 1 A PL 90G (mg)	Factor 2 B Sodium Cholate(mg)	Factor 3 C Tween 80 (mg)	Response 1 Vesicle size (nm)	Response 2 EE (%)	PDI	Zeta Potential (mV)	Assay (%)
200	55	30	109.20 ± 0.14	69.61 ± 0.65	0.362 ± 0.069	-37.4 ± 2.97	101.42 ± 0.20
400	40	50	158.30 ± 8.49	91.16 ± 0.24	0.407 ± 0.006	-40 ± 0.99	99.03 ± 0.21
400	55	30	157.70 ± 1.41	84.56 ± 0.17	0.458 ± 0.006	-40.2 ± 0.57	99.89 ± 0.10
200	25	30	80.63 ± 0.67	76.61 ± 0.02	0.267 ± 0.001	-27.1 ± 1.70	99.49 ± 0.22
400	25	30	161.90 ± 1.56	91.13 ± 0.10	0.495 ± 0.027	-39.75 ± 0.35	98.91 ± 0.20
300	25	10	122.05 ± 5.87	73.10 ± 0.181	0.400 ± 0.005	-39.9 ± 0.71	99.95 ± 0.68
300	40	30	93.51 ± 0.44	79.04 ± 0.89	0.272 ± 0.008	-26.65 ± 0.35	100.86 ± 0.28
300	55	50	126.60 ± 1.13	77.51 ± 0.54	0.429 ± 0.037	-40.7 ± 5.23	100.34 ± 0.47
200	40	50	108.00 ± 1.41	74.39 ± 0.29	0.374 ± 0.024	-36.9 ± 0.71	98.77 ± 0.30
300	40	30	93.56 ± 0.51	79.94 ± 0.40	0.272 ± 0.008	-26.65 ± 0.35	101.26 ± 0.98
200	40	10	112.85 ± 2.62	69.45 ± 0.13	0.309 ± 0.008	-38.85 ± 1.20	99.70 ± 0.10
400	40	10	171.70 ± 10.47	81.65 ± 0.03	0.481 ± 0.034	-40.95 ± 1.63	98.97 ± 0.31
300	55	10	146.05 ± 5.59	62.61 ± 0.08	0.438 ± 0.029	-39.15 ± 1.77	99.26 ± 0.50
300	25	50	113.85 ± 1.20	74.71 ± 0.26	0.309 ± 0.008	-36.05 ± 1.34	98.91 ± 0.20
300	40	30	95.87 ± 0.07	79.54 ± 0.30	0.272 ± 0.008	-30.95 ± 1.06	100.65 ± 0.29

Table 5.3. BBD experimental design runs and responses for QCN loaded transferosomes

Factor 1 A PL 90G (mg)	Factor 2 B Sodium Cholate(mg)	Factor 3 C Tween 80 (mg)	Response 1 vesicle size (nm)	Response 2 EE (%)	PDI	Zeta Potential (mV)	Assay (%)
300	55	50	90.36 ± 2.76	88.09 ± 1.13	0.293 ±0.005	-22.23 ± 0.91	100.03 ± 0.44
300	25	50	123.97 ± 1.82	83.36 ± 0.25	0.414 ± 0.029	-27.93 ± 0.46	100.83 ± 0.34
400	55	30	139.00 ± 1.31	92.40 ± 0.18	0.409 ± 0.018	-35.00 ± 0.79	98.73 ± 0.69
200	25	30	91.21 ± 4.18	86.88 ± 0.11	0.443 ± 0.012	-28.73 ± 0.64	101.26 ± 0.78
400	25	30	163.33 ± 6.51	84.16 ± 0.34	0.446 ± 0.076	-31.53 ± 0.60	100.41 ± 0.22
300	40	30	136.30 ± 3.87	79.08 ± 0.54	0.369 ± 0.044	-30.37 ± 0.55	100.50 ± 0.66
300	40	30	134.37 ± 5.17	78.44 ± 0.08	0.303 ± 0.070	-30.67 ± 0.40	100.24 ± 0.80
200	40	10	133.23 ± 4.71	84.66 ± 0.40	0.464 ± 0.017	-33.50 ± 0.44	99.49 ± 0.65
300	40	30	137.43 ± 2.22	80.92 ± 0.25	0.366 ± 0.049	-29.80 ± 1.22	100.44 ± 0.54
400	40	10	158.13 ± 0.58	84.24 ± 0.14	0.328 ± 0.071	-31.97 ± 0.81	101.83 ± 0.11
300	55	10	127.77 ± 3.55	82.00 ± 0.08	0.414 ± 0.015	-37.20 ± 2.00	99.79 ± 0.90
200	40	50	72.27 ± 1.51	87.13 ± 0.16	0.281 ± 0.009	-23.33 ± 0.72	101.20 ± 0.75
300	25	10	134.77 ± 1.05	79.18 ± 0.11	0.410 ± 0.016	-29.70 ± 0.66	98.91 ± 0.79
200	55	30	99.13 ± 6.94	83.37 ± 0.25	0.479 ± 0.017	-30.87 ± 0.31	100.84 ± 0.77
400	40	50	148.87 ± 2.35	93.44 ± 0.17	0.378 ± 0.002	-31.00 ± 1.06	101.75 ± 0.22

The resultant data pertaining to vesicle size and entrapment efficiency were incorporated into the analytical software for a comprehensive ANOVA analysis (partial sum of squares -type III). This enabled the evaluation of the model's suitability and determination of the significance of individual variables. The response values obtained from the diverse trial formulations were integrated into the model matrix, aiming to identify the model that exhibited the most optimal fit. The quadratic model was determined to be the most suitable fit for the experimental results

with $p > 0.001$. The ANOVA statistics summary (indicating the suitability of the model) is presented in **Table 5.4**. The lack fit for both the responses was not significant relative to the pure error.

Table 5.4. ANOVA analysis for prepared transferosomes using BBD design

Parameter	TFD		QCN	
	Response 1 vesicle size (nm)	Response 2 EE (%)	Response 1 vesicle size (nm)	Response 2 EE (%)
Standard deviation	4.28	1.03	5.28	0.96
Mean	123.52	77.67	125.42	84.49
C.V %	3.46	1.33	4.21	1.13
R-squared	0.9922	0.9937	0.9855	0.9839
Adjusted R-squared	0.9781	0.9823	0.9594	0.9549
Pred R-squared	0.8843	0.9055	0.7965	0.9030
Adeq precision	26.853	34.908	21.178	17.860

Furthermore, the *p*-values corresponding to each influencing factor, that aids in understanding their impact on the measured responses are mentioned in **Table 5.5**

Table 5.5. **ANOVA** analysis for all dependent variables

Source	*p*-value for TFD		*p*-value for QCN	
	Response 1 Vesicle size (nm)	Response 2 EE (%)	Response 1 Vesicle size (nm)	Response 2 EE (%)
A	**0.0001**	**0.0001**	**0.0001**	**0.0064**
B	**0.0039**	**0.0008**	**0.0142**	**0.0062**
C	**0.0127**	**0.0001**	**0.0005**	**0.0005**
AB	**0.0122**	0.8413	**0.0284**	**0.0017**
AC	0.3635	0.0772	**0.0044**	**0.0169**
BC	0.2456	**0.0013**	0.0666	0.3630
A^2	**0.0002**	**0.0006**	0.9979	**0.0001**
B^2	**0.0042**	**0.0022**	**0.0154**	**0.0293**
C^2	**0.0002**	**0.0004**	0.1652	**0.0073**
Lack of fit	0.1305	0.1138	0.2056	0.8567

5.4.1.1. Effect of independent variables on vesicular Size

The representation of the impact of independent variables on the vesicular size of TFD or QCN loaded transferosomes are depicted through 3D graphs and 2D contour plots (**Figure 5.3 & 5.4**). Furthermore, the mathematical model derived using MLRA was expressed in terms of coded factors, as presented in the following equation (eq 5.3 & 5.4).

Vesicle size for TFD $= + 94.67 + 29.87\,A + 7.64\,B\,-5.74\,C\,-8.19\,AB\,-2.14\,AC\,-2.81\,BC +21.63$ $A^2 +11.06\,B^2 +21.41\,C^2$ ...eq 5.3

Vesicle size for QCN $= + 133.10 + 26.94\,A - 6.89\,B\,-15.02\,C\,-8.06\,AB + 12.99\,AC\,-6.18$ $BC\,-0.0075\,A^2\,-9.92\,B^2\,-4.47\,C^2$ ...eq 5.4

In this equation, a positive symbol signifies a synergistic effect of the independent variable on the response, whereas a negative coefficient indicates an antagonistic effect. The vesicle size of TFD and QCN was influenced by statistically significant terms (p-value < 0.100). For TFD transferosomes, significant model terms are A, B, C, AB, A², B², and C², while for QCN transferosomes, significant model terms are A, B, C, AB, AC, and B², as outlined in **Table 5.5**. The vesicle size of TFD-loaded transferosomes ranged from 80.63 ± 0.67 nm to 171.70 ± 10.47 nm, while that of QCN-loaded transferosomes ranged from 72.27 ± 1.51 nm to 163.33 ± 6.51 nm. The overall data revealed that an increase in the vesicle size of TFD-loaded transferosomes was associated with an increase in concentrations of PL 90G and sodium cholate. Conversely, a marginal reduction in vesicle size was observed with an increase in the concentration of tween 80. In the case of QCN-loaded transferosomes, an increase in vesicle size was noted with increasing concentrations of PL 90G. On the contrary, a slight reduction in vesicle size was observed with an increase in the concentrations of sodium cholate and tween 80. Additionally, perturbation graphs were employed as visual representations to analyze the sensitivity of responses to variations in key factors as represented in **Figure 5.7a & 5.7b**. A steep slope or curvature suggested a high sensitivity of the response to changes in that factor, while a comparatively flat line indicated a lack of sensitivity to the factor. The graphical representation indicated that factors A and C exhibited a pronounced curvature, while factor B demonstrated a moderate curvature in relation to the vesicle size of TFD. In the case of QCN, factor A displays a steeper curve, whereas factors B and C show a moderate curvature.

5.4.1.2. Effect of independent variables on % EE

The impact of independent variables on the % EE of TFD or QCN-loaded transferosomes was illustrated through 3D graphs and 2D contour plots (**Figure 5.5 & 5.6**). Additionally, the coded factors influencing encapsulation efficiency were defined in equation (5.5 & 5.6).

EE for TFD $= + 79.51 + 7.30\,A - 2.66\,B + 3.87C + 0.11\,AB + 1.14\,AC + 3.32\,BC +4.08\,A^2 -$ $3.10\,B^2\,-4.42\,C^2$ …eq 5.5

Chapter 5

EE for QCN = + 79.48 + 1.53 A + 1.53 B + 2.74 C +2.94 AB + 1.68 AC + 0.48 BC +5.72 A^2 +1.51B^2 +2.17 C^2

...eq 5.6

The EE of TFD and QCN were affected by statistically significant terms (p-value < 0.100). For TFD transferosomes, significant model terms were A, B, C, BC, A², B², and C²,while for QCN transferosomes, significant model terms were A, B, C, AB, AC, A², B², and C² as outlined in **Table 5.4.** The percentage encapsulation efficiency for TFD-loaded transferosomes ranged from 62.61 ± 0.08% to 91.16 ± 0.24%, while for QCN-loaded transferosomes, it spanned from 78.44 ± 0.08 % to 93.44 ± 0.17%. As indicated by the data, TFD-loaded transferosomes exhibited an increase in %EE with an increase in concentrations of PL 90G and tween 80, while a decrease in %EE was observed with an increased concentration of sodium cholate. Conversely, for QCN-loaded transferosomes, an increase in %EE was noted with elevated concentrations of PL 90G, sodium cholate, and tween 80. The perturbation graphs depicted in **Figure 5.7c & 5.7d** illustrate that factor A exhibits a greater curvature, whereas factors B and C display a moderate slope for both TFD and QCN transferosomes.

Apart from dependent variables, PDI, ZP and % assay for the executed runs were detailed in Table 1 and 2 for TFD and QCN respectively. The PDI was ranged from 0.267 ± 0.001 to 0.495 ± 0.027 for TFD transferosomes and 0.281 ± 0.009 to 0.479 ± 0.017 for QCN transferosomes indicating the narrow size distribution of the nanovesicles and negative ZP was observed for all nanovesicles indicating high stability [33]. The negative ZP exhibited by the vesicles is a result of the alignment of the negatively charged phosphatidyl group outwardly, while the choline group is oriented inwardly within the phospholipid head group during the bilayer formation in the aqueous phase [34].

Out of the 15 experimental runs for both TFD and QCN-loaded transferosomes, the formulation containing 400 mg of PL 90G demonstrated high entrapment efficiency along with an increased vesicle size and PDI. Subsequently, it was excluded when selecting the formulation using numerical optimization.
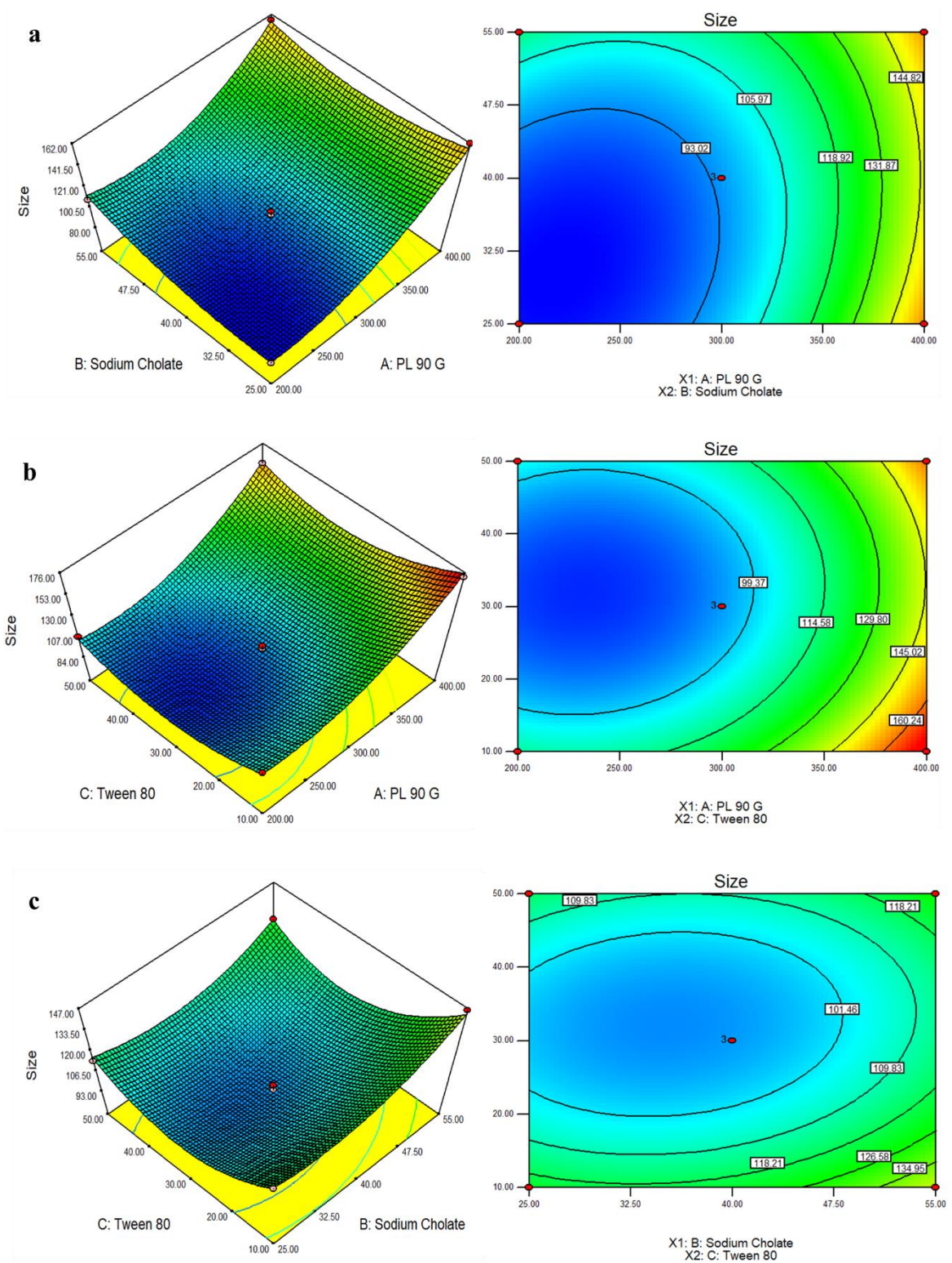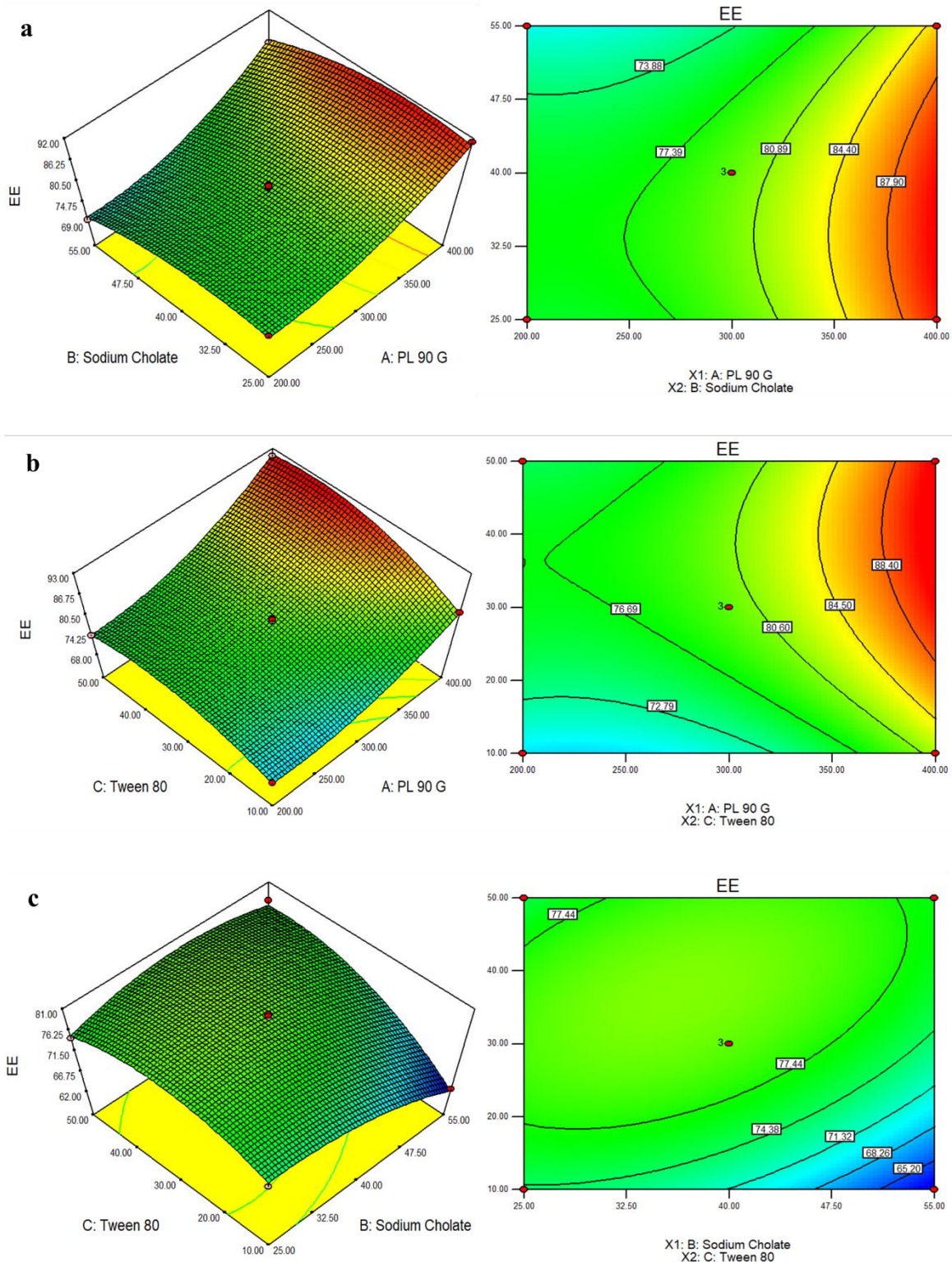
Figure 5.3. 3D and contour plots illustrating the impact of factors on the vesicle size of TFD-loaded transferosomes
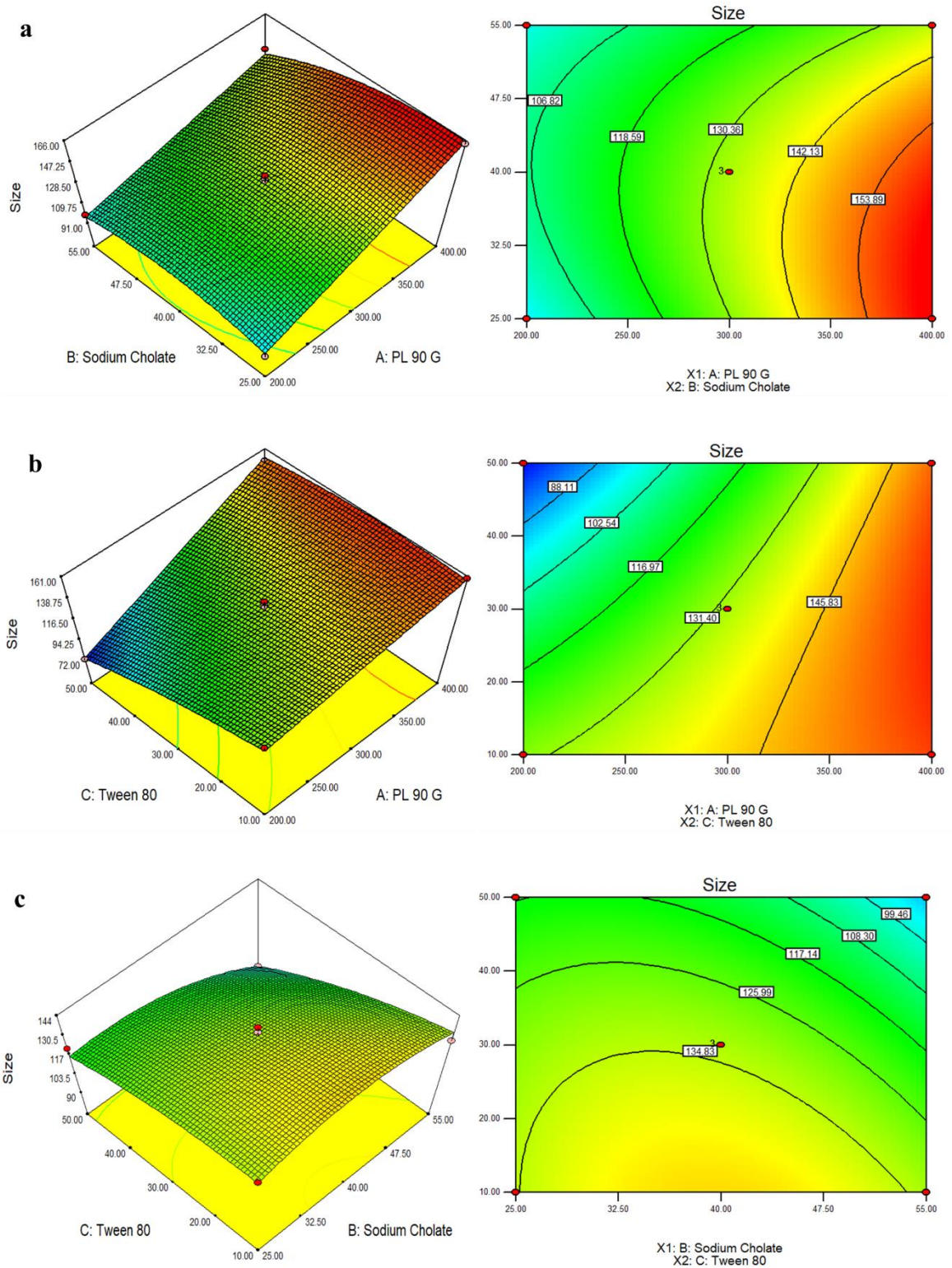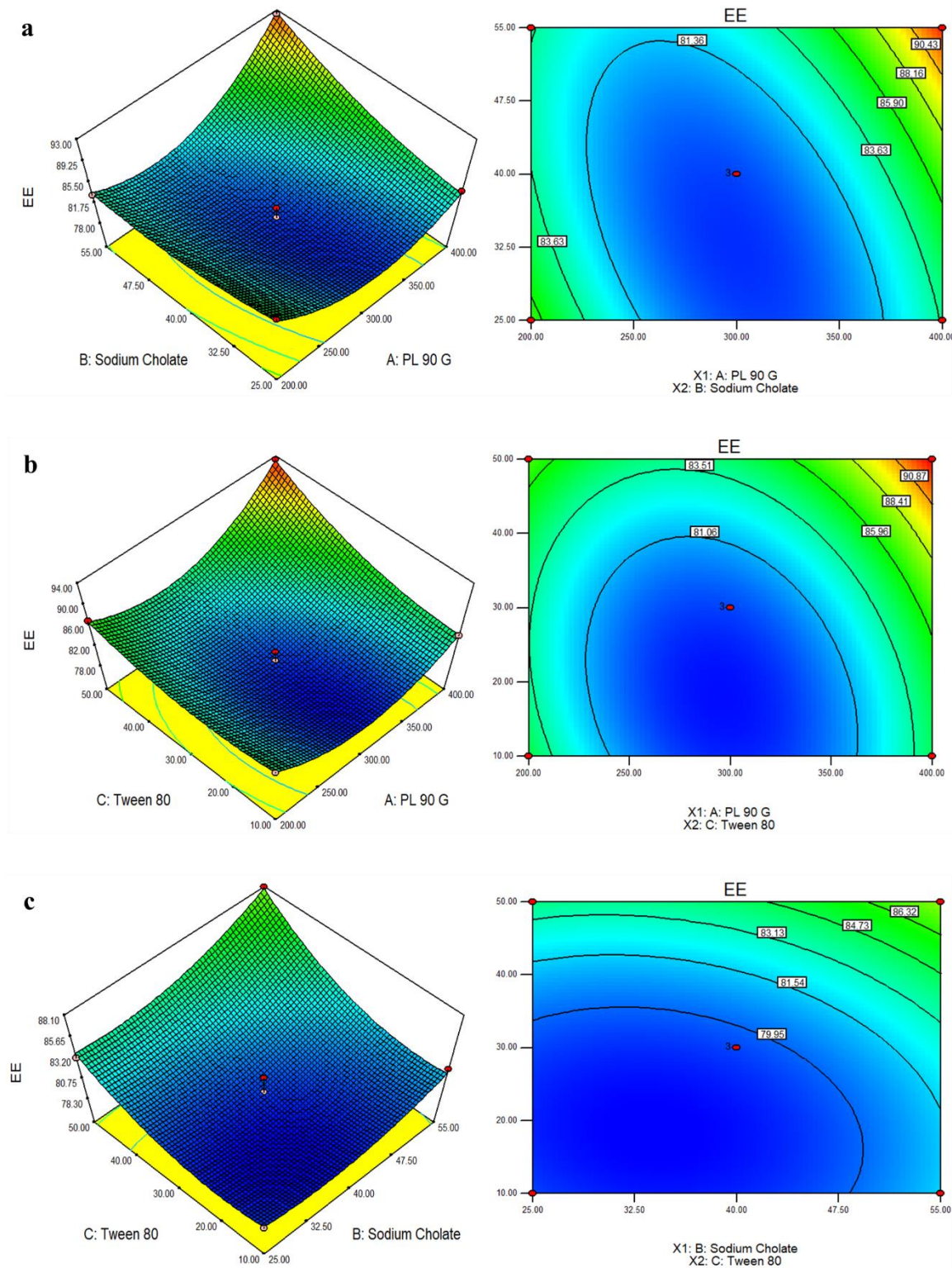
Figure 5.4. 3D and contour plots illustrating the impact of factors on the vesicle size of QCN-loaded transferosomes
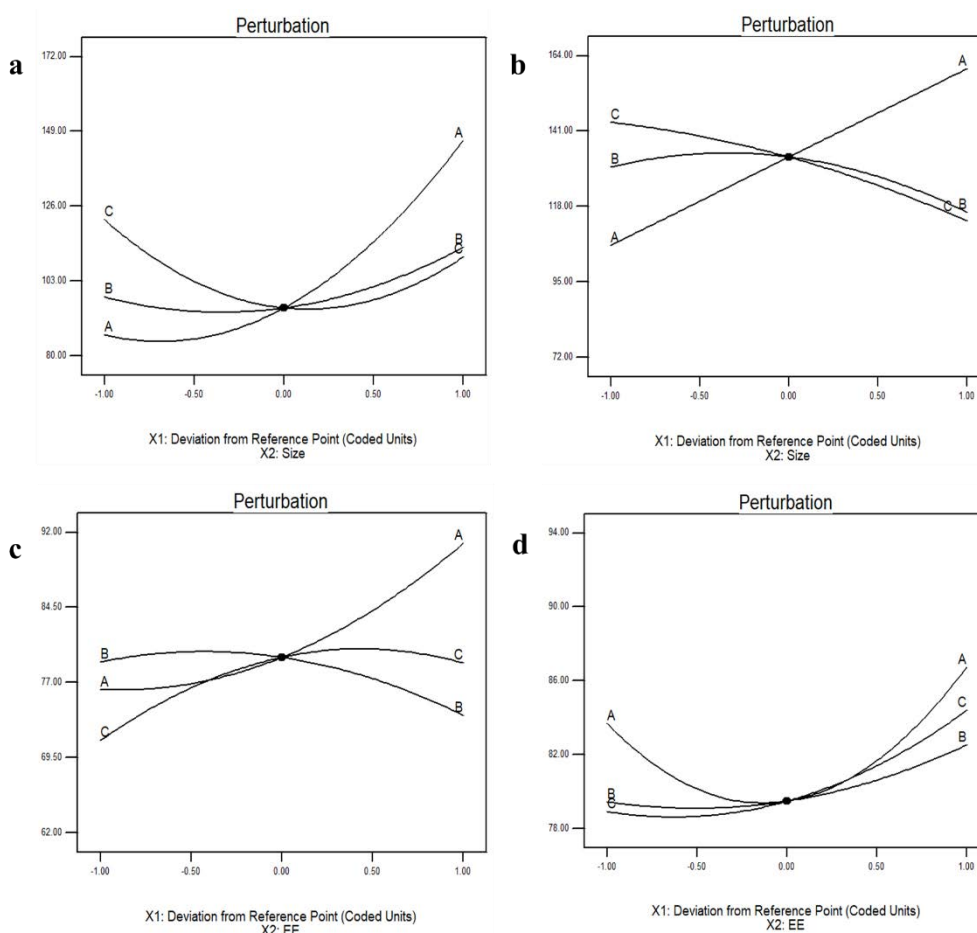
Figure 5.5. 3D and contour plots illustrating the impact of factors on the EE of TFD-loaded transferosomes

Figure 5.6. 3D and contour plots illustrating the impact of factors on the EE of QCN-loaded transferosomes

Figure 5.7. Perturbation graph for the effect of factors on a) vesicle size of TFD; b) vesicle size of QCN; c) EE of TFD; d) EE of QCN

5.4.1.3. Model validation and selection of optimized formulation

The validation process of the developed method employed model diagnostics graphs following QbD principles. The linear correlation plots as depicted in **Figure 5.8** exhibited a high degree of correspondence between the predicted and actual values. This alignment serves as strong evidence for the validity and efficacy of the developed method.

The numerical and graphical methods were employed for formulation optimization using Design Expert software. The selection criteria involved maximizing entrapment efficiency while minimizing vesicle size. The MODR was established and has been visually depicted in **Figure 5.9**, with the optimized zone highlighted in yellow color. A flag was used to indicate the selected composition within this optimized zone.
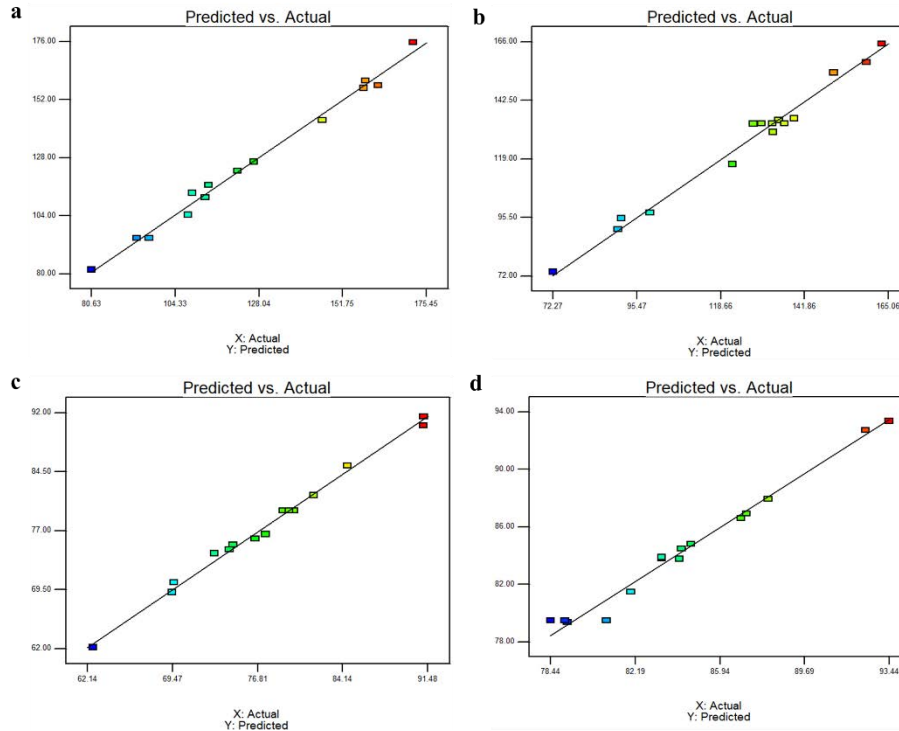
Figure 5.8. Linear correlation plots for a) vesicle size of TFD transferosomes; b) vesicle size of QCN transferosomes; c) EE of TFD transferosomes; d) EE of QCN transferosomes
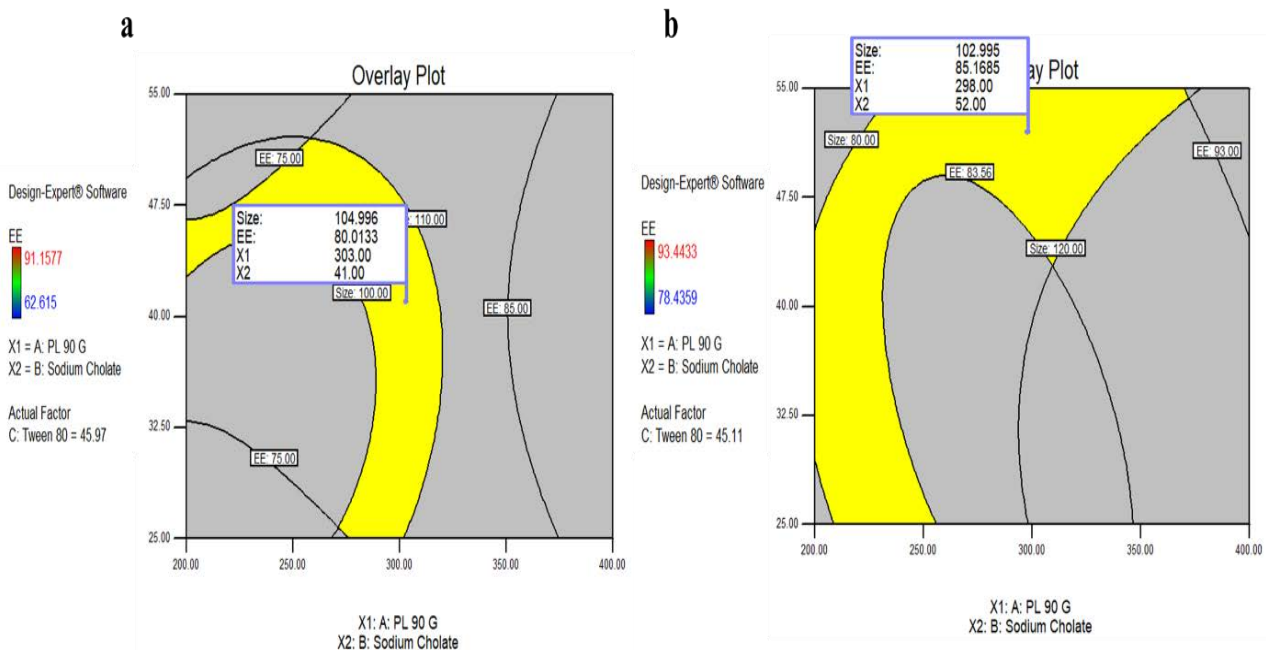
Figure 5.9. MODR for the a) TFD transferosomes; b) QCN transferosomes

The optimization procedure aimed to achieve a desirability value approaching 1, indicating the optimal composition. The desirability graphs are represented in **Figure 5.10**

Figure 5.10. Desirability graph for a) vesicle size of TFD transferosomes; b) vesicle size of QCN transferosomes; c) EE of TFD transferosomes; d) EE of QCN transferosomes

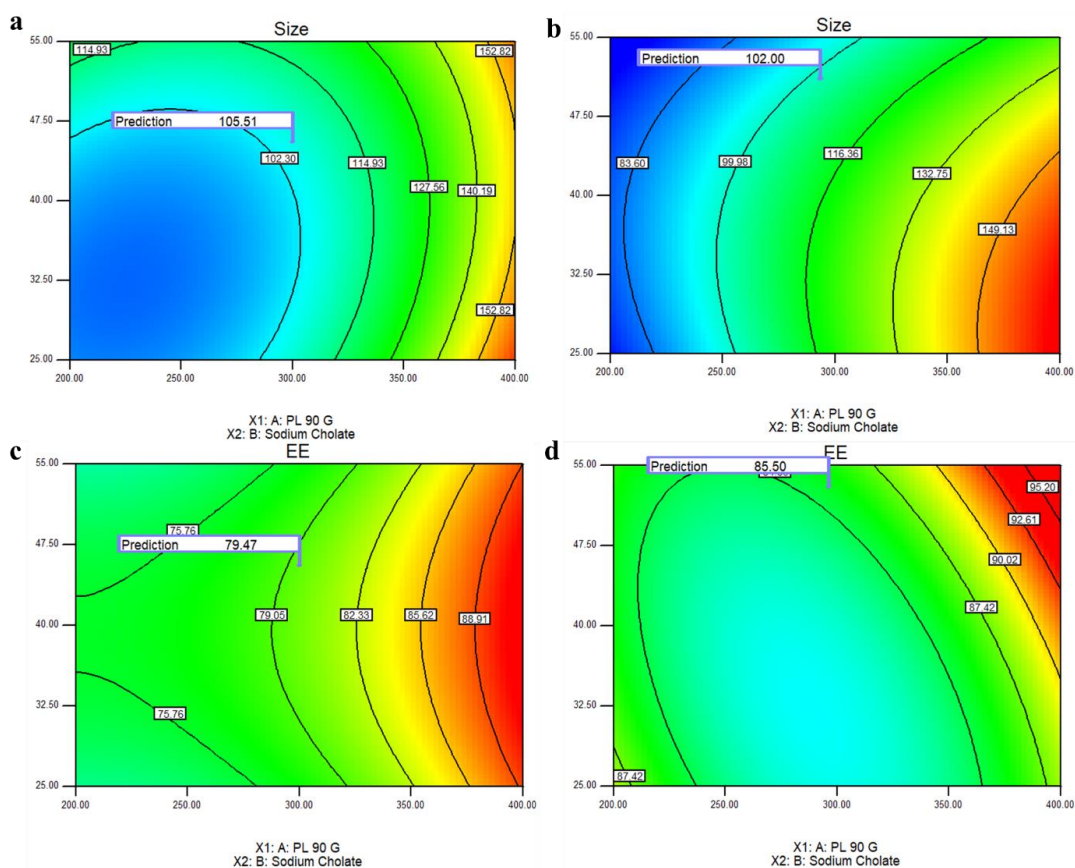Subsequently, the final optimized formulation suggested by QbD was prepared using the thin film hydration method, as described earlier. The optimized composition for TFD-loaded transferosomes comprised of PL 90G (300 mg), sodium cholate (40 mg), and tween 80 (45 mg). Similarly, for QCN-loaded transferosomes, the optimized composition includes PL 90G (300 mg), sodium cholate (50 mg), and tween 80 (45 mg). The remaining process parameters were kept constant. The optimized formulations are shown in **Figure 5.11a**.

5.4.2. Vesicular size, PDI and ZP determination

The vesicular size of the optimized TFD-loaded transferosomes was found to be 107.80 ± 2.68 nm, with a PDI of 0.283 ± 0.008, and the ZP was found to be -32.10 ± 1.98 mV. Similarly, for QCN transferosomes the vesicular size was found to be 96.32 ± 3.32 nm exhibiting a PDI of 0.289 ± 0.005, and the ZP values was determined to be -30.70 ± 1.14 mV. The optimized formulation along with vesicle size and ZP graphs are shown in **Figure 5.11 b-e.**
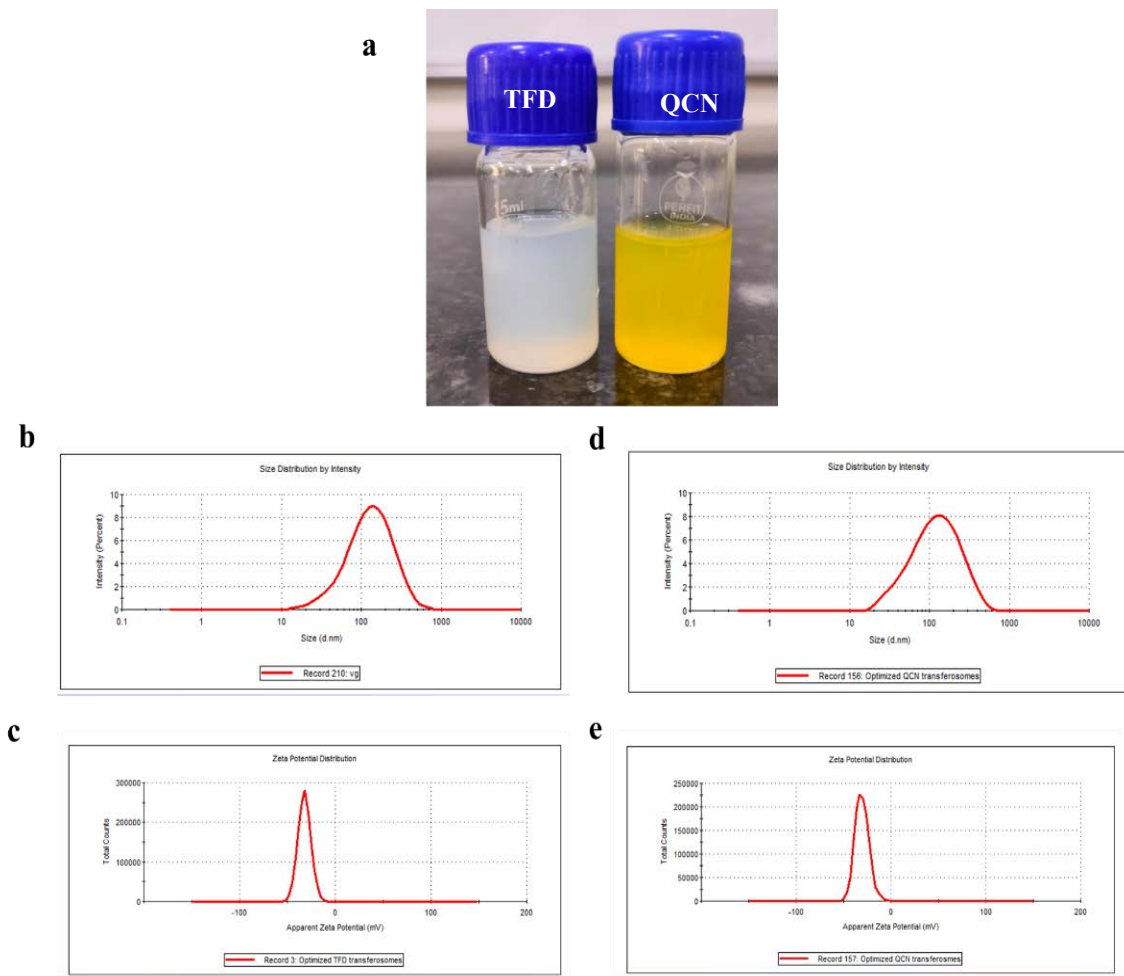
Figure 5.11. a) TFD loaded transferosomes and QCN loaded transferosomes; b) vesicle size of TFD transferosomes; c) ZP of TFD transferosomes; d) vesicle size of QCN transferosomes and e) ZP of QCN transferosomes

5.4.3. Determination of % EE and % DL

The EE of the optimized TFD transferosomes and QCN transferosomes were found to be 79.92 ± 0.20 % and 89.55 ± 0.10 %, respectively. The % drug loading of TFD transferosomes and QCN transferosomes were found to be 2.07 and 3.37 respectively.

5.4.4. Drug content determination

The % assay for all optimized formulations using QbD approach were in the range of 98 to 101 %. For the optimized TFD transferosomes was found to be 99.92 ± 0.14 % and for QCN transferosomes 99.52 ± 0.21 %.

5.4.5. Characterization by ATR-IR

The FTIR spectra of free TFD, free QCN, blank transferosomes, TFD-loaded transferosomes, and QCN-loaded transferosomes are illustrated in **Figure 5.12**. The FTIR spectra of TFD showed characteristic peaks at 3299 cm^{-1} (-NH- stretch of acetamide group), 2220 cm^{-1} (-C≡N

group), 1549 cm^{-1} N-H bending (amide), 1325 cm^{-1} (-CF-bond), 1635 cm^{-1} (- C=O), 1405 (-C-N stretching) [35]. The FTIR spectra of QCN showed characteristic peaks at 3403 and 3283 cm^{-1} for OH groups stretching, 1360 cm^{-1} (OH bending of phenol), 1664 cm^{-1} (C=O Aryl ketonic stretch), 1606, 1555, and 1515 cm^{-1} (C=C aromatic ring stretch), 1314 cm^{-1} (C-H in Aromatic hydrocarbon), 1262 cm^{-1} (C-O Stretch of phenol) [36]. The FTIR spectra of blank transferosomes exhibited similarities to both TFD and QCN transferosomes, occurring at identical wavenumbers. Characteristic bands for TFD and QCN were not detected in the drug-loaded transferosomes, confirming the encapsulation of TFD and QCN within the transferosome vehicles.
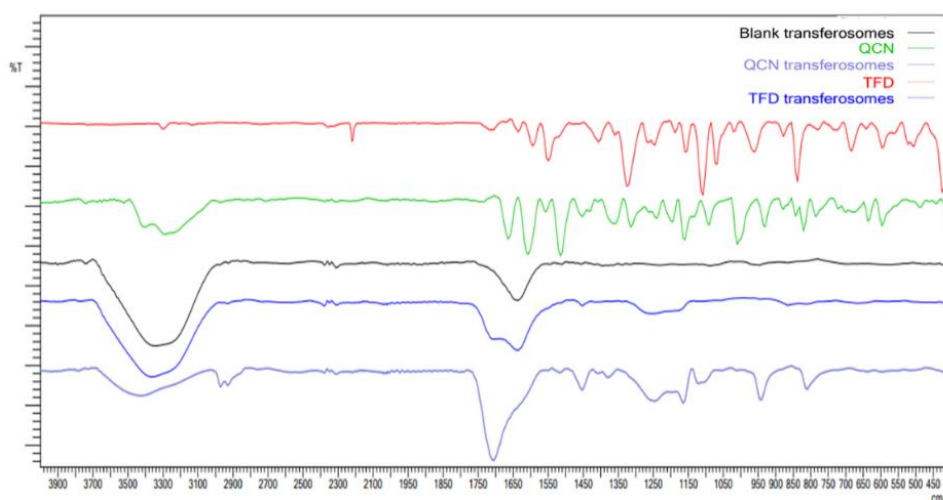
Figure 5.12. ATR-IR spectrum for characterization of transferosomes

5.4.6. *In-vitro* drug release

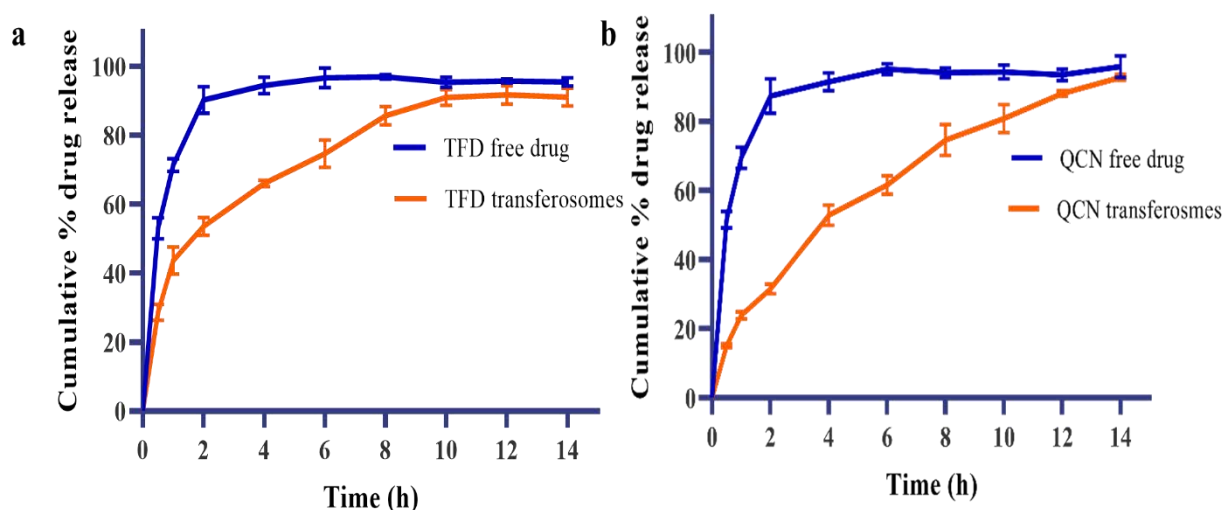The drug release profiles of both TFD transferosomes and QCN transferosomes are presented in **Figure 5.13**. Within 2 h, 90.25 ± 3.845 % of the drug was released from free TFD solution, while 53.54 ± 2.567 % of the drug was released from TFD transferosomes. Notably, TFD transferosomes demonstrated controlled release up to 10 h, achieving a 91.11 ± 2.58 % drug release. Similarly, in the case of QCN, 87.31 ± 4.921 % of the drug was released from free QCN solution within 2 h, compared to only 31.48 ± 1.379 % released from QCN transferosomes. Notably, QCN transferosomes demonstrated controlled release for up to 12 h, achieving a 92.69 ± 2.098% drug release. Both the TFD and QCN transferosomes displayed controlled release over an extended period, in contrast to the free drug [25].

Figure 5.13. *In-vitro* drug release profile for a) TFD transferosomes and b) QCN transferosomes (n=3, Mean ± SD).

5.4.7. Lab scale-up studies

The lab scale-up investigations involved increasing the batch size from 10 mL to 50 mL for optimized batch of TFD and QCN transferosomes. The various process parameters for preparation of transferosomes are detailed in **Table 5.3**. For the 50 mL batch size, the vesicle size of TFD transferosomes was determined to be 109.26 ± 0.436 nm with PDI of 0.281 ± 0.006 and a ZP of -30.87 ± 0.31 mV. Similarly, for QCN transferosomes, the vesicle size was determined to be 103.28 ± 1.50 nm, with a PDI of 0.282 ± 0.004 and a ZP of -33.50 ± 0.44 mV. The % EE was found to be 77.87 ± 0.32 % and 88 ± 0.20 % for TFD and QCN transferosomes, respectively. Based on the findings, it can be inferred that there is no significant difference between the 10 mL and 50 mL batch sizes, thus indicating their suitability for future studies involving scale-up processes.

5.4.8. Evaluation of TFD and QCN loaded combination transferosomal gel

5.4.8.1. Physical Appearance, pH and drug content determination

The combination gel was translucent, with a pale-yellow color. It had homogeneous texture with good consistency. The pH of the gel was found to be 5.6 ± 0.3, demonstrating compatibility with the skin which typically ranges from 5.4 to 5.9. The % assay of the gel was found to be 98.91 ± 1.51 % and 99.22 ± 1.71 % for TFD and QCN, respectively.

5.4.8.2. Vesicle size, PDI and ZP of combination loaded gel

The mean vesicle size of transferosomes within the gel was determined to be 113.9 ± 7.497 nm with PDI of 0.288 ± 0.242 and ZP of -35.1 ± 0.519 mV.

5.4.8.3. Rheology

Viscosity and flow curves

The topical gel exhibited an average viscosity of 8677.10 ± 34.64 mPa at a consistent shear rate of 10 1/s, (**Figure 5.14a)**, and demonstrated time-independent behavior. The graph (**Figure 5.14 b**) showed the relationship between apparent viscosity (η) and shear rate ($\dot{\gamma}$) for the gel. It demonstrated a decrease in viscosity as shear rate was increased, indicating a characteristic non-Newtonian flow, specifically pseudo-plastic or shear-thinning behavior, consistent with findings reported for carbopol dispersions at a concentration of 0.5 % w/v. The shear flow curve for shear stress *vs* shear rate is depicted in **Figure 5.14c**. The flow curve exhibits the characteristic Herschel-Bulkley shape, highlighted in orange color, typical of non-Newtonian fluids [19,37–39].

Amplitude sweep test

The amplitude sweep test was performed to determine the linear viscoelastic region (LVR) of the material. The elastic nature of the material was measured by G' and viscous nature of the material was measured by G". The LVR was observed within the low stress amplitude range, exhibiting consistent moduli for both G' and G" as illustrated in **Figure 5.14d**. Within the LVR region, the predominance of G' over G" signifies the gel's elastic behavior. In this region, the microgels retain their structural integrity, deforming elastically while remaining relatively stationary within their cages. As soon as the moduli started to decrease (indicated by red color on the storage modulus), the structure was disturbed till the end of the LVR region, where the linearity limit, (or yield point) was attained. In this yield zone, the initial structural strength of the gel diminished, although the sample predominantly retained the properties of solid matter or a gel. Beyond this, crossover point (known as the flow point) was observed, where G' equals G" indicating the onset of flow behavior as stress amplitudes increased [19].

Frequency sweep test

The frequency sweep test result for the gel was depicted in **Figure 5.14e**. It showed that with an increase in frequency, G' remained relatively constant, whereas there was a slight elevation in G". Additionally, G' was notably larger than G", which is a characteristic commonly observed in viscoelastic gels and cross-linked systems.

The rheological assessment suggested that the formulated combination gel exhibited non-Newtonian flow behavior, particularly featuring shear thinning characteristics. This property facilitates effortless spreading upon application to the skin, enhancing its usability and effectiveness. Furthermore, both the amplitude sweep test and frequency sweep test revealed

the viscoelastic nature of the gel with strong microgel structure. This characterization indicated that the gel possessed the ability to both store and dissipate energy under varying conditions, highlighting its potential for stable and effective performance in topical applications.
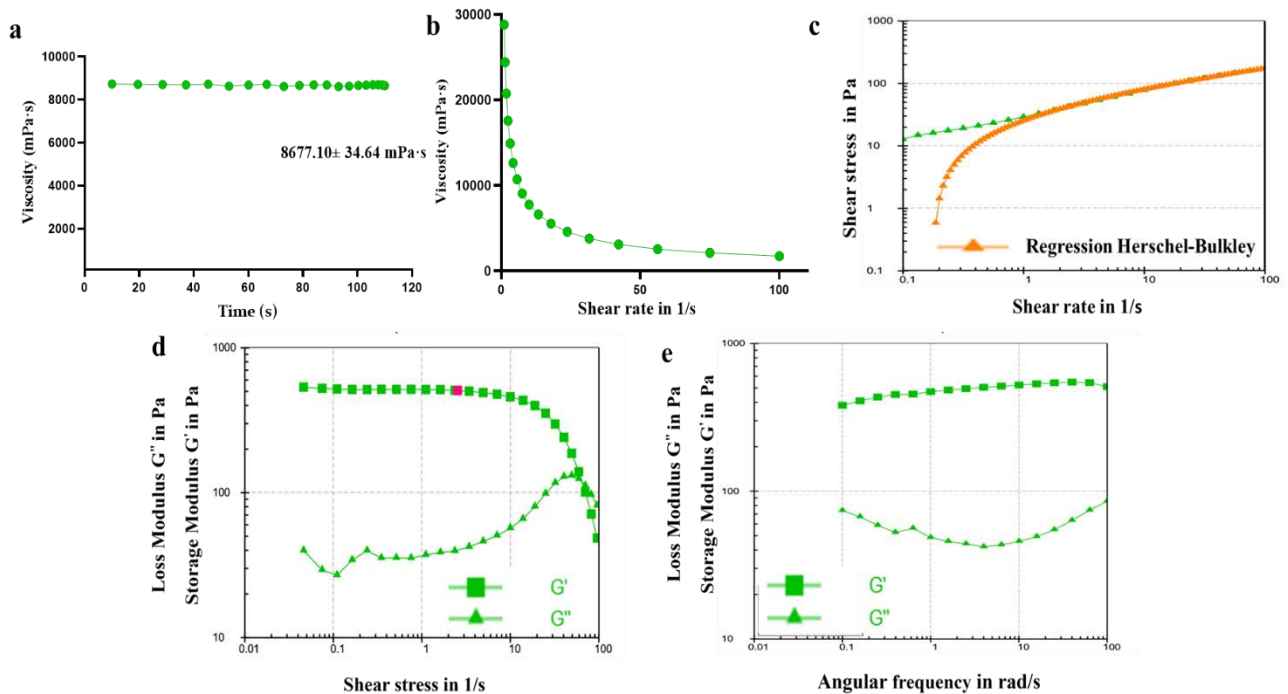
Figure 5.14. a) Viscosity at constant shear; b) viscosity at varied shear rate; c) flow curve for combination gel; d) amplitude sweep test; e) frequency sweep test for combination gel

5.4.9. *In-vitro* cell line studies

5.4.9.1. NO assay

The effect of free TFD, free QCN, TFD transferosomes, QCN transferosomes, combination free drug gel, and combination transferosomal gel on NO levels was assessed using Griess reagent. The results are depicted in **Figure 5.15a**. Data analysis revealed that incorporation of TFD and QCN into transferosomal gel led to a significant ($p < 0.05$) decrease in nitrite levels compared to the free drug gel at tested concentration ranges. Also, the combination of TFD and QCN was more effective compared to individual treatment.

5.4.9.2. TNF-α and IL-6 production in RAW 264.7 cells

The effect of various formulations on production of TNF-α and IL-6 was evaluated in LPS stimulated RAW 264.7 cells and the resultant data has been represented in **Figure 5.15 b & c**. The analysis of both figures leads to the conclusion that the inclusion of TFD and QCN in transferosomes results in a substantial and statistically significant increase ($p < 0.05$) in the inhibition of TNF-α and IL-6 in RAW 264.7 cells compared to the free drug. Furthermore, the

combination of TFD and QCN exhibits a synergistic effect, indicating enhanced efficacy compared to the individual drugs. This highlights the potential use of transferosomal combination gel as a promising approach to improve therapeutic outcomes in the management of RA.

Figure 5.15. Effect of various formulation on the production of a) NO assay b) TNF-α; c) IL-6 in RAW 264.7 cells (n=3, Mean ± SD). **** $p < 0.0001$; *** $p < 0.001$; ** $p < 0.01$; * $p < 0.05$ and ns
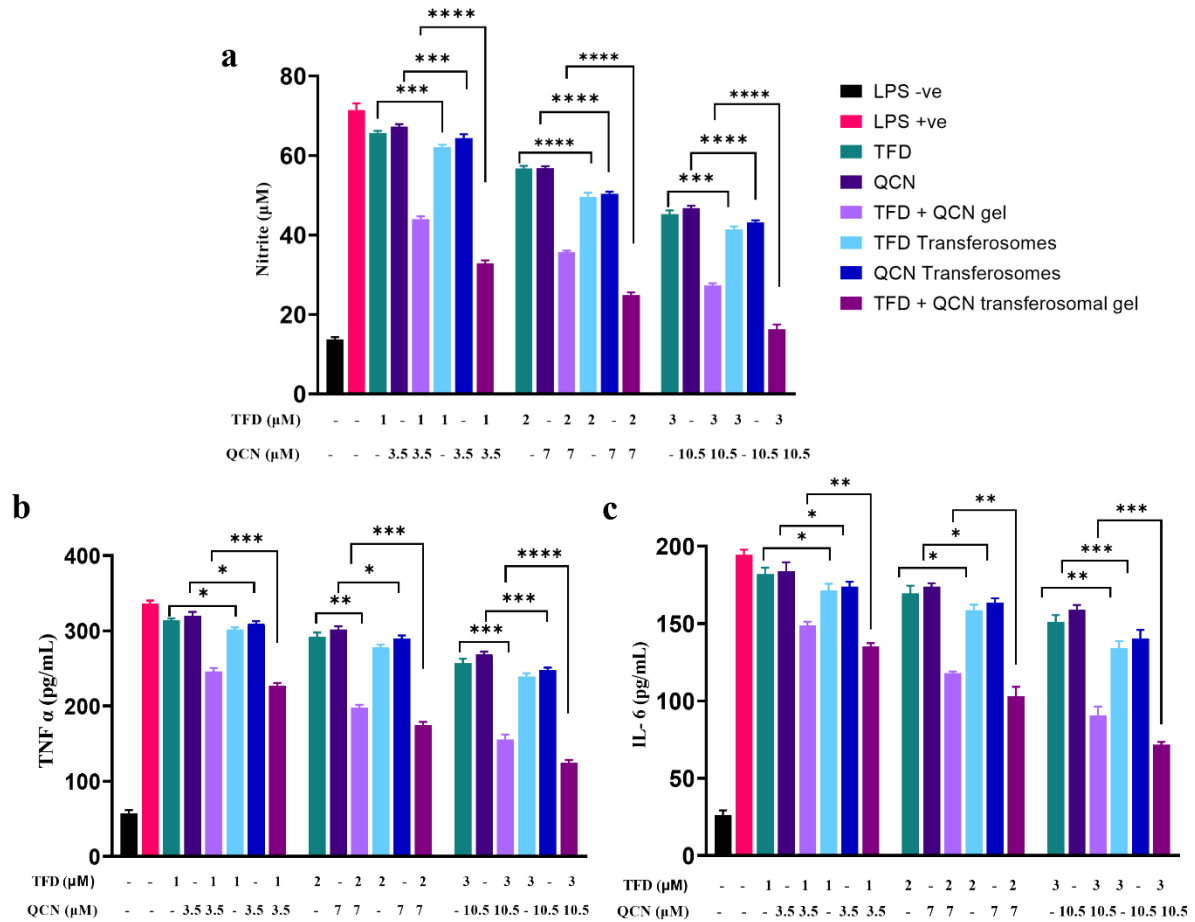
5.4.9.3. Cell viability in HaCaT cells

The cytotoxic potential of free TFD, free QCN, TFD transferosomes, QCN transferosomes, combination free drug gel, and combination transferosomal gel was assessed in HaCaT cell lines, as depicted in **Figure 5.16**. The formulation demonstrated comparable cell viability with no statistical difference ($p < 0.05$) to that of the free drug, suggesting that the prepared combination transferosomal gel, along with the excipients, did not induce toxicity in the cell lines [40].
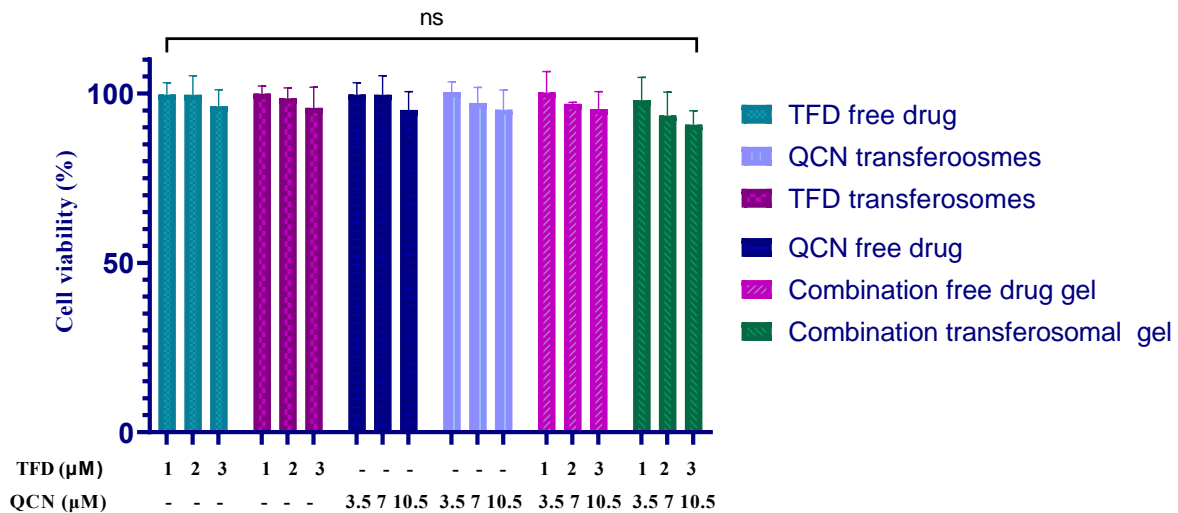
Figure 5.16. Effect of various formulation on the cell viability of HaCaT cells (n=3, Mean ± SD). ns- not significant

5.4.10. *Ex-vivo* **skin permeation and skin retention studies**

An *ex-vivo* skin permeation study was conducted using rat skin and the cumulative drug permeation over a 24 h time period is presented in **Figure 5.17a** for both the free drug loaded combination gel and transferosomal combination gel. After a 12 h duration, there was a significant ($p < 0.0001$) increase in the amount permeated from the combination transferosomes-loaded gel when compared to the gel loaded with both the free drugs. After 24 h , the drug permeation through the skin was found to be 11.98 ± 0.75 µg/cm^2 for TFD and 13.52 ± 0.81 µg/cm^2 for QCN from the free drug-loaded gel. In contrast, the transferosomal loaded gel exhibited higher permeation, with values of 18.72 ± 0.49 µg/cm^2 for TFD and 41.78 ± 0.69 µg/cm^2 for QCN, respectively. The flux through the skin was determined to be 0.51 ± 0.13 and 0.46 ± 0.22 µg/cm^2/h for TFD and QCN in the free drug-loaded gel, while for the transferosomal gel, the flux was 0.74 ± 0.02 and 1.54 ± 0.13 µg/cm^2/h, respectively.

After 24 h , the drug retained in the skin was found to be 1.44 µg/cm^2 for TFD and 0.17 µg/cm^2 for QCN from the gel containing the free drug. In contrast, the transferosomal gel showed higher retention, with values of 3.16 µg/cm^2 for TFD and 2.54 µg/cm^2 for QCN. The investigation yielded the conclusion that the permeation of TFD and QCN from transferosomes increased in comparison to free drug-loaded gels as shown in **Figure 5.17b**. This enhancement can be attributed to the presence of surfactant in the transferosomes, that contributes to the flexibility and elasticity of liposomes. Additionally, the smaller size of the transferosomes further improved permeation of the drugs [41].
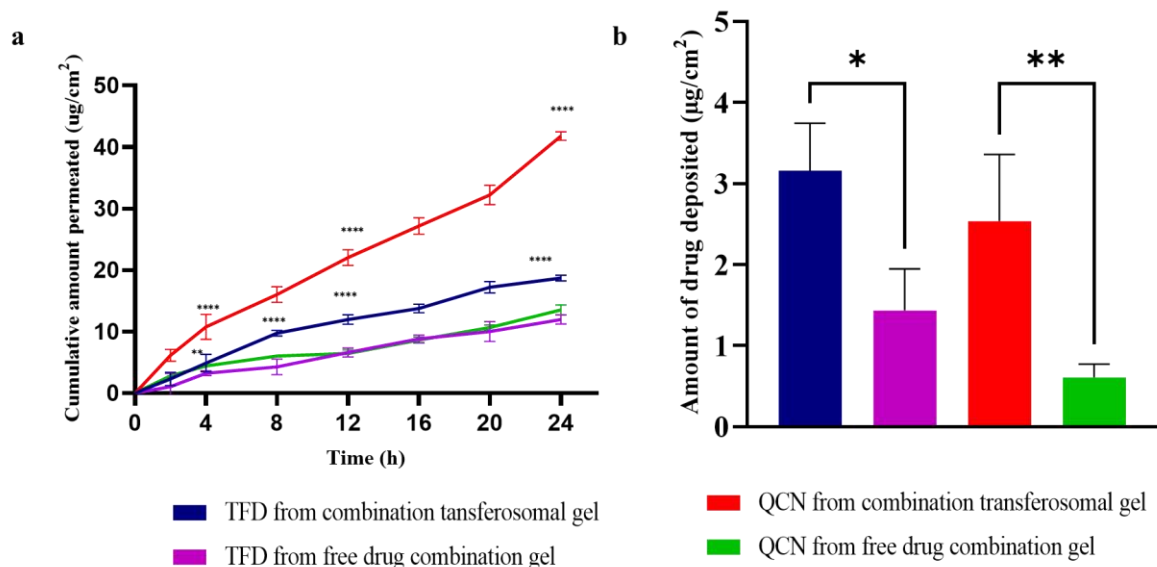
Figure 5.17. a) *Ex-vivo* skin permeation studies; b) *ex-vivo* skin retention studies (n=3, Mean ± SD). **** $p < 0.0001$; *** $p < 0.001$; ** $p < 0.01$; * $p < 0.05$ and ns

5.4.11. Storage stability

The combinational transferosomal gel was evaluated for vesicle size, PDI, and ZP over a 45-days storage period, with the results presented in **Table 5.6.** The findings demonstrated that no significant changes in these parameters were observed indicating the stability of the gel.

Table 5.6. Stability data for TFD and QCN loaded transferosomal gel

Parameter	0 days	15 days	30 days	45 days
Vesicle size (nm)	105.1 ± 3.27	101.4 ± 2.16	110.7 ± 1.83	115.8 ± 4.15
PDI	0.291 ± 0.003	0.217± 0.002	0.301 ±0.004	0.288 ± 0.004
ZP (mV)	32.65 ± 1.82	34.22 ± 1.06	31.82 ± 0.85	33.72 ± 1.72

5.5. Conclusion

The TFD and QCN transferosomes were successfully optimized using QbD approach incorporating the BBD with 15 experimental runs. The optimized composition resulted in a smaller size and enhanced stability, primarily due to the negative zeta potential facilitated by the incorporation of sodium cholate. Characterization by ATR-IR further confirmed the

encapsulation of TFD and QCN. The *in-vitro* release study demonstrated sustained release of drug from transferosomes up to 10 h and 12 h for TFD and QCN transferosomes respectively. The optimized transferosomes were successfully loaded into the Carbopol 974P gel and evaluated. The rheological studies demonstrated that the combination transferosomal gel exhibits non-Newtonian behavior with shear-thinning properties comparable to those of Carbopol gels. The anti-inflammatory activity in RAW 264.7 cells demonstrated that the transferosomal gel was effective in reducing the levels of NO and proinflammatory cytokines (such as TNF-α and IL-6) levels compared to free drug loaded gel. Additionally, cell viability studies in HaCaT cells demonstrated the non-cytotoxicity of the formulation and showed similar cell viability to the free drug. The *ex-vivo* studies revealed that the combination transferosomal gel exhibited increased permeation and retention of TFD and QCN compared to free drug combination loaded gel. This indicates the effectiveness of transferosomal gel in overcoming major barriers of the skin such as *stratum corneum*. The storage studies have confirmed that the transferosomal gel maintains its stability over a period of 45 days. The TFD and QCN loaded transferosomal gel was successfully prepared and evaluated.

Chapter 5

References

1. Köhler, B. M., Günther, J., Kaudewitz, D., & Lorenz, H. M. (2019). Current therapeutic options in the treatment of rheumatoid arthritis. *Journal of Clinical Medicine*, *8*(7), 938.

2. Gokhale, J. P., Mahajan, H. S., & Surana, S. S. (2019). Quercetin loaded nanoemulsion-based gel for rheumatoid arthritis: In vivo and in vitro studies. *Biomedicine and Pharmacotherapy*, *112*, 108622.

3. Anita, C., Munira, M., Mural, Q., & Shaily, L. (2021). Topical nanocarriers for management of Rheumatoid Arthritis: A review. *Biomedicine & Pharmacotherapy, 141*,111880.

4. Hagen, M., & Baker, M. (2017). Skin penetration and tissue permeation after topical administration of diclofenac. *Current Medical Research and Opinion*, *33*(9), 1623–1634.

5. Opatha, S. A. T., Titapiwatanakun, V., & Chutoprapat, R. (2020). Transfersomes: A promising nanoencapsulation technique for transdermal drug delivery. *Pharmaceutics*, *12*(9), 1–23.

6. Van Hoogevest, P., & Fahr, A. (2019). Phospholipids in cosmetic carriers. In *Nanocosmetics: From Ideas to Products*. Springer International Publishing, 95–140.

7. Tamilarasan, N., Yasmin, B. M., Anitha, P., Umme, H., Cheng, W. H., Mohan, S., Ramkanth, S., & Janakiraman, A. K. (2022). Box–behnken design: Optimization of proanthocyanidin-loaded transferosomes as an effective therapeutic approach for osteoarthritis. *Nanomaterials 2022, Vol. 12, Page 2954*, *12*(17), 2954.

8. Mahmoud, D. B., ElMeshad, A. N., Fadel, M., Tawfik, A., & Ramez, S. A. (2022). Photodynamic therapy fortified with topical oleyl alcohol-based transethosomal 8-methoxypsoralen for ameliorating vitiligo: Optimization and clinical study. *International Journal of Pharmaceutics*, *614*, 121459.

9. Duangjit, S., Opanasopit, P., Rojanarata, T., & Ngawhirunpat, T. (2013). Evaluation of meloxicam-loaded cationic transfersomes as transdermal drug delivery carriers. *AAPS PharmSciTech*, *14*(1), 133-140.

10. Jose, A., Ninave, K. M., Karnam, S., & Venuganti, V. V. K. (2018). Temperature-sensitive liposomes for co-delivery of tamoxifen and imatinib for synergistic breast cancer treatment. *Journal of Liposome Research*, *29*(2), 153–162.

11. Kathuria, H., Handral, H. K., Cha, S., Nguyen, D. T. P., Cai, J., Cao, T., Wu, C., & Kang, L. (2021). Enhancement of skin delivery of drugs using proposome depends on drug lipophilicity. *Pharmaceutics*, *13*(9), 1457.

12. Moyá, M. L., López-López, M., Lebrón, J. A., Ostos, F. J., Pérez, D., Camacho, V., Beck,

I., Merino-Bohórquez, V., Camean, M., Madinabeitia, N., & López-Cornejo, P. (2019). Preparation and characterization of new liposomes. Bactericidal activity of cefepime encapsulated into cationic liposomes. *Pharmaceutics 2019, 11*(2), 69.

13. Saha, P., Singh, P., Kathuria, H., Chitkara, D., & Pandey, M. M. (2023). Self-assembled lecithin-chitosan nanoparticles improved rotigotine nose-to-brain delivery and brain targeting efficiency. *Pharmaceutics*, *15*(3), 851.

14. Khatoon, K., Rizwanullah, M., Amin, S., Mir, S. R., & Akhter, S. (2019). Cilnidipine loaded transfersomes for transdermal application: Formulation optimization, in-vitro and in-vivo study. *Journal of Drug Delivery Science and Technology*, *54*, 101303.

15. Uwaezuoke, O., Du Toit, L. C., Kumar, P., Ally, N., & Choonara, Y. E. (2022). Linoleic acid-based transferosomes for topical ocular delivery of Cyclosporine A. *Pharmaceutics*, *14*(8), 1695.

16. Xie, X., Li, Z., Zhang, L., Chi, Q., Yang, Y., Zhang, H., Yang, Y., & Mei, X. (2015). A novel accelerated in vitro release method to evaluate the release of thymopentin from PLGA microspheres. *Pharmaceutical Development and Technology*, *20*(5), 633–640.

17. Karnam, S., Jindal, A. B., & Paul, A. T. (2024). Implementing analytical quality by design in reversed phase-high performance liquid chromatography for simultaneous estimation of teriflunomide and quercetin: Applicability in dual drug loaded topical microemulsion. *Journal of Liquid Chromatography & Related Technologies*, 1–18.

18. Joshi, A., Kaur, J., Kulkarni, R., & Chaudhari, R. (2018). In-vitro and ex-vivo evaluation of raloxifene hydrochloride delivery using nano-transfersome based formulations. *Journal of Drug Delivery Science and Technology*, *45*, 151–158.

19. Varges, P. R., Costa, C. M., Fonseca, B. S., Naccache, M. F., & De Souza Mendes, P. R. (2019). Rheological characterization of Carbopol® dispersions in water and in water/glycerol solutions. *Fluids 2019, 4*(1), 3.

20. Sharma, V., Kumar, R., Arora, N., Singh, S., Sharma, N., Anand, A., Jain, S. K., & Sharma, S. (2020). Effect of heat treatment on thermal and mechanical stability of NaOH-doped xanthan gum-based hydrogels. *Journal of Solid State Electrochemistry*, *24*, 1337–1347.

21. Matsuno, H., Yudoh, K., Katayama, R., Nakazawa, F., Uzuki, M., Sawai, T., Yonezawa, T., Saeki, Y., Panayi, G. S., Pitzalis, C., & Kimura, T. (2002). The role of TNF-alpha in the pathogenesis of inflammation and joint destruction in rheumatoid arthritis (RA): A study using a human RA/SCID mouse chimera. *Rheumatology*, *41*(3), 329–337.

22. Srirangan, S., & Choy, E. H. (2010). The role of interleukin 6 in the pathophysiology of

rheumatoid arthritis. *Therapeutic Advances in Musculoskeletal Disease*, *2*(5), 247–256.

23. Yoshida, Y., & Tanaka, T. (2014). Interleukin 6 and rheumatoid arthritis. *BioMed Research International*, *2014*, 698313.

24. Caddeo, C., Manca, M. L., Peris, J. E., Usach, I., Diez-Sales, O., Matos, M., Fernàndez-Busquets, X., Fadda, A. M., & Manconi, M. (2018). Tocopherol-loaded transfersomes: In vitro antioxidant activity and efficacy in skin regeneration. *International Journal of Pharmaceutics*, *551*(1–2), 34–41.

25. Sana, E., Zeeshan, M., Ain, Q. U., Khan, A. U., Hussain, I., Khan, S., Lepeltier, E., & Ali, H. (2021). Topical delivery of curcumin-loaded transfersomes gel ameliorated rheumatoid arthritis by inhibiting NF-κβ pathway, *Nanomedicine*, *16*(10), 819–837.

26. Alsaidan, O. A., Elmowafy, M., Shalaby, K., Alzarea, S. I., Massoud, D., Kassem, A. M., & Ibrahim, M. F. (2023). Hydrocortisone-loaded lipid-polymer hybrid nanoparticles for controlled topical delivery: Formulation design optimization and in vitro and in vivo appraisal. *ACS Omega*, *8*(21), 18714–18725.

27. Lee, E. H., Kim, A., Oh, Y. K., & Kim, C. K. (2005). Effect of edge activators on the formation and transfection efficiency of ultradeformable liposomes. *Biomaterials*, *26*(2), 205–210.

28. Liu, D., Hu, H., Lin, Z., Chen, D., Zhu, Y., Hou, S., & Shi, X. (2013). Quercetin deformable liposome: preparation and efficacy against ultraviolet B induced skin damages in vitro and in vivo. *Journal of Photochemistry and Photobiology B: Biology*, *127*, 8–17.

29. Alharbi, W. S., Almughem, F. A., Almehmady, A. M., Jarallah, S. J., Alsharif, W. K., Alzahrani, N. M., & Alshehri, A. A. (2021). Phytosomes as an emerging nanotechnology platform for the topical delivery of bioactive phytochemicals. *Pharmaceutics*, *13*(9), 1475.

30. Ćirin, D. M., Poša, M. M., & Krstonošić, V. S. (2012). Interactions between sodium cholate or sodium deoxycholate and nonionic surfactant (Tween 20 or Tween 60) in aqueous solution. *Industrial and Engineering Chemistry Research*, *51*(9), 3670–3676.

31. Mahmood, S., Taher, M., & Mandal, U. K. (2014). Experimental design and optimization of raloxifene hydrochloride loaded nanotransfersomes for transdermal application. *International Journal of Nanomedicine*, *9*, 4331–4346.

32. El Zaafarany, G. M., Awad, G. A. S., Holayel, S. M., & Mortada, N. D. (2010). Role of edge activators and surface charge in developing ultradeformable vesicles with enhanced skin delivery. *International Journal of Pharmaceutics*, *397*(1–2), 164–172.

33. Bakr, M. M., Shukr, M. H., & ElMeshad, A. N. (2020). In situ hexosomal gel as a promising tool to ameliorate the transnasal brain delivery of vinpocetine: Central

composite optimization and in vivo biodistribution. *Journal of Pharmaceutical Sciences*, *109*(7), 2213–2223.

34. Albash, R., Abdelbary, A. A., Refai, H., & El-Nabarawi, M. A. (2019). Use of transethosomes for enhancing the transdermal delivery of olmesartan medoxomil: In vitro, ex vivo, and in vivo evaluation. *International Journal of Nanomedicine*, *14*, 1953–1968.

35. Mehta, B., Prajapat, P., & Gohil, Y. (2017). Development and validation of stability indicating RP-HPLC method for estimation of teriflunomide in active pharmaceutical ingredient. *The Pharma Innovation Journal*, *6*(9), 440–449.

36. Catauro, M., Papale, F., Bollino, F., Piccolella, S., Marciano, S., Nocera, P., & Pacifico, S. (2015). Silica/quercetin sol–gel hybrids as antioxidant dental implant materials. *Science and Technology of Advanced Materials*, *16*(3), 035001.

37. Divoux, T., Tamarii, D., Barentin, C., Teitel, S., & Manneville, S. (2012). Yielding dynamics of a Herschel-Bulkley fluid: A critical-like fluidization behaviour. *Soft Matter*, *8*(15), 4151–4164.

38. Nagaraja, S., Basavarajappa, G. M., Attimarad, M., & Pund, S. (2021). Topical nanoemulgel for the treatment of skin cancer: Proof-of-technology. *Pharmaceutics*, *13*(6), 902.

39. Herrada-Manchón, H., Fernández, M. A., & Aguilar, E. (2023). Essential guide to hydrogel rheology in extrusion 3D printing: How to measure it and why it matters? *Gels*, *9*(7), 517.

40. Chen, M., Shamim, M. A., Shahid, A., Yeung, S., Andresen, B. T., Wang, J., Nekkanti, V., Meyskens, F. L., Kelly, K. M., & Huang, Y. (2020). Topical delivery of carvedilol loaded nano-transfersomes for skin cancer chemoprevention. *Pharmaceutics*, *12*(12), 1151.

41. Malviya, N., A, P., & Alexander, A. (2023). Comparative study on ethosomes and transferosomes for enhancing skin permeability of sinapic acid. *Journal of Molecular Liquids*, *383*, 122098.

Chapter 6

Evaluation of Teriflunomide and Quercetin Transferosomal gel in Complete Freund's Adjuvant Induced Rat Model

Chapter 6

6.1. Introduction

The TFD and QCN combination showed synergistic activity in *in-vitro* cell line studies. However, it is imperative to assess the efficacy of the topical transferosomal combination gel in the *in-vivo* studies. A variety of adjuvants have been utilized to induce arthritogenic signals in animal models. These include collagen type I or II, lipopolysaccharides, complete or incomplete Freund's adjuvant, carrageenan, pristine, formalin, 6-sulfanilamidoindazole, and squalene. The *in-vivo* activity of the developed formulations was assessed using the CFA model, which is a well-established method, and widely used for inducing arthritis in experimental animals. It contains killed *Mycobacterium tuberculosis* suspended in mineral oil. CFA is characterized by a more severe and systemic manifestation when compared with arthritis induced by adjuvants devoid of antigens. This model mimics several aspects of RA, making it a reliable system for evaluating the efficacy of potential antiarthritic agents [1,2]. In this model, localized inflammation is initiated through the administration of CFA into the rat footpad by subplantar route. Subsequently, there is a notable increase in erythrocyte sedimentation rate (ESR), blood neutrophil count, and leukocyte count, that is observed commencing on the fourth day post-CFA injection. Within 1-2 weeks after induction, hyperalgesia and edema manifest in the ankle and dorsal tarsal region, that is attributed to extensive neutrophil infiltration and synovial lining proliferation [3]. This cascade stimulates immune cells to release pro-inflammatory mediators (TNF-α, IL-6, IL-1β, IL-12 and MMP) and epithelial-neutrophil activating peptide (ENA) in the synoviocytes of the affected joint, resulting in vasodilation and increased permeability of blood vessels in the paw tissue [4,5].

The formulation of transferosomes incorporating TFD and QCN was optimized using a systematic QBD approach, aimed at enhancing skin permeability. As demonstrated in section 5.4.10, the transferosomal gel demonstrated augmented skin permeability and retention, evaluated using rat abdominal skin. Also, the *in vitro* cell line studies demonstrated transferosomes exhibited more effective in proinflammatory cytokine inhibition compared to free drug. So, the primary objective of this study was to assess the effectiveness of a combination transferosomal gel in reducing arthritic manifestations in a rat model induced with CFA in comparison to a gel containing free drug combination. Additionally, the experiment was conducted using two dosage levels (low and high), both individually and in combination, to evaluate the efficacy of the combination in alleviating arthritic symptoms.

6.2. Materials and methods

6.2.1. Materials

As mentioned in chapter 3, TFD (99.9 % pure) was obtained as a gift sample from the MSN Laboratories Private Limited (Sangareddy,India). QCN (> 98 % purity) was purchased from Yucca Enterprises (Mumbai, India). CFA was procured from Sigma, India. The ELISA kits were purchased from Elabscience (Houston, USA).

6.2.2. Animals

The *in-vivo* studies were performed as per the protocol (IAEC/RES/33/08) approved by the Institutional animal ethical committee's (IAEC) guidelines BITS-Pilani, Pilani campus, Rajasthan. Female Wistar rats weighing 250 ± 10 gm were housed in standard laboratory conditions, maintained at a temperature of 25 ± 2 °C and a relative humidity of 55 ± 10 %. The animals were provided with standard laboratory diet and water *ad libitum* at the central animal facility (CAF) at BITS-Pilani.

6.2.3. Skin irritation study

Female rats were systematically selected and divided into five experimental groups, with each group comprising three animals. Group 1 (normal control); group 2 (5 % SLS); group 3 (transferosomal topical gel with 2 mg/kg of TFD and 7 mg/kg of QCN); group 4 (free drug loaded combination gel with 2 mg/kg of TFD and 7 mg/kg of QCN); and group 5 (blank gel). The day prior to the experiment, the hairs on the dorsal side of the rats' skin were removed using a shaver. Subsequently, application sites were visually inspected for erythema. Images were captured at the end of 48 h after application. After completion of the 48 h time period, a single animal from each group was scarified, and histopathological analysis was conducted utilizing hematoxylin and eosin (H&E) staining [6].

6.2.4. Evaluation of antiarthritic activity in CFA induced rat

For the experiment, female Wistar rats were selected and assigned to 16 groups, each comprising 6 animals, as presented in the **Table 6.1**.

Table 6.1. Experimental groups for CFA induced model assessment

Groups	Treatment
Group -1	Normal control (arthritis uninduced group)
Group - 2	Disease control group (CFA induced group)
Group - 3	Topical low dose - free TFD gel
Group - 4	Topical low dose - free QCN gel
Group - 5	Topical low dose - free drug combination gel
Group - 6	Topical low dose -TFD transferosomal gel
Group - 7	Topical low dose - QCN transferosomal gel
Group - 8	Topical low dose - combination transferosomal gel
Group - 9	Topical high dose - free TFD gel
Group – 10	Topical high dose - free QCN gel
Group – 11	Topical high dose - free drug combination gel
Group – 12	Topical high dose - TFD transferosomal gel
Group – 13	Topical high dose - QCN transferosomal gel
Group – 14	Topical high dose - combination transferosomal gel
Group - 15	High dose oral TFD solution
Group - 16	Placebo transferosomal gel

Note.

High dose is 2 mg/kg of TFD and 7 mg/kg of QCN

Low dose is 1 mg/kg of TFD and 3.5 mg/kg of QCN

High dose oral TFD is 2 mg/kg

The anti-arthritic efficacy was studied for all treatment groups as mentioned in **Table 6.1**. Except for group 1, all animals in each group received a subplantar injection of 120 µL of CFA into the right hind paw, marking the commencement of the study as day zero. The treatment regimen commenced on the 7th day after induction and continued until the 27th day. It involved topical application of the formulations to the induced paw (for groups 3 to 14 and 16), as well as oral administration (for group 15) once a day. Throughout the experiment, the animals were housed in a controlled environment, with unrestricted access to a standard pellet diet and water. The schematic representation of the *in-vivo* experimental design is represented in **Figure 6.1**.
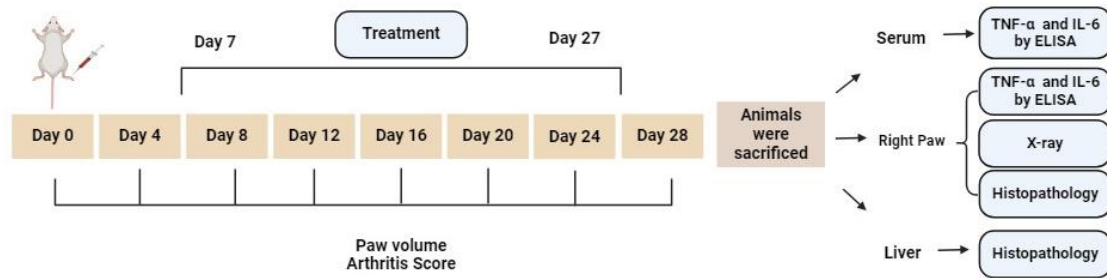
Figure 6.1. Schematic representation of the *in-vivo* experimental design

6.2.4.1. Measurements of paw volume

The volume of the right hind paw was measured using plethysmometer (UGO basile) at regular interval of 0, 4, 8, 12, 16, 20, 24 and 28th day. Changes in the paw volume were determined using equation 6.1.

$$\% \text{ Increse in paw volume} = \frac{\text{paw volume of control} - \text{paw volume of test}}{\text{paw volume of control}} \times 100 \qquad \text{…eq 6.1}$$

6.2.4.2. Arthritic score

The scores were assigned to the rats' right paw in each group based on a scale ranging from 0 to 4: wherein 0 indicated no swelling or erythema, 1 represented slight swelling and/or erythema, 2 denoted low to moderate edema, 3 indicated pronounced edema with limited joint use, and 4 signified excessive edema. The scores were noted at regular intervals of 0, 4, 8, 12, 16, 20, 24 and 28th day.

6.2.4.3. Determination of pro-inflammatory cytokine level in serum

Blood samples were collected on the 28th day of the experiment from all groups and allowed to clot for some time. Then centrifuged at 10,000 rpm at 4 ºC for 15 min. The obtained serum was analyzed for TNF-α and IL-6 levels using an ELISA kit, following the manufacturer's protocol [7].

6.2.4.4. Determination of pro-inflammatory cytokine levels in paw tissue

After the 28th day, the animals were euthanized, and paw tissues were harvested from each experimental group. The harvested tissues were rinsed with ice-cold phosphate-buffered saline (PBS). Following this, the paw tissue was diced into small fragments, homogenized for 10 min, and then centrifuged at 10000 rpm for 15 min. The resulting supernatant was then utilized for the analysis of pro-inflammatory cytokine assessment, specifically TNF-α and IL-6, employing an ELISA kit (Elabscience), in accordance with the manufacturer's protocol [7].

6.2.4.5. Radiographic analysis

For radiographic evaluation, one animal from each group was euthanized, and the right paw with the ankle joint was collected specifically for X-ray imaging for detailed examination of joint structure and any potential abnormalities.

6.2.4.6. Histopathological observation of rat paw tissue

After completion of study, one animal from each group was euthanized, and the ankle joint of the right hind paw was dissected for histopathological examination. The dissected samples were stored in 10% formalin solution until further processing. Subsequently, the tissues were embedded in paraffin wax to create solid blocks. The blocks were sectioned into 5 mm thick slices using a microtome and stained with Masson's trichrome stain. Imaging was performed using a compact light microscope (Zeiss). The assessment involved analyzing the level of collagen deposition in the rat paw tissue [8,9].

6.2.4.7. Histopathology of the liver

Following the 28-day study period, one animal from each group was euthanized, and liver tissue samples were obtained. These samples were rinsed with ice-cold PBS saline, prepared for histopathological examination as described above. The samples were then stained using H&E. The assessment criteria for liver sections involved observing fibrous connective tissue proliferation (FCP), inflammatory cell infiltration (IC), and portal inflammation (PI) [10].

6.3. Statistical analysis

Each experiment was conducted thrice, and the findings were presented as the mean with standard deviation. Statistical analysis involved employing two-way ANOVA for *in-vivo* paw volume and arthritic score measurement; one-way ANOVA for *in-vivo* serum sample and plasma tissue analysis for evaluation of pro-inflammatory cytokine through GraphPad Prism (v 7.0), with significance levels set at $p < 0.05$.

6.4. Results and Discussion

6.4.1. Skin irritation study

To assess the compatibility of the topical gels, a 48 h skin irritation study was conducted. The study involved observing skin reactions before and after application to different treatment groups. The images were captured 48 h after application and are presented in **Figure 6.2** for visual comparison. No signs of edema and erythema were observed in all groups except group 2 (5% SLS group).
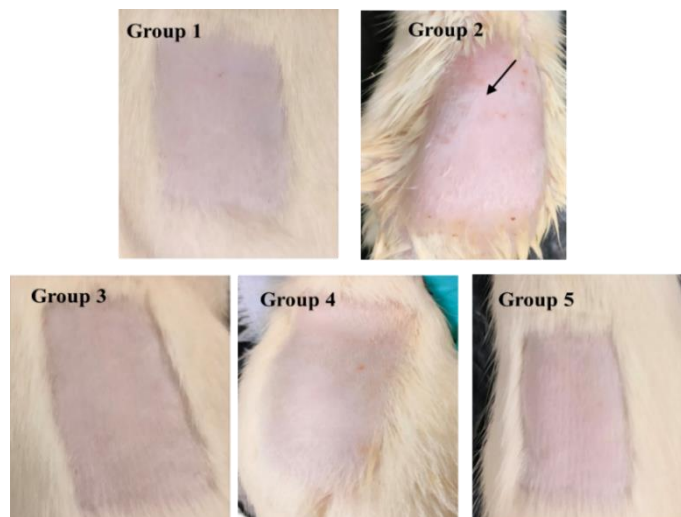
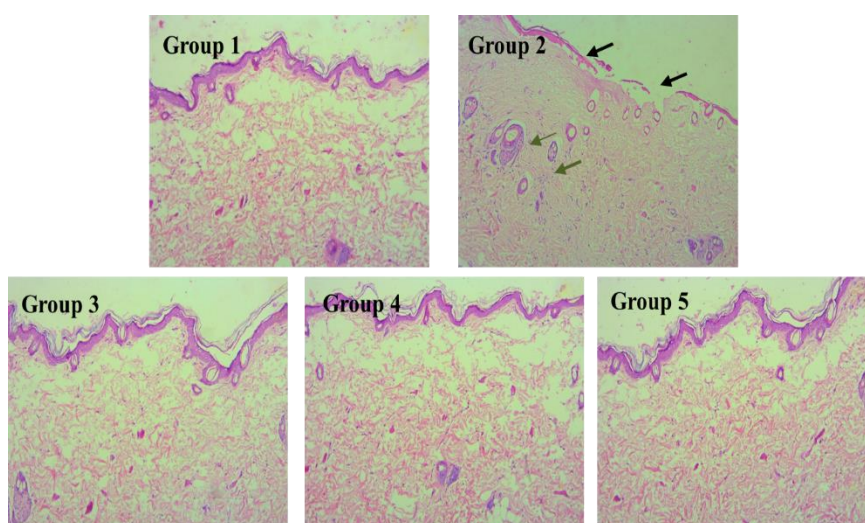**Figure 6.2.** Images of *in-vivo* skin irritation study for topical formulations taken after 48 h. (Black arrows indicates erythema and edema).

After 48 h of application, skin samples were evaluated for histopathological observations, and the corresponding images are presented in **Figure 6.3**. The epidermal layer exhibited a thin structure, as observed in group 1 (normal control) with no evidence of necrosis. A similar pattern was noted in group 3 (transferosomal topical gel with 2 mg/kg of TFD and 7 mg/kg of QCN); group 4 – (free drug loaded combination gel with 2 mg/kg of TFD and 7 mg/kg of QCN); and Group 5 (blank gel). On the other hand, group 2 (5 % SLS) displayed a damaged epidermal layer along with necrosis. This suggests that the prepared topical formulations are safe for use without any observed indications of skin irritation.

Figure 6.3. Histopathology images for *in-vivo* skin irritation study. (Black arrows indicate dermal damage, green arrows indicate necrosis).

6.4.2. Antiarthritic activity

6.4.2.1. Measurements of paw volume

The antiarthritic activity was assessed in the CFA-induced rat paw edema model. The data illustrating the percent increase in paw volume for all groups are depicted in **Figure 6.4**. A significant increase ($p < 0.05$) in paw volume after four days post-induction with CFA was observed in all groups with the exception of group 1. Subsequently, in the CFA induced group (group 2), progressive increase in paw volume was observed, reaching exacerbation after 12 days and continuing until the end of the 28-day period. This was accompanied by noticeable swelling and fissures with paw volume of 70.72 ± 1.27 %. Following this, placebo gel treated group (Group 16) also showed increase in paw volume of 59.31 ± 3.34 %, although less pronounced compared to group 2.

The free QCN gel at low and high doses (group 4 and 10) exhibited an increase in paw volume compared to the QCN transferosomal gel (group 7 and 13), that can be attributed to the enhanced permeability achieved by encapsulation into transferosomes. Similar trends were observed with the free TFD gel at low and high doses (group 3 and 9) and the TFD transferosomal gel (group 7 and 12).

The high dose oral TFD group (group 15) exhibited a higher paw volume, measuring 29.59 ± 3.08 %, compared to the same dosage administered through topical TFD transferosomal gel (group 12), with a paw volume of 23.37 ± 2.60 % at the end of 28th day. This suggests that topical administration leads to a more significant reduction ($p < 0.0001$) in paw volume at equivalent dosages, likely owing to its localized effect.

The TFD and QCN combination transferosomal gel, administered at both low (group 8) and high doses (group 14) demonstrated a notable reduction in paw volume compared to monotherapy, indicating the efficacy of combination therapy. Particularly, the high-dose combination transferosomal gel, (group 14) exhibited a statistically ($p < 0.001$) more substantial decrease in paw volume (14.19 ± 4.10 %) compared to low dose combination transferosomal gel (25.53 ± 2.853 %).

The low dose TFD and QCN combination transferosomal gel (group 8) exhibited a paw volume of 25.53 ± 2.853 %, whereas high dose oral TFD solution (group 15) exhibited a paw volume of 29.59 ± 3.08 %. There was no statistically significant difference observed between both groups at the end of 28th day. This suggests that achieving the same activity may be possible with a low-dose combination gel compared to a high-dose oral TFD, indicating the potential for dose reduction
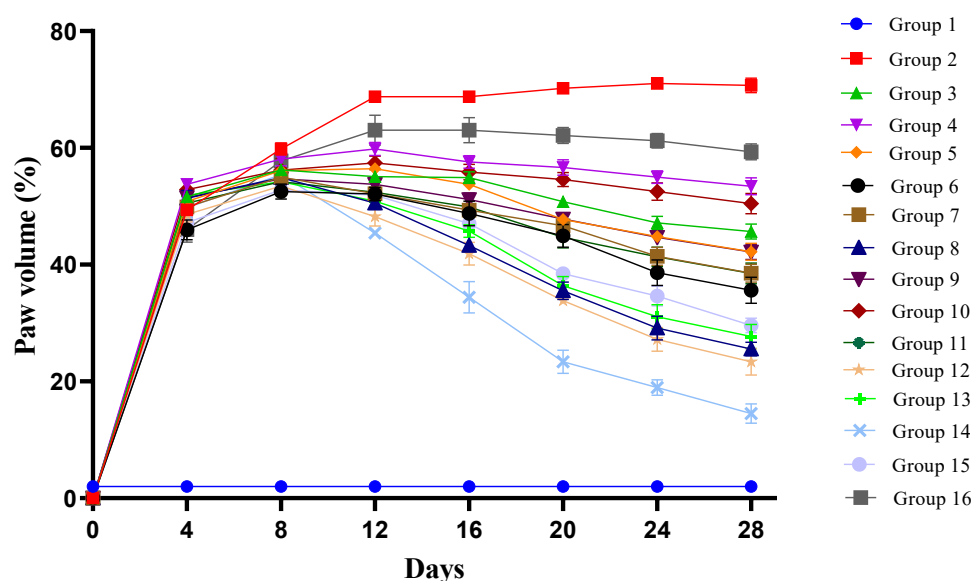
Figure 6.4. Effect of different treatment groups on paw volume (n = 6, mean ± SD,)

6.4.2.2. Arthritic Score

The arthritic index quantifies the severity of joint inflammation by assessing the scores of the paws following arthritis induction. **Figure 6.5** illustrates the arthritic scores assigned to all groups. After fourth day of induction, the arthritic score increased for all groups except group 1, indicating the onset of a proliferative phase characterized by inflammation, hyperplasia, and macrophage activities within the synovial membrane.

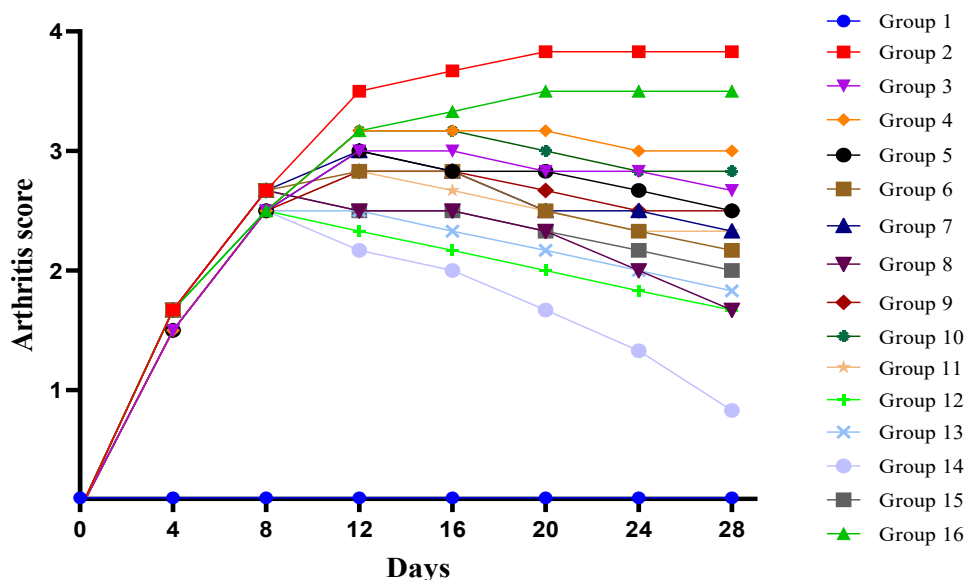**Figure 6.5**. Effect of different treatment groups on arthritic score (n = 6, mean ± SD)

The arthritic score for CFA induced group (group 2) was found to be 3.83 ± 0.54 at the end of 28th day. The score was reduced to 1.67 ± 0.32 and 0.83 ± 0.21 for low dose (group 8) and high

dose TFD and QCN combination transferosomal gel (group 14) respectively. The results revealed a statistically significant difference between the CFA control group and the high-dose combination transferosomal gel (group 14), resulting in a reduction in arthritic manifestations, including paw volume, erythema, redness, and swelling.

6.4.2.3. Determination of pro-inflammatory cytokine level in serum and paw tissue

The concentrations of pro-inflammatory cytokines namely TNF-α and IL-6, were assessed using ELISA, and the findings are presented in the corresponding **Figure 6.6a** & **b** for serum and **Figure 6.6c** & **d** for paw tissue, respectively.
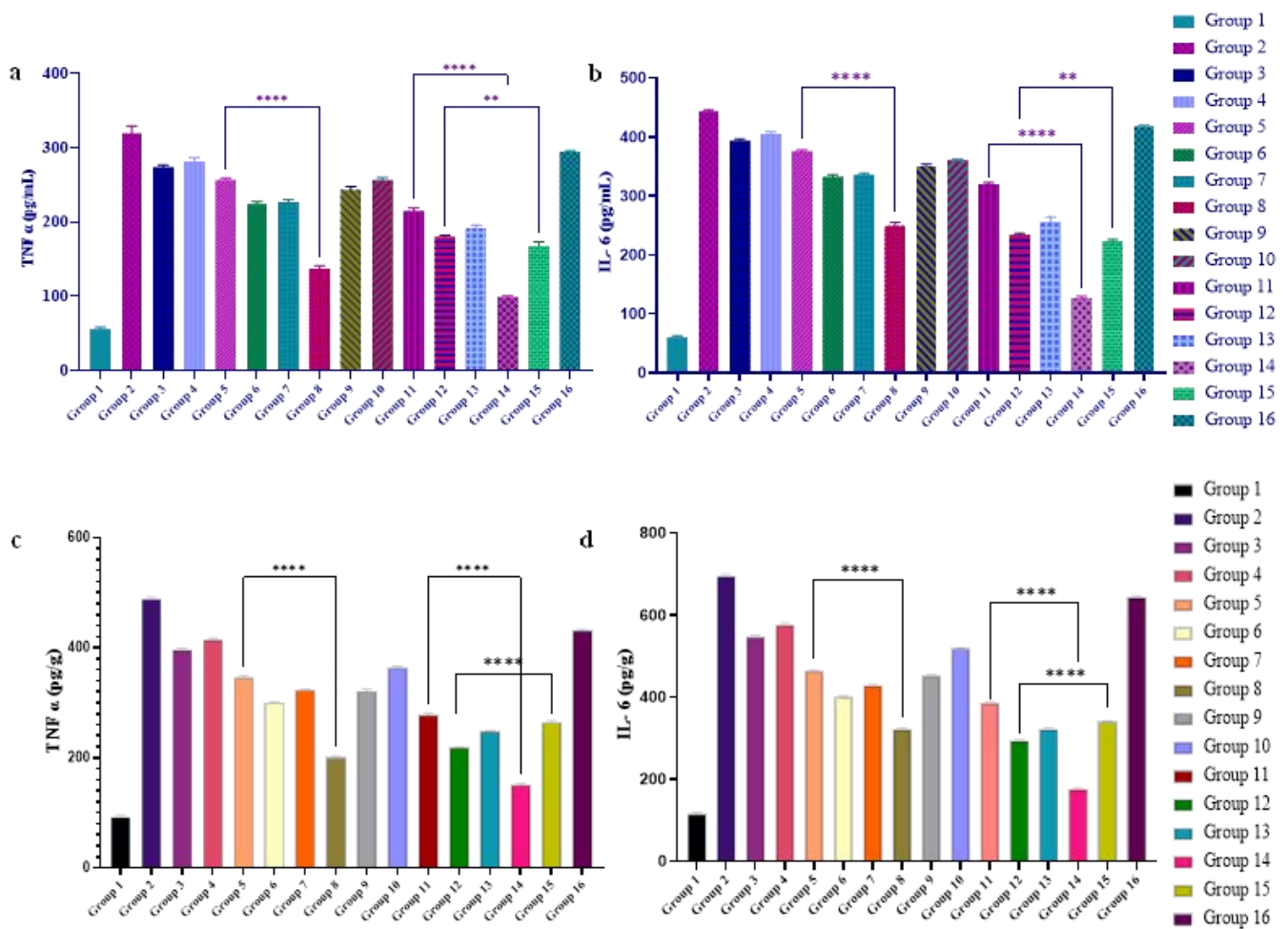
Figure 6.6. Impact of various formulations on serum levels of a) TNF-α; b) IL-6 and impact on paw tissue levels of c) TNF-α; d) IL-6 in rats (n = 3, mean ± SD).

One way ANOVA   **** $p < 0.0001$; *** $p < 0.001$; ** $p < 0.01$; * $p < 0.05$

The results suggest that the encapsulation of drugs within nanovesicles enhanced their inhibitory efficacy against TNF-α and IL-6 in the *in-vivo* studies. Compared to free drug loaded gel at both low (group 3, 4, 5), and high doses (group 9,10,11), all the transferosome loaded gel at similar dose exhibited more inhibitory activity in groups 6,7,8, 12,13 and 14. Also, the combination of TFD and QCN transferosomal gel in group 8 and 14 exhibited statistically significant ($p < 0.0001$) decrease in the TNF-α and IL-6 levels compared to individual transferosomal gel, as observed in both serum and paw tissue.

The administration of a high dose oral TFD group (group 15) led to a notable decrease ($p < 0.001$) in TNF-α and IL-6 levels in serum compared to TFD transferosomal gel at an equivalent dose (group 12). Conversely, compared to oral administration of TFD (group 15), topical application of TFD transferosomal gel at the same dose (group 12) demonstrated a statistically significant ($p < 0.0001$) reduction in pro-inflammatory cytokine levels in paw tissue. These findings indicate that topical delivery offers an effective approach for mitigating the levels of pro-inflammatory cytokines compared to oral administration at equivalent dosages in local tissue, by directly targeting the affected area.

6.4.2.4. Radiographic analysis

Radiographical analysis enabled the observation of joint space reduction and soft tissue inflammation in the CFA-induced model. **Figure 6.7** includes X-ray images obtained after treatment accompanied by rat paw images. Analysis of the data demonstrated a more pronounced joint space reduction and increase in soft tissue inflammation in the CFA induced group (group 2) and the placebo transferosomal gel (group 16). Similar trends were noted in the groups administered with the free TFD and QCN gel (group 3, 4, 5, 9, 10, 11). No joint space reduction or soft tissue inflammation was observed in the normal control group (group 1), and comparable findings were noted in the high dose TFD and QCN combination transferosomal gel (group 14) compared monotherapy, indicating the efficacy of topical combination therapy for the treatment of RA.

Figure 6.7. Rat paw and x-ray images following 28 days of treatment in CFA-induced model; (orange arrow indicates the inflammation in soft tissue and blue arrow indicates the reduction in joint space)

6.4.2.5. Histopathological observation of rat paw tissue

Histopathological analysis of the paw tissue was conducted using Masson's Trichome staining, and representative histopathological images were presented in **Figure 6.8.** The blue color observed beneath the epidermis signifies the presence of collagen fibrils, while the red staining indicates the presence of cytoplasm, red blood cells, and muscle tissue. The extent of blue-colored collagen (indicated by a black arrow) corresponds to the relative quantity of total deposited collagen fiber, reflecting various processes including collagen synthesis, degradation, and remodeling. The data clearly indicate that collagen deposition was significantly higher in group 2 and 16 compared to the normal control group (group 1). Collagen deposition was found to be higher with both low and high doses of free drug-loaded gel (group 3, 4, 5, 9, 10, 11) compared to the gel loaded with transferosomes (group 6, 7, 8, 12, 13, 14). Group 14 exhibited a lower level of collagen deposition, and it was comparable to group 1. Furthermore, in comparison to the groups 12 and 13, the combination transferosomal gel (group 14) demonstrated a more pronounced decrease in collagen deposition. This highlights the effectiveness of the high dose transferosomal combination gel in attenuating collagen deposition for the treatment of RA.
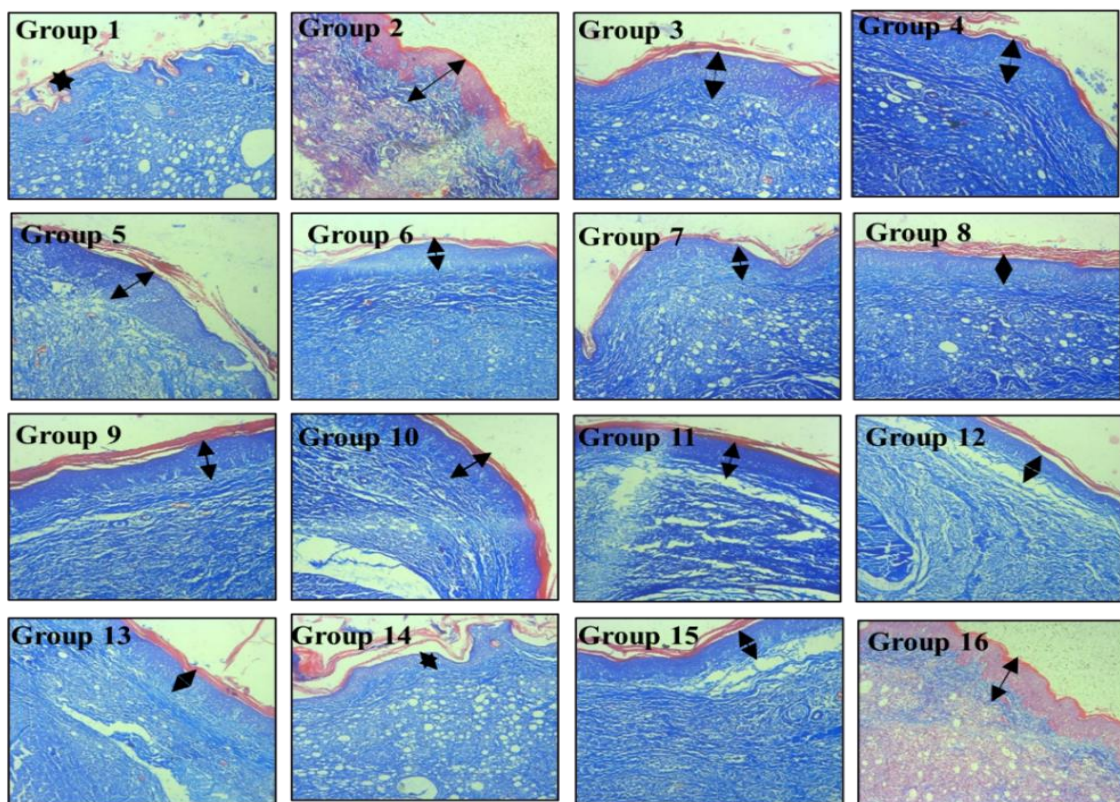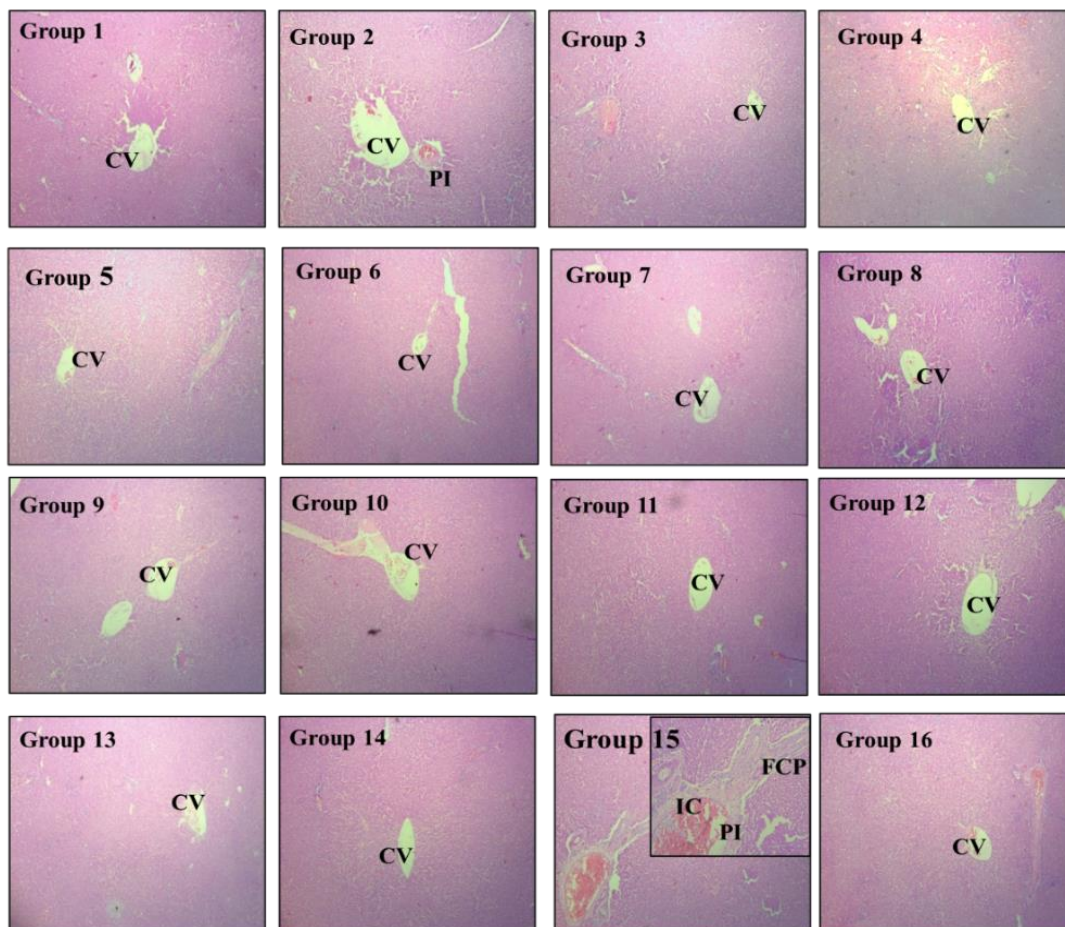

Figure 6.8. Histopathology of rat paw tissue stained by Masson's trichome stain. (The black arrow indicates the collagen fibrils thickness.

6.4.2.6. Histopathology of the liver

The histopathological images using H&E staining were shown in **Figure 6.9.** At the end of the study, the alteration in hepatocellular structure was evaluated following treatment with various formulations. The data revealed that the normal control group (group 1) exhibited normal hepatocellular structure, while CFA control group showed minor portal inflammation (PI). The high dose oral TFD group (group 15) exhibited notable fibrous connective tissue proliferation (FCP), inflammatory cell infiltration (IC), and portal inflammation (PI) as similar to reported by Pandey et al. 2021. However, at an equivalent dosage of groups 12 and 14, no evident signs of changes in hepatocellular structure were observed, indicating superiority over other treatment groups. TFD has been documented to induce significant hepatotoxicity upon oral ingestion [11]. However, in our investigation, administering TFD at equivalent dose *via* both oral and topical routes revealed that oral ingestion elicited minor alterations in hepatocellular morphology, while topical application of TFD in transferosomal gel formulation did not produce discernible changes in histopathology of the liver [12].

Figure 6.9. Histopathology of rat liver stained using H&E. **CV** – Central Vein; **FCP** – Fibrous Connective tissue Proliferation; **IC** – Inflammatory cell Infiltration

Chapter 6

The *in-vivo* anti-arthritic activity in the CFA model was assessed for various parameters including paw volume, arthritic score, X-ray analysis, inhibition of proinflammatory cytokines in serum and paw tissue, and histopathological examination of paw and liver tissue. The findings indicated that the transferosomal gel demonstrated greater efficacy compared to the gel loaded with free drug. This highlights the advantage of employing nanocarriers to enhance permeability for therapeutic applications. The enhanced permeability of transferosomes can be attributed to their smaller size and negative ZP, which aligns with findings by Miatmoko et al. 2022, observed increased skin permeability with the use of anionic surfactant sodium cholate due to the negatively charged nature of the *stratum corneum*. Additionally, the minimal interaction of transferosome vesicles with the skin layer facilitates easier diffusion of encapsulated active ingredients into deeper skin layers [13,14].

Furthermore, the combination of transferosomal gel at both low and high doses demonstrated increased anti-arthritic activity compared to monotherapy. This was due to the combined effect of TFD and QCN. The TFD functions by inhibiting DHODH and has also been reported to inhibit the NF-kB pathway [15]. Similarly, QCN has been reported to inhibit the differentiation of TH17 cells, which are implicated in RA pathogenesis and joint inflammation. Additionally, QCN has been reported to inhibit NF-κB, adenosine deaminase, MAPK [16]. Therefore, the collective impact of both compounds targeting multiple pathways may provide improved anti-arthritic activity. Zhang, Y et al. 2014 reported similar findings, where the combination of TFD and diclofenac showed enhanced anti-inflammatory effects in Wistar rats induced with CFA [9]. Likewise, Haleagrahara et al. 2018 demonstrated that the combined effect of QCN and methotrexate exhibited notable anti-inflammatory activity in Chicken type II collagen induced C57/BL6 mice.

High-dose oral administration of TFD at 2 mg/kg (group 15) resulted in a similar inhibition of paw volume and arthritic score with the low dose combination transferosomal gel at TFD-1 mg/kg and QCN-3.5 mg/kg (group 8). This suggests that topical administration of combination transferosomal gel allows for dose reduction, potentially minimizing systemic side effects associated with oral dosage through localized action. Also, topical administration resulted in a slight reduction of proinflammatory mediators in paw tissue compared to oral administration, indicating a localized action which may reduce systemic exposure to the drug. This may be due to the deposition of more amount of drug at the local tissue [17].

The histopathology of the liver showed minimal changes in hepatocellular structure following oral administration of TFD. In contrast, no such alterations were observed with topical transferosomal gel administration at an equivalent dose. Similar findings were observed by

Cao, Y., et al. 2019, where oral administration of TFD led to increased inflammatory cell infiltration, but this effect was absent in topical TFD microemulsion. Additionally, Pandey, S., et al. 2022, reported similar observations, where oral Aubagio® resulted in portal inflammatory reaction in liver histopathology. Hepatotoxicity may occur due to high systemic exposure to TFD. However, topical administration results in reduced or no toxicity, likely due to lower systemic exposure to TFD. Roth et al. 2011, also found that applying diclofenac topically is a viable alternative to oral NSAIDs, resulting in lower systemic exposure. Oral NSAID use was associated with increased liver enzymes and creatinine levels, along with greater decreases in creatinine clearance and hemoglobin compared to topical administration [18]. Thus, topical application presents a potential means to decrease systemic drug exposure.

In summary, the increased effectiveness of the topical transferosomal gel in treating arthritis may stem from its direct diffusion into local tissue, as governed by Fick's law of diffusion [19]. Hagen et al. 2017 noted that relatively low systemic absorption occurs through dermal microcirculation after topical application [20]. Additionally, Bae et al. 2016 found higher concentrations of the TFD in synovial tissue compared to non-application sites in *in-vivo* micropig knee joint tissue deposit studies [21]. Similarly, Shinkai et al. 2011 reported direct diffusion of ketoprofen into skin and joint tissue after topical application [22]. Collectively, these findings suggest that the topical approach could be effective for localized treatment of RA.

6.5. Conclusion

The *in-vivo* efficacy studies in CFA-induced rat paw edema model illustrated the effectiveness of the combination transferosomal gel in reducing paw volume and mitigating other arthritis manifestations. Additionally, liver histopathology showed minimal hepatocellular structural changes with oral TFD administration, contrasting with topical TFD administration. The study concluded that the combination of TFD and QCN transferosomal gel holds promise for the effective treatment of RA through localized delivery by direct diffusion, and allows for the potential dose reduction of TFD. Consequently, it may alleviate systemic side effects.

Chapter 6

References

1. Fehrenbacher, J. C., Vasko, M. R., & Duarte, D. B. (2012). Models of inflammation: Carrageenan- or complete freund's adjuvant (CFA)-induced edema and hypersensitivity in the rat. *Current Protocols in Pharmacology, 56*(1)*,* 5-4.

2. Noh, A. S. M., Tan, D. C., Khir, N. A. M., Shafin, N., & Ismail, C. A. N. (2022). A Review on complete freund's adjuvant-induced arthritic rat model: Factors leading to its success. *IIUM Medical Journal Malaysia*, *21*(4), 3–12.

3. Pearson, C. M., Waksman, B. H., & Sharp, J. T. (1961). Studies of arthritis and other lesions induced in rats by injection of mycobacterial adjuvant. v. Changes affecting the skin and mucous membranes. Comparison of the experimental process with human disease. *The Journal of Experimental Medicine*, *113*(3), 485–510.

4. Noh, A.S.M., Chuan, T.D., Khir, N.A.M., Zin, A.A.M., Ghazali, A.K., Long, I., Ab Aziz, C.B. & Ismail, C.A.N.,(2021). Effects of different doses of complete freund's adjuvant on nociceptive behaviour and inflammatory parameters in polyarthritic rat model mimicking rheumatoid arthritis. *PloS One, 16*(12), e0260423.

5. Szekanecz, Z., Halloran, M.M., Volin, M.V., Woods, J.M., Strieter, R.M., Haines III, G.K., Kunkel, S.L., Burdick, M.D. & Koch, A.E. (2000). Temporal expression of inflammatory cytokines and chemokines in rat adjuvant-induced arthritis. *Arthritis & Rheumatism,* 43(6), 1266-1277.

6. Sana, E., Zeeshan, M., Ain, Q.U., Khan, A.U., Hussain, I., Khan, S., Lepeltier, E. & Ali, H. (2021). Topical delivery of curcumin-loaded transfersomes gel ameliorated rheumatoid arthritis by inhibiting NF-κβ pathway. *Nanomedicine, 16*(10), 819-837.

7. Lal, R., Dhaliwal, J., Dhaliwal, N., Dharavath, R. N., & Chopra, K. (2021). Activation of the Nrf2/HO-1 signaling pathway by dimethyl fumarate ameliorates complete freund's adjuvant-induced arthritis in rats. *European Journal of Pharmacology*, *899*, 174044.

8. Burayk, S., Oh-Hashi, K., & Kandeel, M. (2022). Drug discovery of new anti-inflammatory compounds by targeting cyclooxygenases. *Pharmaceuticals*, *15*(3), 282.

9. Abdelkader, D. H., Elekhnawy, E., Negm, W. A., El-Masry, T. A., Almukainzi, M., Zayed, A., & Ulber, R. (2022). Insight into fucoidan-based PEGylated PLGA nanoparticles encapsulating methyl anthranilic acid: In vitro evaluation and in vivo anti-inflammatory study. *Marine Drugs, 20*(11), 694.

10. Pandey, S., Rai, N., Mahtab, A., Mittal, D., Ahmad, F.J., Sandal, N., Neupane, Y.R., Verma, A.K. & Talegaonkar, S.(2021). Hyaluronate-functionalized hydroxyapatite nanoparticles laden with methotrexate and teriflunomide for the treatment of rheumatoid

arthritis. *International Journal of Biological Macromolecules*, 171, 502-513.

11. Bar-Or, A. (2014). Teriflunomide (Aubagio®) for the treatment of multiple sclerosis. *Experimental Neurology, 262*, 57-65.

12. Mahtab, A., Rabbani, S.A., Neupane, Y.R., Pandey, S., Ahmad, A., Khan, M.A., Gupta, N., Madaan, A., Jaggi, M., Sandal, N. & Rawat, H. (2020). Facile functionalization of teriflunomide-loaded nanoliposomes with chondroitin sulphate for the treatment of rheumatoid arthritis. *Carbohydrate Polymers, 250,* 116926.

13. Miatmoko, A., Marufah, N.A., Nada, Q., Rosita, N., Erawati, T., Susanto, J., Purwantari, K.E., Nurkanto, A., Purwati & Soeratri, W. (2022). The effect of surfactant type on characteristics, skin penetration and anti-aging effectiveness of transfersomes containing amniotic mesenchymal stem cells metabolite products in UV-aging induced mice. *Drug Delivery, 29*(1), 3443-3453.

14. Sinico, C., Manconi, M., Peppi, M., Lai, F., Valenti, D., & Fadda, A. M. (2005). Liposomes as carriers for dermal delivery of tretinoin: In vitro evaluation of drug permeation and vesicle-skin interaction. *Journal of Controlled Release 103*(1), 123–136.

15. Manna, S. K., & Aggarwal, B. B. (1999). Immunosuppressive leflunomide metabolite (A77 1726) blocks tnf-dependent nuclear factor-κb activation and gene expression. *The Journal of Immunology*, *162*(4), 2095–2102.

16. Tang, M., Zeng, Y., Peng, W., Xie, X., Yang, Y., Ji, B., & Li, F. (2022). Pharmacological aspects of natural quercetin in rheumatoid arthritis. *Drug Design, Development and Therapy*, *16*, 2043-2053.

17. Bae, J., & Park, J. W. (2016). Topical delivery of leflunomide for rheumatoid arthritis treatment: Evaluation of local tissue deposition of teriflunomide and its anti-inflammatory effects in an arthritis rat model. *Drug Development and Industrial Pharmacy*, *42*(2), 254–262.

18. Roth, S. H., & Fuller, P. (2011). Diclofenac topical solution compared with oral diclofenac: A pooled safety analysis. *Journal of Pain Research*, *4*, 159-167.

19. Matharoo, N., Mohd, H., & Michniak-Kohn, B. (2024). Transferosomes as a transdermal drug delivery system: Dermal kinetics and recent developments. *Wiley Interdisciplinary Reviews. Nanomedicine and Nanobiotechnology*, *16*(1), e1918.

20. Hagen, M., & Baker, M. (2017). Skin penetration and tissue permeation after topical administration of diclofenac. *Current Medical Research and Opinion*, *33*(9), 1623–1634.

21. Xi, H., Cun, D., Xiang, R., Guan, Y., Zhang, Y., Li, Y., & Fang, L. (2013). Intra-articular drug delivery from an optimized topical patch containing teriflunomide and lornoxicam

for rheumatoid arthritis treatment: Does the topical patch really enhance a local treatment? *Journal of Controlled Release*, *169*(1–2), 73–81.

22. Shinkai, N., Korenaga, K., Okumura, Y., Mizu, H., & Yamauchi, H. (2011). Microdialysis assessment of percutaneous penetration of ketoprofen after transdermal administration to hairless rats and domestic pigs. *European Journal of Pharmaceutics and Biopharmaceutics, 78*(3), 415-421.

Chapter 7

Summary and Conclusion

Chapter 7

Summary and conclusion

The intricate cascade of immune-mediated processes culminates in the progressive deterioration of joint integrity and subsequent functional impairment observed in RA. Effective management of RA necessitates a combination therapy approach to address its diverse underlying pathways comprehensively. Various reports have been documented for the effectiveness of combining synthetic molecules with natural products for RA management. TFD belongs to the synthetic DMARDs and the first line of choice for the treatment of RA. Natural products have also been documented to demonstrate anti-inflammatory and anti-arthritic properties by interfering with multiple pathways involved in the pathogenesis of RA. In the present investigation, the combination of TFD with various natural products such as ANG, QCN, RES, RUT, and TAN IIA underwent screening for synergistic effect analysis in *in-vitro* RAW264.7 cells. Based on the inhibitory activity observed on NO production, pro-inflammatory cytokines, and ROS measurement, the combination of TFD and QCN exhibited significant synergistic activity with low CI value compared to all tested combinations and thus was selected for further investigation. Due to severe hepatotoxicity and systemic effects linked to oral administration of TFD, and the low solubility and poor bioavailability associated with QCN, topical administration *via* transferosomes was selected with the aim to enhance permeability and achieve localized action. For the analysis of TFD and QCN, a simple and cost-effective UV-visible spectrophotometric method was successfully developed for simultaneous estimation using the absorption factor method. Additionally, a simple and rapid HPLC method was developed utilizing the QbD approach incorporating CCD. The developed method underwent validation in accordance with ICH guidelines.

The TFD or QCN transferosomes were successfully optimized using QbD approach incorporating the BBD with 15 experimental runs. The optimization of the method was accomplished using numerical and graphical methods, including desirability graphs and MODR. The optimized composition for TFD loaded transferosomes comprised of PL 90G (300 mg), sodium cholate (40 mg), and tween 80 (45 mg). Similarly, for QCN-loaded transferosomes, the optimized composition included PL 90G (300 mg), sodium cholate (50 mg), and tween 80 (45 mg). The optimized composition resulted in a smaller size and enhanced stability, primarily due to the negative zeta potential facilitated by the incorporation of sodium cholate. ATR-IR characterization studies confirmed the encapsulation of the drug within the transferosomes. The *in-vitro* release study showed sustained release from transferosomes, achieving 91.11 ± 2.58 % release in 10 h for TFD and 92.69 ± 2.098 % in 12 h for QCN. In contrast, the maximum drug release from the free drug solution observed within 2 h. The TFD

and QCN transferosomes were loaded into Carbopol 974P at a ratio of 1:3.5 based on *in-vitro* cell line studies. The rheological studies revealed the non-Newtonian flow behavior of the gel, characterized by shear thinning properties. Additionally, both the amplitude sweep test and frequency sweep test demonstrated the viscoelastic nature of the gel, highlighting a robust microgel structure. The combination of transferosomal gel exhibited significantly ($p < 0.001$) greater inhibitory activity against NO, TNF-α and IL-6 in *in-vitro* RAW 264.7 cells compared to free drug loaded gel. Furthermore, the MTT assay conducted on HaCaT cell lines indicated that the incorporation of TFD and QCN into the transferosomal gel did not affect cell viability, suggesting the non-toxicity of the excipients used. Also, *ex-vivo* studies revealed significantly enhanced permeation ($p < 0.0001$) compared to the free drug, indicating effectiveness in crossing the major epidermal barrier of the skin.

Skin irritation studies in female Wistar rats indicated compatibility of the prepared transferosomal gel with the skin. This was further confirmed by histopathological analysis of skin samples showing no signs of irritation. Efficacy studies in the CFA-induced paw model was successfully developed and conducted over 28 days with the treatment regimen initiated from 7th day after induction and continued till 27th day. Paw volume and arthritic score measurements taken at regular time intervals throughout the study period revealed the greater inhibitory activity of the transferosomal combination gel compared to the free drug-loaded gel. Similarly, from the X-ray analysis, NO inhibition, proinflammatory cytokines inhibition in serum and paw tissue, and histopathological examination of paw tissues revealed the efficacy of transferosomal combination gel in treating CFA-induced model. This may be attributed to the enhanced penetration facilitated by using transferosomes. Additionally, the enhanced activity observed in the combination gel may be attributed to the combined effects of TFD and QCN, that target multiple pathways. TFD is reported to act by inhibiting DHODH and has also been reported to inhibit the NF-κB pathway. Similarly, QCN has been reported to inhibit the differentiation of TH17 cells and to inhibit NF-κB, adenosine deaminase, and MAPK.

In animal studies oral administration of TFD caused slight hepatocellular alterations, while topical TFD transferosomes showed no such changes in liver histopathology. Also, inhibition of proinflammatory cytokine levels in serum was greater with oral TFD compared to topical application, whereas contrasting results were observed in paw tissue. This could be attributed to localized action, that potentially may reduce systemic levels of the drug. Moreover, the low-dose combination transferosomal gel exhibited similar activity compared to the high oral dose TFD solution, as evidenced by paw volume and arthritic score measurements. The comprehensive study concluded that the combination of TFD and QCN transferosomal gel

holds promise for the effective treatment of RA through localized delivery by direct diffusion, and may reduce the systemic side effects by allowing for a dose reduction of TFD.

Future perspectives

Following studies based on the present outcomes can be planned

➢ The mechanism underlaying the synergy activity of TFD and natural products can be further evaluated using molecular level experimental studies of various markers

➢ The prepared transferosomes requires further commercial scale-up and toxicity studies

➢ Further *in-vivo* studies are necessary in guinea pigs and rabbits to determine the concentration at the site of action

➢ The developed TFD and QCN combination-loaded transferosomal gel can be further investigated in clinical studies

➢ The developed transferosomal combination gel can be extended for delivery through other routes, such as the intra-articular

Appendices

Appendix I

List of Patents and Publications

Patent

- Atish T. Paul, **Karnam Sriravali** and Anil. B Jindal "A composition and formulation of nano-vesicles for combinatorial delivery including a process of preparation" filed at Indian patent office (Application No. 202411000945) dated 05 January 2024.

Publications from thesis

- **Karnam Sriravali**, Anil B. Jindal, and Atish T. Paul (2024). Implementing analytical quality by design in reversed phase-high performance liquid chromatography for simultaneous estimation of teriflunomide and quercetin: Applicability in dual drug loaded topical microemulsion. *Journal of Liquid Chromatography & Related Technologies*, *47*(6-10), 104-121.

- **Karnam Sriravali**, Mahipal Reddy Donthi, Anil B. Jindal, and Atish T. Paul (2024). Recent innovations in topical delivery for management of rheumatoid arthritis: A focus on combination drug delivery. *Drug Discovery Today*, 104071.

- **Karnam Sriravali**, Anil B. Jindal, and Atish T. Paul "Quality by Design-based Optimization of Teriflunomide and Quercetin Combinational Topical Transferosomes for the Treatment of Rheumatoid Arthritis" (under review- IJPHARM-D-24-02774).

- **Karnam Sriravali**, Utkarsh Jagtap, Anil B. Jindal, Atish T. Paul "Assessment of synergistic anti-inflammatory effects of teriflunomide, a synthetic DMARD, in combination with selected natural products in LPS-stimulated RAW264.7 cells (under communication- SAJB-D-24-02440).

- **Karnam Sriravali**, Anil B. Jindal, and Atish T. Paul .Simultaneous Estimation of Teriflunomide and Quercetin in Dual Drug Loaded Transferosomes: A UV Spectrophotometric Approach Utilizing the Absorption Factor Method (under communication-Accreditation and Quality Assurance - ID 776f452d-493d-4eb0-abeb-b6578becd032)

Other publications

- **Karnam, Sriravali**, Anil B. Jindal, Charu Agnihotri, Bhim Pratap Singh, and Atish T. Paul (2023). Topical Nanotherapeutics for Treating MRSA-Associated Skin and Soft Tissue Infection (SSTIs). *AAPS PharmSciTech*, *24*(5), 108.

- **Karnam, Sriravali**, Jindal, Anil B., Bhim Pratap Singh, and Atish T. Paul (2022). Plant-associated endophytic fungi and its secondary metabolites against drug-resistant pathogenic microbes. In *Antimicrobial resistance* (pp. 253-288). Springer, Singapore.

Appendix II

Bibliography of the Supervisor

Paul Atish Tulshiram

Dr. Paul Atish Tulshiram is Associate Professor at Department of Pharmacy, BITS-Pilani, Pilani Campus, India. He completed his bachelor's from University of Pune, Maharashtra. He pursued M.S and Ph.D in Natural Products from National institute of Pharmaceutical Education and Research (NIPER) S.A.S Nagar, Punjab. He completed post-doctorate from the National Centre for Natural Products Research (University of Mississippi, USA) in the research group of Prof. Ikhlas Khan. His current research interest is Evaluation of anti-inflammatory and anti-obesity natural products and their synergistic evaluation in biochemical assays and cell lines. He has completed 7 research grants from DST-SERD, DST(SEED), DBT, ICMR and Industry. He has published more than 60 research articles in reputed international journals and contributed 24 official monographs on polyherbal formulations in the Ayurvedic Pharmacopeia of India. He has been granted 3 patents in the area of natural products and their derivatives and 7 patents are under evaluation. He has provided guidance to 6 doctoral students and is presently supervising 9 doctoral candidates. He is a reviewer of various journals of reputed publishers such as ACS, Elsevier, Wiley, Bentham, etc., and also for funding agencies such as DST-SERB and South African Medical, Research Council.

Appendix II

Bibliography of the Co- supervisor

Anil. B. Jindal

Dr. Anil Jindal is an Associate Professor at the Department of Pharmacy BITS Pilani and has over a decade of experience in drug delivery technology and nanomedicine. His primary research focus revolves around the development of nanoformulations for efficient drug delivery in both human and animal infectious diseases. He obtained his PhD from ICT, Mumbai, M. Pharm from Bombay College of Pharmacy, Mumbai, and B.Pharm from the University of Rajasthan. Dr. Jindal has also worked with well-known pharmaceutical companies such as Pfizer and IPCA before joining BITS Pilani. He has published more than 45 research and review papers in high-impact factor journals and 15 book chapters, covering a diverse range of topics in drug delivery, nanomedicine, and pharmaceutical sciences. He has been listed in Stanford University list of top 2% of scientists worldwide for three consecutive years (2021, 2022 and 2023). Throughout his career, Dr. Jindal has been the recipient of several prestigious research awards, including the Prof. ML Khorana Memorial Award, Eudragit Award, and SERB Early Career Research Award, all of which highlight his significant contributions to the field. He has successfully edited/co-edited two significant books in the domain of drug delivery: "Pharmaceutical Process Engineering and Scale-up Principles" and "Nanomedicine for the Prevention and Treatment of Infectious Diseases," both of which were published by Springer in 2023. He has successfully developed and commercialised the product, "BEAUTISAN" through an industry-sponsored project, now available for purchase in the US market. Additionally, Dr. Jindal has been serving as a Managing Theme Editor for the esteemed journal Advanced Drug Delivery Reviews (Impact Factor 16.01 in 2023) since July 2022. Dr. Jindal's expertise as an expert reviewer is highly sought after, with invitations to review grant applications for government funding agencies such as DBT and SERB. Furthermore, he has lent his expertise as a reviewer for reputed journals in the field, including Advanced Drug Delivery Reviews, Journal of Drug Delivery Science and Technology, AAPS PharmSciTech, Molecular Pharmaceutics, and PLOS ONE, among many others.

Appendix II

Bibliography of the Candidate

Karnam Sriravali

Karnam Sriravali is Research scholar from Department of Pharmacy, BITS-Pilani, Pilani campus, Rajasthan, India. She has completed B.Pharm from SSJ college of Pharmacy, Hyderabad, Telangana. She has completed M.Pharm in Pharmaceutics from BITS-Pilani, Hyderabad campus, India. She also has 1 year of industry experience as a Research Scientist-I, specialization in pharmaceutical R&D, particularly in topical formulation, at Aizant Drug Research Solutions Pvt. Ltd. Hyderabad, Telangana. She joined as a project associate in the DST funded project at BITS-Pilani and registered for Ph.D program under the supervision of Prof. Paul Atish Tulshiram in the year 2019. Her research area includes nano formulation for synthetic and natural products for the treatment of Rheumatoid arthritis.